ACS SYMPOSIUM SERIES 1128

Physical Methods in Food Analysis

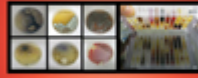

EDITED BY
Michael M. Tunick and
Charles I. Onwulata

Physical Methods in Food Analysis

Downloaded by 142.58.101.27 on July 29, 2013 | http://pubs.acs.org
Publication Date (Web): July 24, 2013 | doi: 10.1021/bk-2013-1138.fw001

In Physical Methods in Food Analysis; Tunick, M., et al.;
ACS Symposium Series; American Chemical Society: Washington, DC, 2013.

Downloaded by 142.58.101.27 on July 29, 2013 | http://pubs.acs.org
Publication Date (Web): July 24, 2013 | doi: 10.1021/bk-2013-1138.fw001

In Physical Methods in Food Analysis; Tunick, M., et al.;
ACS Symposium Series; American Chemical Society: Washington, DC, 2013.

ACS SYMPOSIUM SERIES **1138**

Physical Methods in Food Analysis

Michael H. Tunick, Editor
U.S. Department of Agriculture, Agricultural Research Service
Wyndmoor, Pennsylvania

Charles I. Onwulata, Editor
U.S. Department of Agriculture, Agricultural Research Service
Wyndmoor, Pennsylvania

Downloaded by 142.58.101.27 on July 29, 2013 | http://pubs.acs.org
Publication Date (Web): July 24, 2013 | doi: 10.1021/bk-2013-1138.fw001

Sponsored by the
ACS Division of Agricultural and Food Chemistry, Inc.

American Chemical Society, Washington, DC

Distributed in print by Oxford University Press

In Physical Methods in Food Analysis; Tunick, M., et al.;
ACS Symposium Series; American Chemical Society: Washington, DC, 2013.

Library of Congress Cataloging-in-Publication Data

Physical methods in food analysis / Michael H. Tunick, editor, U.S. Department of Agriculture, Agricultural Research Service, Wyndmoor, Pennsylvania, Charles I. Onwulata, editor, U.S. Department of Agriculture, Agricultural Research Service, Wyndmoor, Pennsylvania ; sponsored by the ACS Division of Agricultural and Food Chemistry, Inc.
pages cm. -- (ACS symposium series ; 1138)
Includes bibliographical references and index.
ISBN 978-0-8412-2884-9 (alk. paper)
1. Food--Analysis. I. Tunick, Michael. II. Onwulata, Charles.
TX541.P478 2013
664′.7--dc23

2013027642

Downloaded by 142.58.101.27 on July 29, 2013 | http://pubs.acs.org
Publication Date (Web): July 24, 2013 | doi: 10.1021/bk-2013-1138.fw001

The paper used in this publication meets the minimum requirements of American National Standard for Information Sciences—Permanence of Paper for Printed Library Materials, ANSI Z39.48n1984.

Copyright © 2013 American Chemical Society

Distributed in print by Oxford University Press

All Rights Reserved. Reprographic copying beyond that permitted by Sections 107 or 108 of the U.S. Copyright Act is allowed for internal use only, provided that a per-chapter fee of $40.25 plus $0.75 per page is paid to the Copyright Clearance Center, Inc., 222 Rosewood Drive, Danvers, MA 01923, USA. Republication or reproduction for sale of pages in this book is permitted only under license from ACS. Direct these and other permission requests to ACS Copyright Office, Publications Division, 1155 16th Street, N.W., Washington, DC 20036.

The citation of trade names and/or names of manufacturers in this publication is not to be construed as an endorsement or as approval by ACS of the commercial products or services referenced herein; nor should the mere reference herein to any drawing, specification, chemical process, or other data be regarded as a license or as a conveyance of any right or permission to the holder, reader, or any other person or corporation, to manufacture, reproduce, use, or sell any patented invention or copyrighted work that may in any way be related thereto. Registered names, trademarks, etc., used in this publication, even without specific indication thereof, are not to be considered unprotected by law.

PRINTED IN THE UNITED STATES OF AMERICA

Foreword

The ACS Symposium Series was first published in 1974 to provide a mechanism for publishing symposia quickly in book form. The purpose of the series is to publish timely, comprehensive books developed from the ACS sponsored symposia based on current scientific research. Occasionally, books are developed from symposia sponsored by other organizations when the topic is of keen interest to the chemistry audience.

Before agreeing to publish a book, the proposed table of contents is reviewed for appropriate and comprehensive coverage and for interest to the audience. Some papers may be excluded to better focus the book; others may be added to provide comprehensiveness. When appropriate, overview or introductory chapters are added. Drafts of chapters are peer-reviewed prior to final acceptance or rejection, and manuscripts are prepared in camera-ready format.

As a rule, only original research papers and original review papers are included in the volumes. Verbatim reproductions of previous published papers are not accepted.

ACS Books Department

Downloaded by 142.58.101.27 on July 29, 2013 | http://pubs.acs.org
Publication Date (Web): July 24, 2013 | doi: 10.1021/bk-2013-1138.fw001

Preface

Downloaded by 137.207.120.173 on July 29, 2013 | http://pubs.acs.org
Publication Date (Web): July 24, 2013 | doi: 10.1021/bk-2013-1138.pr001

A symposium titled "Physical Methods in Food Analysis" was presented at the Fall National Meeting of the American Chemical Society (ACS) in Philadelphia in August 2012. The symposium was sponsored by the ACS Division of Agricultural and Food Chemistry, Inc. (AGFD), which is in the forefront in the dissemination of knowledge about food chemistry. This book includes ten chapters based on the talks given at that symposium. Chapter 1 describes how poppy, cotton seed, soybean, and canola seed oils can be examined with reverse phase high performance thin layer chromatography and viscosity measurements in an attempt to differentiate between them. Continuing with the theme of distinguishing between foods, Chapter 2 discusses the use of ultrahigh pressure liquid chromatography accurate mass quadrupole time-of-flight mass spectrometry with electrospray ionization for analyzing flavonoid-based compounds in onions, for the purpose of varietal identification. Chapter 3 details the use of high performance liquid chromatography-mass spectrometry for quality control and product standardization of the East Asian botanical *jiaogulan*. In Chapter 4, lanthanide-sensitized luminescence spectrometry is applied to detection of tetracyclines and fluoroquinolones in food. Chapter 5 shows how glycemic index may be determined for extruded grains blended with whey protein or cashew pulp. Polymethoxyflavones and derivatives, which occur in citrus fruits, are described in Chapter 6 along with chromatographic techniques for analyzing them. Chapter 7 discusses rheology as a method for looking at characteristics of bioplastics. The book wraps up with three chapters centering on color. Blue pigments, which are scarce in nature, are covered in Chapter 8 along with methods for separating and identifying them. In Chapter 9, resonance Raman spectroscopy was used to identify blue and red forms of anthrocyanins in grapes at various pH levels. A description of color changes in polydiacetylene-based smart packaging, and Raman spectroscopic methods for measuring them, are found in Chapter 10.

We thank our authors for sharing their results with us in the symposium and this book. We also thank AGFD for providing a forum for the symposium and financial support.

Michael H. Tunick
Dairy & Functional Foods Research Unit
Eastern Regional Research Center
Agricultural Research Service
U.S. Department of Agriculture
600 East Mermaid Lane
Wyndmoor, PA 19038
michael.tunick@ars.usda.gov (e-mail)

Charles I. Onwulata
Director, Office of the Chief Scientist
U.S. Department of Agriculture
Jamie L. Whitten Building, Room 338A
1400 Independence Avenue, SW -- Mailstop 0110
Washington, DC 20250
charles.onwulata@osec.usda.gov (e-mail)

Downloaded by 137.207.120.173 on July 29, 2013 | http://pubs.acs.org
Publication Date (Web): July 24, 2013 | doi: 10.1021/bk-2013-1138.pr001

Downloaded by UNIV SOUTH DAKOTA on July 29, 2013 | http://pubs.acs.org
Publication Date (Web): July 24, 2013 | doi: 10.1021/bk-2013-1138.ch001

Chapter 1

High-Performance Thin Layer Chromatography and Raman Microscopy of Cotton and Other Seed Oils

Ivan C. Lee,* Adam Gamson, and Jonathan Mitchell

U.S. Army Research Laboratory, Sensors and Electron Devices Directorate, 2800 Powder Mill Road, Adelphi, Maryland 20783, U.S.A.
***E-mail: ivan.c.lee2.civ@mail.mil.**

Cotton seed oil is a renewable resource that can potentially be blended with fossil fuels for power generation. The primary objective of this work was to identify analytical techniques that can be performed on the field to discern poppy seed oil from cotton seed oil. It was determined that it is feasible to distinguish poppy and cotton seed oil samples using reverse phase high performance thin layer chromatography (HPTLC) and viscosity measurement. Other seed oils including soybean and canola seed oils were also evaluated to understand the limitations of these analytical techniques. Viscosity measurement was determined to be effective to distinguish cotton seed oil from poppy or soybean seed oil, but it failed to distinguish cotton and canola seed oils. To maximize the HPTLC separation of the oils without pretreatment, different solvent mixtures were studied: isopropyl alcohol, 1-butanol, methanol, hexane, dioxane, and distilled water. The purpose of mixing solvents was to tailor a solution with moderate polarity to achieve the best separation with the HPTLC plates. The most promising mixtures were butanol-methanol at the ratio of 80:20% and 90:10%. In the 80:20 mixture, R_f values increased in the order of poppy, canola, cotton, and soybean, while in the 90:10 mixture the order was reversed. With this technique the oil polarity can be ranked in increasing polarity: poppy < canola < cotton < soybean. This showed that the various compounds making up the oil have varying levels of polarity, and thus lessen in concentration

Not subject to U.S. Copyright. Published 2013 by American Chemical Society
In Physical Methods in Food Analysis; Tunick, M., et al.;
ACS Symposium Series; American Chemical Society: Washington, DC, 2013.

at varying levels as the analyte moves up the plate. Raman spectroscopy (microscopy) was employed to characterize the oils by locating cis C=C vibrational peak at 1654cm^{-1} on the oil smear that decreased as the analyte moved up the stationary phase.

Introduction

Seed oil is an important food commodity with varying levels of nutritional value (*1*, *2*). Some inexpensive seed oils have also become renewable materials for production of alternative fuels (*3*, *4*), plasticizers (*5*), and lubricants (*6*, *7*). Furthermore, seed oil-diesel blends can potentially be used as a fuel for compression ignition engine (*8*, *9*). For these reasons, it is imperative for the consumer to be able to discern one seed oil from another.

Each seed oil has a unique composition of triacylglycerides (TAGs), tocopherols, phytosterols, and phospholipids. TAGs, the most prevalent characteristic of seed oils, consist of a glycerol backbone and three fatty acid esters. Figure 1 is an illustration of a generalized TAG structure. These fatty acid esters are commonly a mixture of 14, 16, 18, 20 and 22 carbon chains with different degrees of saturation. Chromatography has been used to characterize lipid contents and fatty acid distribution of phospholipids in oils (*10–18*). Table 1 shows the TAG composition of various seed oils. Meanwhile, it should be noted that there is natural variability of fatty acids in seed oils. For example, Dowd et al. proposed biosynthesis pathways to explain the effects of genotype and environment on fatty acid profiles of cotton seed oil (*Gossypium hirsutum* L.) (*19*). In additional to TAG quantification, quantification of cylcopropenoid acids of cottonseed also attracts some attentions in the literature (*13–15*). Furthermore, mechanical properties such as refractive index, density, viscosity and surface tensions of different seed oils have been compared (*16*, *17*).

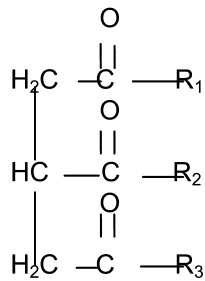

Figure 1. Chemical structure of triacylglyceride (TAG).

Meanwhile, thin layer chromatography (TLC) is a simple tool for separating analytes in a sample, in that it takes advantage of a two-phase system to discern chemicals (*20–24*). The first phase is the stationary (solid or liquid) phase, which typically has characteristics suitable for interacting with one or more analytes, either by physical interaction or chemical interaction; the second is the mobile

In Physical Methods in Food Analysis; Tunick, M., et al.;
ACS Symposium Series; American Chemical Society: Washington, DC, 2013.

Downloaded by UNIV SOUTH DAKOTA on July 29, 2013 | http://pubs.acs.org
Publication Date (Web): July 24, 2013 | doi: 10.1021/bk-2013-1138.ch001

(liquid or gas) phase, which serves as the medium for carrying the analyte through the stationary phase. Separation is achieved by the unique properties of each analyte that cause them to pass through the stationary phase at different velocities. Plate selection is one of the most important parameters for effective separation. Spot broadening can be reduced by using a plate coated with finer particles. In addition, solvent selection can be another difficult and challenging issue of developing an effective TLC experiment. Based on solvent theory and the work of many researchers, a seven-solvent scheme can be created for rapid investigation of solvent mixtures to achieve optimal separation. Typically, previous HPTLC studies involve pretreatment processing of seed oils to break down the chemical structure of TAGs, which limits the usefulness of HPTLC for seed oil identification outside the laboratory environment.

Downloaded by UNIV SOUTH DAKOTA on July 29, 2013 | http://pubs.acs.org
Publication Date (Web): July 24, 2013 | doi: 10.1021/bk-2013-1138.ch001

Table 1. TAG composition of various seed oils

Seed Oil	*C14:0*	*C16:0*	*C16:1*	*C18:0*	*C18:1*	*C18:2*	*C18:3*
Poppy (P. Somniferum)		12		3	20	65	
Cotton	0.9	21.1		2.2	19.2	55.1	0.6
Canola		4.5		1.5	60.5	21.2	9.7
Soybean		7-14		1-6	19-30	44-62	4-11

The purpose of this study is to develop a simple analytical method so that pure cotton seed oil and pure poppy seed oil can be distinguished outside a laboratory environment. However, this study was not intended to detect adulteration or to quantify the level of adulteration for a given oil. This study is organized as follows. First, the viscosity of the seed oils was determined as a function of temperature in order to understand the usefulness and limitations of viscosity measurement for seed oil identification. Next, chromatographic separation of these seed oils was investigated. To achieve the best separation of the oils with the HPTLC plates, solvents of varying polarity were mixed and tested. Finally, the HPTLC plates were characterized with Raman spectroscopy (microscopy) to track the movement of seed oil components with specific functional groups.

Procedures

Materials and Reagents

The cotton and soybean oil samples were obtained from undisclosed commercial vendors through Army Aberdeen Test Center, MD. Poppy and canola seed oil samples were extracted by mechanical pressing of corresponding seeds.

The viscosity of seed oil was measured using a Size 1B Ubbelohde viscometer (Cannon Instrument Co.) in a temperature-controlled ethylene glycol/water mixture bath. Three viscosity measurements were conducted at each bath temperature of 22, 30, 35, 40, and 50 °C.

Two important factors in performing effective HPTLC separation are plate and solvent selections. Specifically, reverse phase HPTLC was used, meaning that the stationary phase consisted of a glass backbone and a thin layer of silica gel treated with non-polar functional groups. The naturally polar silica gel can be modified through a process called hydrosilylation so that the surface is terminated with a C-18 chain rather than OH (*25*, *26*). This will allow the non-polar carbon chains of the fatty acids that compose TAGs to interact with the stationary phase and achieve separation. In addition, these reverse phase HPTLC plates also contained a fluorescent indicator that emitted light at 254 nm. This wavelength required the use of a handheld UV lamp for detection.

Downloaded by UNIV SOUTH DAKOTA on July 29, 2013 | http://pubs.acs.org
Publication Date (Web): July 24, 2013 | doi: 10.1021/bk-2013-1138.ch001

All solvents were purchased from Sigma Aldrich with a purity exceeding 99%. All TLC and HPTLC plates were purchased from Analtech through Sigma Aldrich. Plates of two different sizes, (10 cm x 10 cm) and (7.5 cm x 2.5 cm), were used. In GC or HPLC experiments a single separation column is used repeatedly, but a new separation plate is needed for each HPTLC experiment. For studying solvent formulations, the larger plates (10 cm x 10 cm) were used so that all four oils were simultaneously investigated and directly compared on a single plate with the same solvent concentration. This experiment was performed 5 times on different plates. This eliminated concerns regarding variations between plates and of experimental conditions such as temperature. Although the exact R_f values could varied up to 10% from plate to plate, the ranking order of R_f values for these oil samples remained the same for each experiment with the same solvent concentration. The emphasis here is the ranking order of R_f value for the seed oils. We could have performed 5 R_f measurements of the same type of seed oil on each 10 cm x 10 cm plate at each solvent concentration. But for the purpose of illustrating R_f value ranking order, it is more meaningful to report R_f values of each seed oil on a specific plate instead of the average R_f values for all plates with standard deviation error bars. In addition, the smaller plates (7.5 cm x 2.5 cm) were used to demonstrate the usefulness of vibrational spectroscopy or microscopy in tandem with HPTLC. These smaller plates are big enough to allow simultaneous comparison of two different oil samples, but they are small enough to be placed onto the microscope stage.

Solvent Preparation

The dielectric constant of various solvents was compared to that of water in order to decide which solvent to use. Table 2 shows the dielectric constant of the solvent candidates at various temperatures. We initially screened single solvents and binary solvent mixtures with IPA-dioxane, IPA-H_2O, butanol-H_2O, and methanol-H_2O. Aside from simple trial and error, solvents were chosen to be moderately polar so that the oils would achieve maximum separation using TLC. As in all chromatography, TLC uses a biphasic mobile and stationary system for separation. Oils are generally non-polar, and the strength of the association of the

analyte to the stationary phase versus the mobile phase is how unique R_f values are obtained. In order for the non-polar analyte to adsorb on the plate, the silica backbone was modified with C-18 chains to become non-polar. Therefore, a polar mobile phase was necessary, and in order to pinpoint differences between oils, a moderately polar solvent is desired. After deciding to use a mixture of 1-butanol and methanol, it was necessary to identify the optimal mixture composition. This was accomplished by running several pure samples in solvents of varying volume composition ratios of butanol and methanol.

Downloaded by UNIV SOUTH DAKOTA on July 29, 2013 | http://pubs.acs.org
Publication Date (Web): July 24, 2013 | doi: 10.1021/bk-2013-1138.ch001

Table 2. Dielectric constant of various organic solvents

Chemical	*Dielectric Constant*	*Temp (°C)*
1-Butanol	17.8	68
Isobutanol	18.7	68
Dioxane	2.2	77
Hexane	1.9	68
Isopropanol	18.3	68
Methanol	33.1	68

Before applying the samples onto the TLC or HPTLC plates, the solvent must first be mixed and added to a transparent developing chamber. Once the desired solvent has been prepared, the appropriate volume of solvent should be poured into the chamber to the depth of 1 cm. After the solvent has settled in the chamber, the chamber was closed to allow it to become saturated with the vapors of the solvent.

Sample Application and Separation

In order to prepare a plate for separation, a line was drawn across the plate 2 cm from the bottom with a pencil. Tic marks between 0.2 and 0.5 μL were made where samples would be placed and were applied using a micro-syringe. Between each sample application, the micro-syringe was rinsed with the solvent. Once all samples were applied to the plate, the plate was inserted into the developing chamber with the pencil line parallel to the solvent and near the bottom of the chamber. The plates were removed from the developing chamber before the solvent front reached the top of the plate. The solvent front was then marked with a pencil and allowed to dry in the air. The R_f values were calculated by dividing the distance the sample traveled by the distance the solvent front traveled up the plate. Figure 2 displays the lengths required for R_f calculations.

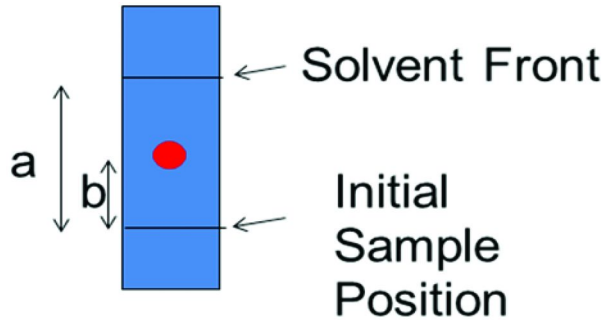

Figure 2. Determination of R_f values of HPTLC.

Downloaded by UNIV SOUTH DAKOTA on July 29, 2013 | http://pubs.acs.org
Publication Date (Web): July 24, 2013 | doi: 10.1021/bk-2013-1138.ch001

Raman Microscopy

The resulting HPTLC plates (2.5 cm x 7.5 cm plates) with cotton seed oil, poppy seed oil, canola oil, or soybean oil were characterized using a confocal Raman microscope (HORIBA, LabRam ARAMIS) with sub-micron spatial resolution. A 532nm He-Ne laser was used as the source. The microscope objective magnification was set at 100x, and the 600 gr/mm grating was selected. Spectrum noise and detector saturation were minimized by adjusting the exposure time to 2 s and the accumulation number of scans to 16. The spectra with oil samples were then compared to spectra of a clean HPTLC slide and a slide with TLC solvent.

Results and Discussion

Viscosity Measurement

Figure 3 illustrates the changes in seed oil viscosity with temperature. Canola and cotton seed oils have similar kinematic viscosity at all temperatures. Soybean seed oil has a lower kinematic viscosity than canola and cotton seed oils, and the unfiltered or filtered poppy seed oil has the lowest viscosity. The kinematic viscosity of cotton seed oil was determined to be 74.6 mm^2/s at 22 °C and decreased exponentially with temperature. The viscosity measurements are fitted to a curve using a power function (Equation 1) or an exponential function (Equation 2)

$$V = A * T^B \qquad (1)$$

$$V = A * e^{(B*T)} , \quad (2)$$

where V represents kinematic viscosity in mm^2/s, and T represents temperature in degrees Celsius. The fitting parameters with the power function and the exponential function are shown in Table 3. Both functions fit the experiment data very well with R^2 values around 0.99. With these fitting parameters, viscosity can be readily calculated at any environmental temperature between 22 and 50

°C, and is specific for each oil type. The implication is that we can confirm the identity of an unknown seed oil by comparing its measured viscosity to the expected viscosity of standard seed oils at any environmental temperature.

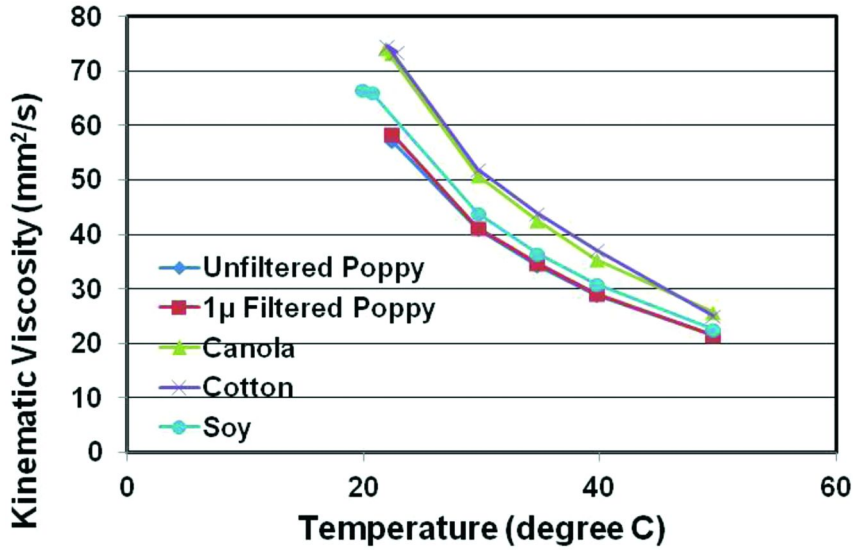

Figure 3. Viscosity measurement of seed oils in a temperature bath at various temperatures.

Table 3. Fitting Parameters for kinematic viscosity (V, mm2/s) as a function of temperature (T, °C)

	$V = A * T^B$			$V = A * e^{(B*T)}$		
Oil	***A***	***B***	***R²***	***A***	***B***	***R²***
Unfiltered Poppy	2541	-1.218	0.999	120.5	-0.035	0.9899
1 micron filtered Poppy	2805	-1.243	0.9988	125.0	-0.036	0.9894
Canola	3914	-1.281	0.9983	168.2	-0.039	0.9916
Cotton	4440	-1.312	0.9917	176.2	-0.040	0.9961
Soy	2315	-1.178	0.9964	137.6	-0.037	0.9929

Viscosity is a simpler and more direct method for observing differences in oils, requiring less effort and equipment than other methods. As shown in Figure 3, this technique was able to distinguish cotton seed oil from poppy and soybean oils effectively. While usefulness of viscosity measurement is without question, it

In Physical Methods in Food Analysis; Tunick, M., et al.;
ACS Symposium Series; American Chemical Society: Washington, DC, 2013.

Downloaded by UNIV SOUTH DAKOTA on July 29, 2013 | http://pubs.acs.org
Publication Date (Web): July 24, 2013 | doi: 10.1021/bk-2013-1138.ch001

does have its limitations. It was difficult to distinguish canola seed oil from cotton seed oil solely based on viscosity measurement. When viscosity fails to provide a clear answer, HPTLC is an invaluable tool for providing supplementary data that can be used to easily differentiate between the oils in question.

Furthermore, usefulness of viscosity measurement could be limited by seed oil processing. Effects of refining, bleaching, de-colorization, and winterizing have shown to be small for seed oils including canola, soybean and other oils (*27*, *28*). However, degree of unsaturation and molecular size of fatty acids can affect the kinematic viscosity (*28*, *29*). For example, Toscano et al. have demonstrated that unsaturated oils and small size molecules of fatty acids have a lower viscosity (*28*). Wakeham and Magne have shown that hydrogenation of cottonseed oil plays an important role in seed oil viscosity (*29*). They summarized the relationship and viscosity data with a series of isotherms. From these isotherms, we can read off the viscosity once we know the iodine number of the cotton seed oil. Conversely, we found that viscosity behavior of our cotton seed oil sample is consistent with the U.S.P. grade "unhydrogenated" cotton seed oil (with iodine number = 101) used by Wakeham and Magne. It is important to note that hydrogenation lowers the iodine number and increases the viscosity. Therefore, "unhdydrogenated" cotton seed oil in this study (with iodine number of about 100) represents the lower limit of viscosity.

Meanwhile, Ozcan and Atalay investigated the degree of unsaturation among 8 different poppy seeds, and they found that these seeds have similar degree of unsaturation as indicated by a narrow range of their iodine number varying from 122.0 to 129.5 (*30*). Although poppy seeds would have a different set of viscosity-iodine number isotherms than cottonseed oil, the viscosity of our unhydrogenated poppy seed is outside the range of viscosity of cottonseed oils as determined by Wakeham and Magne (*29*). Hydrogenation of poppy seed oil would increase its viscosity, and it is possible that hydrogenated poppy seed oil could be within the viscosity range of cottonseed oils. But, it is highly unlikely that the viscosity any cotton seed oil sample (hydrogenated or unhydrogenated) can be as low as the viscosity of an unhydrogenated poppy seed sample evaluated at this study.

Downloaded by UNIV SOUTH DAKOTA on July 29, 2013 | http://pubs.acs.org
Publication Date (Web): July 24, 2013 | doi: 10.1021/bk-2013-1138.ch001

Quantitative Analysis with HPTLC Plates

Initially, the solvent mixtures of interest were schemed using TLC plates. While no quantitative data could be extracted from the regular TLC plates, these initial experiments were integral in learning the types of mixtures to test with the HPTLC plates. The reason that regular TLC was insufficient was twofold. First, the solvent front was nearly impossible to distinguish from the oil sample mark due to trace "fingers" left by the solvent; second, the run time using regular TLC plates was 4-5 h. The "fingers" were likely a result of the type of plate used. The regular TLC plates were modified so that the C-18 hydrocarbon strongly interacted with the silica backbone but was not chemically bound. It is believed that the unbound hydrocarbons also migrated with the solvent up the TLC plate.

HPTLC solves the aforementioned problems in TLC by using an optimized coating for the plate. HPTLC plates are simple to precondition, have improved dosage methods, and are easier to analyze due to a uniform dosage system. The

main innovation is the uniform coating of smaller SiO_2 molecules. Due to the smaller particle size, the coating can be more densely packed. Using the van der Meer equation for theoretical plates that is commonly seen in other forms of chromatography, we get the following relation:

$$N=L/H\,, \quad (3)$$

where N represents the number of theoretical plates, L represents the column length, and H represents the height of the plates. With decreasing particle size, the effective H decreases; therefore, N increases. As N grows, separation between spots is better achieved.

Only the most promising solvent mixtures, including mixtures of IPA-hexane, methanol-dioxane, and butanol-methanol, were evaluated on the HPTLC plates. These solvents were chosen based on polarity, which was gauged by the dielectric constant, found in Table 2. Most of these solvents were mixed to create moderately polar solutions. First, HPTLC tests were run using solvents consisting of pure IPA, pure butanol, and pure dioxane. After these initial runs, mixtures of IPA and hexane were performed with IPA concentrations of 25% - 75% in increments of 25%. Over the range of mixtures, the poppy seed oil had R_f values of: 0.66, 0.74, and 0.72 at IPA concentrations of 75%, 50%, and 25% IPA. Cotton seed oil had R_f values of 0.69, 0.75, and 0.74 over these concentrations. It was determined that the poppy and cotton seed oils had similar values with IPA-hexane solvent, so this binary solvent was not further considered.

The next solvent mixture studied was methanol-dioxane, ranging from 100% methanol to 100% dioxane, varying by increments of 25%. Dioxane was chosen over hexane due to the phase separation of methanol and hexane. Figure 4 shows the R_f values for poppy, cotton, canola, and soybean oils in the various methanol-dioxane mixtures, where the oils again have similar R_f values and are difficult to distinguish. Moreover, as the methanol concentration increased, the R_f values decrease to 0. An R_f value of 0 indicates that the analyte did not dissolve in the mobile phase and was not carried up the column with the solvent. Conversely, an R_f value of 1 would indicate that the analyte completely dissolved in the solvent and had no interaction with the stationary phase. Furthermore, the increase in percent methanol caused the R_f values to go to 0, indicating that highly polar solvents would not be capable of separating oils due to a lack of interaction. The selection of a solvent was vital to the separation of the oil samples and led to the decision to use a solvent mixture that would be less polar than methanol.

The third solvent mixture studied was butanol-methanol, ranging from 60% to 100% butanol in increments of 10%. In this set of solutions, the data for the 100% methanol run was also included. The butanol-methanol mixtures were run in 10% increments based on the promising data obtained from the 100% butanol run, and the apparent lack of migration shown by the 100% methanol run. The concentration of butanol was decreased in each run until no migration was seen. Figure 5 shows an actual HPTLC plate with the fluorescent indicators that illustrates the indirect method of detection. The oil spots are indicated by a lack of fluorescent activity. As Figure 6 illustrates, there were two butanol-methanol concentrations that gave the oil samples the desired uniqueness for the purpose

Downloaded by UNIV SOUTH DAKOTA on July 29, 2013 | http://pubs.acs.org
Publication Date (Web): July 24, 2013 | doi: 10.1021/bk-2013-1138.ch001

of this study: 80:20 and 90:10. Additional evaluations consisted of checking the reproducibility of the results, as well as using some two-dimensional plates. Poppy oil has the lowest R_f value in the 80:20 concentration and the highest at 90:10, going from 0.38 to 0.62. At 80:20 concentration the descending order of R_f values was soybean, cotton, canola, and poppy, while at 90:10 the order was poppy, canola, soybean, and cotton. Cotton has the R_f range of 0.44 to 0.53, canola 0.41 to 0.57, and soybean 0.45 to 0.69. As shown in Table 2, methanol is much more polar than 1-butanol. Therefore, as the percent of butanol rises, the solvent mixture becomes less polar. Using these results, the optimum solvent composition for oil separation was chosen such that there was a distinction between several of the samples.

Downloaded by UNIV SOUTH DAKOTA on July 29, 2013 | http://pubs.acs.org
Publication Date (Web): July 24, 2013 | doi: 10.1021/bk-2013-1138.ch001

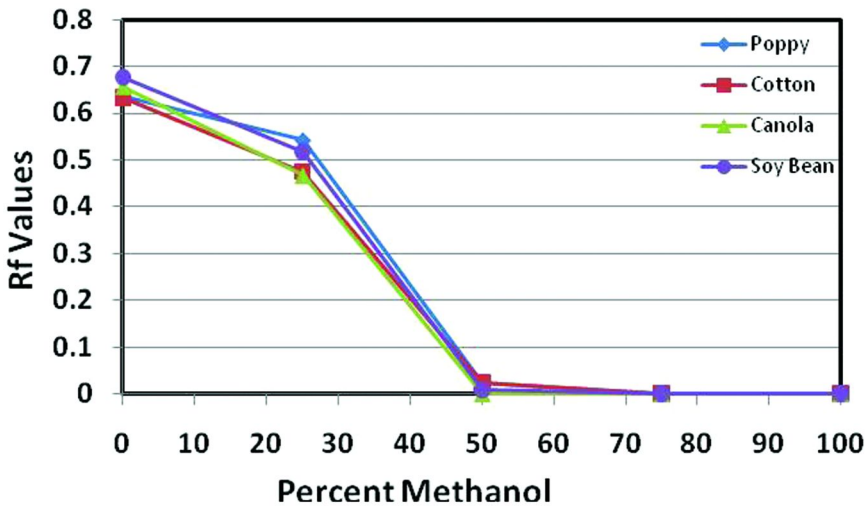

Figure 4. R_f values of poppy, cotton, canola and soybea seed oils in methanol-dioxane mixtures from 0:100 to 100:0.

The switch in order of R_f values in the 80:20 and 90:10 butanol-methanol mixtures can be explained by the relative strength between the solvent-analyte interaction and the analyte-solid interaction. Methanol has a shorter alkyl chain than butanol; therefore, methanol is more polar than butanol. In other words, the 80:20 butanol-methanol mixture is more polar than the 90:10 mixture. These results imply that, in the 80:20 mixture, poppy seed oil has a weaker solvent-analyte interaction than analyte-solid interaction, while canola has a relatively stronger solvent-analyte interaction than analyte-solid interaction. However, in the 90:10 mixture, poppy seed oil has a stronger solvent-analyte interaction than analyte-solid interaction, while canola has a relatively weaker solvent-analyte interaction than analyte-solid interaction. Therefore, it can be concluded that poppy seed oil is less polar than canola seed oil. Likewise, the oil polarity can be ranked in increasing polarity: poppy < canola < cotton < soybean.

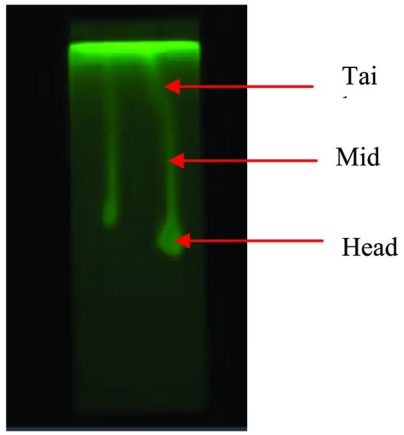

Figure 5. An image of HPTLC of seed oils in a solvent mixture of 80:20 butanol-methanol. Right-poppy seed oil; Left-cotton seed.

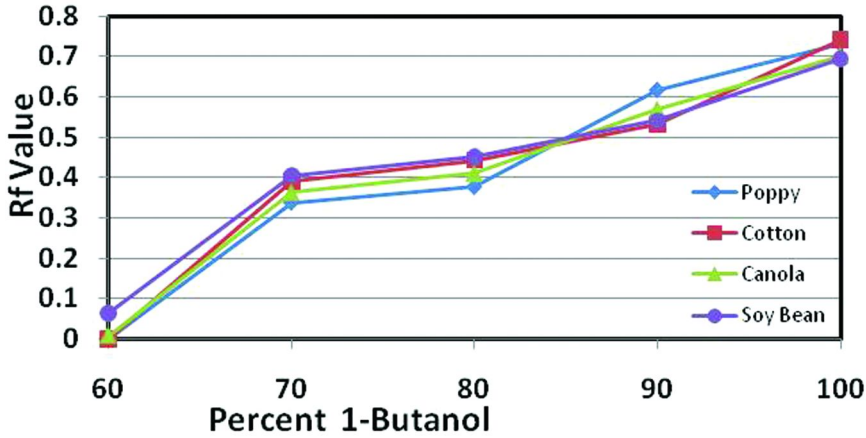

Figure 6. R_f values of poppy, cotton, canola and soy seed oils in 1-butanol: methanol mixtures from 0:100 to 100:0.

Raman Spectroscopy/Microscopy

For a given seed oil, the fatty acid chains in the triglyceride structure could be different in length and in degree of saturation. These differences affect the solvent-analyte interaction and the analyte-solid interaction. The triglycerides containing more unsaturated fatty acids move at a different velocity on the stationary phase than the triglycerides containing more saturated fatty acids. Therefore, the movement of triglyceride can be tracked by monitoring characteristic vibrational peaks of unsaturated fatty acids. Raman microscopy

Downloaded by UNIV SOUTH DAKOTA on July 29, 2013 | http://pubs.acs.org
Publication Date (Web): July 24, 2013 | doi: 10.1021/bk-2013-1138.ch001

revealed two characteristic peaks that appeared in each oil spectra on three locations (head, middle, and tail) of each oil smear as in Figure 5. Figure 7 displayed the Raman spectrum for each oil at the head region of the oil smear. Previously, these characteristic peaks at 1654 cm^{-1} and 3009 cm^{-1} are assigned to be the stretching mode of cis-C=C bond in the C=C-H portion of triglyceride and the stretching mode of C-H bond in the C=C-H portion, respectively (*31–33*). The peaks remained consistently in the same wavenumber for each oil sample, only varying by 3 cm^{-1} at most. Figure 8 displayed the Raman spectra along the oil smears of poppy and cotton seed oil samples. The peaks, all appearing relatively strong in the head region, were shown to decrease in relative intensity as the middle and tail regions were inspected.

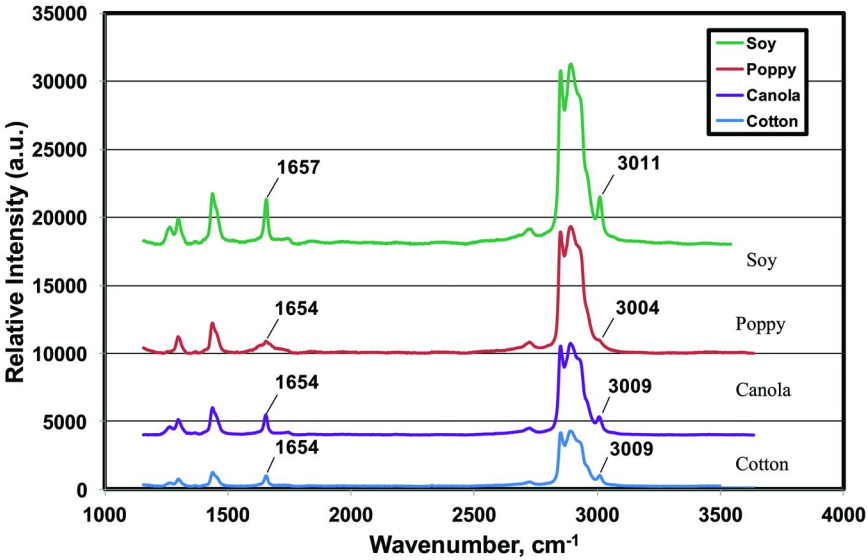

Figure 7. Comparison of Raman spectra for poppy, cotton, canola and soybean seed oil samples on HPTLC Plate.

Although the cotton seed oil and the poppy seed oil showed the similar feature, the geometric coordinates for the "heads" were defined by the Rf value of each oil on the plate as shown in Figure 5. The relative intensity was seen to vary between oils, perhaps indicating some differentiation between the types. Further analysis of the ratio of the characteristic solvent peak at 1437 cm^{-1} and the analyte peak at 1654 cm^{-1} shows a trend that is indicative of which oil is being studied, as well as the regression of the characteristic oil bonds as the analyte moves from the head region toward the tail (Table 4). It can be observed that the exact change in ratios between oils can vary notably, but all show a progression of increased ratio between the observed 1437 cm^{-1} peak and the 1654 cm^{-1} peak as the head, middle, and tail regions are studied. This supports the concept that the compounds in the oils carrying the C=C bonds have a stronger affinity to the stationary phase and, thus, thin out as the analyte travels up the mobile phase.

Downloaded by UNIV SOUTH DAKOTA on July 29, 2013 | http://pubs.acs.org
Publication Date (Web): July 24, 2013 | doi: 10.1021/bk-2013-1138.ch001

Downloaded by UNIV SOUTH DAKOTA on July 29, 2013 | http://pubs.acs.org
Publication Date (Web): July 24, 2013 | doi: 10.1021/bk-2013-1138.ch001

(a)

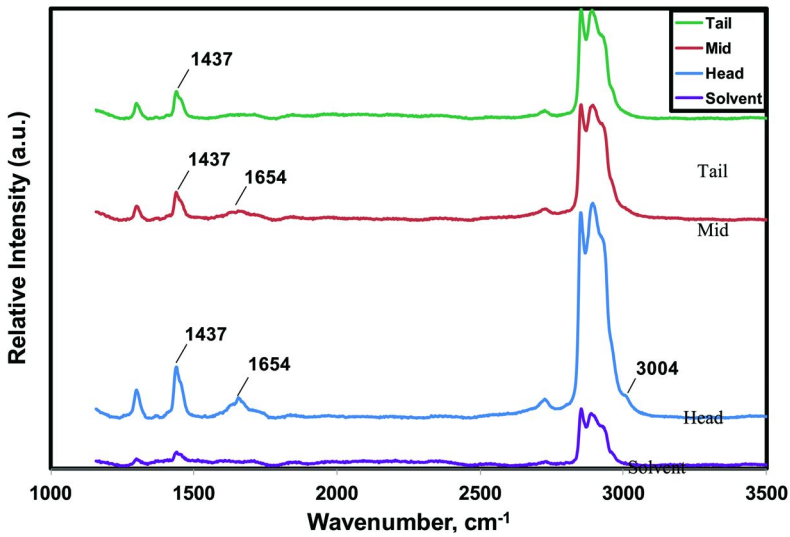

(b)

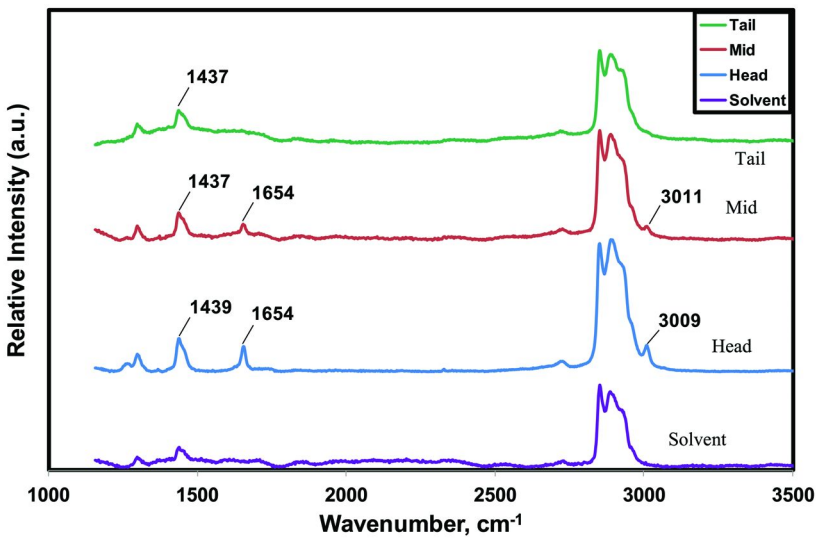

Figure 8. Raman Spectra along the oil smear after separation on HPTLC Plate in Figure 5: (a) poppy seed oil, and (b) cotton seed oil.

Table 4. Ratio of Solvent Peak (1437) to Oil Peak (1654)

	Head	*Middle*	*Tail*
Cotton	2.27	2.86	-
Poppy	2.54	3.04	-
Canola	2.48	4.82	-
Soy	1.91	2.44	4.04

Downloaded by UNIV SOUTH DAKOTA on July 29, 2013 | http://pubs.acs.org
Publication Date (Web): July 24, 2013 | doi: 10.1021/bk-2013-1138.ch001

Conclusions

Two important factors in performing HPTLC are plate and solvent selection. Due to the biphasic separation of chromatography, it is possible to use a given characteristic of the sample of interest to distinguish it from a mixture. For different seed oils, polarity serves as a good basis for separation. Knowing that oils are non-polar, the HPTLC plates with a non-polar backbone were chosen, and a polar solvent was needed. Identifying the solvent to achieve optimal separation was more difficult than choosing the stationary phase since the solvent's polarity needed to be flexible for best results. Finally, two solvent mixtures were selected for separating. They were 80% butanol and 20% methanol, as well as 90% butanol and 10% methanol. These two were chosen because they showed good separation and had a reversal of order of R_f values of the samples. This indicates that the mobile and stationary phase interactions with the analyte were changing in between those solvents. At 80:20 butanol-methanol, the oils had R_f values of 0.38, 0.41, 0.44, and 0.45 for poppy, canola, cotton, and soybean, while at 90:10 butanol-methanol, the values were 0.53, 0.54, 0.57, and 0.62 for cotton, soybean, canola, and poppy. Further analysis of the HPTLC plates with Raman spectroscopy showed that the oils contained a characteristic peak at 1654 cm^{-1} that would decrease in comparison to the solvent peak at 1437 cm^{-1} as the analyte moved from the head region to the tail region. This showed that the shape of the analyte steaks on the plates are formed due to the various compounds composing the oil having varying affinities to the non-polar background and, thus, lessen in concentration as the analyte moves up the plate. Viscosity measurement could be a supplementary technique to distinguish cotton seed oil from soybean oil, although these two oils have similar R_f values with 80:20 butanol-methanol solution.

Future Works

Current work has demonstrated that HPTLC can be combined with vibrational microscopy to identify the movement of individual components in a seed oil, in particular the cis C=C containing compounds. We can potentially focus our attention on measuring intensity of some specific vibrational modes, for example the stretching vibration of cis C=C bond at about 1654 cm^{-1}. Then we can obtain a spatial 3-D mapping of this vibrational mode for HPTLC separation of each

seed oil. In other words, we can measure the peak intensity ratio such as in Table 4 across the whole surface of a HPTLC plate. Current vibration microscopy has the capability to scan the HPTLC slides with multiple coordinates sequentially as defined by meshing. Such practice is time intensive on the order of magnitude of 1 day for a HPTLC plate of the size of a microscope slide (2.5 cm x 7.5 cm). However, with future advance in imaging technology, this 3-D mapping could be achieved with minutes or seconds.

Furthermore, there is a need to detect adulteration of seed oil, and additional studies can be performed on the mixture of seed oils to find out the feasibility of detection outside the laboratory environment. Currently, detection of the adulteration of pure oil mixtures with cheaper substitutes has been achieved by various advanced laboratory analytical methods including vibrational spectroscopy (*32*, *33*) and GC-MS (*34*).

Downloaded by UNIV SOUTH DAKOTA on July 29, 2013 | http://pubs.acs.org
Publication Date (Web): July 24, 2013 | doi: 10.1021/bk-2013-1138.ch001

Acknowledgments

Dr. Karen Gaskell at the University of Maryland provided helpful suggestions with the Raman microscopy. William Allmon at the U.S. Army Research Laboratory provided the extracted the canola and poppy seed oils from the seeds for this study. John Wills at the U.S. Army Aberdeen Test Center Corp provided the cotton and soybean oil samples.

References

1. Jukanti, A. K.; Gaur, P. M.; Gowda, C. L. L.; Chibbar, R. N. *Br. J. Nutr.* **2012**, *108*, S11–S-26.
2. Anjum, F. M.; Nadeem, M.; Khan, M. I.; Hussai, S. *Br. Food J.* **2012**, *114*, 544–552.
3. Fukuda, H.; Kondo, A.; Noda, H. *J. Biosci. Bioeng.* **2001**, *92*, 405–416.
4. Wadumesthrige, K.; Ara, M.; Salley, S. O.; Ng, K. Y. S. *Energy Fuels* **2009**, *23*, 2229–2234.
5. Fogassy, G.; Pan, K.; Figueras, F.; Gassagnau, P.; Rouzeau, S.; Courault, V.; Gelbard, G.; Pinel, C. *Appl. Catal., A* **2011**, *393*, 1–8.
6. Schuster, H.; Rios, L. A.; Weckes, P. P.; Hoelderich, W. F. *Appl. Catal., A* **2008**, *348*, 266–270.
7. Campanella, A.; Rustoy, E.; Baldessari, A.; Baltanas, M. A. *Bioresour. Technol.* **2010**, *101*, 245–254.
8. Krishna, B. M.; Mallikarjuna, J. M. *J. Renewable Sustainable Energy* **2009**, *1*, 023106.
9. Abolle, A.; Kouakou, L.; Planche, H. *Biomass Bioenergy* **2009**, *33*, 1116–1121.
10. Yoshida, H.; Tomiyama, Y.; Yoshida, N.; Saiki, M.; Mizushina, Y. *J. Am. Oil Chem. Soc.* **2008**, *85*, 535–541.
11. Yoshida, H.; Tomiyama, Y.; Tanaka, M.; Mizushina, Y. *Eur. J. Lipid Sci. Technol.* **2007**, *109*, 600–607.
12. Skipski, V. P.; Peterson, R. F.; Barclay, M. *Biochem. J.* **1964**, *90*, 374–378.

13. Fisher, G. S.; Schuller, W. H. *J. Am. Oil Chem. Soc.* **1981**, *58*, 943–946.
14. Obert, J. C.; Hughes, D.; Sorenson, W. R.; McCann, M.; Ridley, W. P. *J. Agric. Food Chem.* **2007**, *55*, 2062–2067.
15. Sheehan, E. T.; Schneider, D. L.; Vaich, M. G. *J. Agric. Food Chem.* **1972**, *20*, 119–121.
16. Alvarado, J. D. Mechanical Properties of Vegetable Oils and Fats. *Grasas Aceites* **1995**, *46*, 264–269.
17. Erol, A. S.; Oxcan, M. M.; Er, F. *Asian J. Chem.* **2011**, *23*, 1851–1853.
18. Yoshida, H.; Tomiyama, Y.; Yoshida, N.; Mizushina, Y. *Food Chem.* **2009**, *115*, 1424–1429.
19. Dowd, M. K.; Boykin, D. L.; Meredith, W. R.; Campbell, B. T.; Bourland, F. M.; Gannaway, J. R.; Glass, K. M.; Zhang, J. *J. Cotton Sci.* **2010**, *14*, 64–73.
20. Hendrikse, P. W.; Harwood, J. L.; Kates, M. In *The Lipid Handbook*, 2nd ed.; Gunstone, F. D., Harwood, J. L., Padley, F. B., Eds.; Chapman & Hall: London, U.K., 1994; pp 319−358.
21. Yoshida, H.; Tomiyama, Y.; Yoshida, N.; Mizushina, Y. *Eur. J. Lipid Sci. Technol.* **2006**, *108*, 149–158.
22. Krist, S.; Stuebiger, G.; Bail, S.; Unterweger, H. *J. Agric. Food Chem.* **2006**, *54*, 6385–6389.
23. Erinc, H.; Tekin, A.; Ozcan, M. M. *Grasas Aceites* **2009**, *60*, 375–381.
24. Sherma, J. In *Handbook of Thin-Layer Chromatography*; Sherma, J., Fried, B., Eds.; Chromatographic Science Series and Volumne 89; Marcel Dekker Inc.: New York, 2003; pp 1−46.
25. Mischki, T.; Lopinski, G.; Wayner, D. *Langmuir* **2009**, *25*, 5626–5630.
26. Plumere, N.; Speiser, B.; Dietrich, B.; Albert, K.; Pesek, J.; Matyska, M. *Langmuir* **2009**, *25*, 13481–13487.
27. Lang, W.; Sokhansanj, S.; Sosulski, F. W. *J. Am. Oil Chem. Soc.* **1992**, *69*, 1054–1055.
28. Toscano, G.; Riva, G.; Foppa Pedretti, F.; Duca, D. *Biomass Bioenergy* **2012**, *46*, 511–516.
29. Wakeham, H.; Magne, F. C. *Ind. Eng. Chem.* **1944**, *36*, 568–570.
30. Ozcan, M. M.; Atalay, C. *Grasas Aceites* **2006**, *57*, 169–172.
31. Schonemann, A.; Edwards, H. G. M. *Anal. Bioanal. Chem.* **2011**, *400*, 1173–1180.
32. Zhang, X. F.; Zou, M. Q.; Qi, X. H.; Liu, F.; Zhang, C.; Feng, Y. *J. Raman Spectrosc.* **2011**, *42*, 1784–1788.
33. Lopez-Diez, E. C.; Bianchi, G.; Goodacre, R. *J. Agric. Food Chem.* **2003**, *51*, 6145–6150.
34. Krist, S.; Stuebiger, G.; Bail, S.; Unterweger, H. *J. Agric. Food Chem.* **2006**, *54*, 6385–6389.

Downloaded by UNIV SOUTH DAKOTA on July 29, 2013 | http://pubs.acs.org
Publication Date (Web): July 24, 2013 | doi: 10.1021/bk-2013-1138.ch001

Downloaded by UNIV OF ROCHESTER on July 29, 2013 | http://pubs.acs.org
Publication Date (Web): July 24, 2013 | doi: 10.1021/bk-2013-1138.ch002

Chapter 2

Nontargeted Unknown LC(ESI-)-Q/TOF MS Approaches for Food Verification

Jihyun Lee,[1] Jerry Zweigenbaum,[2] and Alyson E. Mitchell*,[1]

[1]Department of Food Science and Technology, University of California, Davis, One Shields Avenue, Davis, California 95616
[2]Agilent Technologies, 2850 Centerville Road, Wilmington, Delaware 19808
***E-mail: aemitchell@ucdavis.edu.**

In this study, an ultrahigh pressure liquid chromatography accurate mass quadrupole time-of-flight mass spectrometry with electrospray ionization (UHPLC-(ESI)QTOF MS/MS) method for varietal separation of onions was examined. Non-targeted and data mining (unknown analysis) extraction approaches were employed and are discussed. Herein, nineteen flavonoid-based compounds were identified in all onion varieties using accurate mass formula searching. Principal component analysis (PCA) indicated that varietal identification, based upon the content of these 19 flavonoids, might be possible with the collection of a more comprehensive dataset. In addition, a molecular formula extraction algorithm was used to find all compounds in each variety without any attempt in identification. This new approach employes statistical methods to filter out non-differentiating unknown compounds and then PCA to determine if varietal differentiation could be made.

Introduction

Epidemiological studies indicate people who consume diets rich in fruits and vegetables have a reduced risk of chronic diseases (*1*, *2*). Fruits and vegetables are primary dietary sources of vitamins, minerals, fiber and a wide array of non-essential but biologically active phytochemicals including: polyphenolic antioxidants (e.g. flavonoids, carotenoids (e.g. lycopenes, β-carotene), alkaloids, glucosinolates, etc.). Biologically active phytochemicals encompass a wide range

© 2013 American Chemical Society
In Physical Methods in Food Analysis; Tunick, M., et al.;
ACS Symposium Series; American Chemical Society: Washington, DC, 2013.

of chemical structures and chemical activities and have tremendous variability in foods (*3*). To date, there is limited understanding of the influence of cultivar variability, growing season, growing region, processing, storage, formulation and packaging on the chemical composition of bioactives in foods. This lack of knowledge makes the medicinal or functional use of foods difficult, and results in a true manufacturing challenge; that is delivering a food-based product with a consistent level of specific bioactives. Moreover, many of these biologically active phytochemicals are unique in their profiles within a food or species and a more complete understanding of these profiles will lead to analytical advancements in source authentication and in detecting adulteration.

Downloaded by UNIV OF ROCHESTER on July 29, 2013 | http://pubs.acs.org
Publication Date (Web): July 24, 2013 | doi: 10.1021/bk-2013-1138.ch002

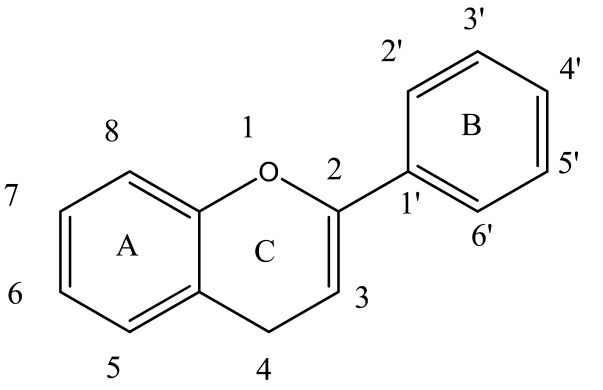

Flavan nucleus

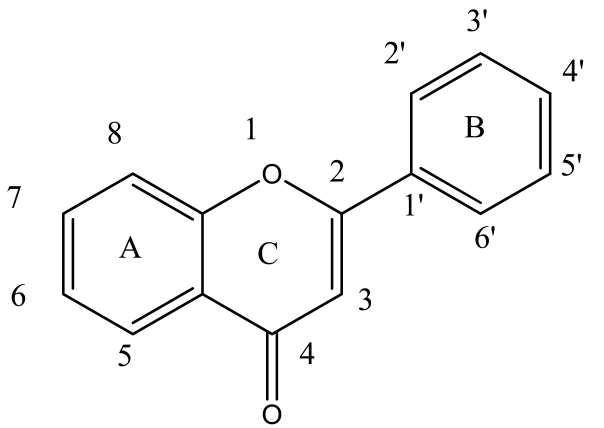

4-oxo-flavonoid nucleus

Figure 1. Structure of the Flavonoid Backbone.

In Physical Methods in Food Analysis; Tunick, M., et al.;
ACS Symposium Series; American Chemical Society: Washington, DC, 2013.

Downloaded by UNIV OF ROCHESTER on July 29, 2013 | http://pubs.acs.org
Publication Date (Web): July 24, 2013 | doi: 10.1021/bk-2013-1138.ch002

Table 1. Variety Comparisons of Flavonoids in the Outer Layers of Onions (mg/100 g DW)[a]

Variety	*quercetin 3,4′-O-diglucoside*	*quercetin 3-O-glucoside*	*quercetin 4′-O-glucoside*	*isorhamnetin 4′-O-glucoside*	*quercetin aglycone*	*sum*
Cougar	541 ± 4 f	42 ± 1 c	480 ± 4 e	79 ± 0 f	256 ± 2 b	1398 ± 3 e
Don Victor	10 ± 0 a	Below LOQ[b]	56 ± 1 a	7 ± 0 a	20 ± 0 a	93 ± 2 a
Gobi	95 ± 3 d	10 ± 0 b	103 ± 2 c	21 ± 1 d	30 ± 0 a	258 ± 4 c
Milestone	49 ± 0 c	54 ± 1 d	536 ± 3 f	17 ± 0 c	1047 ± 29 c	1703 ± 30 f
Natasha	36 ± 3 b	4 ± 0 a	89 ± 2 b	12 ± 0 b	26 ± 0 a	167 ± 5 b
Warrior	242 ± 1 e	10 ± 0 b	230 ± 2 d	34 ± 0 e	23 ± 0 a	539 ± 3 d

[a] Values are mean ± SD. Mean values followed by the different letters (a-f) within each column are significantly different at $p < 0.05$. [b] Detected but below LOQ (Limit of Quantitation). Source: Reproduced with permission from reference (*2*). Copyright 2011 American Chemical Society.

Flavonoids are the most abundant subclass of plant-derived polyphenolic bioactive compounds and more than 6,000 flavonoids have been identified (*1*). Flavonoids are secondary metabolites that play critical roles in plant protection against environmental stress such as solar UV-B radiation (*1*). The flavonoid backbone is composed of two aromatic rings (A and B) connected via a three-member carbon bridge (C6-C3-C6) (Figure 1). The 4-oxo-flavonoids have a carbonyl group on the 4 position of the C-ring. The B-ring is typically attached at the 2 position of the C-ring in most flavonoids. Isoflavones are exceptions to this in that the B ring is attached at the 3 position. Based on the other substitutions and conjugations, flavonoids are subdivided into flavonones, flavonols, isoflavones, anthocyanidins, flavanols, flavanones, and proanthocyanidins. The flavonols most frequently found in plants are those with B-ring hydroxylation in the 3′,4′-positions (quercetin), 4′-position (kaempferol), and 3′,4′,5′-positions (myricetin).

Typically plants convert flavonoids into glycosylated-conjugates as these are more water-soluble and can be stored in aqueous plant compartments (e.g. vacuoles). Glycosides greatly increase the chemical diversity and complexity of the base flavonoid structure. The dominant types of flavonoid glycoside vary among species and cultivars (*2*, *4*). For example, in apples, quercetin is present as a mixture of 3-O-galactoside, 3-O-glucoside, 3-O-rhamnoside, and 3-O-rutinoside, whereas it occurs primarily as the 4′-O-glucoside in onions (*2*, *4*, *5*). The flavonoid glycoside composition affects gastrointestinal absorption and bioavailability in animals (*5*, *6*). For example, enzymatic conversion of hesperidin (hesperetin 7-*O*-glucose-rhamnose) to hesperetin 7-glucoside increases bioavailability two-fold (*7*). Whereas, the consumption of a purified quercetin 4′-*O*-glucoside, or onion dominating in quercetin 4′-*O*-glucoside, presented the same pharmacokinetic parameters over 24 h (*8*), but differed from the quercetin aglycone over 13 h (*6*).

Onions are a primary source of flavonoids in the Western diet (*9*). Flavonoid profiles in onions are relatively simple. Previous studies identified five primary flavonoids in onions by LC-(ESI)MS/MS which include: quercetin 3,4′-*O*-diglucoside, quercetin 3-*O*-glucoside, quercetin 4′-*O*-glucoside, isorhamnetin 4′-*O*-glucoside and quercetin aglycone (*2*). Additionally, studies indicate that there is large variation of flavonoids and their glycosides in different varieties of onions (Table 1). The predominant factor influencing the complement of flavonoids in food is genetics. Therefore, the profile of flavonoids is unique to a species and varieties within that species. Because profiles are unique there is the potential that they may be used as tools for authenticating varietals.

Herein we describe a study in which onions were used as a model to explore the application of UHPLC-(ESI)QTOF MS/MS for the non-targeted analysis (without standards) of onion flavonoids in order to establish varietal differences. Identifying the composition of flavonoids in a particular variety, and how they contrast between varieties, can be accomplished by using chromatography coupled to accurate mass TOF MS. Because TOF acquires mass spectral data by pulsing ions entering the flight tube in an orthogonal beam, full spectra are always collected unlike scanning instruments. The data captured is accurate enough to determine the elemental composition of the flavonoids therefore

Downloaded by UNIV OF ROCHESTER on July 29, 2013 | http://pubs.acs.org
Publication Date (Web): July 24, 2013 | doi: 10.1021/bk-2013-1138.ch002

allowing identification without standards (*10*). However, even with the data, the true identification may be difficult because there might be isomers and possible other compounds with the same elemental composition. Other techniques such as NMR can be used to increase the probability of identification. In contrast to targeted analysis (*11–13*), which requires the use of analytical standards to determine figures of merit for detection, identification, and quantification, non-targeted analysis employs technology with sufficient analytical 'power' to make a tentative identification from a list of compounds without having standards. An analogous example of this is the use of Kovats indices with gas chromatography (*14–16*). Today, accurate mass TOF MS provides the capability to measure pseudo-molecular ions with accuracy to better than 3 ppm (*17*, *18*). This provides the power to tentatively identify compounds using a library (list), in this case flavonoids.

Downloaded by UNIV OF ROCHESTER on July 29, 2013 | http://pubs.acs.org
Publication Date (Web): July 24, 2013 | doi: 10.1021/bk-2013-1138.ch002

This initial approach begins with a general survey of these chemically diverse compounds within a sample. This "survey" can then be searched against a database of flavonoids for tentative identification using the molecular formula (based upon exact mass) of each compound in the database. The formula search approach allows comparison of the exact mass, the theoretical isotope spacing, and the relative abundance mass of the adducted molecule (pseudo-molecular ion) to the measured masses found in the data. This procedure makes the assumption that the flavonoid composition can distinguish one variety of onion from another. Once a list of tentatively identified flavonoids is generated from the different varieties, they are further examined by PCA. This statistical approach allows the determination of whether these compounds will provide differentiation of variety. Given a sufficient dataset of varietal replicates, and that these compounds can make these distinctions, a mathematical model (for MS data typically partial least squares discrimination, PLSD, or support vector machine, SVM) (*19*) is constructed to predict variety. The prediction capability of the model truly demonstrates the selected set of compounds ability to establish variety. There are many examples of using both PCA and modeling for food authenticity and verification (*20–24*).

Another approach is to extract all possible compounds found in the single MS LC/ TOF MS data for the different varieties and then filter the found "unknown compounds" based on their presence in one variety and absence in another. The filtering should include not only the presence or absence, but relative concentration as well. This complex extraction or mining of the data may provide differentiation of variety without having to actually identify the actual distinguishing compounds (*25*). This approach, *unknown analysis,* allows one to apply statistical manipulations to compare the general chemical composition of individual varieties for identification. Combining the approach of non-targeted determination (i.e., the database search for flavonoids with the approach of unknowns) gives a varietal differentiation process of non-targeted unknown analysis.

MS/MS providing structural information, is necessary to increase the probability of true identification of the individual flavonoids tentatively identified by single LC/TOF MS; as accurate mass of a pseudo-molecular ion provides only an accurate molecular formula. Compounds that are statistically important

in differentiating samples using this approach, can be searched against larger databases; but again MS/MS is required for improved identification and true structural confirmation. It must be cautioned that the characterization obtained using this approach is limited to only those compounds that 1) are extracted in the sample preparation procedure and 2) those compounds that respond (ionize) to the instrumental technology employed.

Materials and Methods

Samples

Onions were obtained from Gills Onions, LLC (Oxnard, CA) in the summer of 2011. The flavonoid composition was characterized in the four different yellow onion varieties (Cowboy, Chief, Vaquero, and Sommerset) and three red onion varieties (Red Rock, Salsa, and Merenge).

Downloaded by UNIV OF ROCHESTER on July 29, 2013 | http://pubs.acs.org
Publication Date (Web): July 24, 2013 | doi: 10.1021/bk-2013-1138.ch002

Sample Extraction

The flavonoid extraction was performed following the method of Lee and Mitchell (*2*). Inner layers have limited anthocyanidins (red color). Briefly, after separating inner layers of the onion samples from the outer layer of onions, inner layers were lyophilized and extracted with 80% methanol for 20 minutes. The total extraction process was done in triplicate.

UHPLC-(ESI)QTOF MS Analysis

The instrumental methodology was kept broad to obtain as much "coverage" as possible. A reversed-phase UHPLC gradient, from high water content to high organic modifier, was used to separate polar to less polar compounds. Electrospray ionization was used as it generally can ionize a broad range of compounds, with exception of those that are relatively non-polar. Under these conditions, most flavonoids should respond well, however their relative response is highly impacted by their variation and conjugation. Some may respond only in positive ion mode and some only in negative and those that respond in both may have much higher ionization efficiency in one or the other. In addition, electrospray is subject to ion suppression and enhancement effects, and given the typical complexity of food, these effects are expected (*26*). Thus relative response is a poor indicator of concentration and concentration can only be obtained by comparison to standards of these compounds. To get an accurate measure of concentration, one needs to perform standard addition or use stable isotopes of the compounds to assess matrix effects.

Analysis was performed on an Agilent 1290 Infinity ultra-high pressure liquid chromatography system coupled to a 6530 accurate mass quadrupole time-of-flight mass spectrometer (UHPLC-(ESI)QTOF MS/MS) with electrospray ionization (ESI) via Jet Stream Technology (Agilent Technologies, Santa Clara, CA, USA). The UHPLC was equipped with a binary pump with integrated vacuum degasser (G4220A), an auto sampler (G4226A) with thermostat (G1330B), and

thermostatted column compartment (G1316C). The 80% methanolic extracts were separated on a Poroshell 120 C_{18} column (2.1 x 100, 2.7 μm, Agilent Technologies). The flow rate was 0.4 mL/min and the injection volume was 5 μL. The mobile phase consisted of a linear gradient of 0.1% formic acid in water (A) and 0.1% formic acid in acetonitrile (B) as follows: 5–10% B, 0–5 min; 10–12% B, 5–8 min; 12–15% B, 8–10 min; 15% B, 10–15 min; 15–55% B, 15–18 min; 55–90% B, 18–20 min. The column was re-equilibrated between injections for 4 min with initial mobile phase.

To identify all possible flavonoids, total ion spectra were collected over a mass range of m/z 100–1000 in negative mode at an acquisition rate of 1.0 spectra/s. The drying gas temperatures and flow rate were 225 °C and 8.0 L/min, respectively. The sheath gas temperature and flow rate were 300 °C and 10.0 L/min, respectively. The nebulizer gas pressure, skimmer voltage, octopole RF, and fragmentor voltage were 45 psi, 65V, 750 V, and 125 V, respectively. The capillary voltage was 2.5 kV. Continuous internal calibration was performed during analysis to achieve the desired mass accuracy of recorded ions with the ions of m/z of 119.0363 (proton abstracted purine) and 966.0007 (formate adduct of protonated hexakis (1H, 1H, 3H-tetrafluoropropoxy)phosphazine or HP-921).

Downloaded by UNIV OF ROCHESTER on July 29, 2013 | http://pubs.acs.org
Publication Date (Web): July 24, 2013 | doi: 10.1021/bk-2013-1138.ch002

Data Analysis

Using the open-access databases such as Phenol-Explorer (http://www.phenol-explorer.eu/) and Chemspider (http://www.chemspider.com/), 250 possible flavonoids and flavonoid conjugates were identified. The molecular formula of each flavonoid is imported into a Personal Compound Database and Library (PCDL) manager and used to create a flavonoid database (Agilent Technologies) containing the exact mass calculated from the molecular formula, other useful textual data, and the structure in mol file format (if available). This general flavonoid database can then be customized for a particular food. For example, herein flavonoid database was constricted to the flavonoids that could be plausibly be present in onions (e.g. isoflavones were excluded, etc.,). Using this approach, the list of flavonoids was reduced to 150 compounds. These 150 compounds were used to create a flavonoid database customized for analysis of onions. Using this customized flavonoid database and the "find-by-formula" option in the MassHunter Qualitative Analysis Software (Agilent Technologies), accurate mass tolerances were set and used to search each data file for ions of expected adducts (e.g., H^+, Na^+), dimers, trimers, etc. Potential flavonoids were identified based on a comparison of accurate mass, abundance of the isotopes, and isotope spacing with the calculated theoretical masses and abundances (performed automatically in MassHunter Qualitative Analysis). This is termed a "targeted" search for "non-target" compounds. That is we are looking specifically for all the compounds in the database without having standards. If standards are available, retention times can be also be added to the database and used as figure of merit for determining whether those specific compounds are present in the sample. The total ion chromatogram (TIC), shown of Merenge inner layers appears somewhat non-descript and not complex (Figure 2). However, there are many ions of compounds "hidden" under the TIC and whether these match a

flavonoid of interest can be discovered by specific search of the database using the "find-by-formula" algorithm. This algorithm extracts the ion (m/z) of each adduct specified determined from the exact monoisotopic mass of the formula within the tolerance specified (e.g. 10 ppm), and for as many charge states as specified (e.g. z=1, 2 and 3 but for the flavonoids only a charge state of z = 1 is used) and then integrates the resulting chromatogram. If a peak is found then all ions in that peak are evaluated against the theoretic isotopes expected for the molecular formula in the database. A score is calculated from those results and if that score exceeds a threshold set by the analyst, the compound is listed as found. If many peaks are found each is listed unless a retention time is specified. In that case then only the peak with the matching retention time is listed.

The other approach to the many ions found under the non descript TIC is a data mining (unknown) extraction of the compounds present using a "molecular feature extraction" algorithm. This algorithm takes all ions that represent chromatographic peaks (thus eliminating background ions) and groups them by adduct clusters, possible isotopes, dimers, trimmers etc. all taken together as molecular features without any determination of identity. Each feature is then calculated back to a "molecular mass" again without any identification assigned.

Both approaches provide a "list" of compounds, one tentatively identified from the database search, the other a list of "unknowns." After processing, these lists of compounds are converted into compound exchange format files (.cef files) for each sample and exported to data mining and statistical analysis software. In this case, Mass Profiler Professional (MPP) was used for data mining (Agilent Technologies). For data processing, other commercial software such as MarkerLynx software (Waters, Milford, MA, USA), Metabolic Profiler (Bruker Daltonic & Bruker BioSpin, Billerica, MA, USA), and Sieve (Thermo Fisher Scientific, Waltham, MA, USA) and freely available tool such as XCMS can be used (*27*). Statistical packages such as Minitab, R, and SAS can be used after data mining and data is exported as text or .csv format.

Downloaded by UNIV OF ROCHESTER on July 29, 2013 | http://pubs.acs.org
Publication Date (Web): July 24, 2013 | doi: 10.1021/bk-2013-1138.ch002

Results and Discussion

Database Mining Results

From the *find by formula* algorithm, the following 19 flavonoids were tentatively identified based upon "find-by-formula" criteria in seven onion varieties: delphinidin3-O-(6″-malonyl-glucoside), dihydromyricetin3-*O*-rhamnoside, dihydroquercetin, isorhamnetin, isorhamnetin 4′-*O*-glucoside, kaempferol, kaempferol 3-*O*-(6"-malonyl-glucoside), kaempferol 3,7-*O*-diglucoside, kaempferol 3-*O*-acetyl-glucoside, kaempferol 3-*O*-rutinoside, kaempferol 3-*O*-xylosyl-rutinoside, quercetin, quercetin 3,7,4′-triglucoside, quercetin -*O*-diglucoside, quercetin 3,4′-*O*-diglucoside, quercetin 3-*O*-glucoside, quercetin 3-*O*-rhamnoside, and quercetin 4′-*O*-glucoside. For unequivocal confirmation of identity, further MS/MS analysis and comparisons with MS/MS spectra and retention times of standards would be needed.

Downloaded by UNIV OF ROCHESTER on July 29, 2013 | http://pubs.acs.org
Publication Date (Web): July 24, 2013 | doi: 10.1021/bk-2013-1138.ch002

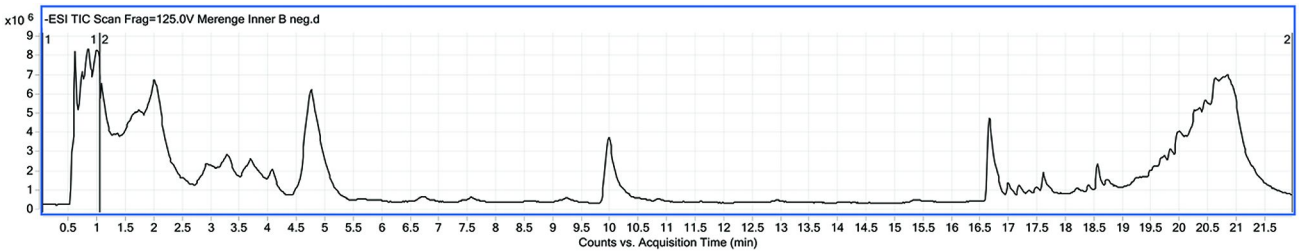

Figure 2. Total Ion Chromatogram of Merenge Onion Variety.

Downloaded by UNIV OF ROCHESTER on July 29, 2013 | http://pubs.acs.org
Publication Date (Web): July 24, 2013 | doi: 10.1021/bk-2013-1138.ch002

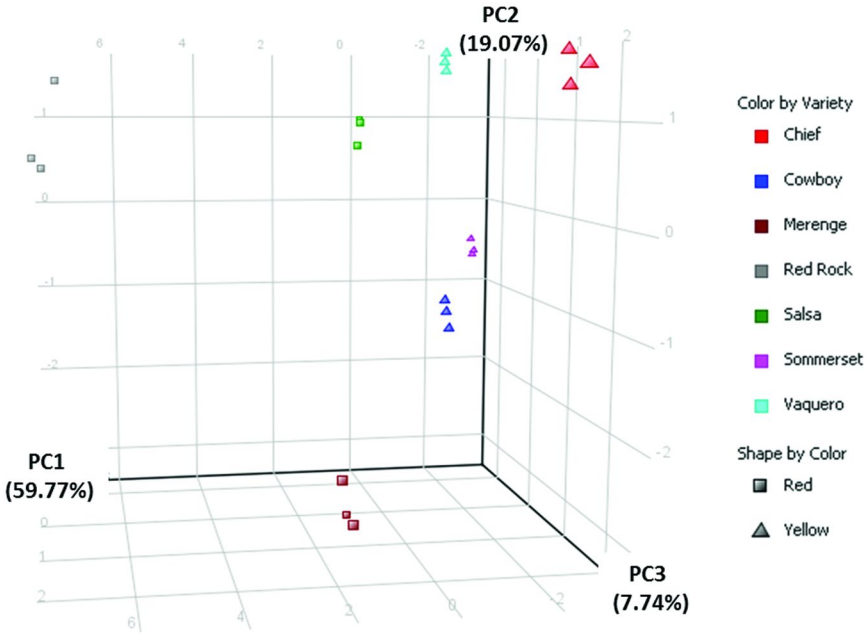

Figure 3. Principal Component Analysis on 19 Targeted Unknowns for Varietal Difference.

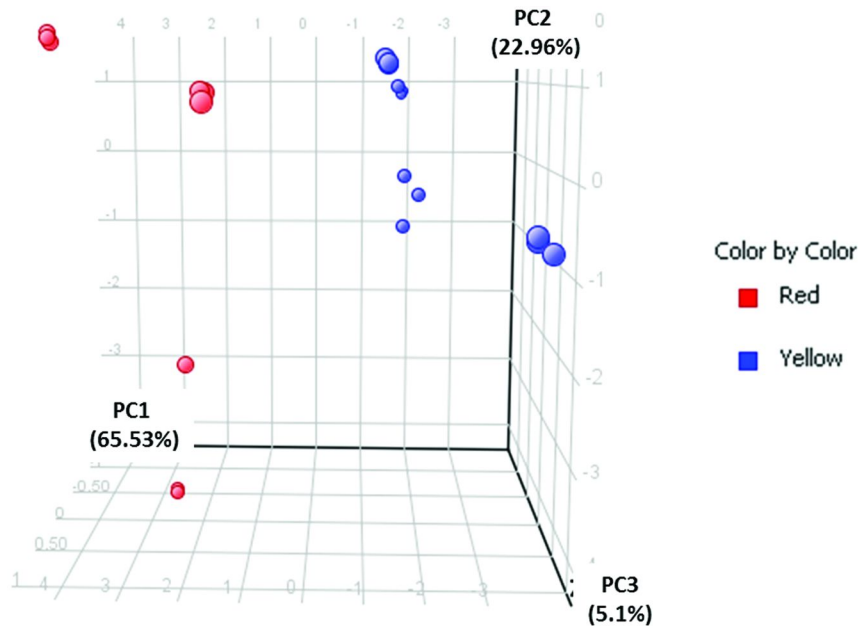

Figure 4. Principal Component Analysis on 19 Target Compounds for Color Difference.

Principal Component Analysis (PCA) on 19 Targeted Unknowns for Varietal and Color Difference

A PCA of the 7 varieties of onions based on the 19 compounds discovered in the database search show good separation of some of the varieties (Figure 3). Because analyses were on the "inner" layers of the onions, and extraction solvents excluded anthocyandins, the "distinction" of variety is not based upon obvious differences in pigment related compounds (e.g. anthocyanidin levels). One could argue that the Cowboy and Summerset varieties are not being separated, and that Chief, Vaquero and Salsa group together. The Redrock and Merenge verities have distinct separation from the other varieties (both are red varieties).

PCA analysis of the 7 varieties (herein 4 yellow and 3 red varieties were analyzed) indicate that there is no distinction between them based upon color although, there is some correlation along the x-axis (note the triplicate analysis of each variety are tightly grouped) (Figure 4).

Downloaded by UNIV OF ROCHESTER on July 29, 2013 | http://pubs.acs.org
Publication Date (Web): July 24, 2013 | doi: 10.1021/bk-2013-1138.ch002

Principal Component Analysis on Unidentified Compounds for Varietal and Color Difference

It is important to note that PCA of all the unknown compounds found by the unknown approach would be non-descript that is there is no assumption that compounds found may describe a variety. In the case of the flavonoid approach, these compounds were sought as descriptive. Prior to PCA, the data was normalized so that compounds in high concentration do not overly weigh PCA. Then, the list of unknowns must first be filtered to assure consistency within a variety, that is filtering by frequency within a group, and then filtered from variety to variety for distinction. The compounds that are statistically important in differentiating the samples, were filtered using ANOVA and/or fold change (how much that compound changed from one variety to the next), and then PCA was performed. Once compounds that were not common within a variety were eliminated and then those that were common from variety to variety the molecular feature extraction could be used to evaluate the general composition of the different varieties and whether color can be determined by these "unknown" compounds provides interesting and possibly distinguishing results (Figure 5). Again the ability of a model using this data to predict color or variety would be demonstrative in using the "unknown" compound data for differentiation. As Chief and Merenge are well separated in the PCA, the loadings and this list of compounds can be evaluated to find the compounds that can differentiate the two. The top 10 compounds tentatively identified responsible for colored differentiation are 6,8-dihydroxy kaempferol, kaempferol 3-*O*-(6"-malonyl-glucoside), kaempferol diglucoside-1, kaempferol diglucoside-2 (this is an isomer with a different retention time), kaempferol 3-*O*-acetyl-glucoside quercetin, quercetin 3,4′-*O*-diglucoside, quercetin diglucoside-1, quercetin diglucoside-2 (isomer with a different retention time), quercetin 3-*O*-rhamnoside and dihydroquercetin. However, there are a number of possible compounds for each formula generated from the data. Again, MS/MS can help determine which compound is actually present in the samples.

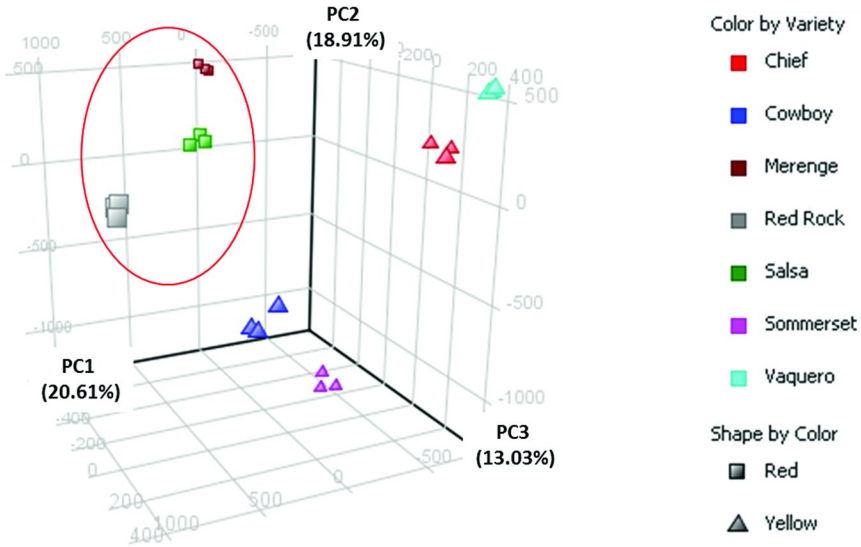

Figure 5. Principal Component Analysis on Unidentified Compounds for Varietal and Color Difference.

Conclusions

A flavonoid library for onions was developed using PCDL manager and included 150 entries. Nineteen flavonoid and flavonoid glycosides were identified in the methanolic extracts of 7 varieties of onions. Principal component analysis on these 19 target compounds demonstrates separation in varietal difference and color difference. Non-target analysis resulted in similar results. Tentative identification of the top 10 flavonoids is associated in the PCA space with color and variety differences. Although, more sampling of varieties grown under different conditions over time are needed to establish clear correlations, it appears that the non-targeted analysis of flavonoids by UHPLC-(ESI)QTOF MS/MS can be used to establish varietal differences.

Acknowledgments

The authors thank Gills Onions, LLC, Oxnard, CA for providing onions for this work. We also thank Dr. Susan Ebeler of the UC Davis and Steven Fischer of the Agilent Technologies for invaluable scientific input and help with advanced data processing.

Downloaded by UNIV OF ROCHESTER on July 29, 2013 | http://pubs.acs.org
Publication Date (Web): July 24, 2013 | doi: 10.1021/bk-2013-1138.ch002

References

1. Hertog, M. G.; Hollman, P. C. *Eur. J. Clin. Nutr.* **1996**, *50*, 63–71.
2. Lee, J.; Mitchell, A. E. *J. Agric. Food Chem.* **2011**, *59*, 857–863.
3. Dillard, C. J.; German, J. B. *J. Sci. Food Agric.* **2000**, *80*, 1744–1756.
4. Boyer, J.; Liu, R. *Nutr. J.* **2004**, *3*, 5–19.
5. Lee, J.; Mitchell, A. E. *J. Agric. Food Chem.* **2012**, *60*, 3874–3881.
6. Hollman, P.; de Vries, J.; van Leeuwen, S.; Mengelers, M.; Katan, M. *Am. J. Clin. Nutr.* **1995**, *62*, 1276–1282.
7. Nielsen, I. L. F.; Chee, W. S. S.; Poulsen, L.; Offord-Cavin, E.; Rasmussen, S. E.; Frederiksen, H.; Enslen, M.; Barron, D.; Horcajada, M.-N.; Williamson, G. *J. Nutr.* **2006**, *136*, 404–408.
8. Graefe, E. U.; Wittig, J.; Mueller, S.; Riethling, A. K.; Uehleke, B.; Drewelow, B.; Pforte, H.; Jacobasch, G.; Derendorf, H.; Veit, M. *J. Clin. Pharmacol.* **2001**, *41*, 492–499.
9. Formica, J. V.; Regelson, W. *Food Chem. Toxicol.* **1995**, *33*, 1061–1080.
10. Huang, N.; Siegel, M.; Kruppa, G.; Laukien, F. *J. Am. Soc. Mass Spectrom* **1999**, *10*, 1166–1173.
11. Alder, L.; Greulich, K.; Kempe, G.; Vieth, B. *Mass Spectrom. Rev.* **2006**, *25*, 838–865.
12. Halket, J. M.; Waterman, D.; Przyborowska, A. M.; Patel, R. K. P.; Fraser, P. D.; Bramley, P. M. *J. Exp. Bot.* **2005**, *56*, 219–243.
13. Krauss, M.; Singer, H.; Hollender, J. *Anal. Bioanal. Chem.* **2010**, *397*, 943–951.
14. Kováts, E. *Helv. Chim. Acta* **1958**, *41*, 1915–1932.
15. Lee, J.; Taylor, D. R. *Chromatographia* **1982**, *16*, 286–289.
16. van Den Dool, H.; Dec. Kratz, P. *J. Chromatogr., A* **1963**, *11*, 463–471.
17. Broecker, S.; Herre, S.; Wüst, B.; Zweigenbaum, J.; Pragst, F. *Anal. Bioanal. Chem.* **2011**, *400*, 101–117.
18. Hayashida, M.; Takino, M.; Terada, M.; Kurisaki, E.; Kudo, K.; Ohno, Y. *Leg. Med.* **2009**, *11*, S423–S425.
19. Datta, S.; Pihur, V. *Methods Mol. Biol.* **2010**, *593*, 205–229.
20. Arvanitoyannis, I. S.; Vaitsi, O.; Mavromatis, A. *Crit. Rev. Food Sci. Nutr.* **2008**, *48*, 799–823.
21. Arvanitoyannis, I. S.; Vaitsi, O. B. *Crit. Rev. Food Sci. Nutr.* **2007**, *47*, 675–699.
22. Chukwumah, Y.; Walker, L.; Vogler, B.; Verghese, M. *Food Chem.* **2012**, *132*, 525–531.
23. Moco, S.; Bino, R. J.; Vorst, O.; Verhoeven, H. A.; de Groot, J.; van Beek, T. A.; Vervoort, J.; de Vos, C. H. R. *Plant Physiol.* **2006**, *141*, 1205–1218.
24. Reid, L. M.; O'Donnell, C. P.; Downey, G. *Trends Food Sci. Technol.* **2006**, *17*, 344–353.
25. Vaclavik, L.; Lacina, O.; Hajslova, J.; Zweigenbaum, J. *Anal. Chim. Acta* **2011**, *685*, 45–51.
26. King, R.; Bonfiglio, R.; Fernandez-Metzler, C.; Miller-Stein, C.; Olah, T. *J. Am. Soc. Mass Spectrom.* **2000**, *11*, 942–950.
27. Katajamaa, M.; Oresic, M. *J. Chromatogr., A* **2007**, *1158*, 318–328.

Downloaded by UNIV OF ROCHESTER on July 29, 2013 | http://pubs.acs.org
Publication Date (Web): July 24, 2013 | doi: 10.1021/bk-2013-1138.ch002

Downloaded by UNIV OF DELAWARE MORRIS LIB on July 29, 2013 | http://pubs.acs.org
Publication Date (Web): July 24, 2013 | doi: 10.1021/bk-2013-1138.ch003

Chapter 3

HPLC/MS Fingerprinting Techniques for Quality Control of *Gynostemma pentaphyllum* (Thunb.) Makino Samples

Zhuohong Xie,[1] Haiming Shi,[*,2] and Liangli (Lucy) Yu[1,2]

[1]Department of Nutrition and Food Science, University of Maryland-College Park, 0112 Skinner Bldg., College Park, Maryland 20742, U.S.A.
[2]Institute of Food and Nutraceutical Science, Key Lab of Urban Agriculture (South), School of Agriculture & Biology, Shanghai Jiao Tong University, 800 Dongchuan Road, Shanghai 200240, China
[*]E-mail: hmshi@sjtu.edu.cn.

Gynostemma pentaphyllum (Thunb.) Makino is a perennial vine widely grown in Asia. It has been an ingredient for foods and beverages and marketed in many countries including the United States. This chapter reviews HPLC-UV/ELSD/MS fingerprinting methods in characterizing *G. pentaphyllum* botanical samples. The chapter also discusses the combination of fingerprinting and chemometrical analysis for quality assessment of *G. pentaphyllum*. The comparison of compiled data and discussion in this review may promote the use of *G. pentaphyllum* in nutraceutical and functional foods. Last, the current limitation and future directions on *G. pentaphyllum* fingerprinting analysis were addressed.

Introduction

Gynostemma pentaphyllum (Thunb.) Makino, known as jiaogulan, is a botanical material traditionally used in food, vegetables and tea. It is easily grown in poor soil and is widely spread over China, Korea, Japan, Thailand and Vietnam. Growing evidence has suggested that *G. pentaphyllum* products may have health benefits against cardiovascular diseases (*1*), diabetes (*2*), cancer (*3*),

© 2013 American Chemical Society
In Physical Methods in Food Analysis; Tunick, M., et al.;
ACS Symposium Series; American Chemical Society: Washington, DC, 2013.

hepatitis (*4*) and neural diseases (*5*, *6*) and may alleviate oxidative stress (*7*, *8*), inflammation (*4*, *9*) and fatigue (*10*). Bioactives in *G. pentaphyllum* may include polysaccharides, flavonoids, saponins (gypenosides), carotenoids, chlorophylls and sterols, while flavonoids and saponins were considered the major bioactives in most biological and nutritional studies (*11*, *12*).

The outstanding health benefits as a result of consumption of *G. pentaphyllum* have promoted commercialization of this botanical. *G. pentaphyllum* has been made into a variety of commercial products and marketed widely in many countries including the United States (*13*). Recent studies in our lab and from others (*9*, *14*, *15*), however, have indicated that chemical composition varied greatly in commercially available *G. pentaphyllum* products. Difference in chemical composition may lead to potential variance in health related effects, effective dosage, stability, shelf life, flavor, functional properties, as well as safety. Therefore, chemical profile of *G. pentaphyllum* samples should be identified and monitored for quality control. To assure the concentration of bioactive composition, a quantification of single or several chemical(s) is not sufficient since quality of a botanical relies on its overall chemical components. On the other hand, obviously it is not feasible to detect and identify every single component in a botanical. To solve this paradox, chemical fingerprinting method has been introduced as a strategy for quality assessment (*16*, *17*). This approach simultaneously compares the chemical profile for multiple components and provides accurate, precise and rapid results.

For quality control and product standardization purposes, this manuscript reviews the current progress on fingerprinting in *G. pentaphyllum* samples utilizing different techniques. Sample extraction methods, identification and quantitation of individual flavonoids and saponins and chemometrical analysis were also included for discussion. The comparison of compiled data and discussion in this review may promote the use of *G. pentaphyllum* in nutraceutical and functional foods.

Sample Extraction Methods

Flavonoids

Flavonoids belong to the larger group of phenolic compounds, which are widely present in plants. The basic structure of flavonoid consists of two aromatic rings, linked by a three-carbon bridge. In plant they are mostly in glycoside form, in which phenolic hydrogen(s) is/are substituted by sugar moiety (moieties). With difference in substitution location, sugar moiety, double bond position, individual flavonoids may have different polarities and solubilities. In literature (*11*, *18–20*), solvents including methanol, ethanol, methanol/water (1:1, v/v), methanol/chloroform (1:1, v/v) and acetone, with sonication or Soxhlet extraction were used to maximize extraction efficiency for flavonoids. Xie et al. has conducted an investigation for overall extraction efficiency for *G. pentaphyllum* flavonoid extraction (*21*). As shown in Table I, methanol (MeOH) had the best efficacy for total flavonoids and quercetin extraction at 37.5 mg of rutin equivalents (RE)/g and 0.6 mg/g, while MeOH/H_2O (1:1, v/v) was able

In Physical Methods in Food Analysis; Tunick, M., et al.;
ACS Symposium Series; American Chemical Society: Washington, DC, 2013.

Downloaded by UNIV OF DELAWARE MORRIS LIB on July 29, 2013 | http://pubs.acs.org
Publication Date (Web): July 24, 2013 | doi: 10.1021/bk-2013-1138.ch003

to extract the highest level of rutin (10.9 mg/g) in sonication. The data was consistent with Kao's study (*11*). On the other hand, although having similar efficiency, MeOH/H_2O mixture was less preferable because water in the extraction mixture was relatively difficult to be removed or replaced for further biological experiments. Soxhlet extraction was more efficient than sonication. In short, Soxhlet extraction with methanol was able to extract the highest total flavonoids and rutin and quercetin concentrations in *G. pentaphyllum*.

Saponins

Saponins are another class of glycosides present in plants, which are composed of sapogenin, hexoses and galacturonic acid. Saponins in *G. pentaphyllum* are also named gypenosides. The major type of saponins in *G. pentaphyllum* is triterpenoid. Saponins have similar polarity as flavonoids and therefore similar solvent systems have been implemented to extract saponins as to flavonoids. Both pure methanol and MeOH/H_2O have been used for extracting gypenosides from different *G. pentaphyllum* samples with high efficacy (*11*, *14*, *22*). The above solvent systems might extract both the flavonoids and gypenosides, along with other impurities. Flavonoid determination was well tolerant to the presence of gypenosides due to flavonoids' strong response in UV signal (*9*). On the other hand, to minimize the signal interference of flavonoids when detecting gypenosides in evaporative light scattering detector (ELSD) or mass spectroscopy (MS), a purification process including the use of macropore resin column and C18 cartridge might lower the difficulty for subsequent isolation and analysis (*11*, *22*).

Detection and Quantification of Individual Compounds

Flavonoids

Flavonoids are one large group of bioactives and important health contributors present in *G. pentaphyllum*. Flavor-3-ol is the major type of flavonoids detected in *G. pentaphyllum*. The most prominent flavonoids in *G. pentaphyllum* are rutin and quercetin. The rutin content possessed large variance among samples from different studies. As reported by Xie et al., one commercial *G. pentaphyllum* sample had no detectable rutin content (*9*). In a subsequent study, diploid leaf *G. pentaphyllum* sample was found to have rutin content of 23 mg/g botanical (*21*). The quercetin content also varied greatly in amount. In Kao and Tsai's studies, quercetin glycosides were found but no free quercetin was reported (*11*, *20*). On the other hand, the highest level of quercetin was detected in commercial *G. pentaphyllum* sample in Zhao and other's study (*23*). The difference in amount and type of flavonoid seems to be affected by sources, genotypes, environment factors, and storage condition, which as a result may alter health beneficial properties of *G. pentaphyllum*. Thus, the determination of individual flavonoids may serve as an important measure of botanical quality of *G. pentaphyllum*. Rutin and quercetin was identified and quantified by comparison of retention times,

Downloaded by UNIV OF DELAWARE MORRIS LIB on July 29, 2013 | http://pubs.acs.org
Publication Date (Web): July 24, 2013 | doi: 10.1021/bk-2013-1138.ch003

maximal wavelength absorbance and mass spectra with standard chemicals. Due to the lack of chemical standards, the identification of other flavonoids relied most on comparing the chromatographic and mass spectrometric behaviors with those reported in literature, while the quantification was through internal standards.

Saponins

Saponins have shown many promising bioactivities and may be the bioactives responsible for numerous health beneficial properties of *G. pentaphyllum*. Approximately 169 gypenosides have been reported to date (*24*). Detection and quantification of saponins in *G. pentaphyllum* was challenging because most chemical standards were not commercially available and many gypenosides shared the same formula which caused difficulty resolving them in mass spectrometry. Kao and his colleagues were able to quantify gypenosides through internal standards but didn't identify the majority of gypenosides (*11*). Another study identified over 100 gypenosides based on chemical standards and database, yet some of the shared-formula gypenosides were not resolved (*14*). In Lu and other's study, four gypenosides were identified and quantified based on the standards they possessed (*15*). The determination of individual gypenosides aids evaluation of quality of *G. pentaphyllum*.

Downloaded by UNIV OF DELAWARE MORRIS LIB on July 29, 2013 | http://pubs.acs.org
Publication Date (Web): July 24, 2013 | doi: 10.1021/bk-2013-1138.ch003

Chromatographic/Evaporative Light Scattering/Mass Spectrometric Fingerprinting Methodology

Fingerprinting technique was introduced and accepted by World Health Organization (WHO) (*25*) in 1991 and State of Food and Drug Administration of China (SFDA) (*26*) for quality control of botanicals. This technique has the advantage of systematic characterization of chemical profiles in samples or products. Recently numerous studies have shown applications for quality evaluation of different herbs and traditional Chinese medicines (*27–29*). To determine the flavonoid and gypenoside profiles in *G. pentaphyllum*, a series of fingerprinting methods utilizing UV detectors, evaporative light scattering detector (ELSD) and mass spectrometry (MS) detectors were developed and validated (*14*, *15*, *21–23*). For flavonoid fingerprinting, because of the high reproducibility, strong response, high signal to noise ratio and high selectivity, UV detectors are suitable for detection and generation of flavonoid chemical profiles. On the other side, saponins are absence of chromophore and therefore the response and quality of signals in UV detectors were inferior to those in ELSD or MS detectors. In practical use, gypenoside fingerprintings were determined either by a UV wavelength at the lower end (203 nm), by ELSD detector or MS detector (*14*, *15*, *22*).

Because of the excellent response and selectivity, a flavonoid fingerprinting produced by Xie and his colleagues (*21*) served as an example here to elucidate the procedure involved in *G. pentaphyllum* fingerprinting development and validation. The flavonoid fingerprinting study aimed to develop and apply this quality

control approach to *G. pentaphyllum* samples of two different genotypes (diploid vs tetraploid) and two different plant parts (leaf vs whole-plant). The sixteen samples include four diploid leaf samples (2L1-2L4), four diploid whole-plant (stems and leaves) samples (2W1-2W4), four tetraploid leaf samples (4L1-4L4), and four tetraploid whole-plant (stems and leaves) samples (4W1-4W4). In order to maximize peak separation within reasonable retention time, a gradient program using two mobile phases was developed. HPLC procedure using UV detector was validated for precision, repeatability and stability. The precision was conducted by analysis of five consecutive injections of the same sample solution. The repeatability was evaluated by determination of five different sample solutions prepared from the same botanical sample. The stability was examined by analysis of injections at different time points (0, 2, 4, 8, 16 and 24 h). The similarities of all injections were over 0.900 ($R > 0.900$), suggesting that the HPLC procedure was valid and effective. In this method, an authentic *G. pentaphyllum* sample was purchased from National Institute for the Control of Pharmaceutical and Biological Products. The fingerprint of this botanical sample was selected as a reference fingerprint. The peaks in all fingerprints were numbered and the most obvious peak was characterized as reference peak (peak 5, rutin) (Figure 1). Areas of peak 5 in all samples were normalized to the same level and those of other peaks were normalized proportional to the area of peak 5. In Figure 1, 2L2, 2W3, 4L3, 4W2 were representative chromatograms of diploid leaf, diploid whole-plant, tetraploid leaf and tetraploid whole-plant samples respectively, while REF indicated that of reference botanical mentioned above. As seen in Figure 1 and Table II, there were a total of 24 peaks detected in all samples including the reference botanical. Seven common peaks (peaks 5, 6, 8, 10, 11, 14 and 17) were detected in all samples. The chromatograms were artificially grouped into 4 regions, according to differences among samples. In region I, peaks 1-4 were exclusively found in tetraploid leaf and whole-plant samples. None of these four peaks were detected in the reference botanical or diploid samples. Most common peaks (peaks 5, 6, 8, 10, and 11) existed in region II. No difference was observed between leaf and whole-plant samples of the same genotype in region I and II. Peak 7 was only detected in the sixteen samples but not in the reference botanical. Peak 9 was only found in tetraploid samples but not in diploid samples. In region III, there were two other common peaks (peaks 14 and 17) in all samples, although large variance existed regarding the peak areas. There were more peaks in the reference botanical than in other samples. Peaks 15 and 16 were exclusively found in the reference botanical. Peak 18 was only detected in diploid samples and the reference botanical. On the other side, peaks 13 and 19 were only found in diploid leaf samples and the reference botanical. Peak 12 was observed in leaf samples and the reference botanical. In region IV, peak 24 was detected in diploid samples and the reference botanical, and peak 22 was only detected in diploid leaf sample and the reference botanical. Peaks 20, 21, and 23 were specific for reference botanical. By direct comparison of fingerprints, chromatogram of diploid leaf sample was most similar to that of reference botanical (Figure 1). It is also noteworthy that quantity of individual flavonoids may vary greatly in *G. pentaphyllum* samples. In summary, the flavonoid fingerprinting approach provides useful information to distinguish *G. pentaphyllum* samples.

Downloaded by UNIV OF DELAWARE MORRIS LIB on July 29, 2013 | http://pubs.acs.org
Publication Date (Web): July 24, 2013 | doi: 10.1021/bk-2013-1138.ch003

Downloaded by UNIV OF DELAWARE MORRIS LIB on July 29, 2013 | http://pubs.acs.org
Publication Date (Web): July 24, 2013 | doi: 10.1021/bk-2013-1138.ch003

Table I. Effects of extraction solvent and method on flavonoid content of *G. pentaphyllum**

	Solvent	*TFC (mg RE/g)*	*Rutin content (mg/g)*	*Quercetin content (mg/g)*
Sonication	MeOH	37.54 ± 1.86d	9.79 ± 0.05d	0.60 ± 0.00c
	EtOH	20.44 ± 1.64b	4.19 ± 0.57c	0.30 ± 0.04b
	MeOH:H_2O (1:1, v/v)	30.46 ± 1.00c	10.94 ± 0.85d	0.50 ± 0.06c
	MeOH:$CHCl_3$ (1:1, v/v)	28.11 ± 2.39c	2.66 ± 0.15b	0.52 ± 0.01c
	Acetone	12.25 ± 0.51a	1.04 ± 0.04a	0.14 ± 0.00a
Soxhlet	MeOH	45.63 ± 2.82e	11.06 ± 0.02d	1.02 ± 0.01d

* Sample 4L3 was used in all tests. Different letters represent significant differences ($P < 0.05$). TFC stands for total flavonoid content by spectrometric methods. RE stands for rutin equivalents. Rutin and quercetin content were flavonoid profile obtained by HPLC. Reproduced with permission from reference (*21*). Copyright 2011, American Chemical Society.

Downloaded by UNIV OF DELAWARE MORRIS LIB on July 29, 2013 | http://pubs.acs.org
Publication Date (Web): July 24, 2013 | doi: 10.1021/bk-2013-1138.ch003

Table II. MS fragmentation of the investigated compounds by HPLC-MS*

Peak No.	*RT*	*UV (nm)*	*[M-1]-/ [M+1]+*	*NI/PI*	*Compound*
1	9.63	256,352	755.26/756.75		quercetin-di-(rhamno)-hexoside
2	10.48	264,346	739.23/740.66		kaempferol 3-O-di-p-coumaroylhexoside
3	10.69	266,346	739.30/740.73		kaempferol 3-O-di-p-coumaroylhexoside
4	10.99	264,346	609.21/610.77		quercetin-rhamno-hexoside
5	11.21	256,354	609.19/610.91	1218.87 [2M-1]/633.19 [M+Na]+,464.95 [M+H-Rham], 303.27[M+H-Rham-Glu]	rutin
6	11.71	256,348	609.23/610.79		unknown
7	12.09	264,346	609.25/609.85		unknown
8	12.66	266,348	593.18/-	285.00 [M-H-Rham-Glu]-/617.17[M+Na]+, 503, 287.32 [M+H-Rham-Glu]+	kaempferol-rhamno-hexoside
9	12.86	256,348	593.21/-	284.71[M-H-Rham-Glu]-/617.18[M+Na]+, 503.01, 287.26 [M+H-Rham-Glu]+	kaempferol-3-*O*-rutinoside
10	13.05	254,356	623.19/-	315.20 [M-H-Rham-Glu]-/647.21[M+Na]+, 533.02, 317.25 [M+H-Rham-Glu]+	unknown
11	13.17	254,352	623.19/-	315.20 [M-H-Rham-Glu]-/647.24[M+Na]+, 533.02, 317.25 [M+H-Rham-Glu]+	unknown
12	15.52	266,346	607.21/-	299.09 [M-H-Rham-Glu]-/631.24[M+Na]+, 517.08, 301.30 [M-H-Rham-Glu]+	unknown
13	16.84	268,308	697.25/699.14	675, 643, 299.17/659.16, 627.16, 603.10	unknown

Continued on next page.

Downloaded by UNIV OF DELAWARE MORRIS LIB on July 29, 2013 | http://pubs.acs.org
Publication Date (Web): July 24, 2013 | doi: 10.1021/bk-2013-1138.ch003

Table II. (Continued). MS fragmentation of the investigated compounds by HPLC-MS*

Peak No.	*RT*	*UV (nm)*	*[M-1]-/ [M+1]+*	*NI/PI*	*Compound*
14	17.39	256,360	301.07/-		quercetin
15	19.04	352	329.06/331.28	301.15/661.19 [2M+Na]+	unknown
16	19.74	266,348	329.10/331.25	313.12/315.30	unknown
17	20.33	266,368	285.23/287.27		kaempferol
18	21.04	370	315.16/317.22		unknown
19	21.16	298,368	315.27/317.22		unknown
20	24.24	270,364	299.15/-	/603.08	unknown
21	24.34	270,362	299.12/-	/603.06	unknown
22	26.8	266,366	299.16/-		unknown
23	26.98	272,362	299.16/301.28		unknown
24	27.27	256,370	299.23/-		unknown
25	30.93	266,362	/315.30		unknown

* RT, NI and PI stand for retention time, negative ion mode and positive ion mode respectively. Reproduced with permission from reference (*21*). Copyright 2011, American Chemical Society.

Downloaded by UNIV OF DELAWARE MORRIS LIB on July 29, 2013 | http://pubs.acs.org
Publication Date (Web): July 24, 2013 | doi: 10.1021/bk-2013-1138.ch003

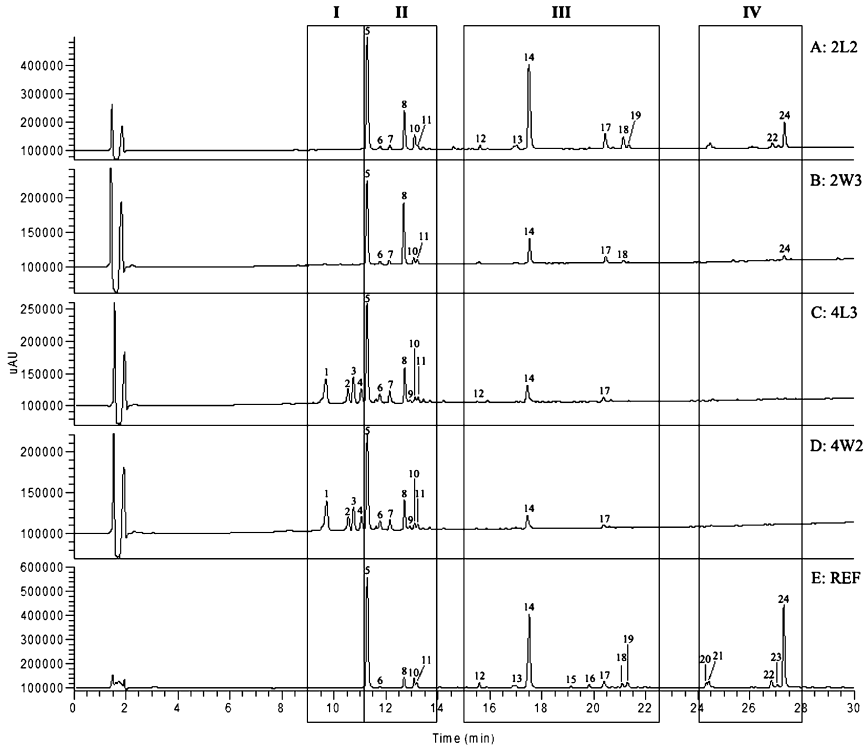

Figure 1. HPLC fingerprint of the representative G. pentaphyllum samples. A) diploid leaf botanical (2L2); B) diploid whole-plant botanical (2W3); C) tetraploid leaf botanical (4L3); D) tetraploid whole-plant botanical (4W2); E) reference botanical. Data was obtained at 256 nm. Reproduced with permission from reference (21). Copyright 2011, American Chemical Society.

Chemometrical Analysis

The HPLC/MS fingerprinting of *G. pentaphyllum* was able to supply a direct impression about the differences among samples. In addition, for quality control purpose, quantitative analyses would be favored to achieve better accuracy and enhanced ability for contaminant detection. Chemometrical analyses including similarity analysis, principal component analysis, and hierarchical clustering analysis were employed for quantitative discrimination of *G. pentaphyllum* samples.

Similarity Analysis

Similarity analysis is an innovative approach to evaluate the differences among samples. In Xie's study (*21*), the chromatograms, after alignment, were compared in Similarity Evaluation System (SES). The coefficient efficiency

In Physical Methods in Food Analysis; Tunick, M., et al.;
ACS Symposium Series; American Chemical Society: Washington, DC, 2013.

(range between 0 and 1) between each sample was determined. A higher value of coefficient efficiency indicates higher similarity between the two samples. As shown in Table III, the similarities between samples within the same group were all above 0.97 except for diploid whole-plant samples. These data implied that samples with certain genotype and plant part were overall consistent and stable. Samples 2W3 and 2W4 fingerprint profiles seemed to deviate from the other two diploid whole-plant samples, with their similarity values with 2W1 and 2W2 lower than 0.93. It should also be noted that similarity value between 2W3 and 2W4 was 0.61, suggesting they share less similarity in flavonoid profiles. The similarity values for dipoid leaf samples 2L1-2L4 to the reference botanical were 0.914286-0.936237, and that for 2W4 was 0.933337, indicating that 2L1-2L4 and 2W4 were similar to the reference botanical in flavonoid profiles. On the other hand, when compared to the reference botanical, the similarity values were below 0.81, 0.49, and 0.47 for samples 2W1-2W3, 4L1-4L4, and 4W1-4W4 (Table III). The similarity analysis of *G. pentaphyllum* samples suggested that diploid leaf samples had a flavonoid profile most similar to the reference botanical.

Downloaded by UNIV OF DELAWARE MORRIS LIB on July 29, 2013 | http://pubs.acs.org
Publication Date (Web): July 24, 2013 | doi: 10.1021/bk-2013-1138.ch003

Principal Component Analysis

Principal component analysis (PCA) is a mathematical procedure to transform a number of possibly correlated variables into a reduced number of orthogonal (unrelated) variables, which are named principal components. It can reduce the dimensions of multivariate problems without losing much information. This procedure has been modified and applied to chemical fingerprinting, in order to reveal the relationship among fingerprints of samples and improve chemometrical analysis (*30*). In PCA of fingerprint, either peak areas or data points (UV/MS) are treated as individual variables and transformed into principal components (PC). The scores plot shows the relationship among samples in a rotated coordinate system. This technique has been used for analysis of flavonoid and gypenoside profiles in several different studies (*15*, *21*, *23*). As an example, in Xie's study (*21*), PCA for peak areas in flavonoid fingerprint (UV) for *G. pentaphyllum* samples was carried out. As shown in Figure 2, PCA scores plot indicated that diploid leaf samples (2L1-2L4), tetraploid leaf samples (4L1-4L4), tetraploid whole-plant samples (4W1-4W4) were well separated between groups while clustered within groups. Diploid whole-plant samples were dispersed in the scores plot. Samples 2W3 and 2W4 were separated from the other two diploid whole-plant samples, which were close to tetraploid whole-plant samples (4W1-4W4) and diploid leaf samples (2L1-2L4) respectively. It seemed that flavonoid profile in diploid whole-plant samples had higher variance among samples. These data showed that samples with certain genotype and plant part were overall consistent and stable except diploid whole-plant samples, which confirmed the results of similarity analysis (Table III). Additionally, diploid leaf samples were closer to the reference botanical in the scores plot, suggesting diploid leaf samples had most similar flavonoid profiles to reference botanical, which agreed with the observation in Figure 1.

Downloaded by UNIV OF DELAWARE MORRIS LIB on July 29, 2013 | http://pubs.acs.org
Publication Date (Web): July 24, 2013 | doi: 10.1021/bk-2013-1138.ch003

Table III. The similarities of the tested *G. pentaphyllum* samples

	2L1	*2L2*	*2L3*	*2L4*	*2W1*	*2W2*	*2W3*	*2W4*	*4L1*	*4L2*	*4L3*	*4L4*	*4W1*	*4W2*	*4W3*	*4W4*	*REF*
2L1	1	0.986124	0.98182	0.982549	0.803492	0.859403	0.656079	0.975242	0.571191	0.496461	0.566273	0.524028	0.48173	0.48772	0.450392	0.481475	0.936237
2L2		1	0.995359	0.995399	0.803781	0.856781	0.654775	0.980101	0.572706	0.492469	0.564566	0.525849	0.472899	0.480477	0.439611	0.470504	0.917554
2L3			1	0.998905	0.812297	0.862195	0.666642	0.981505	0.582484	0.503795	0.573861	0.533374	0.483229	0.490449	0.446903	0.482871	0.920604
2L4				1	0.808627	0.861312	0.663882	0.981636	0.581443	0.500737	0.573	0.533058	0.478852	0.487625	0.443626	0.476198	0.914286
2W1					1	0.982408	0.92577	0.794934	0.821243	0.826733	0.83434	0.793456	0.842474	0.829448	0.829372	0.843837	0.77219
2W2						1	0.915217	0.845239	0.790085	0.780627	0.803021	0.760531	0.788197	0.781007	0.773527	0.779442	0.807741
2W3							1	0.605709	0.892979	0.908558	0.906545	0.880039	0.894734	0.902932	0.880018	0.869591	0.595607
2W4								1	0.50946	0.441372	0.506893	0.457972	0.444409	0.436495	0.412978	0.454206	0.933337
4L1									1	0.97918	0.996025	0.991765	0.936001	0.963231	0.908074	0.908773	0.482403
4L2										1	0.985369	0.97936	0.980258	0.992039	0.964797	0.954639	0.445441
4L3											1	0.993014	0.952263	0.977174	0.929789	0.921749	0.483847
4L4												1	0.937975	0.972046	0.916668	0.898878	0.437149
4W1													1	0.989129	0.99392	0.984846	0.455602
4W2														1	0.979569	0.96028	0.439766
4W3															1	0.976477	0.433885
4W4																1	0.467272
REF																	1

Reproduced with permission from reference (*21*). Copyright 2011, American Chemical Society.

Downloaded by UNIV OF DELAWARE MORRIS LIB on July 29, 2013 | http://pubs.acs.org
Publication Date (Web): July 24, 2013 | doi: 10.1021/bk-2013-1138.ch003

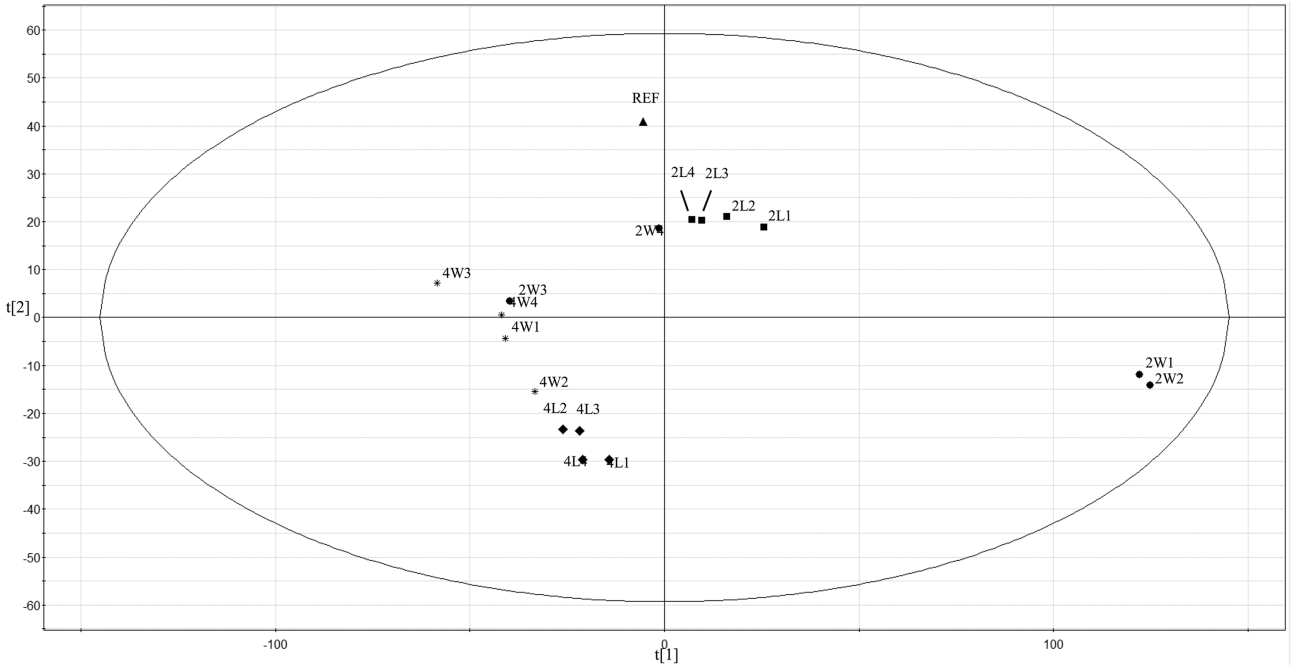

Figure 2. Scores plot of PCA based on UV data. 2L1-2L4 represent diploid leaf botanical; 2W1-2W4 represent diploid whole-plant botanical; 4L1-4L4 represent tetraploid leaf botanical; 4W1-4W4 represent tetraploid whole-plant botanical; REF represents the reference botanical sample. Reproduced with permission from reference (21). Copyright 2011, American Chemical Society.

Downloaded by UNIV OF DELAWARE MORRIS LIB on July 29, 2013 | http://pubs.acs.org
Publication Date (Web): July 24, 2013 | doi: 10.1021/bk-2013-1138.ch003

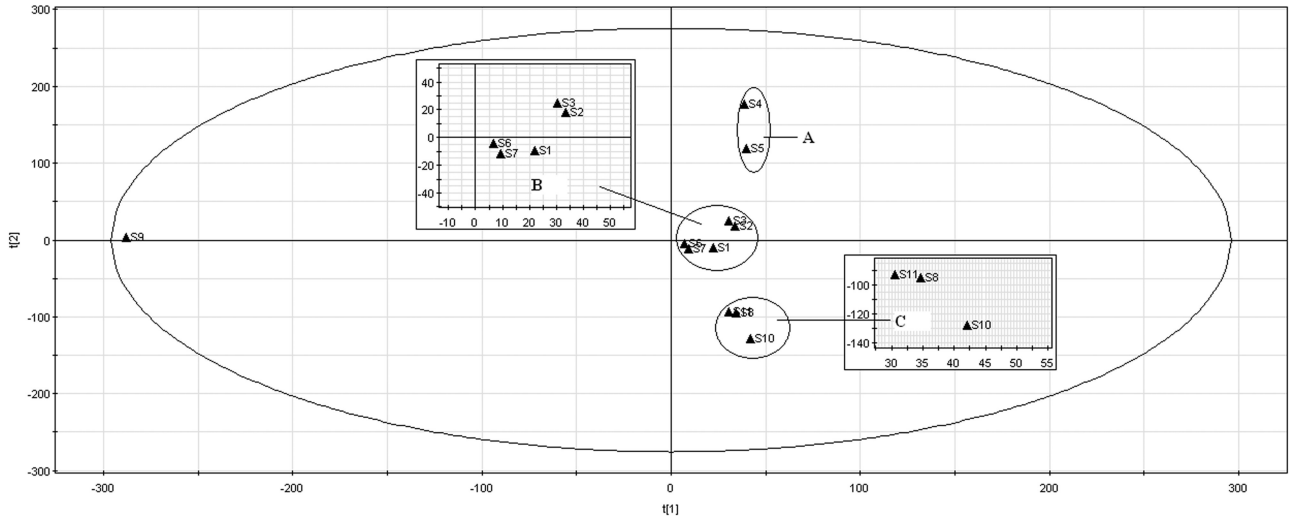

Figure 3. Scores plot of PCA based on MS data. S2-S11 represent commercial G. pentaphyllum samples; S1 represents the reference botanical sample. Reproduced with permission from reference (23). Copyright 2012, Elsevier Ltd.

Downloaded by UNIV OF DELAWARE MORRIS LIB on July 29, 2013 | http://pubs.acs.org
Publication Date (Web): July 24, 2013 | doi: 10.1021/bk-2013-1138.ch003

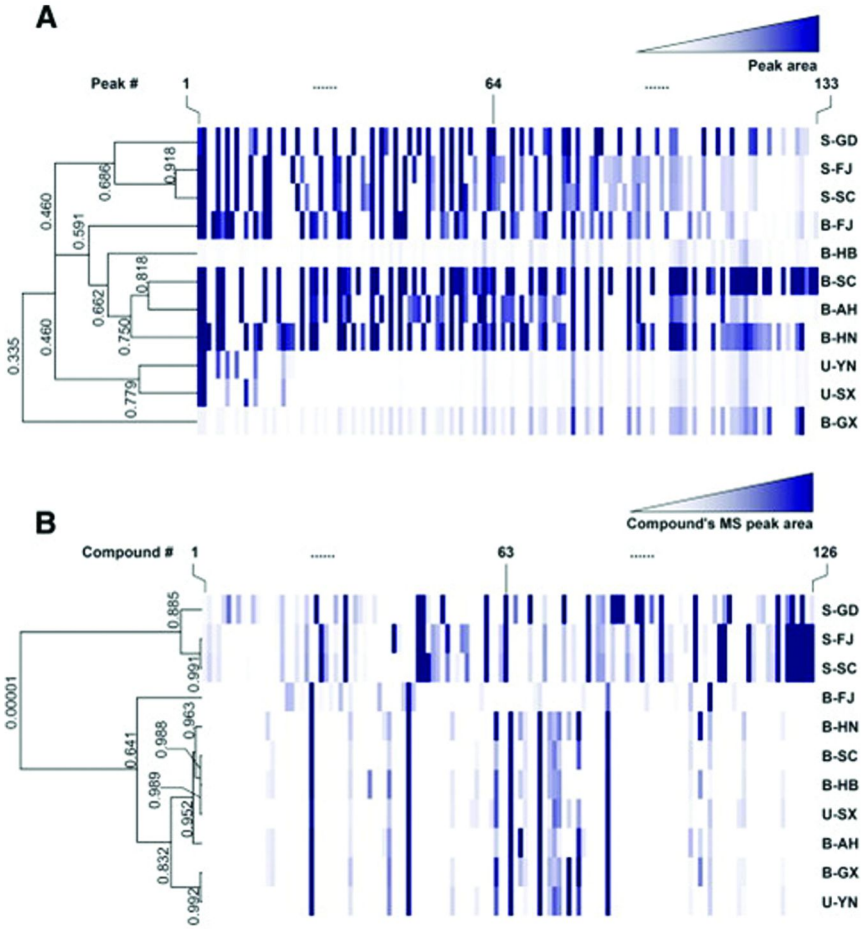

Figure 4. Dendrograms and heat maps of G. pentaphyllum saponins from hierarchical clustering analysis based on A) HPLC-DAD data and B) MS data. Each block in heat map represents one peak. The color intensity of each block indicates the corresponding peak area. Sample codes starting with S indicate sweet taste variant, with B indicate bitter taste variant and with U indicate unspecified samples. Reproduced with permission from reference (14). Copyright 2011, Elsevier Ltd.

MS spectra can also be utilized to perform PCA. In order to compare the differences between PCA of chromatogram and MS spectra, data collected from *G. pentaphyllum* commercial samples were presented here for discussion (*23*). Figure 3 showed PCA scores plot for eleven *G. pentaphyllum* commercial samples using MS spectra data. The samples could be classified into three groups (Group A, B and C) except S9 based on the distances among samples (Figure 2). Group A contained sample S4 and S5; Group B contained S1, S2, S3, S6 and S7; and Group C contained S8, S10, and S11. S9 was far away from the rest of samples

in the scores plot. These data implied that commercial *G. pentaphyllum* differed in chemical profile among samples in different groups, and samples within the same group had similar chemical profiles. The advantage for using MS spectra is to determine more comprehensive chemical profiles. In this case chemical components such as gypenosides that lack UV absorbance are able to be detected. For instance, S11 had a weak signal in UV detection yet a strong response in MS. It turned out to have high concentration in gypenosides similar to S8 and S10, which would have been missed by UV detection. PCA of MS spectra thus offered more rational results regarding varieties of chemicals than PCA of UV data. One possible disadvantage, however, would be the matrix effects generated from solvents and sample extracts, which might interfere with the results. Therefore a more delicate handling and consideration is needed for carrying out PCA based on MS data.

Downloaded by UNIV OF DELAWARE MORRIS LIB on July 29, 2013 | http://pubs.acs.org
Publication Date (Web): July 24, 2013 | doi: 10.1021/bk-2013-1138.ch003

Hierarchical Clustering Analysis

Hierarchical clustering analysis is also a supplemental analysis to identify difference in fingerprinting among samples. The similarities between samples are indicated by similarity score, with a higher score (close to 1) indicating higher similarity. The results are presented as a dendrogram to reveal the similarity and difference among samples. Merged cluster indicates the high resemblance while the split clusters indicate low similarity. The heat map, on the other hand, indicates the peak areas of compounds by color intensity. The advantage of hierarchical clustering analysis is it not only can yield a sharp distinction and a clear relationship between groups, but also provide the fine detail in the variants. In Wu's study (*14*), HPLC-DAD and HPLC-MS data from two taste variants of *G. pentaphyllum* were imported for hierarchical clustering analysis. The results clearly distinguished the two taste variants into two separate groups from MS data but not HPLC-DAD data (Figure 4). The within group similarity scores were much higher than those between groups from MS data, while HPLC-DAD data didn't provide a clear separation of the variants in *G. pentaphyllum* samples, suggesting that MS data are more accurate for hierarchical clustering. The reason may be explained by that MS data were from identified gypenoside peak areas whereas HPLC-DAD data were peaks without identification or prescreening.

In conclusion, this manuscript reviewed current fingerprinting approaches for quality control of *G. pentaphyllum* samples. The fingerprinting technique, identification and quantification of individual bioactives, and the chemometrical analyses provide powerful tools for evaluation of quality and prevention of adulteration for *G. pentaphyllum*. The current limitation lies in the lack of standardized procedure. Different procedure and analysis may yield different forms and values of results. The standardization of procedure may promote industrial adoption in nutraceutical field. A standardized procedure also may facilitate the building of a sample library and therefore be applied to a larger extent. In addition, as chemical composition determines the biological activities of botanicals, the variance in chemical profile in *G. pentaphyllum* may imply different physiological effects in these samples. Thus another aspect may be the investigation about connection between the chemical determination and the

efficacy and availability of *G. pentaphyllum*. The accomplishment of this research may require multidisciplinary collaboration with scientists from nutrition and food science fields. Our recent study investigated biological activities in different genotypes and different plant parts of *G. pentaphyllum*, which may serve as the first step to acquire knowledge on the connection between the chemical profile and the nutraceutical properties (*31*). The review could be used to improve the analytical methodology for *G. pentaphyllum* and its applications in food and nutraceutical field.

Downloaded by UNIV OF DELAWARE MORRIS LIB on July 29, 2013 | http://pubs.acs.org
Publication Date (Web): July 24, 2013 | doi: 10.1021/bk-2013-1138.ch003

References

1. Tanner, M. A.; Bu, X.; Steimle, J. A.; Myers, P. R. *Nitric Oxide* **1999**, *3* (5), 359–365.
2. Yeo, J.; Kang, Y. J.; Jeon, S. M.; Jung, U. J.; Lee, M. K.; Song, H.; Choi, M. S. *J. Med. Food* **2008**, *11* (4), 709–16.
3. Lu, K. W.; Tsai, M. L.; Chen, J. C.; Hsu, S. C.; Hsia, T. C.; Lin, M. W.; Huang, A. C.; Chang, Y. H.; Ip, S. W.; Lu, H. F.; Chung, J. G. *Anticancer Res.* **2008**, *28* (2A), 1093–9.
4. Lin, J. M.; Lin, C. C.; Chiu, H. F.; Yang, J. J.; Lee, S. G. *Am. J. Chin. Med.* **1993**, *21* (1), 59–69.
5. Choi, H. S.; Park, M. S.; Kim, S. H.; Hwang, B. Y.; Lee, C. K.; Lee, M. K. *Molecules* **2010**, *15* (4), 2814–24.
6. Joh, E. H.; Yang, J. W.; Kim, D. H. *Planta Med.* **2010**, *76* (8), 793–5.
7. Li, L.; Lau, B. H. S. *Phytother. Res.* **1993**, *7* (4), 299–304.
8. Lin, C. C.; Huang, P. C.; Lin, J. M. *Am. J. Chin. Med.* **2000**, *28* (1), 87–96.
9. Xie, Z.; Liu, W.; Huang, H.; Slavin, M.; Zhao, Y.; Whent, M.; Blackford, J.; Lutterodt, H.; Zhou, H.; Chen, P.; Wang, T. T. Y.; Wang, S.; Yu, L. *J. Agric. Food Chem.* **2010**, *58* (21), 11243–11249.
10. Ding, Y.; Tang, K.; Li, F.; Hu, Q. *Afr. J. Agric. Res.* **2010**, *5* (8), 707–711.
11. Kao, T. H.; Huang, S. C.; Inbaraj, B. S.; Chen, B. H. *Anal. Chim. Acta* **2008**, *626* (2), 200–211.
12. Razmovski-Naumovski, V.; Huang, T.; Tran, V.; Li, G.; Duke, C.; Roufogalis, B. *Phytochem. Rev.* **2005**, *4* (2), 197–219.
13. Blumert, M.; Liu, J. *Jiaogulan China's "immortality" herb*; Torchlight Publishing Inc.: Badger, CA, 1999.
14. Wu, P. K.; Tai, W.; Choi, R. C.; Tsim, K. W.; Zhou, H.; Liu, X.; Jiang, Z.-H.; Hsiao, W. *Food Chem.* **2011**, *128* (1), 70–80.
15. Lu, J.-G.; Zhu, L.; Lo, K. Y.; Leung, A. K.; Ho, A. H.; Zhang, H.-Y.; Zhao, Z.-Z.; Fong, D. W.; Jiang, Z.-H. *J. Agric. Food Chem.* **2013**, *61* (1), 90–97.
16. Biasioli, F.; Gasperi, F.; Aprea, E.; Colato, L.; Boscaini, E.; Märk, T. *Int. J. Mass* **2003**, *223*, 343–353.
17. Chou, G.; Xu, S. J.; Liu, D.; Koh, G. Y.; Zhang, J.; Liu, Z. *J. Agric. Food Chem.* **2009**, *57* (3), 1076–1083.
18. Lin, L. Z.; Harnly, J. M. *Food Chem.* **2010**, *120* (1), 319–326.
19. Lin, L. Z.; He, X. G.; Lindenmaier, M.; Nolan, G.; Yang, J.; Cleary, M.; Qiu, S. X.; Cordell, G. A. *J. Chromatogr., A* **2000**, *876* (1), 87–95.

20. Tsai, Y.; Lin, C.; Chen, B. *Phytomedicine* **2010**, *18* (1), 2–10.
21. Xie, Z.; Zhao, Y.; Chen, P.; Jing, P.; Yue, J.; Yu, L. *J. Agric. Food Chem.* **2011**, *59* (7), 3042–3049.
22. Liu, F.; Ren, D.; Guo, D.-a.; Pan, Y.; Zhang, H.; Hu, P. *Chem. Pharm. Bull.* **2008**, *56* (3), 389–393.
23. Zhao, Y.; Xie, Z.; Niu, Y.; Shi, H.; Chen, P.; Yu, L. L. *Food Chem.* **2012**, *134* (1), 180–188.
24. Kim, J. H.; Han, Y. N. *Phytochemistry* **2011**, *72* (11–12), 1453–1459.
25. World Health Organization. *Guideline for the Assessment of Herbal Medicines*; WHO: Geneva, Switzerland, 1991.
26. State Drug Administration of China *Chin. Tradit. Pat. Med.* **2000**, *22*, 671–675.
27. Kong, W. J.; Zhao, Y. L.; Xiao, X. H.; Jin, C.; Li, Z. L. *Phytomedicine* **2009**, *16* (10), 950–959.
28. Xie, P. S.; Yan, Y. Z.; Guo, B. L.; Lam, C.; Chui, S.; Yu, Q. X. *J. Pharmaceut. Biomed. Anal.* **2010**, *52* (4), 452–460.
29. Ye, J.; Zhang, X.; Dai, W.; Yan, S.; Huang, H.; Liang, X.; Li, Y.; Zhang, W. *J. Pharmaceut. Biomed. Anal.* **2009**, *49* (3), 638.
30. Chen, P.; Ozcan, M.; Harnly, J. *Anal. Bioanal. Chem.* **2007**, *389* (1), 251–261.
31. Xie, Z.; Huang, H.; Zhao, Y.; Shi, H.; Wang, S.; Wang, T. T. Y.; Chen, P.; Yu, L. *Food Chem.* **2012**, *132* (1), 125–133.

Downloaded by UNIV OF DELAWARE MORRIS LIB on July 29, 2013 | http://pubs.acs.org
Publication Date (Web): July 24, 2013 | doi: 10.1021/bk-2013-1138.ch003

Downloaded by MICHIGAN STATE UNIV on July 29, 2013 | http://pubs.acs.org
Publication Date (Web): July 24, 2013 | doi: 10.1021/bk-2013-1138.ch004

Chapter 4

Lanthanide-Sensitized Luminescence Instrumentation and Methods for Analysis of Tetracycline and Fluoroquinolone Residues in Foods

Guoying Chen,*[,1] Qiongqiong Li,[2] Guyu Liu,[3] Feng Qin,[3] and Yue Du[3]

[1]U.S. Department of Agriculture, Agricultural Research Service, Eastern Regional Research Center, Residue Chemistry & Predictive Microbiology Research Unit, 600 E. Mermaid Lane, Wyndmoor, Pennsylvania
[2]Shanghai Jiaotong University, 800 Dongchuan Road, Shanghai, China
[3]Shanghai Institute for Food and Drug Control, 1500 Zhangheng Road, Shanghai, China
***E-mail: Guoying.Chen@ars.usda.gov.**

Lanthanide-sensitized luminescence (LSL) is highly valuable for analysis of two classes of antibiotic drugs: tetracyclines (TC) and (fluoro)quinolones (FQ). In theory, efficient intrachelate energy transfer enhances LSL's sensitivity and specificity. In practice, time-domain measurement effectively rejects short-life spectroscopic interferences. To take full advantage of LSL, a portable luminescence spectrometer was developed and applied to analysis of TC and FQ residues in food matrices. Implementation of light emitting diode excitation and photomultiplier tube gating technique resulted in improved performance especially signal-to-background ratio. Two applications are demonstrated in this work: quantitation of oxytetracycline, the most prominent antibiotic in shrimp aquaculture, with 12.7 ng/g limit of quantification; and binary screening of four FQs registered in European Union in caprine milk: danofloxacin, flumequine, and enrofloxacin plus its metabolite ciprofloxacin at their maximum residue limits at 30, 50, and 100 ng/g, respectively.

© 2013 American Chemical Society
In Physical Methods in Food Analysis; Tunick, M., et al.;
ACS Symposium Series; American Chemical Society: Washington, DC, 2013.

Introduction

Tetracyclines (TC) and fluoroquinolones (FQ) are two classes of potent, broad-spectrum antibiotic drugs extensively used in human and veterinary medicine. TC alone accounts for more than 50% of antibiotic use in world agriculture due to broad spectrum of activity, low cost, and lack of adverse side effects. FQs are synthesized to confound microorganisms that need spontaneously two mutation genes to survive. However, microbial resistance emerged against TC in the 1950s (*1*), and against FQ in 1980s (*2*). To ensure food safety, agricultural use of these antibiotics and residue limits in foods are regulated in most countries. Effective analytical methodologies are essential to uphold regulations and to protect consumer health.

Downloaded by MICHIGAN STATE UNIV on July 29, 2013 | http://pubs.acs.org
Publication Date (Web): July 24, 2013 | doi: 10.1021/bk-2013-1138.ch004

Analytical strategies for TC and FQ residues in foods fall into quantification or screening category. So far, quantification is dominated by high performance liquid chromatography (HPLC) with UV, fluorescence, or mass spectrometric (MS^n) detectors (*3*, *4*). Besides high-budget instrumentation, delicate sample preparation typically must be performed prior to HPLC to render accurate results, and to protect delicate and expensive LC columns and detectors. Screening, on the other hand, relies upon rapid and low-cost methods to detect presence of residues in food matrices above a threshold derived from tolerance or action level. Typical screening methods are growth inhibition (GI) or enzyme-linked immunosorbent assay (ELISA) (*5*). Alternative methods include microbial competitive receptor assay (Charm II) for TC (*6*) and thin-layer chromatography (TLC) for FQ (*7*). Each of these methods has its own advantages and limitations.

Molecular structures of TC and FQ drugs make them good candidates for lanthanide-sensitized luminescence (LSL) spectrometry using Eu^{III} or Tb^{III}, respectively, as sensitizer. Formation of 1:1 TC:Eu^{III} or FQ:Tb^{III} complexes allows TC→Eu^{III} and FQ→Tb^{III} energy transfer. Because of donor-acceptor proximity and close energy levels, these intrachelate processes are highly efficient leading to enhanced signal intensity in addition to other valuable characteristics: narrow atomic emission peak, large Stokes shift, and extremely long excited-state lifetime (*8*, *9*). From a technical point of view, short-life interferences including fluorescence and scattering can be easily rejected by time-domain measurement. To take full advantage of LSL, a custom luminescence spectrometer was developed, in which light-emitting diode (LED) excitation, photomultiplier tube (PMT) gating, etc. were implemented (*10*). LSL performance was hence significantly enhanced in comparison to commercial desk-top fluorometers, especially signal-to-background ratio (S/B). So far, this fluorescence spectrometer and its predecessors have been applied to analysis of TC and FQ residues in a broad range of food matrices of both animal and plant origins. Described in details below are two examples: eurorpium-sensitized luminescence (ESL) quantitation of oxytetracycline, the most prominent antibiotic in shrimp aquaculture (*11*); and terbium-sensitized luminescence (TSL) screening of four FQs registered in European Union (EU) in caprine milk: danofloxacin (DAN), flumequine (FLU), and enrofloxacin (ENR) plus its metabolite ciprofloxacin (CIP) (*12*).

In Physical Methods in Food Analysis; Tunick, M., et al.;
ACS Symposium Series; American Chemical Society: Washington, DC, 2013.

Materials and Methods

Reagents and Solutions

All analytical-reagent-grade chemicals and solvents were purchased from Sigma-Aldrich (Milwaukee, WI) except enrofloxacin (ENRO) and ciprofloxacin (CIPRO) were provided by Bayer, and danogfloxacin (DANO) was provided by Pfizer. Oasis hydrophilic-lipophilic balance (HLB) cartridges (3 cc/60 mg, and 6 cc/200 mg,) were purchased from Waters (Milford, MA, USA). The reagent solutions included 4 g/L metaphosphoric acid in 10:90 (v/v) methanol−water, 0.5 M acetate buffer at pH 5.7, 0.125 M tris(hydroxylmethyl)aminomethane (tris) buffer at pH 8.5, and saturated Na2EDTA. ESL reagent solutions included 1 mM $Eu(NO_3)_3$−1 mM Na_2EDTA, and 0.25 g/mL cetyltrimethylammonium chloride (CTAC). TSL reagent solutions included 1 mM $Tb(NO_3)_3$, and a 10 mM sodium dodecyl sulfate (SDS) solution. Stock solutions (1 mg/mL) of OTC and target FQs were prepared monthly in methanol and 0.03 M NaOH, respectively; further dilutions were performed daily in water. Deionized (DI) water, prepared with a Barnstead (Dubuque, IA) E-pure system, was used to prepare the above solutions.

Downloaded by MICHIGAN STATE UNIV on July 29, 2013 | http://pubs.acs.org
Publication Date (Web): July 24, 2013 | doi: 10.1021/bk-2013-1138.ch004

Luminescence Spectrometer

The luminescence photometer (Figure 1) was custom built to take full advantage of LSL (*10*). Its optical setup is shown in Figure 2. Multiple sources were used to their advantages. For TC excitation, a 385±5 nm LED NCCU001 (Nichia, Detroit, MI, USA), rated at 80 mW continuous wave (CW) power, was used with a glass excitation filter, ZWB3 (Optima, Elk Glove Village, IL, USA). For FQ excitation, a miniature 2 W RSL3100-10 xenon flask lamp (Perkin Elmer, Santa Clara, CA) was used with an excitation filter set: an interference filter 300FS40-25 (Andover, Salem, NH) plus a glass filter ZWB3 (Optima). The duration of the pulsed beam was 15 μs full width half maximum (fwhm) for the LED, and about 1 μs for the xenon lamp. The beam was loosely focused by a fused silica lens (d=12 mm, fl=20 mm) onto a 1x1 cm quartz sample cuvette. The resulting luminescence signal was collected at 90° using 2 identical double-convex lenses (d=25 mm, fl=25 mm). For Eu luminescence, the emission filters were an HB600 (Optima) plus a 620 nm (fwhm=10 nm) interference filter (Edmund, Barrington, NJ, USA); for Tb luminescence, the emission filter was a 546 nm (fwhm=10 nm) interference filter (Edmund). The photodetector was a PMT module H10304-02 (Hamamatsu, Bridgewater, NJ, USA) which can be gated at a user-defined duration. The energy of LED pulse was monitored by a S1226-44BQ silicon Photodiode (PD) (Hamamatsu); the energy of xenon flash, on the other hand, was monitored by a SG01L-5 silicon carbide PD (Boston Electronics, Brookline, MA, USA). The PD output was integrated for individual pulses and used to compensate pulse-to-pulse energy fluctuation. Both instrument control and signal processing was handled by an IBM ThinkPad T30 laptop computer running a custom LabVIEW (National Instruments, Dallas, TX,

In Physical Methods in Food Analysis; Tunick, M., et al.;
ACS Symposium Series; American Chemical Society: Washington, DC, 2013.

USA) program. A multifunctional card 6062E (National Instruments) provided all the hardware functions including data acquisition, digital input/output, and digital-to-analog conversion. Random baseline fluctuation in amplified PMT output was corrected by software protocol.

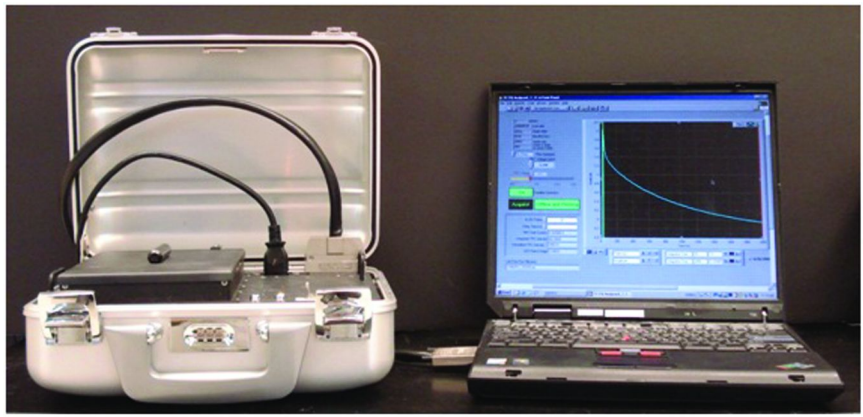

Figure 1. Portable time-resolved fluorescence spectrometer.

Downloaded by MICHIGAN STATE UNIV on July 29, 2013 | http://pubs.acs.org
Publication Date (Web): July 24, 2013 | doi: 10.1021/bk-2013-1138.ch004

Extraction and Cleanup

OTC in Shrimp

Beheaded raw shrimp samples were purchased from local food stores. Tail muscle was minced with a DLC-2A food processor (Cuisinart, East Windsor, NJ, USA) and stored at -80 °C. Partially thawed muscle (2±0.03 g) was weighed into 50 mL polypropylene centrifuge tubes, spiked, and allowed to stand in the dark for 20 min. Homogenization was carried out in 10 mL of 4 g/L metaphosphoric acid in 10:90 (v/v) methanol-water and 1 mL of saturated Na_2EDTA using a Ultra-Turrax T-25 homogenizer (Janke and Kunkel, Cincinnati, OH). With the aid of an Air Admiral portable vacuum pump (Cole-Parmer, Vermon Hills, IL), the homogenate was filtered through Whatman (Florham Park, NJ) #GF/D filter paper (d=55 mm) installed in a Buchner funnel. The muscle pellet and filter paper were extracted again by 20 s vortex mixing in the same extraction medium, followed by filtration through a second #GF/D filter paper. Next, Oasis HLB cartridges (60 mg, 3 mL) were installed in a vacuum manifold, conditioned with 2 mL of methanol and 2 mL of water, loaded with combined filtrates, and washed with 3 mL of water. After the cartridges were dried under vacuum for 1 min, OTC was finally eluted with 2 mL of methanol to test tubes.

Goat milk was purchased from local food stores and stored at 4 °C. Aliquots of 5.0 mL were transferred to 50-mL polypropylene centrifuge tubes and fortified to the desired levels, followed by 10 s vortex mixing. Then, 5 mL of DI water was added to each tube followed by swirl mixing. Oasis HLB (200 mg, 6 mL) cartridges were installed on a vacuum manifold and conditioned with 3 mL of methanol and 5 mL of DI water. After loading and washing with 4 mL of DI water, FQs were finally eluted with 1.5 mL of Methanol to test tubes.

Downloaded by MICHIGAN STATE UNIV on July 29, 2013 | http://pubs.acs.org
Publication Date (Web): July 24, 2013 | doi: 10.1021/bk-2013-1138.ch004

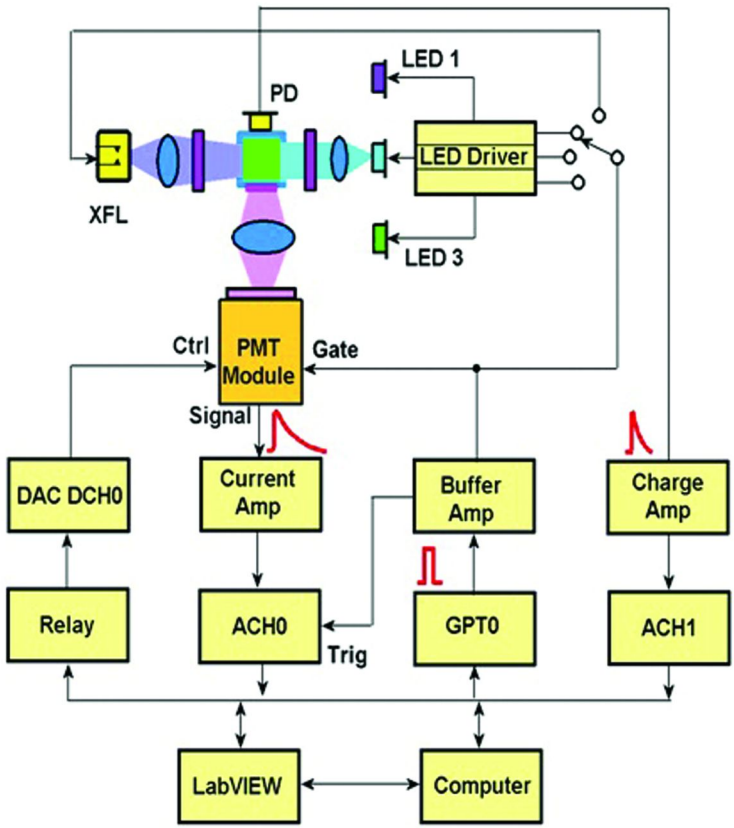

Figure 2. Optical setup of the fluorescence spectrometer.

In Physical Methods in Food Analysis; Tunick, M., et al.;
ACS Symposium Series; American Chemical Society: Washington, DC, 2013.

Luminescence Measurement

ESL

To each OTC eluate, the following reagents were added: 0.5 mL of 1 mM $Eu(NO_3)_3$−1 mM Na_2EDTA, 0.2 mL of 0.25 g/mL CTAC, and 3.3 mL of 0.125 M pH 8.5 tris buffer. Vortex mixing followed. TSL was measured at λ_{ex} = 385 nm and λ_{em} = 620 nm in triplicates; each with a fresh 1.5 mL aliquot. The ESL signal was integrated over 25-1000 μs interval as I_{ESL}. The normalized ESL signal, I_{ESL}/E_{pulse}, where E_{pulse} is the energy of individual LED pulse, was recorded as the final result. In each measurement, 20-pulse averaging was performed to improve signal-to-noise ratio (S/N).

TSL

The eluates were transferred to a 5 mL volumetric flasks, the following TSL reagents were used to rinse the tubes and then added to the flasks: 0.2 mL of 1 mM $Tb(NO_3)_3$, 0.25 mL of 0.5 M sodium acetate buffer (pH 5.7), and 1 mL of 20 mM SDS solution. The flask was filled to mark with water. TSL was measured at λ_{ex} = 300 nm and λ_{em} = 546 nm. The PMT gating duration was set at 15 μs; the resulting TSL signals were integrated from 15 μs to 3.5 ms. Similarly, triplicate readings were acquired and 20-flash averaging was performed.

HPLC-ESI-Tandem Mass Spectrometer

The liquid chromatograph used for validation is an Agilent (Santa Clara, CA, USA) 1200 including a binary pump, a vacuum degasser, and an automatic injector. An Agilent ZOBRAX SB C8 column (5 μm, 150 mm×3.0 mm) was used at 30 °C and 0.3 mL/min flow rate. Injection volume was 20.0 μL. The detector was a triple-quadrupole mass spectrometer Model API 3200 (Applied Biosystems/MDS SCIEX, Concord, Ontario, Canada) with an electrospray ionization (ESI) source. The mass spectrometer was controlled by Analyst 1.5 software. The turbo-ion spray potential was set at +5000 V and the source temperature was set at 500 °C. The spectrometer was operated in the positive mode and analysis were performed in multiple reaction monitoring (MRM) mode. Two product ions were monitored: $[M+H-H_2O-NH_3]^+$ (*m/z* 426) and $[M+H-NH_3]^+$ 135 (*m/z* 444).

Results and Discussion

OTC Extraction and Cleanup

Typically, complexity of animal tissue requires elaborate extraction and cleanup to uphold data integrity and to protect delicate LC columns and expensive detectors such as MS^n. Aqueous media are miscible to animal tissue and dissolve TC drugs better than many organic solvents except alcohols, so they are used

Downloaded by MICHIGAN STATE UNIV on July 29, 2013 | http://pubs.acs.org
Publication Date (Web): July 24, 2013 | doi: 10.1021/bk-2013-1138.ch004

most often. Effective media include 0.1 N succinic acid at pH 4, 0.1 M glycine in 1 M HCl, and, in particular, the prevalent McIlvaine buffer at pH 4 (*13*). In theory, a mild acidic pH maintains TCs in a dominant zwitterionic state that adsorbs better on reverse phase sorbent in subsequent SPE cleanup; and EDTA frees OTC from its complexes with multivalent cations. In practice, however, as a result of rapid protein precipitation, analyte entrapment was observed leading to data fluctuation. Fortunately, dense protein precipitate did not occurred in 4 g/L metaphosphoric acid in 10:90 (v/v) methanol−water. This medium's mild pH (~3) was also ideal for OTC. To promote field assay, centrifugation was replaced by filtration in this work using 2.7 μm Whatman #GF/D binder-free glass microfiber filter, which provided well-balanced performance in speed, load capacity, and filtrate clearness.

Solid phase extraction (SPE) remains the most prominent cleanup approach for animal tissue matrices that fulfills separation, enrichment, and solvent change. Multiple functionalities on TC's common structure render several sorbent types effective including C18, styrene-divinylbenzene, CH-endcapped cyclohexyl, phenyl, and HLB. In this work, HLB sorbent was chosen to avoid OTC-silica interaction and to take advantage of its improved wettability in aqueous media (*14*). This sorbent proved effective: six shrimp samples of different origins yielded an averaged background at 6.4 ng/g with 18.2% RSD.

Downloaded by MICHIGAN STATE UNIV on July 29, 2013 | http://pubs.acs.org
Publication Date (Web): July 24, 2013 | doi: 10.1021/bk-2013-1138.ch004

FQs Extraction and Cleanup

FQs have propensity to bind proteins. To achieve screening at 30-100 ng/g levels without prior HPLC separation, extraction and cleanup are essential. Typically, deproteinization is the first step for milk analysis using acids such as 5% trichloroacetic acid (TCA), or trifluoroacetic acid (TFA) plus organic solvent. To minimize analyte loss due to entrapment, dropwise addition of extraction medium was suggested in milk analysis (*15*) at the cost of productivity. To overcome these problems, protein precipitation was eliminated and SPE was performed in diluted milk. Many sorbent types have been used effectively for FQ-in-milk cleanup including ion-exchange (*16*), C18 (*17*), and HLB (*18*). HLB was chosen in this work that achieved around 72% recovery for both whole and 1% goat milk without a defatting step. The cleanup process took less than 20 min.

Fluorescence Spectrometer

Without prior separation by HPLC or capillary electrophoresis (CE), stand-alone spectrometric detection schemes rely upon intrinsic specificity to tolerate concomitant matrix components. Fortunately, these LSL instrumentation-method combinations achieved high-degree class specificity due to multiple factors: selective excitation, efficient analyte-to-sensitizer energy transfer, selective detection of atomic emission, and time-domain detection that rejects short-life interference emissions including stray source light, scattering from residual turbidity, and fluorescence from matrix components. LED outperformed xenon flashlamp in narrow bandwidth ($\Delta\lambda$=15 nm), clean pulse extinction, and low transient current leading to extremely low noise. Finally, PMT gating technique

significantly enhanced S/N. For shrimp samples spiked with OTC at 100 ng/g, background noise was reduced by six fold vs. Varian Cary Eclipse fluorescence spectrometer.

To effectively target all possible FQs, an excitation filter with broader bandwidth (fwhm=40 nm) was chosen to achieve more uniform excitation among target entities. Water quenching was minimized by using synergistic agent EDTA as well as surfactant CTAC that created a micellar environment. Random signal variation was reduced by averaging over multiple pulse cycles; however, because of the concern on possible OTC photodegradation (*19*), pulse number per aliquot was limited, and a fresh aliquot was used in each measurement.

Downloaded by MICHIGAN STATE UNIV on July 29, 2013 | http://pubs.acs.org
Publication Date (Web): July 24, 2013 | doi: 10.1021/bk-2013-1138.ch004

OTC-in-Shrimp Quantification by ESL

Calibration curves obtained from a randomly selected farm-raised shrimp sample are shown in Figs. 3a-3c. Linear relationship between integrated ESL intensity and OTC concentration is maintained in Figs. 3a-3b; but signal starts to level off in Fig. 3c due to filter effects (*20*). The average RSD was ~2%.

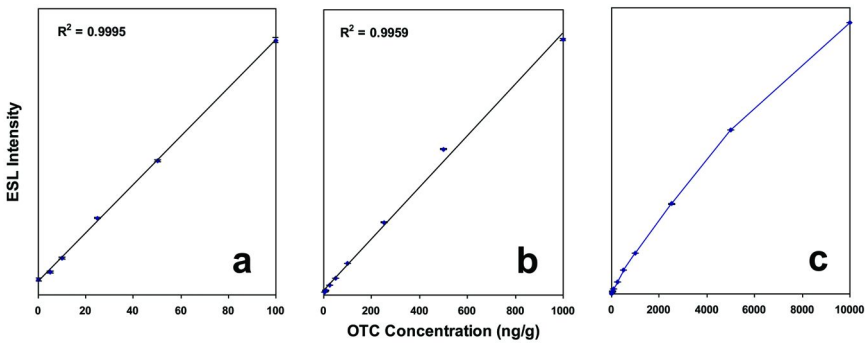

Figure 3. Calibration curves of OTC in shrimp muscle in 5-100 ng/g (a), 5-1000 ng/g (b), and 5-10000 ng/g (c) ranges. Reproduced with permission from reference (11). Copyright 2011 Springer.

ESL signals of six shrimp samples of varied species and origins (2 wild and 4 farmed) before and after fortification with OTC at 100 ng/g is shown in Figure 4. The average background corresponded to 6.4 ng/g with 18.2% RSD. Limit of quantification (LOQ), calculated by background plus 10σ, then divided by slope, was 12.7 ng/g. This LOQ was well below the EU 100 ng/g maximum residue limit (MRL). The background noises originated mainly from matrix interferences; only a minor portion was instrument-related. Conventionally, matrix interferences are minimized by thorough cleanup, or HPLC or CE separation, or high-resolution detection schemes such as MS/MS. These approaches require extra time and labor, expensive instrumentation, and highly trained personnel. In comparison, this ESL method provides simplicity that well serves legislator purpose, yet allows less-

trained personnel to perform assay with confidence. As observed previously, 4-epiOTC metabolite was extracted and detected equally well (*21*), providing an extra advantage over microbial receptor assay and ELISA.

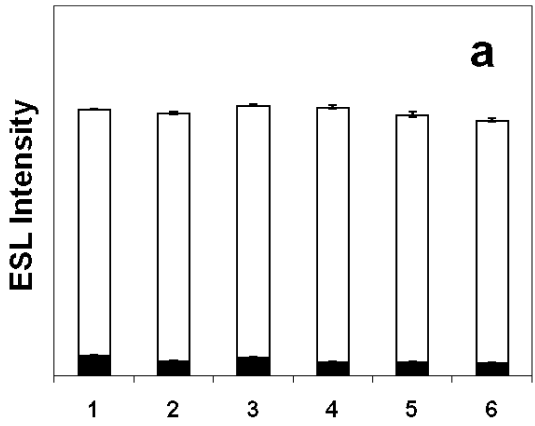

Figure 4. ESL intensities of six shrimp samples spiked with OTC at 0 and 100 ng/g. The error bars indicate ±1 SD. Reproduced with permission from reference (11). Copyright 2011 Springer.

OTC is the most common antibiotic in shrimp aquaculture worldwide; however, caution must be exercised if analyte identity is uncertain. MS is a proven confirmation technique. An alternative solution is partial least-squares (PLS) analysis performed on ESL decay curves. Based on lifetime difference between excited-state TC:Eu^{III} and OTC:Eu^{III} complexes, simultaneous determination of TC and OTC in bovine serum was possible (*22*).

HPLC-MS/MS Validation

Three shrimp samples were randomly selected for HPLC-MS/MS validation: farmed fresh-water shrimp, farmed ocean shrimp, and wild ocean shrimp. After fortification, extraction, and cleanup with the same protocol, the samples were analyzed by HPLC-MS/MS. Quantitation was based on the peak area of primary product ion $[M+H-H_2O-NH_3]^+$ at *m/z* 426. The results at 50, 100, and 2000 ng/g fortification are compared with ESL data in Table 1. Both MS/MS recoveries (79.5%-95.6%) and slightly lower-than-ESL results, based on a reagent-blank calibration curve, were indicative of relatively insignificant matrix suppression. Confirmation of OTC is typically based on retention time and the abundance ratio of secondary product ion $[M+H-NH_3]^+$ to primary ion $[M+H-H2O-NH_3]^+$, [*m/z* 444]/[*m/z* 426].

In Physical Methods in Food Analysis; Tunick, M., et al.;
ACS Symposium Series; American Chemical Society: Washington, DC, 2013.

Downloaded by MICHIGAN STATE UNIV on July 29, 2013 | http://pubs.acs.org
Publication Date (Web): July 24, 2013 | doi: 10.1021/bk-2013-1138.ch004

Table 1. Comparison of HPLC-ESI-MS/MS and ESL results

Shrimp samples	*Fortification concentration (ng g^{-1})*	*n*	*Result (ng g^{-1})*	*RSD*	*Recovery*	*Comparison to ESL (%)*
Sea-water farmed	50	4	39.8	3.0%	79.5%	-24.2%
	100	4	88.3	4.7%	88.3%	-11.2%
	2000	4	1813	3.2%	90.4%	-10.5%
Fresh-water farmed	50	4	40.7	4.1%	81.4%	-22.4%
	100	4	83.2	3.1%	83.2%	-16.3%
	2000	4	1912	3.3%	95.6%	-5.6%
Sea-water wild	50	4	43.2	5.8%	86.5%	-17.4%
	100	4	85.1	3.0%	85.1%	-14.4%
	2000	4	1741	2.1%	87.0%	-14.1%

Downloaded by MICHIGAN STATE UNIV on July 29, 2013 | http://pubs.acs.org
Publication Date (Web): July 24, 2013 | doi: 10.1021/bk-2013-1138.ch004

FQ Screening by TSL

Sensitivity and specificity of TSL are greatly enhanced by efficient intrachelate FQ→Tb^{III} energy transfer, rendering TSL well suited for FQ drug analysis (*9*). However, when the target was not just one FQ but four EU-registered FQs, the situation became more complicated. Firstly, MRLs vary among members from 30 ng/g to 100 ng/g (Table 2). Secondly, structural differences among FQ members result in different excitation and emission spectra, and different quantum yield. Even with a broad excitation bandwidth, TSL responses still vary among members. Our solution was first to identify the lowest responding member (FLU) among four targets at their respective MRLs (Table 2), then establish a single screening threshold based on signals of milk samples (n=18) spiked with 50 ng/g FLU, and applied it to all four targets. The threshold was calculated based on the following formula:

$$\text{Threshold} = \chi_{F50} - 3\sigma_{F50}$$

where χ_{F50} and σ_{F50} are the mean and standard deviation of these TSL data. The advantage of a common threshold is simple binary results. The disadvantage, on the other hand, is sensitivity must be high enough to detect the lowest responding member. For typical food samples, commercial fluorescence spectrophotometers fail to meet this demand due to considerable interference from matrix components. Fortunately, PMT gating technique effectively rejected background noise enabling this photometer to fulfill this screening task. For 30 ng/g DAN in reagents, signal-to-background noise ratio (S/B) in reagent was improved by 5-fold vs. a Varian Cary Eclipse fluorescence spectrometer; and by 30-fold in goat milk in which matrix components played a more significant role.

In Physical Methods in Food Analysis; Tunick, M., et al.;
ACS Symposium Series; American Chemical Society: Washington, DC, 2013.

Table 2. Relative TSL signals of caprine milk spiked with DAN, FLU, ENR, and CIP at their respective MRLs

FQ	*MRL (ng/g)*	*Relative signal*	*SD*	*RSD*	*S/B*
FLU	50	100%	16.5	2.1%	1.13
DAN	30	104%	14.3	1.7%	1.22
ENR	100	308%	28.9	1.2%	5.58
CIP	100	285%	38.0	1.7%	5.09

Downloaded by MICHIGAN STATE UNIV on July 29, 2013 | http://pubs.acs.org
Publication Date (Web): July 24, 2013 | doi: 10.1021/bk-2013-1138.ch004

A screening method can be developed based on a one-to-one signal-concentration relationship. A linear response makes it simple to interpret data and to establish a threshold. In theory, TSL intensity is a linear function of FQ concentration; in practice, linearity is spoiled by filter effects at higher concentrations. Shown in Figs. 5a-5b are the calibration curves of spiked FLU at 0-500 ng/g in caprine milk. Linearity is observed in each decade, but filter effects caused the slope in Fig. 5b to be smaller than that in Fig. 5a.

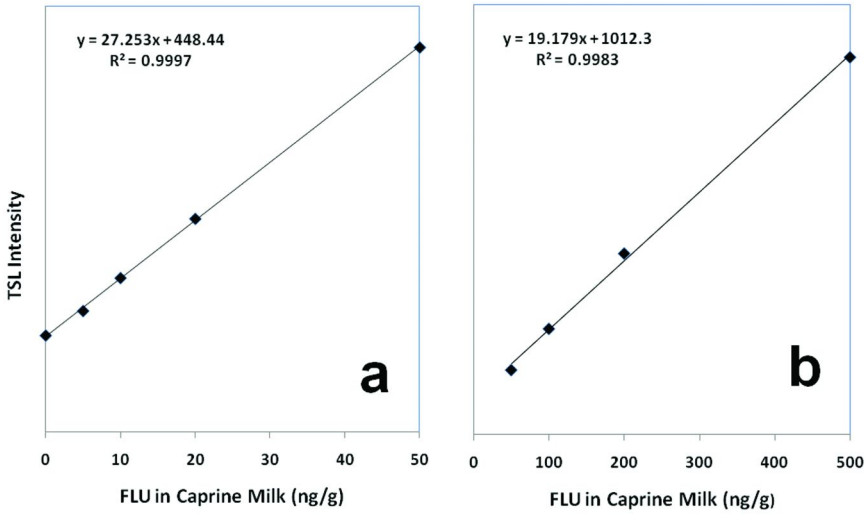

Figure 5. Calibration curves of FLU in caprine milk in 0-50 ng/g (a) and 50-500 ng/g (b) ranges. Reproduced with permission from reference (12). Copyright 2012 Springer.

Blind samples (n=48) were divided into four groups, each spiked with one FQ at random concentrations up to 200% of its MRL. It turned out 25 samples were above respective MRLs and 23 below. Final Screening results are shown in Table 3. All 25 positive samples were classified correctly without false negative. Among 23 negative samples, 11 were screened correctly but 12 were presumed positive.

When a common threshold was derived from the lowest responding member, a higher positive rate was expected for other members. As a rule of screening, presumptive positive is not a final verdict; samples fall into this category must be confirmed further by other quantitative methods such as HPLC-MS/MS during which screening errors will be corrected. The negative verdict, on the other hand, is final. To uphold screening integrity, false negative rate must be minimal.

Table 3. Screening of 48 blind caprine milk samples randomly spiked with FLU, DAN, ENR, and CIP up to 200% of their respective MRLs

Spiked samples		*FLU*	*DAN*	*ENR*	*CIP*	*Screening results*	
n	48	12	12	12	12		48
>MRL	25	5 / 5	8 / 8	8 / 8	4 / 4	Presumptive positive	25
		0	0	0	0	False negative	0
<MRL	25	7 / 4	4 / 1	4 / 2	8 / 4	Negative	11
		3	3	2	4	False Positive	12

The ultimate goal of screening is to identify presence of target residues. Due to reliable performance of this photometer-method combination, this goal was well fulfilled in about 20 min. A rapid and low-cost method is especially valuable for regulatory laboratories that routinely handle large numbers of tests. In comparison to our previous screening protocol for 200 ng/g DAN in beef (*23*), this work enabled screening at 50 ng/g FLU with a signal even lower than that of 30 ng/g DAN, rendering almost an-order-of-magnitude improvement in sensitivity. With centrifugation replaced by filtration, this deployable fluorometer-method is one-step towards field testing. Hopefully, elimination of sample transportation will enable immediate results, timely decision, and minimal market recall.

Though highly specific for FQ drugs as a class, TSL lacks the ability to distinguish individual members that share a common molecular structure, and similar chemical and spectroscopic behavior. These characteristics limit the ability to quantify multiple FQ drugs but enable screening of their presence even including illegal ones. From this point of view, TSL provides extra value in residue monitoring.

Potential Applications and Recent Advancements

Sample preparation is still the bottle-neck of many real-world applications. High intrinsic specificity of LSL allows extraction and cleanup to be simplified to certain extent. If HPLC is excluded from the protocol, the burden to protect

In Physical Methods in Food Analysis; Tunick, M., et al.;
ACS Symposium Series; American Chemical Society: Washington, DC, 2013.

Downloaded by MICHIGAN STATE UNIV on July 29, 2013 | http://pubs.acs.org
Publication Date (Web): July 24, 2013 | doi: 10.1021/bk-2013-1138.ch004

expensive LC columns is also eliminated further enhancing sample throughput. As described above, eluates or filtrates were cleaned up by using SPE cartridges, which fulfilled both analyte isolation and enrichment. Alternatively, both objectives can be fulfilled by using small-format (25x10 mm) C18 sorbent strips, as demonstrated in this laboratory (*23*). At about $0.20/strip, this approach gained cost advantage over conventional cartridge-format SPE. With significantly reduced background noise of this portable spectrometer, higher sensitivity is expected vs. desktop fluorescence spectrometers. The disadvantage of this strip format, however, is limited selections of TLC plate types; besides, such strips are not yet commercially available.

A novel approach known as dispersive liquid-liquid microextraction (DLLME) was developed in 2006 to fulfill both cleanup and enrichment using only a minute amount of chlorinated solvent. Recently, DLLME cleanup was combined with TSL detection to screen residues of ENRO and its metabolite, CIPRO, in swine liver at 500 ng/g tolerance set by the US. Food and Drug Administration (*24*). Even though DLLME gained distinct advantages including rapidity, low cost, and minimal use (450 μL) of chlorinated solvent, reproducibility was found inferior to SPE, and centrifugation steps compromised field deployability.

Thorough cleanup can be achieved by molecularly imprinted SPE (MISPE), as demonstrated by DAN determination in milk (*25*). Elimination of interfering matrix component rendered a very low LOD at 2.0×10^{-9} M. Linear range was 8.4×10^{-9} - 3.4×10^{-7} M. MISPE is especially valuable for high complex matrices such as food or biological samples.

Many technical advances in LSL can gain low-background benefit of the portable spectrometer used in this work. Some examples are cited in this section. TSL can be operated in flow injection analysis (FIA) mode: prior to injection, the analyte formed Tb^{3+} chelate which was transported by a carrier stream to a flow through cell, where it was retained and enriched on a cationic Sephadex resin. Excitation on the resin surface led to TSL signal. Finally, the analyte was eluted by 0.08 M EDTA and the sorbent was renewed. With this scheme, norfloxacin was detected in biological fluids with very low (1.5 ng/mL) LOD (*26*). In another work, silver nanoparticles (AgNPs) was used to enhance TC:Eu emission intensity by 4 times over that in solution phase (*27*). Based on this enhancement effect, TC was determined in milk with satisfactory results, a 4 nM LOD and 10 nM-10 μM linear range. To quantify multiple target analytes without prior separation, chemometrics is a valuable tool. Partial least-squares (PLS) analysis was applied to simultaneous quantitation of two TC analytes (*22*); and multivariate curve resolution-alternating least square (MCR-ALS) was applied to quantitation of three FQ analytes in human serum and elimination of salicylate interference (*28*).

Though most often LSL was applied to direct quantification of ligands or central lanthanide ions, a novel approach is to use lanthanide complexes as probes to indirectly quantify chemical species that either enhance or quench luminescence signal. Successful applications to biochemistry, medicine, and clinical testing are many. By taking advantage of DNA's enhancement effect on luminescence intensity of norfloxacin-Tb^{3+} chelate, herring sperm DNA (hsDNA) and denatured calf thymus DNA (ctDNA) were quantified with a wide 5-1000 ng/mL linear range, and low LODs at 0.9 and 0.6 ng/mL, respectively (*29*).

Downloaded by MICHIGAN STATE UNIV on July 29, 2013 | http://pubs.acs.org
Publication Date (Web): July 24, 2013 | doi: 10.1021/bk-2013-1138.ch004

Similarly, low-density lipoprotein (LDL) in aqueous solution enhanced emission of chlortetracycline (CTC)-Eu^{+3} complex (*30*). This effect, ascribed to shielding of water molecule, a luminescence quencher, from Eu^{+3} coordination sphere, resulted in a 490 ng/mL LOD and an increase in average lifetime from 15 μs to 46 μs. The TC-Eu^{+3} probe was successfully applied to determination of urea hydrogen peroxide in whole blood (*31*), and superoxide dismutase in plant and blood samples (*32*).

On the other hand, many metallic ions quench LSL intensity in aqueous media. A quantification method was developed for Cu^{2+} using Eu^{3+}-TC-hydrogern peroxide complex as a probe. LOD and linear range were 0.2 μM and 0-1.6 μM, respectively (*33*). This method, however, was liable to interferences from other metallic ions, especially Mg^{2+}, Ca^{2+}, and Fe^{3+}, as well as anions such as citrate and phosphate. In a recent study, a Tb^{3+} complex with a quinolone-based dye, cs124, and a polyaminocarboxylate-based ligand, DTPA, was used as a probe for Hg^{2+} detection (*34*). Quenching was found to be dominated by a static mechanism. Because the stability constant of the cs124-DTPA:Hg is 3-4 orders of magnitude higher than that of its Tb counterpart, Hg^{2+} replaced Tb^{3+} resulting in the formation of non-fluorescent cs124-DTPA:Hg. This unique mechanism rendered the method specific for Hg^{2+} detection. Among 14 ions tested, only Fe^{3+} had significant interference. Fortunately, this interference could be easily eliminated by addition of H_2O_2 that reduced Fe_{3+} to non-interfering Fe_{2+}. The method achieved a 4 nM LOD and a linear range of 4-600 nM.

Conclusions

A portable fluorescence spectrometer was developed and applied to LSL analysis of TC and FQ residues in food matrices. Two applications are demonstrated in this work that cover both quantitative and screening strategies. Many obstacles to field deployment were removed, so hopefully applications can be extended to clinical and environmental fields. Some potential applications to biochemical, clinical, and medical testing are also discussed.

Downloaded by MICHIGAN STATE UNIV on July 29, 2013 | http://pubs.acs.org
Publication Date (Web): July 24, 2013 | doi: 10.1021/bk-2013-1138.ch004

Acknowledgments

Christine Haynes is acknowledged for technical assistance.

References

1. Roberts, M. *FEMS Microbiol. Rev.* **1996**, *19*, 1–24.
2. Robicsek, A.; Jacoby, G. A.; Hooper, D. C. *Lancet Infect. Dis.* **2006**, *6*, 629–640.
3. Önal, A. *Food Chem.* **2011**, *127*, 197–203.
4. Hernández-Arteseros, J. A.; Barbosa, J.; Compañó, R.; Prat, M. D. *J. Chromatogr., A* **2002**, *945*, 1–24.
5. Okerman, L.; Croubels, S.; Cherlet, M.; Wasch, K. D.; Backer, P. D.; Hoof, J. V. *Food Addit. Contam.* **2004**, *21*, 145–153.

6. Charm, S. E.; Chi, R. *J. AOAC Int.* **1988**, *71*, 304–316.
7. Juhel-Gaugain, M.; Abjean, J. P. *Chromatographia* **1998**, *47*, 101–104.
8. Hirschy, L. M.; Dose, E. V.; Winefordner, J. D. *Anal. Chim. Acta* **1983**, *147*, 311–316.
9. Gomez-Hens, A.; Aguilar-Caballos, M. P. *TrAC, Trends Anal. Chem.* **2002**, *21*, 131–141.
10. Chen, G. *Appl. Spectrosc.* **2012**, *66*, 341–346.
11. Chen, G.; Liu, G. *Sens. Instrum. Food Qual.* **2011**, *5*, 165–171.
12. Chen, G. *Food Anal. Methods* **2012**, *5*, 1114–1120.
13. Brillantes, S.; Tanasomwang, V.; Thongrod, S.; Dachanantawitaya, N. *J. Agric. Food Chem.* **2001**, *49*, 4995–4999.
14. Li, H.; Kijak, P. J.; Turnipseed, S. B.; Cui, W. *J. Chromatogr., B* **2006**, *836*, 22–38.
15. Moors, M.; Massart, D. L. *J. Pharm. Biomed. Anal.* **1991**, *9*, 129–139.
16. Christodoulou, E. A.; Samanidou, V. F. *J. Sep. Sci.* **2007**, *30*, 2421–2429.
17. Sun, H.; Zhao, W.; He, P. *Chromatographia* **2008**, *68*, 425–429.
18. Herrera-Herrera, A. V.; Hernández-Borges, J.; Rodríguez-Delgado, M. Á. *J. Chromatogr. A* **2009**, *1216*, 7281–7287.
19. Scales, B; Assinder, D. A. *J. Pharm. Sci.* **1973**, *62*, 913–917.
20. Parker, C. A.; Rees, W. T. *Analyst* **1962**, *87*, 83–111.
21. Chen, G.; Liu, G. *Food Addit. Contam. A* **2009**, *26*, 1172–1179.
22. Ibañez, G. A. *Talanta* **2008**, *75*, 1028–1034.
23. Chen, G.; Du, Y. *J. Agric. Food. Chem.* **2011**, *59*, 1058–1062.
24. Chen, G.; Li, Q. *J. Agric. Food. Chem.* **2013**, *61* in press.
25. Kaur, K.; Saini, S. S.; Malik, A. K.; Singh, B. *Spectrochim. Acta A* **2012**, *96*, 790–795.
26. Martínez, E. J. L.; Reyes, J. F. G.; Barrales, P. O.; Díaz, A. M. *Anal. Chim. Acta* **2005**, *532*, 159–164.
27. Tan, H.; Chen, Y. *Sens. Actuators, B* **2012**, *173*, 262–267.
28. Lozano, V. A.; Tauler, R.; Ibañez, G. A.; Olivieri, A. C. *Talanta* **2009**, *77*, 1715–1723.
29. Tong, C.; Hu, Z.; Liu, W. *J. Agric. Food. Chem.* **2005**, *53*, 6207–6212.
30. Teixeira, L. d. S.; Grasso, A. N.; Monteiro, A. M.; Neto, A. M. F.; Vieira, N. D., Jr.; Gidlund, M.; Courrol, L. C. *Anal. Biochem.* **2010**, *400*, 19–24.
31. Courrol, L. C.; Bellini, M. H.; Tarelho, L. V. G.; Silva, F. R. O.; Mansano, R. D.; Gomes, L.; Vieira, N. D., Jr; Shor, N. *Anal. Biochem.* **2006**, *355*, 140–144.
32. Wei, W.; Wang, H.; Jiang, C. *Spectrochim. Acta A* **2008**, *70*, 389–393.
33. Cano-Raya, C.; Ramos, M. D. F.; Vallvey, L. F. C.; Wolfbeis, O. S.; Schäferling, M. *Appl. Spectrosc.* **2005**, *59*, 1209–1216.
34. Tan, H.; Zhang, Y.; Chen, Y. *Sens. Actuators, B* **2011**, *156*, 120–125.

Downloaded by MICHIGAN STATE UNIV on July 29, 2013 | http://pubs.acs.org
Publication Date (Web): July 24, 2013 | doi: 10.1021/bk-2013-1138.ch004

Downloaded by UNIV OF DELAWARE MORRIS LIB on July 29, 2013 | http://pubs.acs.org
Publication Date (Web): July 24, 2013 | doi: 10.1021/bk-2013-1138.ch005

Chapter 5

Estimating the Glycemic Potential of Extruded Food Materials

Charles I. Onwulata* and Audrey E. Thomas-Gahring

U.S. Department of Agriculture, Agricultural Research Service, Eastern Regional Research Center, Dairy & Functional Foods Research Unit, 600 E. Mermaid Lane, Wyndmoor, Pennsylvania 19038
***E-mail: Charles.Onwulata@ars.usda.gov.**

Well-formulated snacks can play a positive role in enhancing health by providing essential nutrients, such as increased levels of protein and fiber, that can mitigate the growing metabolic syndrome associated with obesity. Adding whey protein concentrate (WPC80) and cashew pulp (CP) to corn meal, a major ingredient in extruded snacks in the U.S., or whole grains such as barley and quinoa, or cassava, can increase the amount of protein and fiber, and reduce overall carbohydrate content. The products discussed in this study, barley, cassava, corn meal and quinoa were blended with WPC80 (12.5 wt%) or with CP (12.5 wt%), extruded at a terminal melt temperature of 60°C, and fully cooked by baking at 205°C. The extrudates were analyzed for moisture content, glycemic potential, rapidly available glucose (RAG) determined after 20 min, and slowly available glucose (SAG) measured after 120 min, and confocal scanning laser microscopy. The glycemic potential of the different products was dependent on their unique starch properties; adding WPC80 with or without CP added minimal effects. The products' rapidly available glucose values or potential glycemic index were: quinoa (70%), barley (61%), corn (54%), and cassava (48%). Adding WPC80 with or without CP improved the RAG values for barley and quinoa, but not for cassava which increased from 61 to 77%. Adding WPC80 or CP had no effect on corn products. The RAG values were mostly predictive of each product's glycemic potential.

Not subject to U.S. Copyright. Published 2013 by American Chemical Society
In Physical Methods in Food Analysis; Tunick, M., et al.;
ACS Symposium Series; American Chemical Society: Washington, DC, 2013.

Introduction

Obesity is a growing trend worldwide with implications on health and economic viability of many nations. Modern living with its conveniences such as completely prepared meals has shifted total human energy expenditure negatively, resulting in obesity (*1–3*). Obesity, a significant factor in chronic disease including type 2 diabetes and cardiovascular disease, can be impacted by dietary approaches, most acute with the elderly and those in affluent societies (*4*). Glycemic index, the rate at which plasma glucose accumulates after ingestion of sugars, and glycemic load, the total available glycemic load for a given serving, may affect overall quantity of food consumed (*5*).

The glycemic index (GI) is a physiological assessment of a food's carbohydrate content through its effect on postprandial blood glucose concentrations (*6*). The glycemic index or how fast blood sugar rises with the consumption of carbohydrates or sugars impacts insulin rise and diabetes (*7*) Evidence suggests that low GI and low glycemic load (GL) diets may be protective against the development of chronic and obesity related diseases such as type 2 diabetes and coronary heart disease. Recent studies have suggested a role of GI/GL in weight loss, linking satiety and metabolism to obesity (*8*). Many studies have linked the increased rates of obesity, diabetes, and other health problems associated with metabolic syndrome diseases to lifestyle and diet (*9*, *10*). From the processed foods aspect, the rate of dissolution of food materials may affect levels of nutrients and their availability for absorption within the human digestive system (*11*).

Before food is digested and assimilated, it is first dissolved in the gastric intestinal (GI) tract. It is well recognized that though single-point digestion models are valuable, time-course or kinetic measurements reveal more information on rate and extent of digestion, which can provide estimates of glycemic index (*12*). Wallace et al. (2006) postulated that the blood glucose response for ingested glucose is a linear function of glucose intake over a range of normal intakes and, therefore, that a reference drink of one concentration can be used and a correction factor applied to account for the fact that the reference drink and food are of different weight (*13*). Glycemic glucose equivalent is calculated from measurements of the incremental area under the blood glucose response curve (AUC) for a food of a specified weight divided by the AUC in response to a specified amount of glucose, a measure coined as 'glycemic glucose equivalence' (*13*).

Foods with enhanced health properties can be developed to aid people fighting obesity. At the development stage, in the laboratory, estimates of the extents of dissolution can predict the rate of subsequent digestibility and assimilation. There are many factors that affect how rapidly foods dissolve in the gastric environment such as its composition and processing (*11*). Extrusion is one such process which offers versatility in forming materials for various functional uses and is well suited for creating highly complex fiber products (*14*). A complex product combining cereal grains, flours, whey protein concentrates, and cashew pulp may perform as a low glycemic potential snack particularly by reducing the

Downloaded by UNIV OF DELAWARE MORRIS LIB on July 29, 2013 | http://pubs.acs.org
Publication Date (Web): July 24, 2013 | doi: 10.1021/bk-2013-1138.ch005

In Physical Methods in Food Analysis; Tunick, M., et al.;
ACS Symposium Series; American Chemical Society: Washington, DC, 2013.

rate of glucose digestion in the gut (*15*). For example, we used cassava, quinoa, and barley, as sources of carbohydrate, along with cashew pulp (*Anacardium occidentale* L., 41% fiber) as source of fiber, and whey protein concentrate (80% protein) to increase protein content in extruded, partially cooked (half-product) snacks, which were subsequently fully cooked by baking (*16*). Such new foods could be developed to address issues such as obesity by understanding how rapidly the starch-protein complexes dissolved, assimilated, and their effects in managing obesity and metabolic syndrome diseases (*17*).

Downloaded by UNIV OF DELAWARE MORRIS LIB on July 29, 2013 | http://pubs.acs.org
Publication Date (Web): July 24, 2013 | doi: 10.1021/bk-2013-1138.ch005

Materials and Methods

Materials

Malted barley flour (10% moisture, 2% fat, 14% protein, 1.5% ash, 1.5% non soluble fiber, carbohydrate by difference) was purchased from ConAgra Foods (Omaha, NE). Commercial tapioca pearl made from cassava starch (13% moisture, 1% fat, 1% protein, 1% ash, 3% non soluble fiber, carbohydrate by difference) with small particles ranging from 1 – 2 mm was received gratis from AKFP (American Key Food Products, Closter, NJ). Degermed medium yellow cornmeal (12% moisture, 1% fat, 8% protein, 1% ash, 1% non soluble fiber, carbohydrate by difference) was purchased from AGRICOR, Inc. (Marion, IN). Quinoa, a whole grain grown in the high Andes of South America (11% moisture, 7% fat, 16% protein, 3% ash, 4% non soluble fiber, carbohydrate by difference) was purchased from Quinoa Corporation (Gardena, CA). Whey Protein Concentrate (WPC80), (5% moisture, 8% fat, 80% protein, 4% ash, 0% non soluble fiber, carbohydrate by difference) was purchased from Davisco Foods International, Inc. (Eden Prairie, MN). Cashew pulp (Dwarf cashew variety developed by Embrapa, Brazil Ministry of Agriculture, *Anacardium occidentale* L.), received from Embrapa Food Technology (Rio de Janeiro, Brazil), was prepared from cashew fruits purchased from Nolem Comercial Importadora e Exportadora S.A. (Fortaleza, Brasil; www.nolem.com.br). The cashew fruits were stored in plastic trays at ~10°C. After unpacking and nut removal, cashew "apples" fruit portion were soaked in a 30 ppm chlorine solution for 20 min before pulverization using a Geiger UM 12 cutter (Pinhais, Brazil). The pulp was separated from the juice with a Bonina 025 DF Itametal de-pulping machine (Itabuna, Brazil) fitted with a 0.6 mm aperture sieve. The pulp was dried at 60°C for 24 h in an Embrapa patented electric fruit fan dryer (Brazil #: MU 8302917-6) (Rio de Janeiro, Brazil). Dried pulp with 7% moisture was milled in a TREU hammer/knife mill (Rio de Janeiro, Brazil) fitted with a 0.8 mm sieve. The resulting cashew pulp (CP) (5% moisture, 1.5% fat, 9% protein, 1.7% ash, 41% non soluble fiber, carbohydrate by difference) was blended with the barley, cassava, corn, or quinoa for extrusion of products. The proximate compositions of the ingredient are presented in Table I.

Table I. Proximate composition of starch materials blended with whey protein concentrate (W) and cashew pulp (C)

Product[1]	*Dry matter (g)*	*Protein (%)*	*Fat (%)*	*Ash (%)*	*Fiber (%)*
Barley	92.2	13.4	2.1	1.4	0.8
Barley_W	92.5	19.6	2.6	1.4	0.5
Barley_W_C	92.4	18.6	2.3	1.5	1.6
Cassava	90.0	1.4	0.5	0.4	1.0
Cassava_W	90.0	9.8	1.0	0.6	0.9
Cassava_W_C	90.1	6.5	0.9	0.9	2.4
Corn	92.3	6.6	1.4	0.0	0.0
Corn_W	92.3	14.9	1.3	0.4	0.0
Corn_W_C	92.8	16.3	2.5	0.8	1.6
Quinoa	91.9	13.2	6.8	2.4	0.6
Quinoa_W	92.4	21.5	6.8	2.0	1.0
Quinoa_W_C	92.4	22.2	7.1	2.2	2.2

[1] _W: Product with whey protein concentrate: WPC80 blended in at 12.5 wt%; *_W_C: Product with whey protein concentrate: WPC80 blended in at 12.5 wt%, and cashew pulp: CP blended in at 12.5 wt%.

Downloaded by UNIV OF DELAWARE MORRIS LIB on July 29, 2013 | http://pubs.acs.org
Publication Date (Web): July 24, 2013 | doi: 10.1021/bk-2013-1138.ch005

Extrusion Processing

A ZSK-30 twin screw extruder (Krupp Werner Pfleiderer Co., Ramsey, NJ) with a smooth barrel was used. The extruder has nine zones, and the effective forming zone temperatures were set to 100, 90, 70 and 60°C, respectively, for zones 6, 7, 8, and 9. Zones 1 to 2 were set to 35°C, 3 to 50°C, 4 to 80 and 5 to 90°C. Melt temperature was monitored behind the die. The die plate was fitted with a single flat die of 3 × 30 mm. The screw elements were selected to provide low shear at 300 rpm; the screw profile was published by Onwulata et al. (*18*). Feed was conveyed into the extruder with a series 6300 digital feeder, type T-35 twin screw volumetric feeder (K-tron Corp., Pitman, NJ). The feed screw speed was set at 600 rpm, corresponding to a rate of 6.3 kg/h for all products. Water was added into the extruder at the rate of 1.0 L/h with an electromagnetic dosing pump (Milton Roy, Acton, MA). Half-products were collected after 25 min of processing, dried in a laboratory oven at 60°C for 10 min, and stored at 20°C until thawed at ambient temperature, and analyzed (*16*).

In Physical Methods in Food Analysis; Tunick, M., et al.;
ACS Symposium Series; American Chemical Society: Washington, DC, 2013.

Moisture Content

Moisture content was measured as per Method #925.09, AOAC, 1998, using a vacuum oven (*19*).

Glycemic Index

The *in vitro* rate of the digestion of ground specimens of barley, cassava, corn or quinoa and their blends with WPC80 and CP were measured using methods described by Englyst et al. (*20*), to determine rapidly available glucose (RAG), glucose available in 20 min, and slowly available glucose (SAG), glucose available in 120 min. RAG and SAG were used as *in vitro* predictors of the glycemic response of food formulations.

The chemometric hydrolysis methods are described in detail by Englyst et al. (*21*). For the hydrolysis, 0.8 to 1.5 g milled specimen was incubated with enzyme cocktail consisting of 2.8 mL amyloglucosidase (Sigma Aldrich, St. Louis, MO) and 8.0 ml deionized water (140 AGU/ml amyloglucosidase), 3.0 g pancreatin (Sigma Aldrich, St. Louis, MO), and 20 mL sodium acetate buffer (prepared by dissolving 16.6 g sodium acetate trihydrate (Sigma Aldrich, St. Louis, MO) in 250 mL saturated benzoic acid and made up with deionized water to 1 L. RAG was measured with 0.5 ml hydrolysate removed after 20 min. incubation at 37°C. Another 0.5 mL was removed after 120 min. incubation at 37°C for determining SAG. RAG values are highly correlated to the glycemic index when tested against human subjects (*22*, *23*). After the hydrolysis and digestion procedure, glucose values for RAG and SAG were determined using YSI analyzer model 2700 Select (YSI Life Sciences, Yellow Springs, OH). Glycemic potential was determined as the ratio of glucose in approximately 1 g carbohydrate in dry basis (*22*). Glycemic potential of extruded samples was determined through digestive dissolution. The digestive dissolution media for gastric and intestinal simulation was prepared with enzymes according to Tedeschi et al. (*24*).

Confocal Laser Scanning Microscopy

For confocal laser scanning microscopy (CSLM), extruded half products (4 × 10 mm) were immersed in 20 mL aliquots of 2.5% glutaraldehdye-0.1 M imidazole solution (pH 7.0), to crosslink the protein components and amplify autofluorescence, then stored in sealed vials for 2 h. For imaging, pieces of the products were transferred to MatTek microwell dishes (MatTek Corp., Ashland, MA) and mounted on the stage of a model IRBE optical microscope system equipped with a 20× lens and coupled to a model TCS NT/SP confocal scanner head (Leica Microsystems, Exton, PA). Samples were illuminated with the 488 nm line of an Argon laser and reflection was collected in one channel, green autofluorescence (500 – 540 nm) and in some cases yellow-orange fluorescence (580 – 620 nm) from Nile Red staining was collected in a second and third channel. Overlays of the two or three channels were visualized in extended focus images to resolve the arrangement of components in the powder particles.

Downloaded by UNIV OF DELAWARE MORRIS LIB on July 29, 2013 | http://pubs.acs.org
Publication Date (Web): July 24, 2013 | doi: 10.1021/bk-2013-1138.ch005

Downloaded by UNIV OF DELAWARE MORRIS LIB on July 29, 2013 | http://pubs.acs.org
Publication Date (Web): July 24, 2013 | doi: 10.1021/bk-2013-1138.ch005

Results and Discussion

Cassava, Barley, Corn, and Quinoa

The physical characteristics of the extruded half- and finished-products depended on the carbohydrate source. Extrusion increased solubility of cassava and corn, but not quinoa half-products. WAI increased only for all products. Extrusion increased peak and breakdown viscosity for quinoa and cassava, but adding WPC80 reduced them moderately. Combining WPC80 and CP reduced viscosity most significantly ($P<0.05$). Adding WPC80 and CP improved viscosity properties while extrusion decreased viscosity. Gelatinization temperatures ranging from 100 to 160°C resulted in varying gelation, for cassava (90.3%), quinoa (57.9%), corn (52.0%), and cassava (42.0%). Depending on the structure of material, protein or starch, or type of media, dissolution rates may affect potential glycemic values of foods. Foods can be formulated with whey protein concentrate (WPC) and cashew pulp fiber (CPF) to reduce overall starch content are shown in Figure 1.

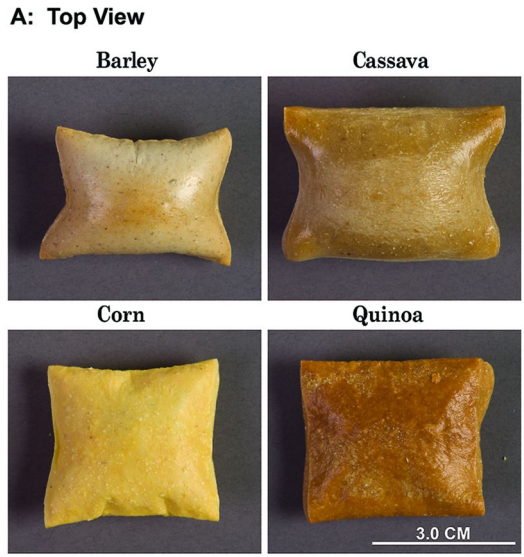

Figure 1. Top view photographs of extruded and baked products containing whey protein concentrate, 80% protein (WPC80), and Cashew Pulp (CP) Barley, Cassava, Corn, and Quinoa.

Glycemic potential was characterized by the rapidly available glucose determined after 20 min (RAG), or the slowly available glucose determined after 120 min (SAG). The food models were barley, cassava, corn meal and quinoa blended with WPC (12.5 wt%) or with CPF (12.5 wt%). The products' rapidly

In Physical Methods in Food Analysis; Tunick, M., et al.;
ACS Symposium Series; American Chemical Society: Washington, DC, 2013.

available glucose values or potential glycemic index were: quinoa (70%), barley (61%), corn (54%), and cassava (48%). Adding WPC with or without CPF improved the glycemic potential values for barley and quinoa from 61 to 77% (Table II). Adding WPC or CPF had no effect on some products such as corn. For low-glycemic product application, mixtures of corn meal, barley flour, quinoa, and cashew pulp or other starches in proportions can help alleviate sucrose-surge stress and may help fight obesity by boosting satiety.

Glycemic potential values were starch-source dependent, meaning that the response depended on the choice of grain or tuber selected. Inclusion of WPC or CPF in some cases decreased the potential glycemic indices RAG or SAG. Ultimately, in some products like cassava with WPC or CPF, RAG may increase, but SAG may decrease. Clearly, the solubility and gelatinization of each starch source differed, and how rapidly or slowly the glucose was digested depended on those responses. The effect of adding WPC or CPF depended on the mode and type of interaction of starch, protein, and fiber. Adding WPC and CPF decreased RAG in barley and corn, neutral to quinoa, and increased RAG for cassava products as shown in Figure 2. Each starch source needs independent study to determine its characteristic interaction effects and glycemic potential within a given dissolution medium.

Downloaded by UNIV OF DELAWARE MORRIS LIB on July 29, 2013 | http://pubs.acs.org
Publication Date (Web): July 24, 2013 | doi: 10.1021/bk-2013-1138.ch005

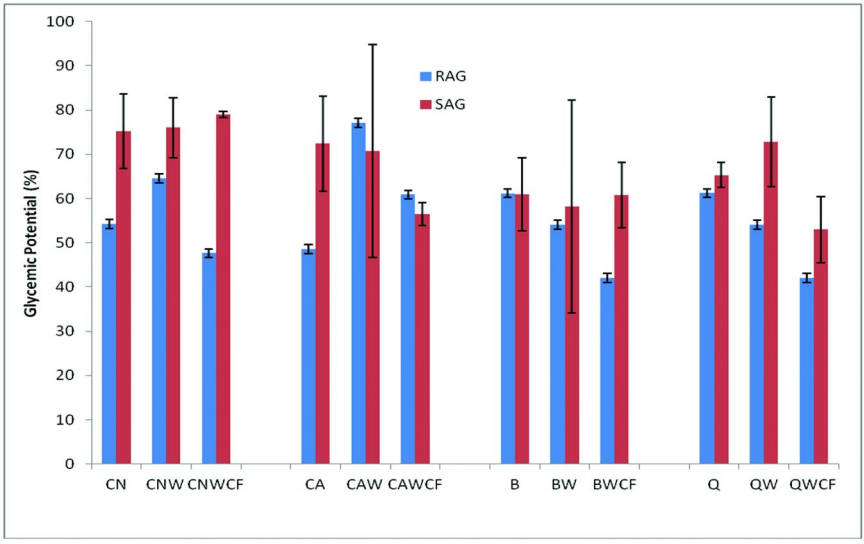

Figure 2. Comparative histograms of the glycemic potential of corn (CN), cassava (CA), barley (B), and quinoa (Q) with whey protein concentrate (W) and cashew fiber (CF), showing both rapidly available glucose (RAG) and slowly available glucose (SAG).

In Physical Methods in Food Analysis; Tunick, M., et al.;
ACS Symposium Series; American Chemical Society: Washington, DC, 2013.

Table II. Proximate composition of starch materials blended with whey protein concentrate (W) and cashew pulp (C)

Product[1]	*Moisture (%)*	*Rapidly Available Glucose*	*Slowly Available Glucose*
Barley	92.2	61.2	60.9
Barley_W	92.5	54.1	58.2
Barley_W_C	92.4	42.0	60.8
Cassava	90.0	54.3	75.2
Cassava_W	90.0	54.6	76.0
Cassava_W_C	90.1	47.6	79.0
Corn	92.3	48.5	72.4
Corn_W	92.3	77.1	70.7
Corn_W_C	92.8	60.9	56.5
Quinoa	91.9	70.3	65.3
Quinoa_W	92.4	69.5	72.8
Quinoa_W_C	92.4	59.6	53.0

[1] _W: Product with whey protein concentrate: WPC80 blended in at 12.5 wt%; _W_C: Product with whey protein concentrate: WPC80 blended in at 12.5 wt%, and cashew pulp: CP blended in at 12.5 wt%. Mean values in a given column with no letter in common are significantly different (P<0.05) by the Bonferroni LSD technique.

There are health benefits from eating products made with whole grains, such as improving atherosclerotic cardiovascular diseases and decreasing body weight (*25*). These health benefits are consistent with epidemiologic studies showing similar effects with incorporating cereal fibers in foods (*26*). Blending and extruding carbohydrate products with whey proteins and fiber results in widely varying physical property responses such as moisture, solubility and water absorption, mainly from interaction or interference of the blended materials with the starch matrix (*27*). Our results also showed similar effects. For example, with corn meal, adding WPC80 with or without CP increased moisture, and decreased solubility; but with cassava, there was a small decrease in moisture and a big increase in solubility. Solubility decreased for barley products. These different responses may be due to varying chemical and physical interactions occurring for extrusion, particularly as the moisture available to protein and starch during gelatinization and denaturation decreased. Diminishing available moisture for denaturation and gelatinization may account for the reduction or increase in percent gelatinization (*16*). Allen et al. (2007) showed that protein concentration and starch type (corn starch or pre-gelatinized waxy starch) affected the water absorption index and water-soluble carbohydrate significantly, and that a covalent complex formed between amylose and whey protein (*28*). Extrusion lowers the

Downloaded by UNIV OF DELAWARE MORRIS LIB on July 29, 2013 | http://pubs.acs.org
Publication Date (Web): July 24, 2013 | doi: 10.1021/bk-2013-1138.ch005

water absorption water vapor due to decreased specific surface area associated with increasing expansion; this resulted in new structures formed. The new structures formed exhibited increased water vapor sorption capacity and specific surface area (*29*).

Confocal Microscopy

In Figure 3, the confocal laser scanning images of dyed extruded barley showing both starch (red) and protein (autofluorescence green). The intensity of the protein follows in increasing order with percent protein (data not shown). Correspondingly, as the protein content of the formulation increased with the addition of WPC80 the green autofluorescence increases. A typical image and material distribution in extruded products is shown for cassava (Figure 4). Figure 4A is the non extruded cassava flour; 4B is the extruded cassava with WPC80, showing directional flow patterns from extrusion shear plane and increased green autofluorescence from proteins, and extruded cassava containing both WPC80 and CP, showing large green autofluorescence bodies and more fiber-like structures from CP. Images containing CP have increased bright yellow areas that correspond to areas where protein, starch, and CP, comingled.

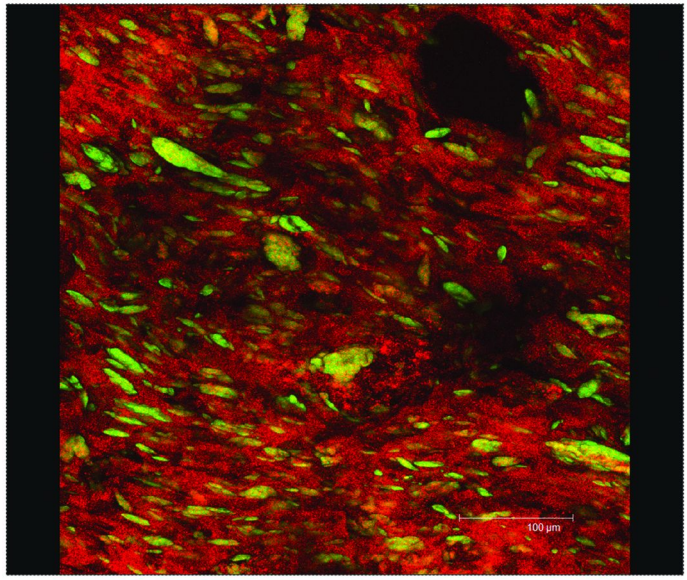

Figure 3. Confocal scanning laser micrograph of extruded partially-cooked (half-product) barley with whey protein concentrate, 80% protein (WPC80), and Cashew Pulp (CP); showing distribution of protein bodies (green autofluorescence), starch (red continuous matrix), and protein-starch complex (bright & dull yellow), and CP fiber as long slender bright yellow lines. Intensity of coloration is associated with concentration of the component.

Downloaded by UNIV OF DELAWARE MORRIS LIB on July 29, 2013 | http://pubs.acs.org
Publication Date (Web): July 24, 2013 | doi: 10.1021/bk-2013-1138.ch005

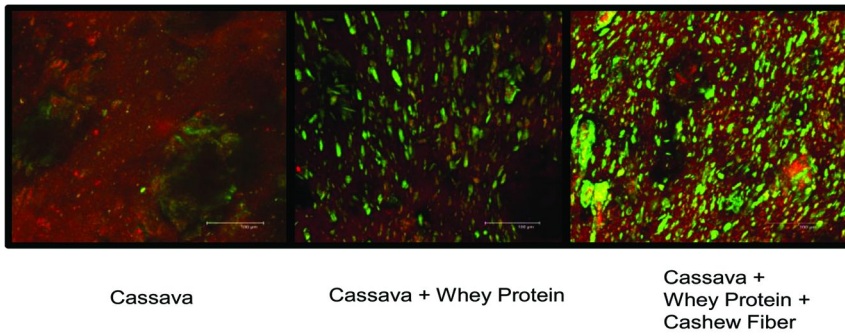

Figure 4. Confocal scanning laser micrographs of extruded cassava (left), Cassava with whey protein concentrate, 80% protein (WPC80), (middle) and cassava with WPC80 and Cashew Pulp (CP) (right); showing distribution of protein bodies (green autofluorescence), starch (red continuous matrix), and protein-starch complex (bright & dull yellow), and CP fiber as long slender bright yellow lines. Intensity of coloration is associated with concentration of the component.

Downloaded by UNIV OF DELAWARE MORRIS LIB on July 29, 2013 | http://pubs.acs.org
Publication Date (Web): July 24, 2013 | doi: 10.1021/bk-2013-1138.ch005

Dietary carbohydrates are digested at different rates in the human small intestine and depending on the botanical source of the starch, the rate at which blood glucose is elevated differs (*23*). In one review, it was shown that slowly absorbed carbohydrate produces beneficial effects on managing chronic diseases, and that highly processed carbohydrates produce fast-releasing sugars, resulting in higher blood glucose levels and greater insulin demand (*30*). Nutrition researchers have developed and correlated *in vitro* digestion methods that estimate or predict the glycemic response of starch based food products using *in vivo* glycemic responses (*23*). For example, Bornet (1989) showed excellent correlation of the percentage of starch hydrolysis *in vitro* to the *in vivo* glycemic response after 30 min. Epidemiological studies show strong links between type 2 diabetes and other metabolic syndromes to consumption of products exhibiting rapidly available glucose, RAG (*31*). Looking strictly at the RAG potential glycemic index for cassava, with glycemic value of 48, would seem to offer an advantage, but including WPC80 negates that benefit, increasing RAG to 77. Adding WPC80 and CP to cassava increased RAG to 61, as well. However, with barley (61) or corn (54), adding WPC80 and CP reduced RAG to 42 for barley and 48 for corn. Englyst et al. (1999) determined that rapidly available glucose (RAG) is an excellent predictor of the glycemic response and explains approximately 61% of the glycemic response measured *in vivo* (*23*). RAG is highly correlated to the glycemic index when tested against human subjects (*22*). For instance, the addition of lentil flour to an extruded snack product lowered the glycemic index, RAG (*32*). Others have found high correlations of *in vitro* starch hydrolysis to the glycemic index and response (*33*). As seen in Figure 4, it is postulated that the

presence of proteins that can complex with starch reduces the rate of breakdown of starch, lowering the glycemic index. Similarly, the presence of fiber may encapsulate or bind starch limiting enzyme access and thereby reducing glycemic index as well (*34*).

Conclusion

Adding whey protein concentrate (WPC80) and cashew pulp (CP) to extruded snacks can reduce overall carbohydrate content. In this study, barley, cassava, corn meal and quinoa were blended with WPC80 (12.5 wt%) or with CP (12.5 wt%), then extruded and baked. The rapidly available glucose values or potential glycemic index were: quinoa (70%), barley (61%), corn (54%), and cassava (48%). Adding WPC80 with or without CP improved the glycemic potential values for barley and quinoa, but not for cassava which increased from 61 to 77%. Adding WPC80 or CP had no effect on corn products. The physical properties, and glycemic potential responses observed for the selected extrusion process conditions and inclusion of WPC80 or CP to the products was carbohydrate-source dependent. Clearly, the solubility and gelatinization of each carbohydrate source differed, and how rapidly or slowly the glucose was digested depended on those responses. The effect of adding WPC80 or CP depended on the interaction of starch, protein and fiber. Adding WPC80 and CP was positive (decreasing RAG) in barley and corn, neutral to quinoa, and negative (increasing RAG) for cassava products. Each carbohydrate source needs independent study for its characteristic interactions and affects. For low-glycemic product application, mixtures of corn meal, barley flour, quinoa, and cashew pulp or other starches in proportions needed to create expanded snack products can help alleviate sucrose-surge stress and may help fight obesity. Product quality characteristics are carbohydrate-source dependent, meaning that the response depends on the choice of grain or tuber selected. Inclusion of WPC80 or CP may or may not decrease the potential glycemic indices RAG or SAG. Ultimately, in some products like cassava with WPC80 or CP, the initial glucose surge (20 min), RAG, may increase, but after 120 min, SAG, decreases.

Downloaded by UNIV OF DELAWARE MORRIS LIB on July 29, 2013 | http://pubs.acs.org
Publication Date (Web): July 24, 2013 | doi: 10.1021/bk-2013-1138.ch005

Acknowledgments

The authors thank Eric Tilman for the extrusion processing, Peter Cooke and Guoping Bao for performing the SEM experiments, and John Phillips for the statistical analyses. Mention of trade names and commercial products in this publication is solely for the purpose of providing information and does not imply recommendation or endorsement by the U.S. Department of Agriculture. USDA is an equal opportunity provider and employer.

References

1. McClellan, F. *The Lancet* **2002**, *359*, 1412.
2. Drewnoski, A. *Nutrition Reviews* **2009**, *67* (Suppl), S36–S39.
3. Sothern, M. S. *Nutrition* **2004**, *20*, 704–708.
4. Houston, D. K.; Nicklas, B. J.; Zizza, C. A. *J. Am. Diet. Assoc.* **2009**, *109*, 1886–1895.
5. Esfahani, A.; Wong, J. M. W.; Mirrahimi, A.; Villa, C. R.; Kendall, C. W. C. *Life* **2011**, *63*, 7–13.
6. Jenkins, D. J.; Wolever, T. M.; Taylor, R. H.; Barker, H.; Fielden, H.; Baldwin, J. M.; Bowling, A. C.; Newman, H. C.; Jenkins, A. L.; Goff, D. V. *Am. J. Clin. Nutr.* **1981**, *34*, 362–366.
7. Bjorck, I.; Granfeldt, Y.; Liljeberg, H.; Tovar, J.; Asp, N-G. *Am J Clin Nutr* **1994**, *59*, 699S–705S.
8. Barclay, A. W.; Petocz, P.; McMillan-Price, J.; Flood, V. M.; Prvan, T.; Mitchell, P.; Brand-Miller, J. C. *Am. J. Clin. Nutr.* **2008**, *87*, 627–637.
9. Esfahani, A.; Wong, J. M.; Mirrahimi, A.; Srichaikul, K.; Jenkins, D. J.; Kendall, C. W. *J. Am. Coll. Nutr.* **2009**, *28* (Suppl), 439S–445S.
10. Barclay, A. W.; Petocz, P.; McMillan-Price, J.; Flood, V. M.; Prvan, T.; Mitchell, P.; Brand-Miller, J. C. *Am. J. Clin. Nutr.* **2008**, *87*, 627–637.
11. Kong, F.; Singh, R. P. *J. Food Sci.* **2008**, *73*, R67–R80.
12. Yong, L. Z.; Chan, C. H.; Garcia, C.; Sopade, P. A. *Carb. Polymers* **2011**, *84*, 162–172.
13. Wallace, A. J.; Monro, J. A.; Hedderley, D. I.; Willis, J. A.; Scott, R. S. *Nutr. Res.* **2006**, *26*, 47–52.
14. Breitenbach, J. *European J. Pharmaceutics and Biopharmaceutics* **2002**, *54*, 107–117.
15. Ayago-Ayerdi, S. G.; Tovar, J.; Osorio-Diaz, P.; Paredes-Lopez, O.; Bello-Perez, L. A. *J. Agric. Food Chem.* **2005**, *53*, 1281–1285.
16. Onwulata, C. I.; Thomas, A. E.; Cooke, P. H.; Phillips, J. G.; Carvalho, C. W. P.; Ascheri, J. L. R.; Tomasula, P. M. *Int. J. Food Prop.* **2010**, *13*, 1–22.
17. Te Morenga, L. A.; Levers, M. T.; Williams, S. M.; Brown, R. C.; Mann *Nutr. J.* **2011**, *10* (40), 1–9.
18. Onwulata, C. I.; Konstance, R. P.; Smith, P. W.; Holsinger, V. H. *J. Food Sci.* **1998**, *63*, 814–818.
19. AOAC. 2000. *Official Methods of Analysis, 14th ed.* Association of Official Analytical Chemists, Washington, DC.
20. Englyst, H. N.; Veenstra, J.; Hudson, G. J. *Brit. J. Nutr.* **1996**, *75*, 327–337.
21. Englyst, H. N.; Kingman, S. M.; Cummings, J. H. *J. Clin. Nutr.* **1992**, *46* (Suppl. 2), S33–S50.
22. Englyst, K. N.; Vinoy, S.; Englyst, H. N.; Lang, V. *Brit. J. Nutr.* **2003**, *89*, 329–339.
23. Englyst, K. N.; Englyst, H. N.; Hudson, G. J.; Cole, T. J.; Cummings, J. H. *Am. J. Clin Nutr.* **1999**, *69*, 448–454.
24. Tedeschi, C.; Clement, V.; Rouvet, M.; Valles-Pamies, B. *Food Hydrocolloids* **2009**, *23*, 1228–1235.

Downloaded by UNIV OF DELAWARE MORRIS LIB on July 29, 2013 | http://pubs.acs.org
Publication Date (Web): July 24, 2013 | doi: 10.1021/bk-2013-1138.ch005

25. Katcher, H. I.; Legro, R. S.; Kunselman, A. R.; Gillies, P. J.; Demers, L. M.; Bagshaw, D. M.; Kris-Etherton, P. M. *Am. J. Clin. Nutr.* **2008**, *87*, 79–90.
26. Jacobs, D. R., Jr.; Gallaher, D. D. *Curr. Ather. Rep.* **2004**, *6*, 415–423.
27. Matthey, F. P.; Hanna, M. A. *Lebens. -Wiss. Technol.* **1997**, *30* (4), 359–366.
28. Allen, K. E.; Carpenter, C. E.; Walsh, M. K. *Int. J. Food Sci. & Technol.* **2007**, *42*, 953–960.
29. Wlodarczyk-Stasiak, M.; Jamroz, J. *J. Food Eng.* **2008**, *85*, 580–589.
30. Augustin, I. S.; Franceschi, S.; Jenkins, D. J. A.; Kendall, C. W. C.; Vecchia, C. L. *Eur. J Clin. Nutr.* **2002**, *56*, 1049–1071.
31. Salmeron, J.; Ascherio, A.; Rimm, E. B.; Coldtz, G. A.; Spiegleman, D.; Jenkins, D. J.; Wing, A. L.; Willett, W. C. *Diabetes Care* **1997**, *20*, 545–550.
32. Hardacre, A. K.; Clark, S. M.; Riviere, S.; Monro, J. A.; Hawkins, A. J. *J. Texture Studies* **2006**, *37*, 94–111.
33. Seal, C. J.; Daly, M. E.; Thomas, L. C.; Bal, W.; Birkett, A. M.; Jeffcoat, R.; Mathers, J. C. *Brit. J. Nutr.* **2003**, *90*, 853–864.
34. Solah, A. S.; Kerr, D. A.; Adikara, C. D.; Meng, X.; Binns, C. W.; Zhu, K.; Devine, A.; Prince, R. L. *Appetite* **2010***doi:*10.1016/j.appet.2010.01.019.

Downloaded by UNIV OF DELAWARE MORRIS LIB on July 29, 2013 | http://pubs.acs.org
Publication Date (Web): July 24, 2013 | doi: 10.1021/bk-2013-1138.ch005

Downloaded by MICHIGAN STATE UNIV on July 29, 2013 | http://pubs.acs.org
Publication Date (Web): July 24, 2013 | doi: 10.1021/bk-2013-1138.ch006

Chapter 6

Progress in Analyses of Citrus Flavonoids

Shiming Li,*[,1] Chih-Yu Lo,[2] and Chi-Tang Ho[1]

[1]Department of Food Science, Rutgers University, 65 Dudley Road, New Brunswick, New Jersey 08901, U.S.A.
[2]Department of Food Science, National Chiayi University, No. 300 Syuefu Road, Chiayi 60004, Taiwan
***E-mail: shiming@rutgers.edu.**

The analyses of citrus flavonoids have been progressed well in recent years due to accelerated and fruitful research in the field of biological activity and health beneficial effects of compounds from citrus genus, particularly methylated flavonoids from citrus peels, such as polymethoxyflavones (PMFs) and 5-hydroxylated polymethoxyflavones (5-OHPMFs). Recent research results and broad application of PMFs and 5-OHPMFs in the areas of nutraceuticals, pharmaceuticals, and functional foods have prompted the identification and quantification of these flavonoids, which serves the basis of characterization and is of great significance. This chapter summarizes the development of characterization of PMFs and 5-OHPMFs from random study to systematic identification to validated and accurate measurement in citrus peels and other matrices containing methylated flavones.

Introduction

Citrus peels provide a rich and perhaps the sole source of polymethoxyflavones (PMFs) and other flavonoids. It has been found in the past decades that PMFs are a group of flavonoid compounds having many health beneficial properties, such as functioning as anti-tumor and cancer chemopreventive agents, antioxidant activity, reduction of DNA damage, suppression of tumor growth by activating apoptosis or inhibiting intracellular signaling thus blocking cell cycle progression (*1*, *2*). PMFs from citrus peel extract (CPE) also exhibit anti-inflammatory activity both at the level of

© 2013 American Chemical Society
In Physical Methods in Food Analysis; Tunick, M., et al.;
ACS Symposium Series; American Chemical Society: Washington, DC, 2013.

gene expression and at the level of enzyme activity (*3–10*), as well as potent efficacy in animal models (*11*). Much more research regarding the biological activity of PMFs and 5-hydroxylated polymethoxyflavones (5-OHPMFs) have been illustrated in literature publications and more explorations of PMFs and 5-OHPMFs in health promoting properties are undergoing at an accelerated pace.

Table I. Most Common PMFs and 5-Demethylated PMFs in Citrus Peels

PMFs	*Structure*	5-OHPMFs	*Structure*
Tangeretin	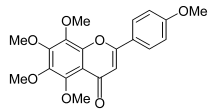	5-Demethyl-tangeretin	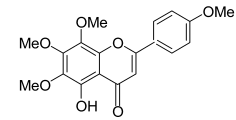
Sinensetin	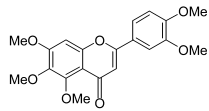	5-Demethyl-sinensetin	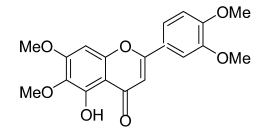
Nobiletin	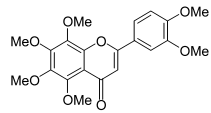	5-Demethyl-nobiletin	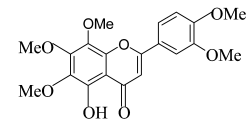
5,6,7,4'-Tetrameth-oxyflavone	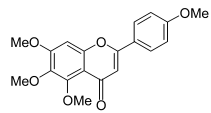	5-Hydroxy-6,7,4'-trimethoxyflavone	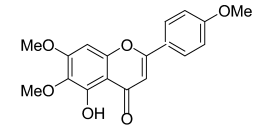
3,5,6,7,8,3',4'-Heptameth-oxyflavone	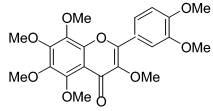	5-Hydroxy-3,6,7,8,3',4'-hexamethoxy-flavone	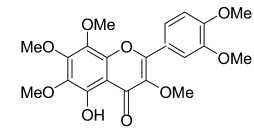
3,5,6,7,3',4'-Hexameth-oxyflavone	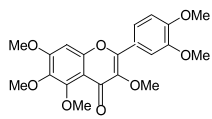	5-Hydroxy-3,6,7,3',4'-pentamethoxy-flavone	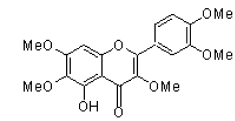

However, to ensure the adequate consistency and reproducibility of efficacious performance in developing therapeutic nutritional products with citrus peel extracts (CPE) in which PMFs and 5-OHPMFs have been mainly identified

In Physical Methods in Food Analysis; Tunick, M., et al.;
ACS Symposium Series; American Chemical Society: Washington, DC, 2013.

Downloaded by MICHIGAN STATE UNIV on July 29, 2013 | http://pubs.acs.org
Publication Date (Web): July 24, 2013 | doi: 10.1021/bk-2013-1138.ch006

as bioactive components, the multimolecular containing CPE must be rigorously evaluated and chemically characterized. Owing to the polymolecular complicity and structural proximity of citrus PMFs and 5-OHPMFs, the research in the field of chemical analysis of CPE has been plagued by inadequate chemical characterization and documentation, which raises many issues and difficulties in comparing bioactivity results across various studies. With the assistance of modern instruments in analytical chemistry and molecular methods existing nowadays, sufficient separation and identification of multiple components can be achieved to avoid this limitation. Hereby, we review the approaches of chemical evaluation of PMFs and 5-OHPMFs and highlight challenges to the field of chemical methods for characterization and quality control for future studies of bioactive natural products.

Downloaded by MICHIGAN STATE UNIV on July 29, 2013 | http://pubs.acs.org
Publication Date (Web): July 24, 2013 | doi: 10.1021/bk-2013-1138.ch006

Quantitative Analysis of Polymethoxyflavones

The separation methods in the analysis of the PMF content in various citrus tissues include GC (*12*), supercritical fluid chromatography (SFC) (*13*, *14*). and HPLC (*15*–*17*). The successful separation of six major PMFs in citrus oil were obtained using GC at high temperature (~310 °C) and were identified by GC-MS, but no quantitative result was reported (*12*). SFC separation with liquid CO_2 and modifier methanol on a packed silica column resulted in good resolution and quantitative analysis for some PMFs in citrus oils (*13*, *14*). Many studies have been reported on the determination of PMFs by HPLC on normal phase or reverse phase (*15*–*17*). Hyphenated HPLC-MS and HPLC-NMR have also been used for the structure elucidation of citrus PMFs.

The validated analytical method for the quantitative analysis of six major PMFs in CPE was pioneered by Wang et al. in 2008 (*18*). In this research, an validated reverse phase HPLC method was successfully developed to separate and quantify the six major PMFs: 5,6,7,4′-tetramethoxyflavone, sinensetin (5,6,7,3′,4′-pentamethoxyflavone), tangeretin (5,6,7,8,4′-penta-methoxyflavone), nobiletin (5,6,7,8,3′,4′-hexaamethoxyflavone), 3,5,6,7,3′,4′-hexamethoxy-flavone, and 3,5,6,7,8,3′,4′-heptamethoxyflavone (Table I).

Due to the unknown correlation between the biological activity and the individual PMF contents in the citrus genus extract, it is of scientific and practical significance to have a validated method to measure PMFs in citrus peel or its extracts. The development of a validated HPLC method with UV detection for the quantitative analyses of the six major PMFs in citrus laid the foundation in exploring the connection between the biological testing and the quantitative analyses of citrus PMFs. The method was developed successfully for direct quantitation of six PMFs in four commercial citrus peel extracts (CPEs) (*18*). This is the first simultaneous quantitative analysis of six PMFs in citrus peel products using liquid chromatography (LC). This LC method was validated in linear range, LOD (limit of detection), LOQ (limit of quantitation), repeatability, intermediate precision and system suitability. Of this developed method, with a 5 µL injection volume, LOD was 0.15 µg/mL and LOQ was 0.5 µg/mL for all standard PMFs. This method allows for a simple and precise determination of PMFs in CPEs. In

addition, it can be readily utilized as an analytical procedure for quality control (QC) of PMFs in CPE related products. The analysis results showed that in the four commercial CPE samples, the actual measured PMF contents did not match with what the manufacturer claimed or labeled. There are big discrepancies found between the PMF content that the manufacture claimed and the content resulted from this LC analysis in individual PMF percentages and total amount of PMFs. For Instance, the actual measured total PMFs in commercial CPE D was at 20.1%, whereas 40% PMFs were claimed by the manufacturer. In contrast, commercial CPE C had 100% of total actually measured PMFs even though only 60% PMFs was claimed by the manufacturer (Table II). More importantly, the percentages and contents of individual PMFs vary across all the four commercial CPEs shown in Table II.

Therefore, the development of this LC method for PMF analysis is of critical importance in establishing a PMF profile of a particular CPE and practical usefulness in quality control to insure a constant resource of CPE marked by individual PMF content. It will bring in the near future maximum benefits in the research and CPE application in biological activity study, since the hurdle of PMF measurement has been removed and the correlation between biological activity and the profile of individual PMFs in CPE becomes feasible.

Downloaded by MICHIGAN STATE UNIV on July 29, 2013 | http://pubs.acs.org
Publication Date (Web): July 24, 2013 | doi: 10.1021/bk-2013-1138.ch006

Table II. Analysis of Six PMFs in CPEs from Different Manufacturers

PMFs	*Weight percentage (%)*			
	CPE A	*CPE B*	*CPE C*	*CPE D*
Sinensetin	3.9	3.2	1.4	1.0
Hexamethoxyflavone	4.1	3.7	0.4	-
Nobiletin	26.1	24.4	33.2	10.5
Tetramethoxyflavone	11.4	12.5	0.6	0.4
Heptamethoxyflavone	31.2	20.7	62.3	-
Tangeretin	15.4	18.1	2.8	8.2
Total% of measured PMFs	**92.1**	**82.6**	**100.7**	**20.1**
Claimed% of total PMFs	**70**	**70**	**60**	**40**

Separation of 5-Hydroxylated Polymethoxyflavones

5-Hydroxylated polymethoxyflavones (5-OHPMFs) have emerged recently because of their potent biological activity compared to their parent polymethoxyflavones (*1*, *8*, *19–24*). However, the analyses of 5-OHPMFs have not been reported until the year 2010 (*25*, *26*) In the analyses of six

5-hydroxylated PMFs, we reported the development of an HPLC-UV analytical method used in the quantification of six 5-OHPMFs in commercially processed and non-processed orange peel extracts (OPE) or other materials which contain 5-demethyated PMFs. The six 5-OHPMFs used as standards in this research were 5-hydroxy-6,7,4′-trimethoxyflavone, 5-demethyltangeretin, 5-demethylsinesetin, 5-hydroxy-3,6,7,3′,4′-pentamethoxyflavone, 5-demethylnobiletin and 5-hydroxy-3,6,7,8,3′,4′-hexamethoxyflavone (*25*).

Upon the HPLC method development, the full baseline separation of the six 5-OHPMFs was obtained with a 30 min gradient elution and a mobile phase system composed of water-acetonitrile-tetrahydrofuran. The other optimized conditions were a Supelco RP-Amide C16 column, column temperature of 25°C, and an injection volume of 10 μL. In this study, linearity was studied in a certain range and detection sensitivity, LOD and LOQ, was also measured. LOD was 0.375 μg/mL for all standards except 5-demethylnobiletin (0.3 μg/mL) and LOQ was 1.25 μg/mL with an exception of 5-demethylnobiletin at 1.0 μg/mL (*25*).

Downloaded by MICHIGAN STATE UNIV on July 29, 2013 | http://pubs.acs.org
Publication Date (Web): July 24, 2013 | doi: 10.1021/bk-2013-1138.ch006

Table III. Analysis of Six 5-OHPMFs in Commercial OPEs

5-Hydroxyl PMFs	*5-OHPMFs weight percentage*				
	OPE A1	*OPE B1*	*OPE C1*	*OPE D1*	*OPE E1*
5-Demethylsinesetin	0	0.10	0.42	4.23	3.91
5-Demethylnobiletin	0	0.04	0.73	18.51	21.30
5-Hydroxy-3,6,7,3′,4′-pentamethoxyflavone	0	0	0	0.58	0.98
5-Hydroxy-3,6,7,8,3′,4′-hexamethoxyflavone	0	0	0	12.47	17.36
5-Hydroxy-6,7,4′-trimethoxyflavone	0	0	0	10.25	11.15
5-Demethyltangeretin	0	0	0	7.46	8.18
Total 5-OHPMFs	0	0.14	1.15	53.50	62.88

Five commercially available orange peel extracts (OPEs), processed or non-processed by the manufacturers, were analyzed for their individual 5-OHPMF contents. These five samples showed quite different profiles in terms of their 5-OHPMF contents and concentrations (Table III), ranging from 0 - 63%. Such differences indicate that samples may have come from different citrus species, extraction techniques, or processing procedures. OPE D1 (53.5% of 5-OHPMFs) and OPE E1 (62.9% of 5-OHPMFs) contain all six 5-OHPMFs with similar percentages of each component in both samples. The four most abundant 5-hydroxy PMFs in percentage decreasing order are 5-demethylnobiletin, 5-hydroxy-3,6,7,8,3′,4′-hexamethoxyflavone,

5-hydroxy-6,7,4′-trimethoxyflavone and 5-demethyltangeretin, which together account for 53% and 62% of the total extracts in OPE D1 and OPE E1, respectively. There are no measurable 5-OHPMFs in extract A1 and B1, only 1% of total 5-OHPMFs in OPE C1 (*25*).

With a different approach, scientists at University of Massachusetts developed a more accurate quantitative method using HPLC coupled with an electrochemical (EC) detector (*26*). Four of 5-hydroxylated PMFs were measured simultaneously at a sensitivity comparable to that of mass spectrometer (MS). The LOD reached as low as 0.65 ng/mL, i.e. ppb scale and fully capable of measuring traces of these 5-hydroxylated PMFs in citrus tissues and biofluids . Furthermore, this validated method could be very useful in nutraceutical and pharmaceutical research of the matrices containing these compounds such as in biofluids (*26*). However, the disadvantage of the EC detector application is that a free hydroxyl group must present on the benzene ring and it is prone to interference by impurities having redox potential.

Downloaded by MICHIGAN STATE UNIV on July 29, 2013 | http://pubs.acs.org
Publication Date (Web): July 24, 2013 | doi: 10.1021/bk-2013-1138.ch006

Simultaneous Measurement of Polymethoxyflavones and 5-Hydroxylated Polymethoxyflavones

Due to recent broad application of PMFs and 5-OHPMFs in medical and nutritional fields,, the validated separation with two LC methods for two divisional groups, i.e. group PMFs with one LC separation method and group of 5-OHPMFs with another analytical method, is not only time consuming, but also inconvenient and laborious to perform an analysis for both PMFs and 5-OHPMFs. We recently developed a validated method for fast separation and simultaneous quantification of six polymethoxyflavones and six 5-demethylated polymethoxyflavones with high performance liquid chromatography coupled with linear ion trap mass spectrometry (*27*). The method was fully validated in linearity, precision, accuracy and recovery. The 12 compounds in Table I, six PMFs and their 5-hydroxy counterparts, six 5-OHPMFs, were for the first time simultaneously analyzed within 20 minutes. The LOD is 0.02-0.23 μg/mL and LOQ 0.05-0.76 μg/mL. With this rapid analytical method, we further performed validation with 12 standard compounds and four of in house acid treated CPEs. The development of this analytical method laid the foundation for screening and structural characterization of PMFs and 5-OHPMFs in CPEs either naturally occurring or via the transformational conversion.

Table IV is an example of the established LC/MS^n method application in the characterization of 12 PMF type compounds (*27*). In the results of this analysis, Liucheng citrus peels contains only 6.6% of PMFs (weight percentage, Table IV). Other citrus peels, such as Ponkan, Murcott and Tonkan, contain 17.4-19.6% PMFs. It is known that with strong acid treatment, the PMFs can be transformed into 5-OHPMFs in the citrus peel extracts. 5-OHPMFs reached 30% in Ponkan citrus extracts after 5 hr, 3N hydrochloride treatment. High yield of 5-demethylnobiletin and 5-demethyltangeretin was obtained under this treatment. The current method is sufficient to satisfy the measurement of both PMFs and their corresponding 5-OHPMFs in a citrus peel matrix in one single analysis (*27*).

Downloaded by MICHIGAN STATE UNIV on July 29, 2013 | http://pubs.acs.org
Publication Date (Web): July 24, 2013 | doi: 10.1021/bk-2013-1138.ch006

Table IV. LC/MS Analysis of PMFs and 5-OHPMFs in Citrus Peel Extracts

Local name	*Total*	*Weight percentage (%) of PMFs*					
		Sines	*HexaMF*	*Nobiletin*	*TetraMF*	*HeptaMF*	*Tangeretin*
Ponkan	17.39	0	0	8.37	0	0	9.02
Liucheng	6.55	1.02	0.55	3.05	0.50	1.13	0.30
Murcott	19.38	0.53	0	12.28	0	1.61	4.96
Tonkan	19.64	0.53	0	12.73	0	3.23	3.15
		Weight percentage (%) of 5-OHPMFs					
After acid treatment	*Total*	*5-Demthyl-sinesetin*	*5-OH-pentaMF*	*5-Demethyl-nobiletin*	*5-OH-triMF*	*5-OH-hexaMF*	*5-demethyl-tangeretin*
Ponkan	30.00	0.15	0	21.33	0.82	0	7.70
Liucheng	10.95	1.82	0.40	5.61	2.40	0.34	0.38
Murcott	19.15	0.48	0	14.43	0.55	0.38	3.30
Tonkan	21.24	1.13	0	15.84	0.11	1.50	2.66

Conclusion and Perspectives

More and more evidence has shown that high content of PMFs and 5-hydroxylated PMFs existing in citrus peels and their extracts may provide reliable and economical resources in biological activity studies and development of efficacious health beneficial products.

This paper reviews the analytical methods for analyzing six major polymethoxyflavones (PMFs) and their six 5-demethylated counter parts (5-OHPMFs) ubiquitously existing in citrus genus. The previous analyses of PMFs in citrus with GC, HPLC, SFC, GC-MS, LC-MS and LC-NMR have been briefly recapitulated. The first practicably generous application of a validated reversed phase LC method in analyses of six dominant PMFs in citrus peels has been thoroughly summarized. Also in this article, the successful development of the first quantitative analysis of six 5-OHPMFs in processed or non-processed citrus peel extracts using LC method is introduced in detail. These analytical methods were validated in a linear range, LOD, LOQ, and system suitability, and they allow for a simple and accurate determination of PMFs and 5-OHPMFs separately in CPEs and other citrus products.

The most up to date robust analytical method has been developed and reviewed in this article. The validated method that can simultaneously analyze both PMFs and 5-OHPMFs, total of 12 compounds isolated in citrus genus. Overall, tremendous progress has been made in the separation of polymethoxyflavones and 5-hydroxy polymethoxyflavones in the past few years. The ultimate goal of the analytical methodology is to serve the bioassay directed efficacious compound quantitative characterization and quality control in research and product development, and to develop high quality products that have long term beneficial impact on human health and wellness.

Downloaded by MICHIGAN STATE UNIV on July 29, 2013 | http://pubs.acs.org
Publication Date (Web): July 24, 2013 | doi: 10.1021/bk-2013-1138.ch006

References

1. Li, S.; Pan, M. H.; Lo, C. Y.; Tan, D.; Wang, Y.; Shahidi, F.; Ho, C-T. *J. Funct. Foods* **2009**, *1* (2), 12.
2. Walle, T. *Semin. Cancer Biol.* **2007**, *17* (5), 354–362.
3. Manthey, J. A.; Grohmann, K.; Montanari, A.; Ash, K.; Manthey, C. L. *J. Nat. Prod.* **1999**, *62*, 441–444.
4. Murakami, A.; Shigemori, T.; Ohigashi, H. *J. Nutr.* **2005**, *135*, 2987S–2992S.
5. Lin, N.; Sato, T.; Takayama, Y.; Mimaki, Y. *Biochem. Pharmacol.* **2003**, *65*, 2065–2071.
6. Choi, S. Y.; Ko, H. C.; Ko, S. Y.; Hwang, J. H. *Biol. Pharm. Bull.* **2007**, *30*, 772–778.
7. Malterud, K. E.; Rydland, K. M. *J. Agric. Food Chem.* **2000**, *48*, 5576–5580.
8. Li, S.; Sang, S.; Pan, M. H.; Lai, C-S.; Lo, C-Y.; Dushenkov, S.; Ho, C-T. *Bioorg. Med. Chem. Lett.* **2007**, *17*, 5177–5181.
9. Murakami, A.; Nakamura, Y.; Torikai, K.; Tanaka, T. *Cancer Res.* **2000**, *60*, 5059–5066.
10. Tanaka, S.; Sato, T.; Akimoto, N.; Yano, M.; Ito, A. *Biochem. Pharmacol.* **2004**, *68*, 433–439.

11. Pan, M-H.; Li, S.; Lai, C-S.; Miyauchi, Y.; Suzawa, M.; Ho, C-T. *Food Sci. Hum. Wellness* **2012**, *1*, 65–73.
12. Stremple, P. *J. High Resolut. Chromatogr.* **1998**, *21*, 587–591.
13. Morin, P.; Gallois, A.; Richard, E.; Gaydou, E. *J. Chromatgr.* **1991**, *586*, 171–176.
14. Dugo, P.; Mondello, L.; Dugo, G.; Heaton, D. M.; Bartle, K. D.; Clifford, A. A.; Myers, P. *J. Agric. Food. Chem.* **1996**, *44*, 3900–3905.
15. Weber, B.; Hartmann, B.; Stockigt, D.; Schreiber, K.; Roloff, M.; Bertram, H.-J.; Schmidt, C. O. *J. Agric. Food. Chem.* **2006**, *54*, 274–278.
16. Manthey, J. A.; Buslig, B. S. *Proc. Fla. State Hortic. Soc.* **2003**, *116*, 410–413.
17. Heimhuber, B.; Galensa, R.; Herrmann, K. *J. Chromatogr.* **1988**, *439*, 481–483.
18. Wang, Z.; Li, S.; Ferguson, S.; Goodnow, R.; Ho, C-T. *J. Sep. Sci.* **2008**, *31*, 30–37.
19. Lai, C-S.; Li, S.; Chai, C-Y.; Lo, C-Y.; Ho, C-T.; Wang, Y-J.; Pan, M-H. *Carcinogenesis* **2007**, *28*, 2581.
20. Lai, C-S; Li, S.; Chai, C-Y.; Lo, C-Y.; Dushenkov, S.; Ho, C-T.; Pan, M-H.; Wang, Y-J. *Carcinogenesis* **2008**, *29*, 2415.
21. Li, S.; Pan, M-H.; Lai, C-S; Lo, C-Y.; Dushenkov, S.; Ho, C-T. *Bioorg. Med. Chem.* **2007**, *15*, 3381.
22. Xiao, H.; Yang, C-S.; Li, S.; Jin, H.; Ho, C-T.; Patel, T. *Mol. Nutr. Food Res.* **2009**, *53*, 398.
23. Sergeev, I. N.; Li, S.; Colby, J.; Ho, C-T.; Dushenkov, S. *Life Sci.* **2005**, *80*, 245.
24. Sergeev, I. N.; Ho, C-T.; Li, S.; Colby, J.; Ho; Dushenkov, S. *Mol. Nutr. Food Res.* **2007**, *51*, 1478.
25. Li, S.; Wang, Y.; Wang, Z.; Xiao, H.; Lo, C. Y.; Rawson, N.; Ho, C. T. *Biomed. Chromatogr.* **2010**, *24*, 838–845.
26. Dong, P.; Qiu, P.; Zhu, Y.; Li, S.; Ho, C. T.; McClements, D. J.; Xiao, H. *J. Chromatogr., A* **2010**, *1217*, 642–647.
27. Lin, Y-S.; Li, S.; Ho, C-T.; Lo, C-Y. *J. Agric. Food. Chem.* **2012**, *60*, 12082–12087.

Downloaded by MICHIGAN STATE UNIV on July 29, 2013 | http://pubs.acs.org
Publication Date (Web): July 24, 2013 | doi: 10.1021/bk-2013-1138.ch006

Downloaded by UNIV OF MICHIGAN ANN ARBOR on July 29, 2013 | http://pubs.acs.org
Publication Date (Web): July 24, 2013 | doi: 10.1021/bk-2013-1138.ch007

Chapter 7

Using Temperature Sweeps To Investigate Rheology of Bioplastics

Michael H. Tunick,*[,1] Charles I. Onwulata,[1] and Peter H. Cooke[2]

[1]U.S. Department of Agriculture, Agricultural Research Service, Eastern Regional Research Center, Dairy & Functional Foods Research Unit, 600 E. Mermaid Lane, Wyndmoor, Pennsylvania 19038
[2]Present address: New Mexico State University, P.O. Box 30001, Las Cruces, New Mexico 88003
***E-mail: Michael.Tunick@ars.usda.gov.**

The viscoelastic properties and microstructure of 20 g per 100 g solutions of calcium caseinate, egg albumin, fish protein isolate, soy protein isolate, wheat gluten, and whey protein isolate were determined under the same heating conditions. Scanning electron microscopy revealed microstructural transformations indicative of changes in bonding that would be expected if the proteins were extruded. Values for elastic modulus (G′) obtained from temperature sweeps from 24 to 70°C showed that solutions of calcium caseinate, egg albumin, and soy protein isolate produced stronger and more ordered networks than solutions of the other three proteins. Activation energies (E_a) calculated from Arrhenius plots were highest for egg albumin, soy protein isolate, and wheat gluten, which undergo sulfhydryl-disulfide bonding when heated; the other proteins produce non-covalent bonds. The strength of protein bonds is determined by G′ and information on the types of bonds involved is provided by E_a, enabling predictions to be made about the matrices obtained by processing at elevated temperatures.

Not subject to U.S. Copyright. Published 2013 by American Chemical Society
In Physical Methods in Food Analysis; Tunick, M., et al.;
ACS Symposium Series; American Chemical Society: Washington, DC, 2013.

Downloaded by UNIV OF MICHIGAN ANN ARBOR on July 29, 2013 | http://pubs.acs.org
Publication Date (Web): July 24, 2013 | doi: 10.1021/bk-2013-1138.ch007

Introduction

Purified proteins are candidates for the production of fortified foods by extrusion, in which water and food powders are mixed, heated as high as 100°C, and shaped by force through a die. The dairy-derived proteins calcium caseinate (CC) and whey protein isolate (WPI) have been co-extruded with wheat fiber and corn meal flour to produce nutritious snacks (*1*). Other proteins such as soy protein isolate (SPI), egg albumin (EA), wheat gluten (WG), and fish protein isolate (FPI) have also been co-extruded with other food materials, with the addition of the proteins improving the functionality of the various food systems (*2*).

Denaturation is required for network formation in proteins, leading to the formation of covalent bonds such as disulfide (S-S) and sulfhydryl-disulfide (SH/S-S) interactions, and non-covalent linkages including hydrogen bonds, hydrophobic interactions, and electrostatic repulsion (*3*). Denaturation, cross-linking, and texturization take place when proteins are extruded (*4*), which means that information on protein microstructure and rheology is vital when heat denaturation of proteins is being considered in processing of food. Scanning electron microscopy (SEM) is typically used for investigating microstructure. Protein solutions may be examined nondestructively by small amplitude oscillatory shear measurements, producing values for storage modulus (G′, a measure of the energy stored per deformation cycle), loss modulus (G″, a measure of the energy dissipated per cycle), tan δ (G″/G′, an indication of relative elastic and viscous behavior), and complex viscosity (η*, the resistance to flow) (*5*). Behavior during heating is examined by a temperature sweep, where the sample temperature is increased while maintaining constant frequency and strain. Activation energy (E_a) may then be calculated by substituting η* and absolute temperature values in the Arrhenius equation (*6*). Proteins in solution and below their gelation temperature are basically disordered polymer coils with sufficient time for disentanglement within the time scale of the oscillation period, which is in the order of seconds and tenths of seconds (*7*). As the temperature rises and aggregation occurs, the amount of disentanglement diminishes, the elasticity of the sample increases, and the G′ value increases while the tan δ value decreases.

Prior Research

CC, EA, FPI, SPI, WG, and WPI have been analyzed by others using small amplitude oscillatory shear and SEM under different experimental conditions to determine their suitability for food formulations. All of these proteins generate a network of some type when heated in solution. Commercially available CC forms a colloidal suspension in water at pH 6-7 (*8*). Aggregated caseinates with varying calcium concentrations were examined with small amplitude oscillatory shear and compared with WG by Stathopoulos and O'Kennedy (*9*), and SEM of CC and other caseinates have undergone fractal analysis by Dziuba et al. (*10*). WPI gels with different calcium levels were examined by electron microscopy by Barbut (*11*). EA and WPI were compared rheologically by Hsieh, Regenstein, and Rao (*12*) and EA microstructure at various pH values was studied by Handa et al.

In Physical Methods in Food Analysis; Tunick, M., et al.;
ACS Symposium Series; American Chemical Society: Washington, DC, 2013.

(*13*). Investigations on the microstructure of SPI gelation behavior were reported by Hermansson (*14*) and temperature sweeps of SPI were carried out by Ahmed, Ramaswamy, and Alli (*7*). Temperature sweeps of 15-18 g/100 g solutions of SPI and WPI at 1.0% strain, 1.00 rad/s, and 1.0°C/min were conducted by Comfort and Howell (*15*), and temperature sweeps of WG under similar conditions were performed by Hayta and Schofield (*16*). Other temperature sweep experiments of WG proteins were performed by Madeka and Kokini (*17*) and by Ahmed, Ramaswamy, and Raghavan (*18*); Amend and Belitz investigated WG by SEM (*19*). Muscle protein from rockfish was subjected to temperature sweeps by Kim et al. (*20*), and rheology of whitefish protein was examined by Ismond and Tonogai (*21*), but studies of the microstructure of FPI solutions have not been reported.

The investigations listed above were performed with various temperatures, concentrations, and other factors. The different experimental parameters used make comparisons between these proteins difficult. The purpose of this work was to compare the viscoelastic properties and microstructure of six protein solutions using the same conditions, with heating to a typical extrusion temperature (70°C) and to provide explanations for the results.

Downloaded by UNIV OF MICHIGAN ANN ARBOR on July 29, 2013 | http://pubs.acs.org
Publication Date (Web): July 24, 2013 | doi: 10.1021/bk-2013-1138.ch007

Materials and Methods

Protein Solutions

Proteins included in this study were CC (Alanate® 309, NZMP North America, Inc., Santa Rosa, CA, U.S.A.), EA (dried egg white; Primera Foods Corp., Cameron, WI, U.S.A.), FPI (primarily from whitefish muscle; SeaTech Bioproducts Corp., Shrewsbury, MA, U.S.A.), SPI (Pro-Fam® 974, ADM Specialty Food Ingredients Division, Decatur, IL, U.S.A.), WG (Wheatpro® 80, ADM), and WPI (Provon® 190, Glanbia Nutritionals, Inc., Monroe, WI, U.S.A.). Preliminary tests indicated that these preparations were typical of those commercially available. Each was dissolved or suspended in distilled deionized water at a concentration of 20 g/100 g water. This concentration was sufficient to allow transitions and interactions to be observed, but not high enough to cause the dissolved proteins to come out of solution. Table I shows the compositional and pH data for the protein powders and solutions.

Rheometry

Solutions and suspensions were placed in an AR-2000 rheometer (TA Instruments, New Castle, DE, U.S.A.) at 22°C using parallel aluminum plates (25.4 mm diameter, 3-4 mm gap), the simplest and most common geometry. Strain sweeps were performed to determine the linear viscoelastic range; 1.0% strain was selected for each specimen. Using the instrument's sealed environmental chamber, samples were heated from 24 to 70°C over a period of 70-85 min at a frequency of 1.00 rad/s, corresponding to a heating rate of 0.54-0.66°C/min. The relatively low heating rate was selected so that transitions could be observed at temperatures corresponding to those seen by thermal analyses. G', G'', tan δ,

In Physical Methods in Food Analysis; Tunick, M., et al.;
ACS Symposium Series; American Chemical Society: Washington, DC, 2013.

and η* were recorded every 2°C. Samples were run in triplicate. Arrhenius plots were obtained by plotting the η* values against reciprocal of absolute temperature T. The resulting sigmoid-shaped curves exhibited straight sections at the higher temperatures. The straight sections followed the Arrhenius equation, $\eta^* = k \exp(-E_a/RT)$, where k is the pre-exponential factor and R is the gas constant, 8.314 J/K mol. By converting η* to log10, E_a is proportional to the slope of the line. Linear regressions, slope, and R^2 values were calculated using Excel software (version 2002 SP-1, Microsoft Corp., Redmond, WA, U.S.A.).

Downloaded by UNIV OF MICHIGAN ANN ARBOR on July 29, 2013 | http://pubs.acs.org
Publication Date (Web): July 24, 2013 | doi: 10.1021/bk-2013-1138.ch007

Table I. Composition of protein powders (according to their manufacturers), and pH values of 20 g/100 g solutions or dispersions of the proteins

Sample	*Protein*	*Moist-ure*	*Fat*	*Carbohy-drate*	*Ash*	*pH*
	(g/100 g)					
Ca caseinate	89.0	<6.0	1.8	1.0	5.0	6.36
Egg albumin	84.2	6.5	0.04	4.6	4.7	6.91
Fish PI[a]	91.5	4.3	3.5	[b]	[b]	5.36
Soy PI	91.0	4.3	0.5	[b]	<5	6.97
Wheat gluten	81.8	7.0	0.6	[b]	0.9	5.34
Whey PI	89.7	3.6	<0.5	[b]	2.9	5.80

[a] PI = protein isolate. [b] Not given by manufacturer.

Scanning Electron Microscopy

All samples were treated with a fixative solution of 2.5 g per 100 g glutaraldehyde-0.1M imidazole buffer at pH 7.2 to preserve the structure, prevent distortion and deterioration, and allow comparison between heated and unheated specimens. Unheated protein solutions were placed in dialysis membrane tubing (Spectrum Laboratories, Rancho Dominguez, CA, U.S.A.) and equilibrated with fixative. After washing in the buffer, the cross-linked protein in dialysis tubing was dehydrated in a graded series of ethanol solutions (50, 75, and 100%) and ethanol freeze-fractured in liquid nitrogen, as described previously (*22*). Specimens that underwent temperature sweeps were immediately removed from the parallel plates of the viscometer at 70°C, placed in fixative, and dehydrated and freeze-fractured as above. The samples were mounted on SEM sample stubs, coated with a thin layer of gold by in a DSM Cold Sputtering Module (Denton Vacuum Co., Cherry Hill, NJ, U.S.A.), and imaged with a Quanta 200 scanning electron microscope (FEI Co., Inc., Hillsboro, OR, U.S.A.), operated in the secondary electron imaging mode.

In Physical Methods in Food Analysis; Tunick, M., et al.;
ACS Symposium Series; American Chemical Society: Washington, DC, 2013.

Results and Discussion

Calcium Caseinate

The four caseins comprising CC have an average molecular weight of 24 kDa. About three-fourths of the casein consists of α_{s1}- and β-casein, which do not contain cysteine residues. CC starts to aggregate and coagulate above 45°C, and dispersions at concentrations in excess of 15 g/100 g protein form gels when heated over 50°C (*8*). In the 20 g/100 g CC dispersions the G′ and G″ values initially decreased with heating, and were < 500 Pa until the temperature reached 44°C (Figure 1 and Table II). All values then began to increase rapidly, eventually exceeding 100 kPa, indicating that a strong and ordered network was forming. Tan δ was in the 0.54-0.97 range from 25 to 46°C, decreased sharply between 42 and 50°C, and decreased slowly thereafter. Tan δ values above 1.00 imply that a specimen is reacting to stress in a more fluid-like and less solid-like manner. Hydrophobic interactions between casein molecules keep casein gels together, and these interactions increase in strength as the temperature increases (*3*). At lower temperatures, however, the moduli decreased as the gel was heated, probably because the casein particles became more compact, resulting in fewer interparticle bonds (*23*).

Downloaded by UNIV OF MICHIGAN ANN ARBOR on July 29, 2013 | http://pubs.acs.org
Publication Date (Web): July 24, 2013 | doi: 10.1021/bk-2013-1138.ch007

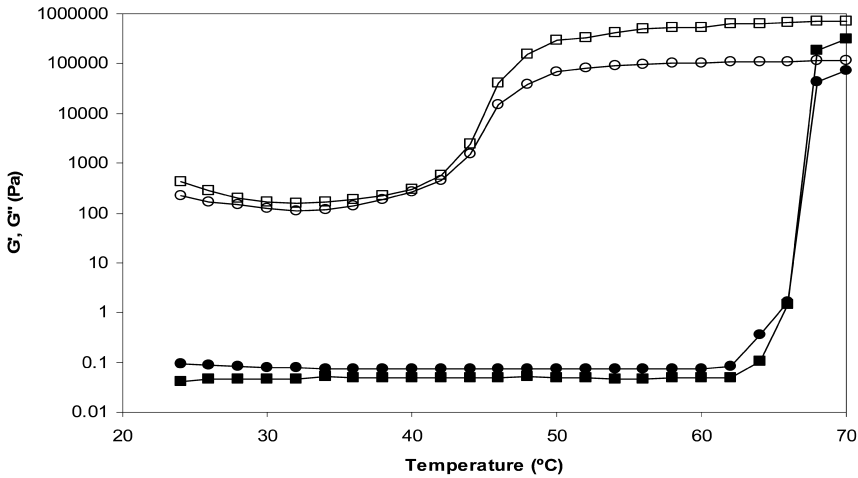

Figure 1. Temperature sweeps of 20 g/100 g solutions of calcium caseinate (open symbols) and whey protein isolate (closed symbols), showing elastic modulus G' (squares) and viscous modulus G" (circles).

The hydrophobic interactions that occur in CC during aggregation are more easily formed than SH/S-S exchanges, leading to a relatively low E_a value (Table II). CC does not undergo sulfide exchanges due to the lack of cysteine in casein. The high G′ and low E_a are suggestive of a strong but easily-formed aggregate.

In Physical Methods in Food Analysis; Tunick, M., et al.;
ACS Symposium Series; American Chemical Society: Washington, DC, 2013.

The SEM images clearly show that CC undergoes microstructural changes upon heating. CC at room temperature consisted of a matrix of strands with pores measuring up to 100 nm in diameter (Figure 2). After heating to 70°C, the matrix changed to spherical particles measuring 200-500 nm in diameter, many of which were connected to each other by filaments. These changes in network geometry imply that casein particles are more compact at lower temperatures and aggregate with intermolecular bonding during heating.

Downloaded by UNIV OF MICHIGAN ANN ARBOR on July 29, 2013 | http://pubs.acs.org
Publication Date (Web): July 24, 2013 | doi: 10.1021/bk-2013-1138.ch007

Table II. Elastic modulus (G′, with standard deviations) and activation energy (E_a, with R^2 values) for 20 g/100 g solutions

Sample[a]	*G′ at 24°C (Pa)*	*Inflection point*[b]		*G′ at 70°C (Pa)*	*E_a (kJ/mol)*	*R^2*
		°C	*G′ (Pa)*			
CC	420 ± 32	44	2400 ± 73	770000 ± 16000	29	0.96
EA	0.052 ± 0.009	58	3.2 ± 1.6	500000 ± 1200	192	0.97
FPI	0.088 ± 0.008	48	0.32 ± 0.03	7000 ± 380	51	0.96
SPI	1400 ± 310	48	7000 ± 770	480000 ± 45000	110	0.98
WG	190 ± 84	56	3000 ± 190	93000 ± 900	107	0.99
WPI	0.037 ± 0.007	68	110000 ± 19000	240000 ± 19000	40	0.98

[a] CC = calcium caseinate, EA = egg albumin, FPI = fish protein isolate, SPI = soy protein isolate, WG = wheat gluten, WPI = whey protein isolate. [b] Measured at the first temperature where G′ was at least twice the previous value.

Whey Protein Isolate

Whey protein is composed of approximately 60 g/100 g β-lactoglobulin (18.4 kDa molecular weight), 22 g/100 g α-lactalbumin (14.2 kDa molecular weight), and 18 g/100 g other proteins (*24*). Figure 1 shows a comparison between the dairy proteins in this study, WPI and CC. The tan δ values of the 20% WPI solutions were > 1.35 until the final reading of 0.93 at 70°C, indicative of a fluid and mobile structure. The values for G′ and G″ were < 0.1 Pa until the temperature reached 68°C (Table II), pointing to a lack of aggregation until the end of the temperature sweep. Similar results were obtained with 15 g/100 g WPI solutions analyzed by Comfort and Howell (*15*) and 15 g/100 g whey protein concentrate solutions analyzed by Havea, Watkinson, and Kuhn-Sherlock (*25*). β-lactoglobulin does not denature until 78°C, but denaturation of α-lactalbumin starts at 62°C (*24*), resulting in the increase observed in G′ and G″.

Non-covalent bonds, especially hydrophobic interactions, are predominant when WPI forms gels in non-alkaline conditions (*3*, *24*), producing a fairly low E_a value of 40.3 kJ/mol (Table II). A value of 28.9 kJ/mol for a 15 g/100 g solution

of WPI at pH 6.00 was found by Dierckx and Huyghebaert (*26*). The E_a and G′ results indicate that WPI forms aggregates nearly as easily as CC, but they are not as strong.

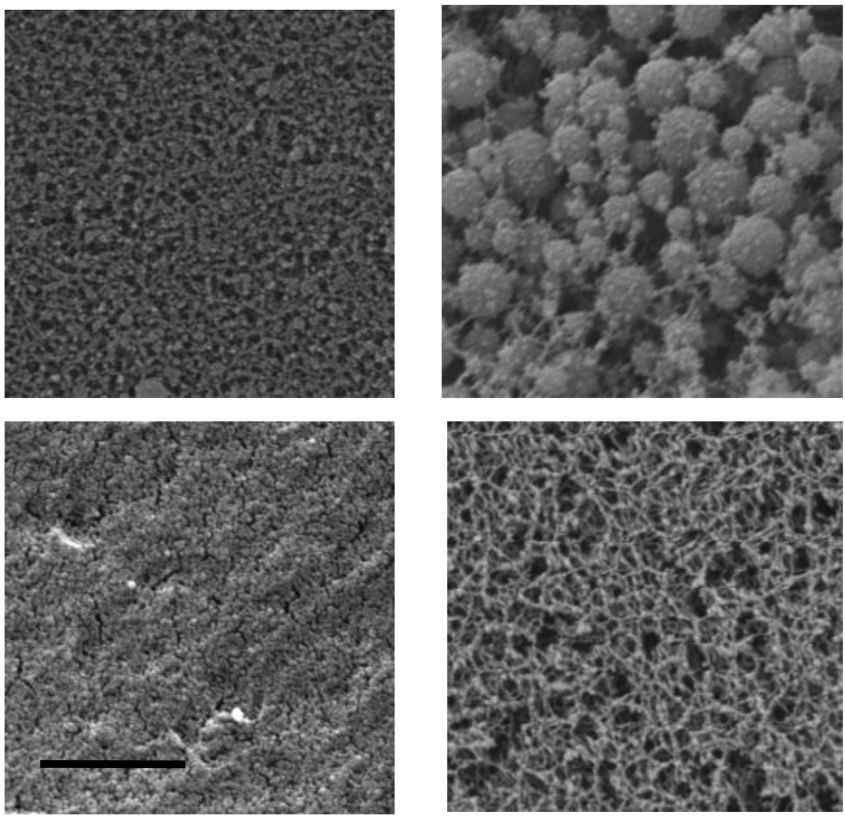

Figure 2. Scanning electron microscopy images of 20 g/100 g solutions of calcium caseinate (top), and whey protein isolate (bottom) prepared at 22°C (left), and after heating to 70°C (right). Bar at lower left = 1000 nm.

The SEM images revealed a tight structure of protein strands at 22°C and a more open mesh of strands and 50-150 μm pores at 70°C (Figure 2). Strands and 100-150 μm pores have been observed by Stading, Langton, and Hermansson in solutions of β-lactoglobulin heated at < 1.0°C/min (*27*). Interpretation of WPI behavior in solution is difficult; for example, only a fraction of whey protein undergoes aggregation at the gel point, and aggregation is highly sensitive to changes in electrostatic properties. β-lactoglobulin forms fractal aggregates that lend themselves to fractal analysis, although the results are controversial (*28*).

In Physical Methods in Food Analysis; Tunick, M., et al.;
ACS Symposium Series; American Chemical Society: Washington, DC, 2013.

Downloaded by UNIV OF MICHIGAN ANN ARBOR on July 29, 2013 | http://pubs.acs.org
Publication Date (Web): July 24, 2013 | doi: 10.1021/bk-2013-1138.ch007

Egg Albumin

EA is comprised of about 65 g/100 g ovalbumin (45 kDa molecular weight) and 15 g/100 g ovotransferrin (also called conalbumin, 76 kDa molecular weight). G′ values were < 0.07 Pa and G″ values were < 0.22 Pa for the EA solutions until 58°C, when all began to increase rapidly (Figure 3 and Table II). Tan δ, which had been > 2.0 to that point, dropped to 0.4 and stayed below 0.2 thereafter. The final value of G′ was seven orders of magnitude greater than the initial value. The transition starting at 58°C corresponds to the onset of ovotransferrin denaturation (*29*), which is responsible for the formation of a soft opaque egg white gel upon heating to 65°C (*30*). Ovotransferrin is the most easily heat-denatured egg white protein, and plays a role in the coagulation step (*31*). Ovalbumin, the only egg white protein with free SH groups, does not start to denature until 84°C (*29*). Heating of EA (and WPI) may cause S-S bonds to form at the start of aggregation, which would lead to cross-linking of protein molecules by intermolecular SH/S-S exchange (*12*).

In addition to having high G′ values after aggregation, the E_a of EA was the highest of the proteins tested (Table II) owing to the high energy of its SH/S-S interactions. While examining ovalbumin aggregates between 75 and 81°C, Hsieh and Regenstein found that E_a decreases as the material polymerizes from dimers (209 kJ/mol) to trimers (188 kJ/mol) to tetramers (167 kJ/mol) (*32*). The E_a value for EA in the present study is within this range. The microstructure of the EA solutions changed from a relatively flat surface with small openings resembling cracks to a network of chains typical of an aggregated gel (Figure 4). The 70°C sample resembled the microstructure of pH 7 egg white gels obtained by Handa et al. after heating to 80°C (*13*). The thickness of the chains is consistent with the formation of a strong network.

Wheat Gluten

WG consists of gliadins (molecular weight 35 kDa) and glutenins (polypeptide chains of 20000 kDa) in roughly equal amounts. These proteins do not exhibit denaturation transitions in solution when the water content is above 60 g/100 g (*33*). Figure 3 shows that the values of G′ and G″ for WG decreased between 24 and 46°C and increased from then on, with the sharpest changes at 54-58°C (for clarity, this is shown in the same figure as the EA results). Tan δ decreased from 0.45 to 0.25 during the sweep, except for an increase in the 54-58°C range. Decreases in G′ and G″ up to 50°C followed by considerable increases were also observed by Hayta and Schofield (*16*). When a WG solution is prepared, the proteins (mainly polymeric glutenins and monomeric gliadins) absorb water and partially unfold, leading to disruption of low-energy intermolecular bonds and relatively small decreases in G′ and G″ (*34*). In temperature sweeps of 25 g/100 g solutions of gliadin at 1°C/min, Madeka and Kokini found that G′ and G″ started to increase around 58°C (*17*). They attributed this result to the onset of SH/S-S interchanges, leading to cross-linking and aggregation reactions between gliadin molecules.

In Physical Methods in Food Analysis; Tunick, M., et al.;
ACS Symposium Series; American Chemical Society: Washington, DC, 2013.

Downloaded by UNIV OF MICHIGAN ANN ARBOR on July 29, 2013 | http://pubs.acs.org
Publication Date (Web): July 24, 2013 | doi: 10.1021/bk-2013-1138.ch007

In WG, the association of α- and γ-gliadins to glutenin by SH/S-S exchange has E_a values of 110 kJ/mol for α-gliadin (which contains three intramolecular S-S bonds) and 147 kJ/mol for γ-gliadin (which contains four such bonds, and thus requires more energy to unfold and expose its sulfur groups) (*35*). The E_a value for WG in the present study (Table II) is comparable to the value of 90 kJ/mol obtained by Hargreaves et al. (*34*).

Except for FPI, WG exhibited the lowest G′ value at 70°C of the proteins tested, suggestive of relatively small changes in its structure during heating. The microstructure of WG did become more granular from 22 to 70°C, but the difference was not obvious (Figure 4). Air bubbles resulting from the mixing of the solution were evident, which was expected since WG entraps air during baking.

Downloaded by UNIV OF MICHIGAN ANN ARBOR on July 29, 2013 | http://pubs.acs.org
Publication Date (Web): July 24, 2013 | doi: 10.1021/bk-2013-1138.ch007

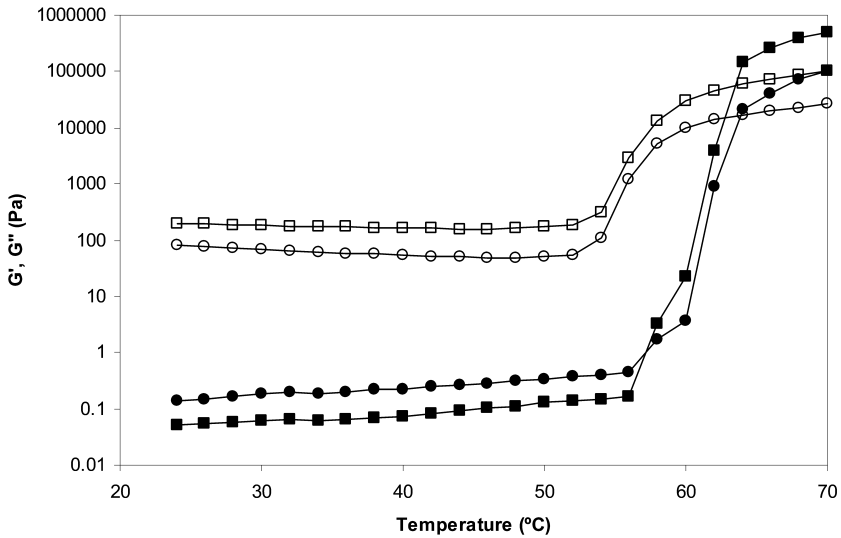

Figure 3. Temperature sweeps of 20 g/100 g solutions of wheat gluten (open symbols) and egg albumin (closed symbols), showing elastic modulus G' (squares) and viscous modulus G" (circles).

Soy Protein Isolate

SPI contains around 40 g/100 g glycinin (320 kDa molecular weight) and 35 g/100 g β-conglycinin (200 kDa molecular weight), and does not denature until 93°C (*36*). The tan δ values of SPI were < 0.3 throughout the sweep (Figure 5). Temperature sweeps of 17 g/100 g SPI solutions performed by Comfort

and Howell (*15*) showed that G′ was greater than G″. They suggested that cross-linking between proteins had occurred before heating, apparently due to some denaturation during manufacture of the isolate. Their values were less than those in the current study due to the more dilute solution they used. Large increases in G′ (from 1.5 to 45 kPa) and G″ (from 0.22 to 12.7 kPa) were observed between 42 and 54°C (Figure 3), also seen by Ahmed, Ramaswamy, and Alli (*7*). Glycinin and β-conglycinin both contain around 40 g/100 g hydrophobic amino acid residues and two or more active free SH groups, meaning that hydrophobic and S-S bonds both contribute to the gel structure (*37*). Soy protein exists in the form of aggregates of various sizes, making the interpretation of temperature effects especially complicated (*7*).

Downloaded by UNIV OF MICHIGAN ANN ARBOR on July 29, 2013 | http://pubs.acs.org
Publication Date (Web): July 24, 2013 | doi: 10.1021/bk-2013-1138.ch007

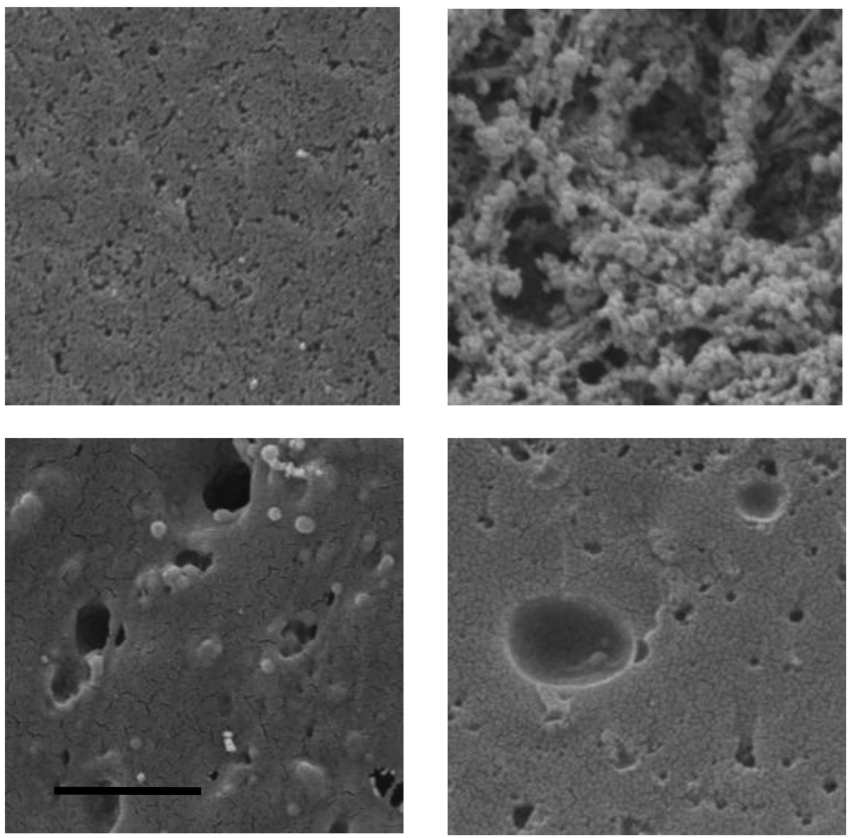

Figure 4. Scanning electron microscopy images of 20 g/100 g solutions of egg albumin (top) and wheat gluten (bottom) prepared at 22°C (left), and after heating to 70°C (right). Bar at lower left = 1000 nm.

The E_a of 110 kJ/mol was similar to that of the WG (Table II), which was expected since both proteins undergo S-S bonding. When performing temperature sweeps of 9.1 g/100 g SPI solutions at 2.3°C/min (four times the heating rate of the present study), Berli et al. obtained E_a values of 165-172 kJ/mol (*38*).

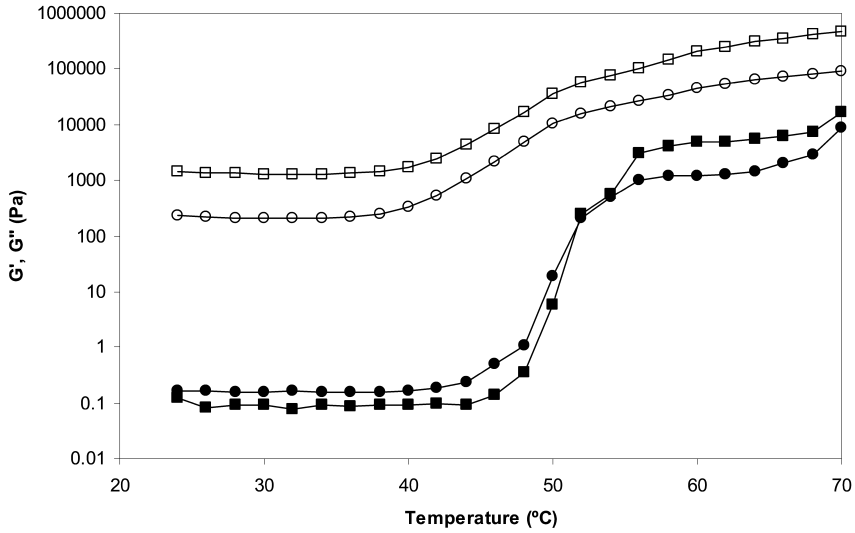

Figure 5. Temperature sweeps of 20 g/100 g solutions of soy protein isolate (open symbols) and fish protein isolate (closed symbols), showing elastic modulus G' (squares) and viscous modulus G" (circles).

Downloaded by UNIV OF MICHIGAN ANN ARBOR on July 29, 2013 | http://pubs.acs.org
Publication Date (Web): July 24, 2013 | doi: 10.1021/bk-2013-1138.ch007

The SEM images of SPI solutions revealed a two-phase system consisting of a mesh of protein strands similar to WPI and a relatively flat surface (Figure 6). The strands were more numerous and the surface was rougher and more granular at 70°C. Glycinin and β-conglycinin formed ordered networks of strands, apparent at both temperatures. Proteins may also form random aggregations, and gels containing aggregations and strands may arise from the same protein (*14*). The microstructures of the SPI solutions appear to show both strands and aggregates, and the relatively high G′ value at 70°C is indicative of a strong structure.

Fish Protein Isolate

The FPI in this study contained the proteins actin (42 kDa molecular weight) and myosin (500 kDa molecular weight), which denature at 83 and 55°C, respectively (*39*). Figure 5 shows that G′, G″, and η* decreased slightly from 32 to 38°C and began to increase rapidly at 48°C (for clarity, these results are shown in the same figure as those for SPI). Small amplitude oscillatory shear analyses at

In Physical Methods in Food Analysis; Tunick, M., et al.;
ACS Symposium Series; American Chemical Society: Washington, DC, 2013.

1.0°C/min by Kim et al. showed a decrease in G′ from 38 to 48°C followed by an increase (*20*). The decrease was attributed to dissociation of the actin-myosin complex and the helix-coil transformation of the myosin tail. The increase that followed resulted from the completion of the unfolding and the start of gelation (*20*). The tan δ was above 1.0 until 52°C, when aggregation took place.

The relatively low E_a was indicative of non-covalent bonding. The G′ value at 70°C was the lowest in this study, pointing to formation of a weak gel.

The SEM images at 22°C showed a mixture of structures, which was not surprising in light of the heterogeneous nature of fish muscle (Figure 6). At 70°C, the surface exhibited fibrous areas along with cavities containing a web-like framework, which suggests that an aggregation of the diverse structures occurred. The low values for FPI throughout the temperature sweep are not surprising in view of the lack of homogeneity in the microstructure.

Downloaded by UNIV OF MICHIGAN ANN ARBOR on July 29, 2013 | http://pubs.acs.org
Publication Date (Web): July 24, 2013 | doi: 10.1021/bk-2013-1138.ch007

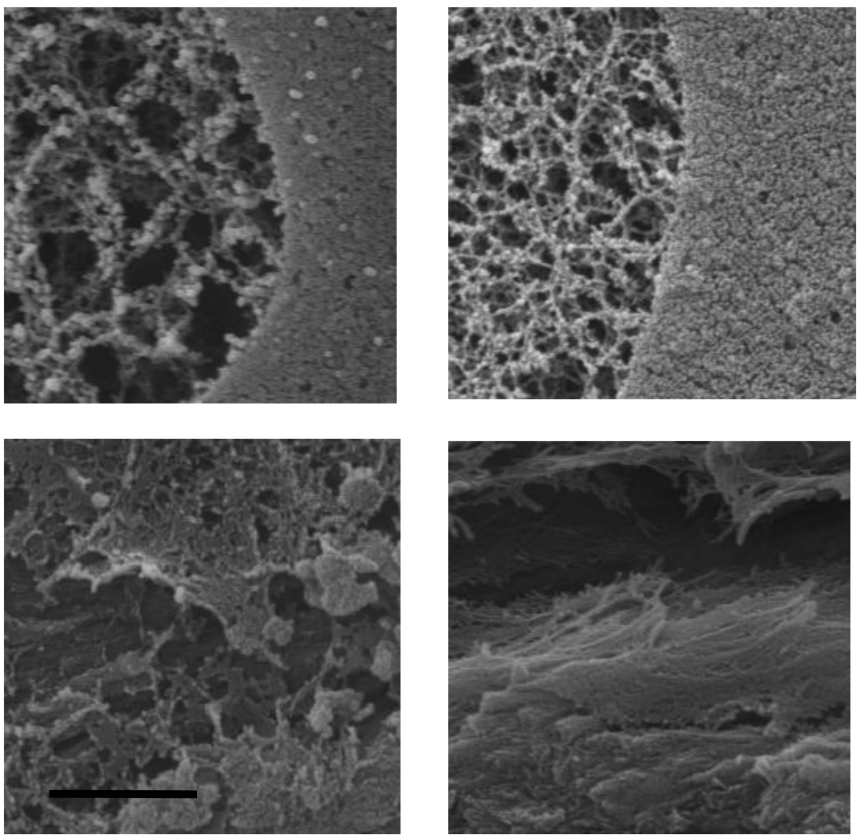

Figure 6. Scanning electron microscopy images of 20 g/100 g solutions of soy protein isolate (top) and fish protein isolate (bottom) prepared at 22°C (left), and after heating to 70°C (right). Bar at lower left = 1000 nm.

In Physical Methods in Food Analysis; Tunick, M., et al.;
ACS Symposium Series; American Chemical Society: Washington, DC, 2013.

Downloaded by UNIV OF MICHIGAN ANN ARBOR on July 29, 2013 | http://pubs.acs.org
Publication Date (Web): July 24, 2013 | doi: 10.1021/bk-2013-1138.ch007

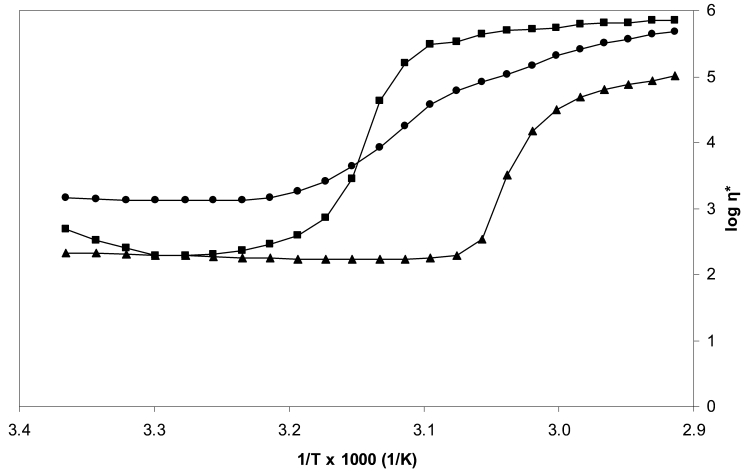

Figure 7. Arrhenius plots of log complex viscosity η vs. reciprocal of absolute temperature T for 20 g/100 g solutions of calcium caseinate (squares), soy protein isolate (circles), and wheat gluten (triangles).*

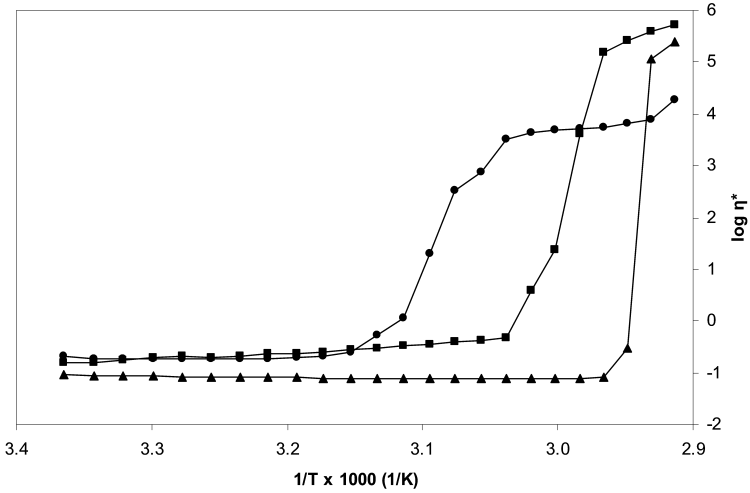

Figure 8. Arrhenius plots of log complex viscosity η vs. reciprocal of absolute temperature T for 20 g/100 g solutions of egg albumin (squares), fish protein isolate (circles), and whey protein isolate (triangles).*

Downloaded by UNIV OF MICHIGAN ANN ARBOR on July 29, 2013 | http://pubs.acs.org
Publication Date (Web): July 24, 2013 | doi: 10.1021/bk-2013-1138.ch007

Comparisons

The final G′ values of the proteins are in Table II. At 70°C, the CC, EA, and SPI exhibited the strongest and most ordered networks, as evidenced by their relatively high G′ values. The WG and WPI were less strong and ordered, and the FPI was a weak gel. Figure 7 shows the Arrhenius plots of CC, SPI, and WG. The lowest η* value for these proteins was 167 Pa·s, and all increased rapidly in the 40-60°C range. The Arrhenius plots of EA, FPI, and WPI are compared in Figure 8. The η* values for EA did not exceed 0.5 Pa·s until 58°C, the values for WPI were below 0.1 Pa·s until 64°C, and the FPI values were the lowest of all. A summary of the apparent bonding interactions, microstructure, and their effects on rheology is shown in Table III. The results presented here are not proof that the suggested bonding and interactions took place, but the agreement with studies by others using different approaches imply that the microstructural and rheological analyses of protein solutions outlined here may be useful in predicting behavior.

Table III. Prior studies of bonding interactions, microstructural appearance, and their effects on rheology of 20 g/100 g solutions of calcium caseinate (CC), egg albumin (EA), fish protein isolate (FPI), soy protein isolate (SPI), wheat gluten (WG), and whey protein isolate (WPI)

Sample	*Possible interactions at 70°C*	*Effect on activation energy*	*Refs.*	*Appearance of microstructure at 70°C*	*Effect on elastic modulus*	*Refs.*
CC	Hydrophobic	Decrease	(*3*)	Connected spheres	Increase	(*3*)
WPI	Non-covalent	Decrease	(*3*, *26*)	Strands	Minor	(*15*, *27*)
EA	Polymerized sulfhydryl-disulfide	Increase	(*32*)	Thick strands	Increase	(*12*, *13*)
SPI	Hydrophobic, sulfhydryl-disulfide	Minor	(*37*, *38*)	Strands and aggregates	Increase	(*1*, *14*)
WG	Sulfhydryl-disulfide	Decrease	(*17*, *34*)	Aggregates	Decrease	(*16*, *19*)
FPI	Non-covalent	Decrease	(*20*)	Fibers and webs	Decrease	(*20*)

Conclusions

The E_a values for the proteins are indicative of the types of bonding taking place, and the G′ values reflect the strength of these interactions. Both are valuable in predicting the structural characteristics of proteins when extruded, as are the

In Physical Methods in Food Analysis; Tunick, M., et al.;
ACS Symposium Series; American Chemical Society: Washington, DC, 2013.

SEM results. Calcium caseinate and soy protein isolate would be expected to form strong matrices when processed at elevated temperatures, and egg albumin and whey protein isolate would also provide strong networks above 65°C. These four proteins underwent microstructural modifications suggestive of changes in bonding. A weaker matrix would arise from processing of wheat gluten, which exhibited minimal microstructural change, and fish protein isolate does not appear to be an option for strong network formation.

Acknowledgments

The authors thank Eric Tilman for sourcing the proteins, Guoping Bao for some of the SEM work, and Phoebe Qi for helpful discussions. Mention of trade names and commercial products in this publication is solely for the purpose of providing information and does not imply recommendation or endorsement by the U.S. Department of Agriculture. USDA is an equal opportunity provider and employer.

Downloaded by UNIV OF MICHIGAN ANN ARBOR on July 29, 2013 | http://pubs.acs.org
Publication Date (Web): July 24, 2013 | doi: 10.1021/bk-2013-1138.ch007

References

1. Onwulata, C. I.; Konstance, R. P.; Smith, P. W.; Holsinger, V. H. *Lebensm.-Wiss. Technol.* **2001**, *34*, 424–429.
2. Areas, J. A. G. *Crit. Rev. Food Sci. Nutr.* **1992**, *32*, 365–392.
3. Bryant, C. M.; McClements, D. J. *Trends Food Sci. Technol.* **1998**, *9*, 143–151.
4. Akdogan, H. *Int. J. Food Sci. Technol.* **1999**, *34*, 195–207.
5. Tunick, M. H. *J. Dairy Sci.* **2000**, *83*, 1892–1898.
6. Tunick, M. H. *Int. Dairy J.* **2010**, *20*, 680–685.
7. Ahmed, J.; Ramaswamy, H. S.; Alli, I. *J. Food Sci.* **2006**, *71*, E158–E163.
8. Singh, H. In *Encyclopedia of Dairy Sciences*; Fuquay, J. W., Fox, P. F., Roginski, H., Eds.; Academic Press: New York, 2002; pp 1976−1982.
9. Stathopoulos, C. E.; O'Kennedy, B. T. *Int. J. Dairy Technol.* **2008**, *61*, 397–402.
10. Dziuba, J.; Babuchowski, A.; Smoczynski, M.; Smietana, Z. *Int. Dairy J.* **1999**, *9*, 287–292.
11. Barbut, S. *Lebensm.-Wiss. Technol.* **1995**, *28*, 598–603.
12. Hsieh, Y. L.; Regenstein, J. M.; Rao, M. A. *J. Food Sci.* **1993**, *58*, 116–119.
13. Handa, A.; Takahashi, K.; Kuroda, M.; Froning, G. W. *J. Food Sci.* **1998**, *63*, 403–407.
14. Hermansson, A.-M. *J. Am. Oil Chem. Soc.* **1986**, *63*, 658–666.
15. Comfort, S.; Howell, N. K. *Food Hydrocolloids* **2002**, *16*, 661–672.
16. Hayta, M.; Schofield, J. D. *J. Sci. Food Agric.* **2005**, *85*, 1992–1998.
17. Madeka, H.; Kokini, J. L. *J. Food Eng.* **1994**, *22*, 241–252.
18. Ahmed, J.; Ramaswamy, H. S.; Raghavan, V. G. S. *J. Cereal Sci.* **2008**, *47*, 417–428.
19. Amend, T.; Belitz, H.-D. *Z. Lebensm.-Unters. Forsch.* **1990**, *190*, 401–409.

20. Kim, Y. S.; Yongsawatdigul, J.; Park, J. W.; Thawornchinsombut, S. *J. Food Biochem.* **2005**, *29*, 517–532.
21. Ismond, M. A. H.; Tonogai, J. R. *J. Food Sci.* **1994**, *59*, 501–503.
22. Tunick, M. H.; Van Hekken, D. L.; Cooke, P. H.; Smith, P. W.; Malin, E. L. *Lebensm.-Wiss. Technol.* **2000**, *33*, 538–544.
23. Van Vliet, T. Y.; Roefs, S. P. F. M.; Zoon, P.; Walstra, P. *J. Dairy Res.* **1989**, *56*, 529–534.
24. deWit, J. N.; Klarenbeek, G. *J. Dairy Sci.* **1984**, *67*, 2701–2710.
25. Havea, P.; Watkinson, P.; Kuhn-Sherlock, B. *J. Agric. Food Chem.* **2009**, *57*, 1506–1512.
26. Dierckx, S.; Huyghebaert, A. *Food Hydrocolloids* **2002**, *16*, 489–497.
27. Stading, M.; Langton, M.; Hermansson, A.-M. *Food Hydrocolloids* **1993**, *7*, 195–212.
28. Foegeding, E. A.; Davis, J. P.; Doucet, D.; McGuffey, M. K. *Trends Food Sci. Technol.* **2002**, *13*, 151–159.
29. Donovan, J. W.; Mapes, C. J.; Davis, J. G.; Garibaldi, J. A. *J. Sci. Food Agric.* **1975**, *26*, 73–83.
30. Yamashita, H.; Ishibashi, J.; Hong, Y.-H.; Hirose, M. *Biosci. Biotechnol. Biochem.* **1998**, *62*, 593–595.
31. Croguennec, T.; Nau, F.; Brulé, G. *J. Food Sci.* **2002**, *67*, 608–614.
32. Hsieh, Y. L.; Regenstein, J. M. *J. Food Sci.* **1992**, *57*, 856–861.
33. Leon, A.; Rosell, C. M.; de Barber, C. B. *Eur. Food Res. Technol.* **2003**, *217*, 13–16.
34. Hargreaves, J.; Popineau, Y.; Le Meste, M.; Hemminga, M. A. *FEBS Lett.* **1995**, *372*, 103–107.
35. Lagrain, B.; Brijs, K.; Delcour, J. A. *J. Agric. Food Chem.* **2008**, *56*, 10660–10666.
36. McKlem, L. K. M.S. Thesis, North Carolina State University, Raleigh, NC, 2002.
37. Apichartsrangkoon, A. *Food Chem.* **2002**, *80*, 55–60.
38. Berli, C. L. A.; Deiber, J. A.; Añón, M. C. *J. Agric. Food Chem.* **1999**, *47*, 893–900.
39. Wright, D. J. In *Developments in Food Proteins*; Hudson, B. J. F., Ed.; Applied Science Publ.: Barking, U.K., 1982; Vol. 1, pp 61−89.

Downloaded by UNIV OF MICHIGAN ANN ARBOR on July 29, 2013 | http://pubs.acs.org
Publication Date (Web): July 24, 2013 | doi: 10.1021/bk-2013-1138.ch007

Downloaded by PURDUE UNIVERSITY on July 29, 2013 | http://pubs.acs.org
Publication Date (Web): July 24, 2013 | doi: 10.1021/bk-2013-1138.ch008

Chapter 8

Isolation and Characterization of Natural Blue Pigments from Underexplored Sources

A. G. Newsome, B. T. Murphy, and R. B. van Breemen*

Department of Medicinal Chemistry and Pharmacognosy, University of Illinois College of Pharmacy, 833 S. Wood Street M/C 781, Chicago, Illinois 60642
***E-mail: Breemen@uic.edu.**

Consumer preference for natural food ingredients has increased in recent decades, and the natural food colorant market has grown to over one billion dollars annually. A variety of red, orange, and yellow natural colorants are approved and in use, but there still exists a lack of available blue and purple natural colorant options. The occurrence of blue colored compounds in the natural world is relatively rare. The isolation, identification, and characterization of natural blue and purple pigments obtained from underexplored natural sources such as from obscure terrestrial organisms and marine microorganisms will be discussed.

Introduction

Recently, consumers have shown a preference for natural over synthetic food colorants because natural colorants are perceived to be safer or even beneficial to health (*1*). As a result, the natural food colorant market has grown to over one billion dollars annually (*1*). Natural food colorants such as β-carotene and annatto extract are now available for replacing the red, orange, and yellow synthetic dyes (*1*, *2*). Despite great market potential, very few natural blue, green, or violet pigments are available for use. A suitable natural blue food colorant would complete the available colorant spectrum by providing the missing primary color that may be used alone or in combination with the existing natural food dyes to provide purple, green, etc. Thus, there are significant incentives for the discovery of new natural blue colorants.

© 2013 American Chemical Society
In Physical Methods in Food Analysis; Tunick, M., et al.;
ACS Symposium Series; American Chemical Society: Washington, DC, 2013.

The overall requirements for a compound to be approved for use in food and beverages are perhaps as demanding as those of a therapeutic drug. For a colorant to reach and be successful in the market, it must be suitable in five major areas of consideration, as follows:

(1) Color intensity: Enables desired colors to be achieved with minimal material, cost or product alteration.
(2) Stability: Must maintain color under the temperature, light, and pH conditions of the application.
(3) Safety: Must be safe for human consumption as demonstrated in both acute and chronic toxicity studies.
(4) Commercial production: Should be obtainable in bulk quantities at competitive cost.
(5) Solubility: For beverage use, water solubility is preferred but not necessary.

Downloaded by PURDUE UNIVERSITY on July 29, 2013 | http://pubs.acs.org
Publication Date (Web): July 24, 2013 | doi: 10.1021/bk-2013-1138.ch008

Regulatory Agency-Approved Food Colorants

The U.S. Food and Drug Administration (FDA) has approved seven synthetic food colorants, and the European Union (E.U.) has approved eight synthetic food colorants (*3*). Among these colorants, two are blue, one is green, and none are violet. The synthetic blue colorant most widely used in the world today is Brilliant Blue FCF (E133, FD&C Blue No. 1). Brilliant blue FCF is used by industry to obtain all shades of blue, violet, and green by mixing with other synthetic colorants.

The approved "natural" food colorants mainly cover the red-orange-yellow portion of the visible spectrum (*1*, *4*). The majority of the red-orange-yellow natural pigments are carotenoids. For example, annatto extract from *achiote* seeds and lycopene from tomatoes are commonly used for obtaining red coloration (*5*). Marigold petals, which are rich in lutein, are commonly added to commercial chicken feed to ensure yellow egg yolks (*6*). Plant sources of the natural orange colorant β-carotene are abundant, but most commercial material is produced synthetically (500+ tons annually) or naturally from cultured microorganisms such as *Dunaliella* (*7*). The anthocyanins, flavanoid-derived pigments responsible for the color of countless flowers and fruits, have been extensively investigated for use as natural food colorants. Over 500 anthocyanins have been isolated to date (*8*, *9*). Their practical commercial use has been very limited since most anthocyanins are too susceptible to chemical degradation. Nearly all anthocyanins are red or purple colored, not blue, at low pH values.

Although green, chlorophylls are only approved for use in drugs and cosmetics at very low levels and are prohibited from use in food by the FDA (*10*). Even where allowed, chlorophylls are heat and acid unstable due to the lability of the Mg^{2+} atom and the phytyl chain and therefore are rarely used. The

In Physical Methods in Food Analysis; Tunick, M., et al.;
ACS Symposium Series; American Chemical Society: Washington, DC, 2013.

blue photosynthetic accessory pigment phycocyanin from *Spirulina platensis* is approved and used in food in Japan and the E.U. (*1*). Phycocyanin has an excellent safety profile and evidence for benefits such as antioxidation, anti-inflammation, and neuroprotection (*11*, *12*). In practice, the use of phycocyanin is limited to solid preparations due to poor solution stability and rapid degradation by light (*13*). Overall, the natural blue or green food colorants in use are few. Structures of the major synthetic and natural food and beverage colorants currently approved for use are shown in Figure 1.

Recently Discovered Marine Blue Pigments

During the past few decades, several blue pigments with new chemical structures have been isolated from the natural world, and perhaps the most interesting examples have come from underexplored marine sources. Purpurone from a marine sponge (*14*) and ammosamide A from the marine *Streptomyces* CNR-698 (*15*) provide natural purple and blue pigments but are too toxic for use as food additives. Complex anthraquinone pigments, such as oxyblepharismin A, have been isolated from the protist *Blepharisma japonicum* (*16*).

Glaukothalin was isolated in 2009 in minor amounts from the marine microorganism *Rheinheimera baltica* (*17*, *18*) and is among the most structurally unusual of all blue chromophores. Initial brine shrimp assay data suggests that glaukothalin is cytotoxic and therefore may function for chemical defense in the marine environment (*17*). A series of compounds based on the azulene chromophore have been isolated from an *Anthogorgia sp.* marine coral (*19*). A new class of blue chromoprotein was recently characterized from the barrel jellyfish, *Rhizostoma pulmo*, but the structure of the chromogenic group has yet to be determined (*20*). A *N*,*N*-decyl analog of the *bis*-pyridal blue pigment indigoidine was isolated from the culture of the marine bacterium *Shewanella violacea* (*21*). None of these compounds are likely to be suitable for use as a food additive due to either toxicity or stability problems, yet these examples demonstrate the structural diversity of blue pigments that are being discovered in underexplored natural environments. Structures of many of these recently discovered natural pigments are shown in Figure 2.

Structural Trends for Natural Blue Chromophores

Two fundamental questions arising during the search for natural blue pigments are, “What makes a compound blue?” and “Why are blue pigments rare in nature?” First, there are many incidences of blue coloration in nature that are not due to blue-pigmented compounds but are instead produced by nanoscale structural patterns, which diffract white light. Blue coloration in the animal kingdom, almost without exception, is due to optical diffraction effects arising from nanoscale structural patterns. Well-known examples include the blue iridescent wings of the Morpho butterfly (*Morpho* sp.) and the feathers of blue birds (*Sialia* sp.). Here, our focus is on blue-pigmented low molecular weight organic compounds.

Downloaded by PURDUE UNIVERSITY on July 29, 2013 | http://pubs.acs.org
Publication Date (Web): July 24, 2013 | doi: 10.1021/bk-2013-1138.ch008

Downloaded by PURDUE UNIVERSITY on July 29, 2013 | http://pubs.acs.org
Publication Date (Web): July 24, 2013 | doi: 10.1021/bk-2013-1138.ch008

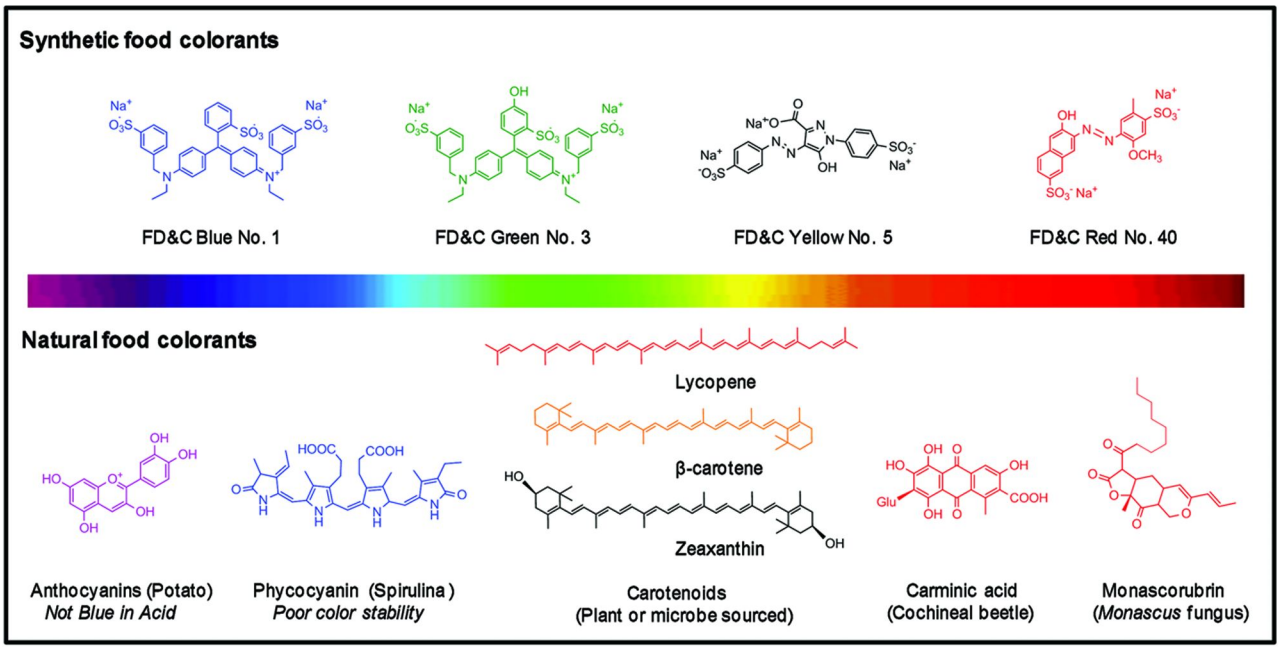

Figure 1. Structures of some major synthetic and natural colorants approved and used commercially in food and beverages today. (see color insert)

Downloaded by PURDUE UNIVERSITY on July 29, 2013 | http://pubs.acs.org
Publication Date (Web): July 24, 2013 | doi: 10.1021/bk-2013-1138.ch008

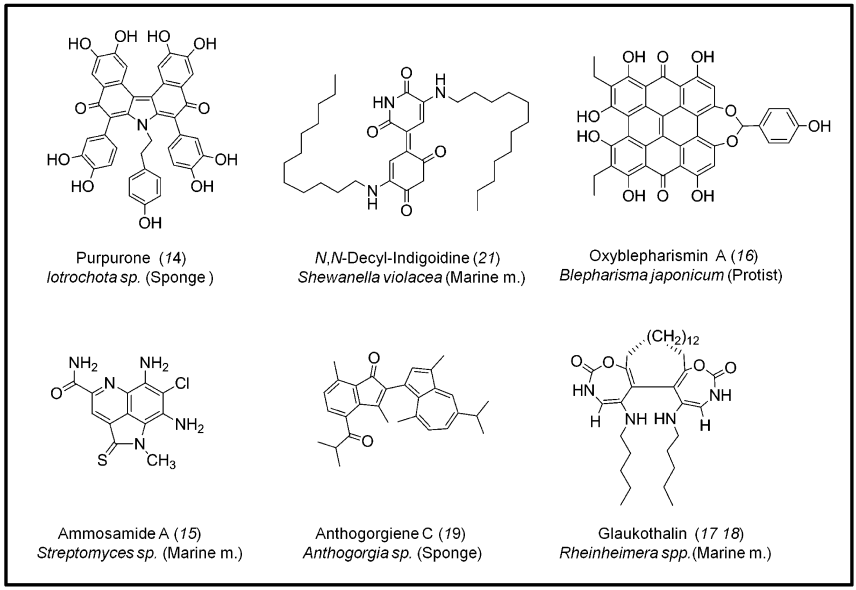

Figure 2. Structures of selected-blue pigmented natural products isolated and characterized from marine organisms within the past 20 years (m. = microorganism).

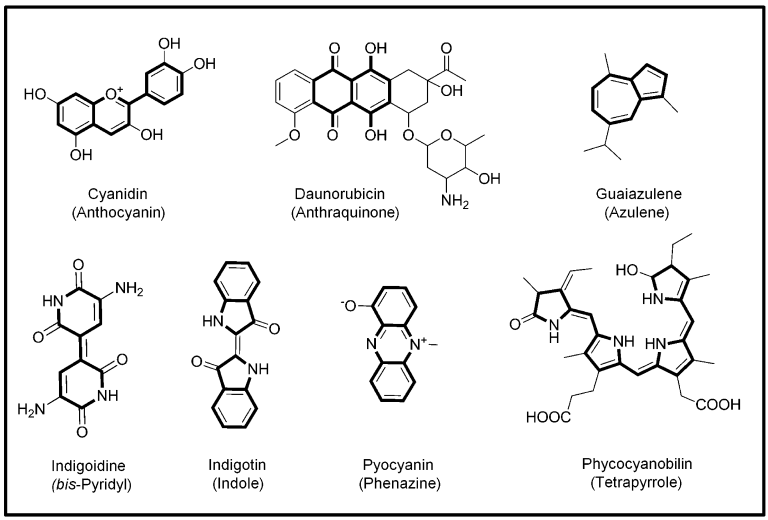

Figure 3. Chemical structures representing each of seven major compound classes of blue-pigmented natural organic compounds. The compound classes are shown in parentheses. The chemical bonds shown in bold font outline the basic structure of each class.

For simple organic compounds, blue color is a quantum mechanical phenomenon, which arises from absorption of photons of the red light range of the visible spectrum (approximately 560-700 nm). In nature, electronic configurations suitable for absorption of photons in the blue range (300-450 nm) as in the carotenoids to produce red, orange, and yellow colors occur by simple conjugation of π bonds. But electronic configurations, which absorb longer wavelength photons in the red range (560-700 nm) to give a blue color, are rare by comparison. Excluding organometallic compounds and proteins, we estimate that ≥ 90% of natural blue pigments reported to date can be placed into one of just seven major structural classes: anthocyanin, anthraquinone, indole, tetrapyrrole, azulene, bis-pyridyl, and phenazine. These seven structure classes and specific examples are shown in Figure 3.

The majority of these structure classes contain N or O atoms associated with ring systems. The vast majority of compounds of the anthocyanin and anthraquinone classes are red or purple, not blue, in acidic conditions. Simply stated, blue pigments are rare in nature because the electronic configurations required for absorption of photons of 560-700 nm are more complex and occur infrequently. It should be noted that some natural blue compounds involve the transition metals (Fe, Cu, etc.). Transition metal complexes are often brightly colored because the quantum mechanical properties of *d* group orbitals often result in the lower energy electronic absorptions required for visible photon absorption. However, natural pigments involving transition elements are generally not practical for food or beverage use since they tend to occur within in protein complexes, precipitate at low pH, or have toxicity problems due to the metal itself.

Downloaded by PURDUE UNIVERSITY on July 29, 2013 | http://pubs.acs.org
Publication Date (Web): July 24, 2013 | doi: 10.1021/bk-2013-1138.ch008

Discovery of Novel Pigments

Because pigments are readily visible, brilliantly colored compounds from terrestrial sources were among some of the earliest natural products to be isolated, and the structure elucidation of these pigments began over a century ago (*22*). While the majority of the natural pigments in terrestrial plants and algae have been identified, there are still examples of uncharacterized pigments from these sources. Our research is focused on the isolation and identification of natural blue pigments from these remaining terrestrial sources such as obscure plants and extremophilic algae as well as the largely unexplored marine microbes. These organisms are likely to be sources of new blue natural products. A summary of the discovery process we are using is shown in Figure 4.

Pigments from Marine-Derived Microbes

A recent biodiversity study found that there are more than 10^5 microbial cells per milliliter of ocean water (*23*). Because the biodiversity of the marine environment is mostly unexplored, the prospects of discovering new compounds

and even new molecular scaffolds from marine microbes are better than from terrestrially sourced microbes. This vast marine microbial diversity makes natural drug discovery and in particular "natural pigment discovery" from the marine environment most appealing. In contrast to pigments of terrestrial organisms, which often serve photosynthetic, UV protectant, or insect attractant roles, microorganisms dwelling in the dark depths of the ocean have little need for absorption of visible light. As indicated by the assortment of marine cultures and fractions from our research in Figure 5, pigments do in fact occur quite commonly in microbes cultured from ocean sediments. Pigmented marine microbe metabolites often have structures suitable for absorption visible light that probably serve ecological or biological roles such as chemical defense completely unrelated to light absorption. The major disadvantage of sourcing the marine environment for consumable natural pigments is the high incidence of undesirable biological activity and toxicity.

Pigment compounds can be detected in microbial cultures by using a simple bioassay consisting of visual inspection of cultures. If extracts, fractions and/or subfractions have already been prepared and characterized in the course of a drug discovery program using techniques such as high-performance liquid chromatography (HPLC) with photodiode array (PDA) absorbance detection, these data files may simply be mined for specific visible absorbances. Therefore, pigment discovery can be incorporated as an accessory into natural products discovery programs such as marine microbial screening with minimal modifications to the operating procedures.

In addition to the discovery of novel pigments in microbial sources, the characterization of pigmented compounds in microbes can also be of general use for rapid chemotaxonomic identification. Often with microextraction of a single Petri culture followed by analysis using HPLC-PDA-high resolution tandem mass spectrometry ($HRMS^2$) analysis, it may be possible to obtain a short list of matching microbial genera or even probable species based on the presence of select classes of pigments without 16S rRNA sequence information. Such early chemotaxonomic information can be practical and informative in terms of project prioritization, strain novelty, and dereplication of other non-pigmented metabolites.

The marine-derived microbial diversity accessed in laboratory culture is highly dependent upon culture methods and the source of the marine samples. For example, some laboratories use heat shock, limited nutrients, etc., (*24*, *26*) to kill the majority of Gram-negative microbes in marine samples prior to culture and then use culture conditions that select for *Actinobacteria* (Gram-positive) since these are spore-forming prolific secondary metabolite producers (*25*, *26*). After pigment-producing strains are selected, the culture, isolation, and characterization of the strains and their pigments are pursued separately. Many solid and liquid marine nutrient media (*e.g.*, A1, M1, ISP2, and TCG) are slightly alkaline (~ pH 8) and close to the pH of the ocean. Unfortunately, many of the pigments that appear blue in alkaline cultures become red under acidic conditions. Blue(alkali)-red(acid) tautomerization behavior is a common characteristic of many pigments of the anthraquinone class (Figure 3).

Downloaded by PURDUE UNIVERSITY on July 29, 2013 | http://pubs.acs.org
Publication Date (Web): July 24, 2013 | doi: 10.1021/bk-2013-1138.ch008

Downloaded by PURDUE UNIVERSITY on July 29, 2013 | http://pubs.acs.org
Publication Date (Web): July 24, 2013 | doi: 10.1021/bk-2013-1138.ch008

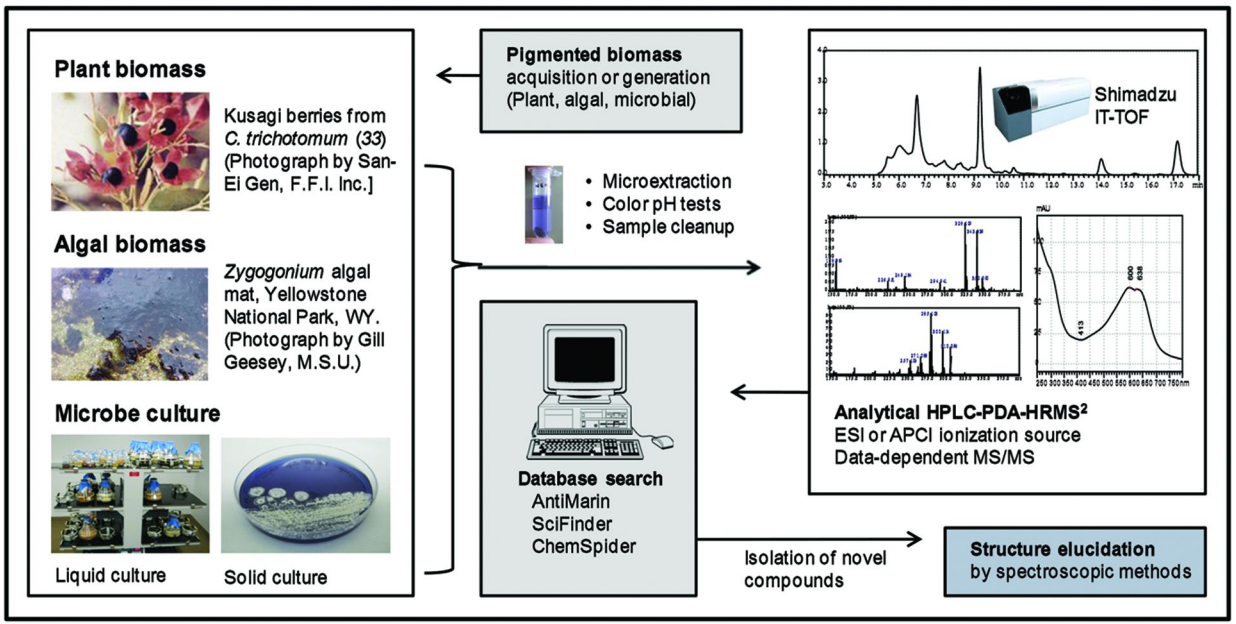

Figure 4. Flow diagram for the isolation and discovery of natural pigments. Pigmented biomass from plants and algae or microbial strains are isolated from environmental samples and extracted on a small scale for analysis by high performance liquid chromatography-photodiode array absorbance detection-high resolution tandem mass spectrometry (HPLC-PDA-HRMS²). Known compounds are dereplicated by comparing their mass spectrometric and spectrophotometric data against compound databases while novel compounds proceed to scale-up for structure elucidation by NMR spectroscopy. (see color insert)

Downloaded by PURDUE UNIVERSITY on July 29, 2013 | http://pubs.acs.org
Publication Date (Web): July 24, 2013 | doi: 10.1021/bk-2013-1138.ch008

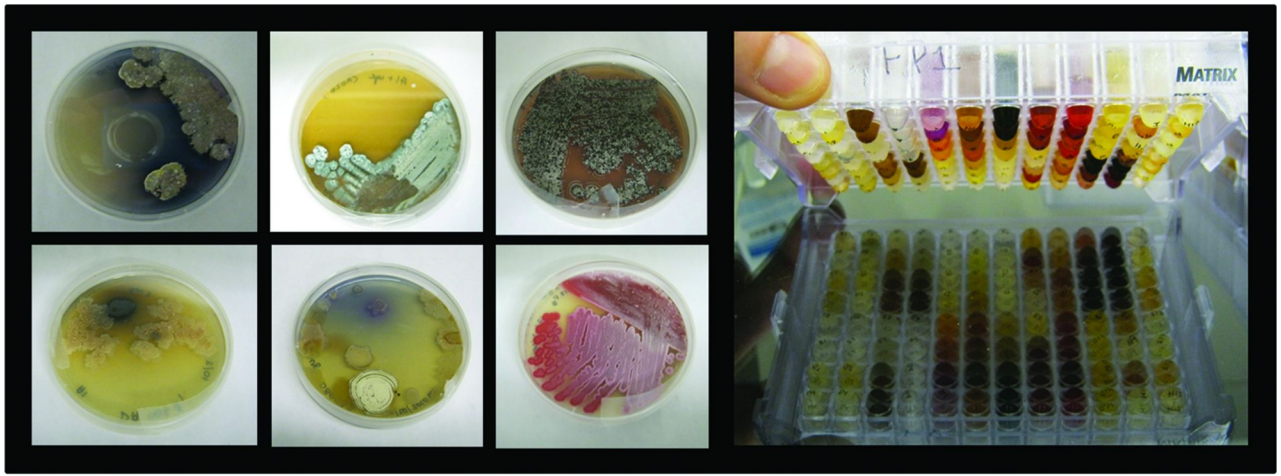

Figure 5. Pigmented marine microbial-derived actinomycete cultures (left) and a 100-well plate fraction library containing extracted secondary metabolites (right). (see color insert)

Microbial Pigment Extraction and Isolation

Microscale extraction of pigment compounds can be much more efficient and rapid than with non-pigmented compounds since the color serves as a rapid visual guide during extraction. In our research, it was often found that a single hyphenated HPLC-PDA-HRMS^2 injection of microextracted pigments from the cells or agar of a single Petri culture could provide enough information to identify pigment metabolites (excluding some minor structural details such as stereochemistry) and even possible microbial genera and species. The initial characterization is aided by the advantage that pigments have a more distinct UV-Vis spectrum as compared to non-pigments. Pigments produced by microbes can be either intracellular or extracellular. In the case of intracellular pigments, the cells must be lysed to release the pigmented contents, which can be achieved using a hypotonic buffer or freeze-thaw cycles. Extracellular pigments are more accessible, but must be separated from the high concentration of salts and other ingredients present in marine growth media. In these cases, pigments have been extracted from water through liquid-liquid extraction, precipitated by addition of a miscible organic solvent (typically, methanol or ethanol), or by solid-phase extraction using a resin such as Amberlite XAD16. Acidification (*e.g.,* 0.1% formic acid) followed by liquid partitioning into ethyl acetate has been a successful approach for most extracellular microbial pigments.

Highly polar pigments are not uncommon and pose an additional analytical challenge. Highly polar compounds are not amenable to liquid-liquid extraction to separate them from salts, and they often show little to no retention on reversed phase stationary phases. Silica gel separation is a mainstay for fractionation of crude natural product extracts but is inappropriate for highly polar pigments that can adsorb irreversibly to the silica. Instead, size-exclusion gel filtration materials such as Sephadex LH-20 or hydrophilic interaction liquid chromatography (HILIC) columns are often successful for fractionation of highly polar compounds. Conveniently, HILIC columns enable the separation of highly polar pigment metabolites using an acetonitrile-water gradient system.

Downloaded by PURDUE UNIVERSITY on July 29, 2013 | http://pubs.acs.org
Publication Date (Web): July 24, 2013 | doi: 10.1021/bk-2013-1138.ch008

Microbial Pigment Analysis and Identification

The microextraction and HPLC-PDA-HRMS^2 methods described below enable the rapid dereplication of individual pigment compounds using the combination of UV-Vis spectra and accurate mass spectrometry data. The primary system used here was a Shimadzu (Columbia, MD) HPLC with a PDA detector connected to a Shimadzu (Kyoto, Japan) Ion Trap – Time of Flight (IT-TOF) mass spectrometer. The use of a PDA detector instead of a less expensive single or dual λ UV detector is a significant advantage for pigment analysis since a complete UV-Vis spectrum can be obtained for each individual pigment constituent. Electrospray is our usual ionization method, but atmospheric pressure chemical ionization (APCI) may be used for more lipophilic pigments. Positive and

negative ion mass spectra are collected in a single run using polarity switching. Tandem mass spectra are collected in a data-dependent mode by computerized selection of the most abundant ions for fragmentation during product ion tandem mass spectra.

In the final preparation of an extract or fraction for HPLC-PDA-HRMS^2 analysis, the sample is generally diluted to a concentration between 50 and 500 μg mL^{-1} in a solvent close to the starting mobile phase composition (*e.g.,* CH_3CN/Water; 20:80, v/v) and centrifuged to remove particulates prior to injection. After the analysis, accurate mass and mass fragmentation data are used to generate a short list of likely chemical formulas. The accurate masses or the chemical formulas are then searched using chemical databases such as Antimarin, Scifinder Scholar, ChemSpider, PubChem, etc. The database matches are further refined by comparison with the UV-Vis spectrum. Other secondary characteristics, which are useful for consideration, include the culture morphology, compound polarity and overall chemical behavior such as acid-base tautomerization.

To demonstrate the use of the rapid microextraction and HPLC-PDA-HRMS^2 dereplication methods, the identification of pigments from the marine strain NE05-AB1 is described as an example. The intracellular violet pigment produced by cells from a 4 cm^2 area of Petri dish culture of strain NE05-AB1 (Lake Michigan, U.S.A.) was scraped from the surface. The pigment extracted readily by sonication in 2 mL of methanol. The extract was centrifuged at 10,000 x g for 15 min, and the supernatant was evaporated to dryness under a stream of nitrogen. The residue was reconstituted in 50 μL of methanol/water (50:50, v/v), centrifuged again and filtered through a 0.2 μm Nylon membrane. Following several HPLC test injections using an analytical C_{18} column, two peaks were collected after a single injection onto a semi-preparative C_{18} column (300 x 10 mm, 5 μm) using a methanol gradient from 10% to 95% over 20 min and detection at 580 nm.

The collected peaks were analyzed by HRMS-PDA-HRMS^n. Because the compounds were highly lipophilic, APCI was chosen instead of electrospray. For the two major compounds, abundant $[M+H]^+$ and $[M-H]^-$ ions were observed which were consistent ($\Delta M < 5$ ppm) with the formulas $C_{20}H_{13}N_3O_3$ (major peak) and $C_{20}H_{13}N_3O_2$ (minor peak). The chemical formulas, UV-Vis spectra, and tandem mass spectra were consistent only with the compounds violacein and deoxyviolacein (*27*) found in chemical databases SciFinder and Antimarin. HPLC-PDA-HRMS data including UV-Vis absorbance spectra, positive ion mass spectra and product ion tandem mass spectra (and fragmentation assignments) are shown in Figure 6.

Many pigmented compounds have been identified from marine-derived strains using similar microextraction and HPLC-PDA-HRMS^2 procedures. In several cases, analysis of the absorbance data, mass spectrometric data and culture morphology enabled the microbial species to be determined even before the 16S rRNA was sequenced. Some of these strains and structures of blue or purple pigments are shown in Figure 7.

Downloaded by PURDUE UNIVERSITY on July 29, 2013 | http://pubs.acs.org
Publication Date (Web): July 24, 2013 | doi: 10.1021/bk-2013-1138.ch008

Downloaded by PURDUE UNIVERSITY on July 29, 2013 | http://pubs.acs.org
Publication Date (Web): July 24, 2013 | doi: 10.1021/bk-2013-1138.ch008

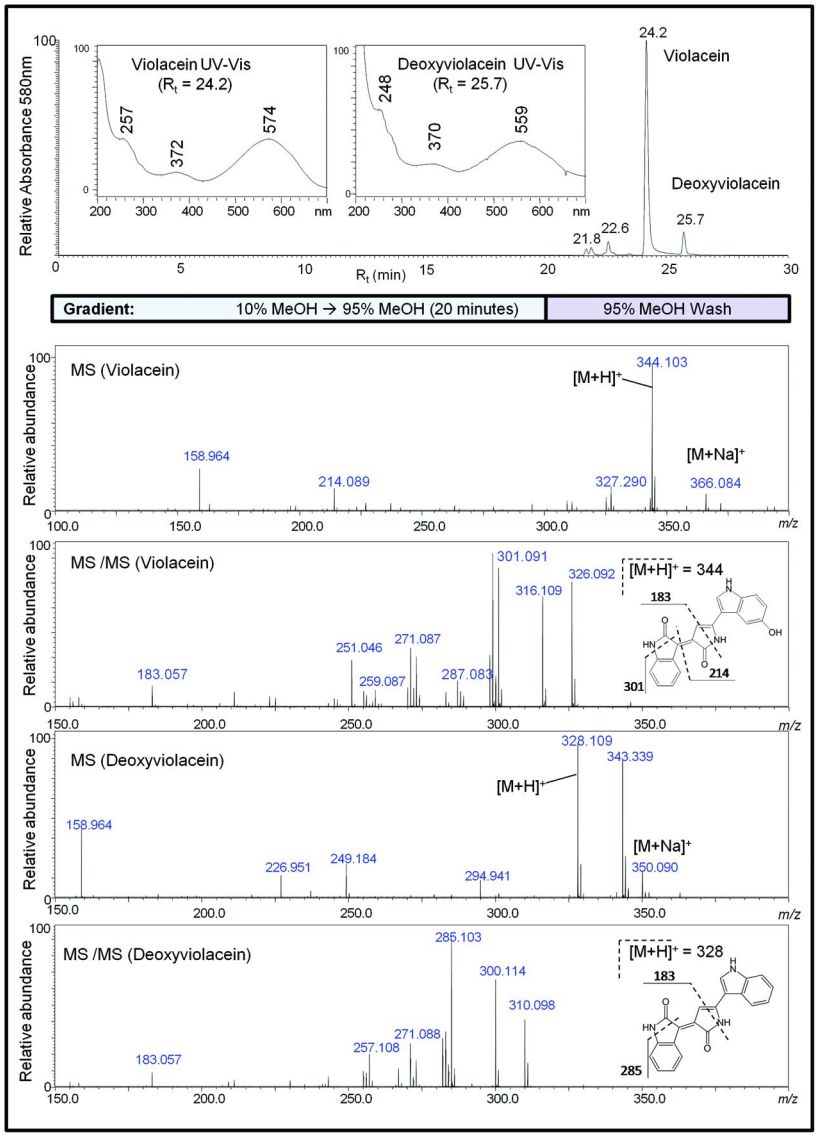

Figure 6. Semi-preparative HPLC chromatogram, UV-Vis spectra, positive ion high resolution mass spectra, and positive ion tandem mass spectra of two violet compounds, identified as violacein and deoxyviolacein, which were obtained from strain NE05-AB1 cultured from marine sediment (Lake Michigan, U.S.A.). (see color insert)

Downloaded by PURDUE UNIVERSITY on July 29, 2013 | http://pubs.acs.org
Publication Date (Web): July 24, 2013 | doi: 10.1021/bk-2013-1138.ch008

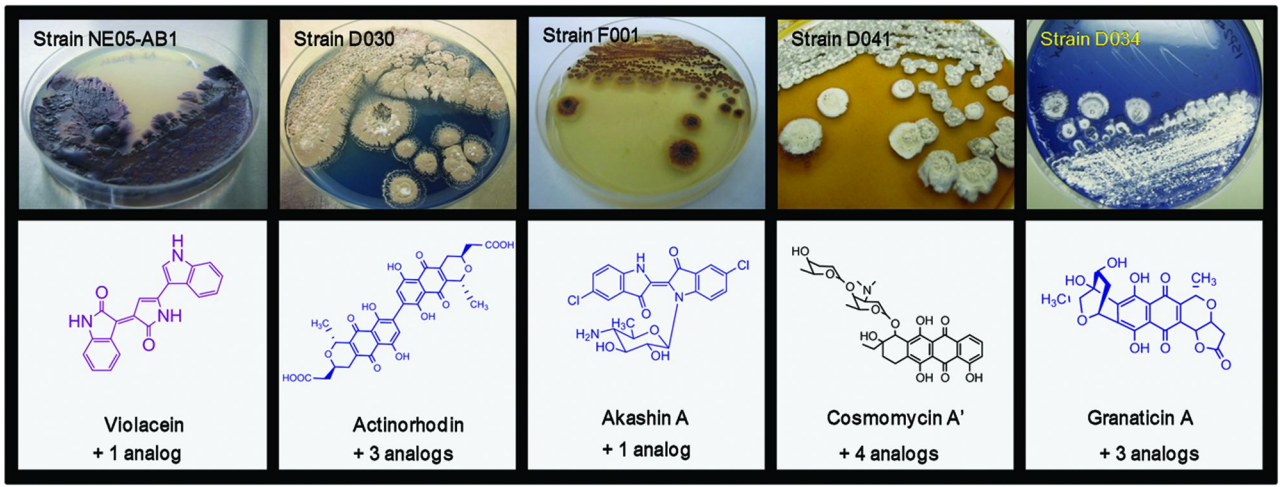

Figure 7. Blue or purple pigmented compounds identified in marine-derived microbial strains. The compound classes were identified by high resolution accurate mass measurements, high resolution tandem mass spectrometry, and UV-Vis spectra. The source strain and collection location are given in parenthesis. (see color insert)

In another example, four anthraquinone pigments were identified in an Amberlite XAD16 resin extract of strain D043 using HPLC-PDA-HRMS^2. The retention times and UV-Vis spectra, and crude 300 MHz NMR were similar but not consistent with a doxorubicin standard. Subsequently, HRMS^2 data were obtained and matched a similar yet structurally and genomically distinct set of anthraquinone antibiotics from *Streptomyces cosmosus* (Cosmomycins A′, B′, A, and B) (*28*). Strain D030 produced an extracellular blue pigment in agar cultures (Figure 7), and the pigment was extracted into water directly from chopped culture agar. Acidification of the blue aqueous extract with 0.1% formic acid tautomerized the pigments into a red form, which extracted readily into ethyl acetate. Actinorhodin and several related congeners were identified from this agar microextract by HPLC-PDA-HRMS^2 (Figure 7). The 16S rRNA sequence of the strain later showed a 100% match with the well studied terrestrial species *Streptomyces coelicolor* (*29*). The chlorinated indigo analog akashin A, reported a few years earlier from a terrestrial *Streptomyces sp.*(*30*), was identified from Strain F001 (Figure 7).

Downloaded by PURDUE UNIVERSITY on July 29, 2013 | http://pubs.acs.org
Publication Date (Web): July 24, 2013 | doi: 10.1021/bk-2013-1138.ch008

Structure Elucidation of Novel Pigments

Spectroscopic evidence for the presence of novel pigmented compounds in a microbial strain can often be established from a single HPLC-PDA-HRMS^2 analysis. The microbe can then be grown on a larger scale to obtain milligram quantities of pure pigmented compounds for isolation and structure elucidation by NMR spectroscopy. From 1 to 40 liters of liquid culture of the microbe may be required. Pigments with high molar absorptivities (ε) may appear abundant even when present at minute levels. When the chromophore class of a novel pigment is known, the quantity of the culture needed to obtain milligram quantities of the pure compounds can be estimated easily. As a practical measure for estimation, the molar absorptivity of any pigment of the same chromophore type may be used from the literature. The concentration of the novel pigment in the sample can then be estimated using absorbance readings from the HPLC-UV/Vis data and Beer's law ($A = \varepsilon cl$). Back-calculation can then provide a rough estimation of the amount of the pigmented compound in the culture (*i.e.* in terms of μg compound per mL of culture) to use as a guideline for the amount of scale-up culture required.

Sometimes, pigment observed in solid cultures may not be produced when transferred to liquid culture of the same media. In this case, scaled-up agar culture may be carried out using any large autoclave-compatible and sealable vessel. In practice, inexpensive and reusable casserole dishes (i.e. 2-quart capacity with glass lid) have worked well for larger scale agar culture. Some microbial strains are very slow growing and may take several months to mature for metabolite extraction. *Actinomycetes* are particularly notorious for slow growth. Since some pigments are light sensitive, microbial cultures should also be protected from light exposure during growth.

For scaled-up extractions, crude pigment extracts are generally fractionated by open column chromatography that facilitate visual detection of the colored bands. Final purification is performed by using semi-preparative HPLC with UV/Vis detection. Reversed phase chromatography will suffice for most

applications, but HILIC or other specialty columns may be required for highly polar, macromolecular or ionic pigmented compounds. High resolution mass spectrometry with accurate mass measurement for elemental composition determination combined with two-dimensional (2D) NMR spectroscopy (preferably using 600 MHz or higher magnet strength) is ideal for structure determination of novel compounds. A usual 2D NMR experiment for natural product structures includes DEPT Q, COSY, HSQC, HMBC, and ROESY. The ROESY experiment measures through-space proton couplings and can provide some stereochemical information, but often additional experiments are required for complete determination of stereochemistry depending upon the compound. When a crystal of an analyte can be obtained, X-ray crystallography in combination with high resolution mass spectrometry can provide the complete structure including absolute stereoconfiguration.

Downloaded by PURDUE UNIVERSITY on July 29, 2013 | http://pubs.acs.org
Publication Date (Web): July 24, 2013 | doi: 10.1021/bk-2013-1138.ch008

Pigments from Underexplored Terrestrial Sources

Although most terrestrial sources of blue natural products have been investigated, the chemical structures of a few blue pigments remain unknown. As examples, the continuing characterization of blue pigments from the blue fruits of *Clerodendron trichotomum*, an Asian shrub, and a high molecular weight purple pigment from an extremophilic *Zygogonium sp.* alga from Yellowstone National Park (WY) are discussed.

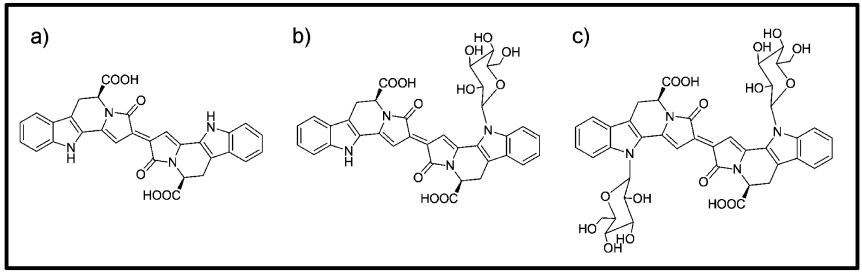

Figure 8. Structures of the alkaloid pigments (a) trichotomine (b) trichotomine G_1 and (c) trichotomine G_2 isolated and characterized from the fruits of Clerodendron trichotomum.

Novel Trichotomine Glycosides from Japanese Kusagi Berry

The blue colored bis-indole alkaloid pigment trichotomine (*31*) and two glycosides thereof (*32*) were isolated and characterized from the berries of the Asian shrub *Clerodendron trichotomum* ("Kusagi") (*33*). Extracts of the Kusagi berry have been used in Japan to produce a blue textile dye. With such elaborate and unusual alkaloid structures, it is perhaps surprising that the pigments have hardly been investigated for other possible uses such as for natural colorants of

food and beverages. Researchers at the natural colorant company San-Ei Gen F.F.I. Inc. (Japan) have generated the most data to date regarding the Kusagi berry pigments. The structures of the known Kusagi berry pigments are shown in Figure 8.

In an effort to identify additional pigment constituents from the Kusagi berry, an extract of wild-collected Kusagi berries from Japan was obtained from San-Ei Gen F.F.I Inc. for our research. The extract was prepared for HPLC-PDA-HRMS^2 analysis as follows. A 10 mL aliquot of the aqueous Kusagi color extract was defatted with hexane (10 mL x 7). A 1 mL aliquot was then centrifuged at 12,000 x g for 15 min, and 20 µL of the supernatant was diluted to 100 µL with deionized water. HPLC-PDA-HRMS^2 analysis of 15 µL of the sample was carried out using a Phenomenex (Torrance, CA) Columbus C_{18} column, 150 x 2.0 mm 3 µm, with a mobile phase system consisting of 10-min gradient from 30% to 70% acetonitrile in water containing 0.1% formic acid (pH 2.8) followed by a 10-min isocratic hold at 70% acetonitrile. The flow rate was 0.2 mL min^{-1}. High resolution accurate mass measurements and data-dependent product ion tandem mass spectra were obtained using a Shimadzu IT-TOF mass spectrometer with positive ion electrospray. Mass and PDA chromatograms and a UV/Vis spectrum are shown in Figure 9.

Downloaded by PURDUE UNIVERSITY on July 29, 2013 | http://pubs.acs.org
Publication Date (Web): July 24, 2013 | doi: 10.1021/bk-2013-1138.ch008

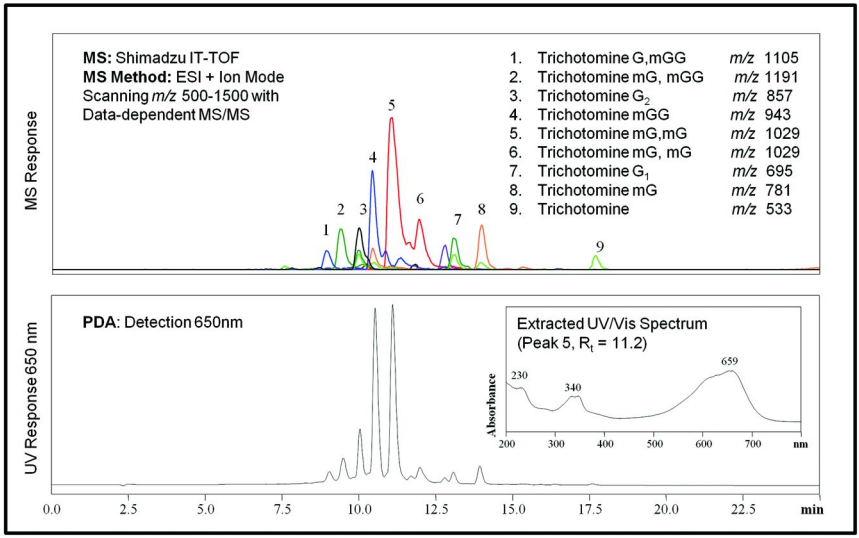

Figure 9. Computer-reconstructed mass chromatograms (top) and PDA chromatogram (bottom) of blue pigment constituents of a Kusagi berry extract. Except for compounds 3, 7, and 9, none of the constituents have been previously reported. G = glycoside, mG = malonylglycoside. (see color insert)

In addition to the accurate masses, absorption spectra, and glycoside fragmentation patterns consistent with trichotomine (**9**), trichotomine G_1 (**7**) and trichotomine G_2 (**3**) (Figure 9), the accurate mass and fragmentation data provide strong evidence for the presence of at least 6 additional glycosylated trichotomine

analogs. The novel glycosides showed fragmentation losses of 248, which are characteristic of glycosides containing malonyl groups, 161 ($C_6H_9O_5$) + 87 ($C_3H_3O_3$) = 248 (malonylglycoside). The product ion tandem mass spectrum of one of the novel analogs (Trichotomine mGG, **4** *m/z* 943) is shown in Figure 10 as an example. The tandem mass spectrum shows a loss of 162 (glycoside) and a loss of 248 (malonylglycoside) suggesting trichotomine analogues with one glycosyl and one malonylglycosyl residue attached. These novel analogues are being purified for structural determination (glycosyl residue identity, stereochemistry, and points of attachment) using NMR spectroscopy.

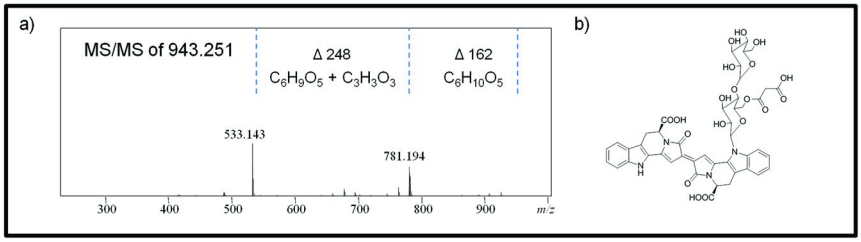

*Figure 10. a) Positive ion electrospray product ion tandem mass spectrum of compound **4** (Figure 9) of m/z 943.251. Accurate mass measurement indicated an elemental composition of $C_{45}H_{42}N_4O_{19}$ (ΔM 0.96 ppm). Note the losses of glycoside and malonylglycoside residues from trichotomine. (b) Proposed structure of **4** consistent with the accurate mass measurement, UV/Vis spectrum and tandem mass spectrum.*

Downloaded by PURDUE UNIVERSITY on July 29, 2013 | http://pubs.acs.org
Publication Date (Web): July 24, 2013 | doi: 10.1021/bk-2013-1138.ch008

Purple Pigment of the Extremophilic *Zygogonium sp.* Algae

The presence of purple pigments in the vacuoles of several members of the *Zygogonium* genus of algae have been documented for over a century (*34–36*). However, none of these purple pigments had been analyzed spectroscopically prior to this work. In our research, pigmented biomass of the alga was obtained from an acid bog in Yellowstone National Park (WY) through a material transfer agreement with Dr. Gill Geesey at Montana State University. The violet pigment was purified by methanol precipitation followed by size-exclusion gel chromatography with Sephadex G_{25}. The process from sample collection to purification is illustrated in Figure 11. Following purification, the pigment was analyzed using MALDI-TOF-MS, FTIR and NMR spectroscopy. The traditional organic spectroscopic data were all characteristic of a polysaccharide substance but offered no clues as to the origin of the purple pigmentation. Molecular weight, glycosyl composition, and glycosyl linkage analysis (performed by the Complex Carbohydrate Research Center at the University of Georgia) indicated the pigment was a polysaccharide (0.85 ± 0.10 wt/wt) of variably branched and linked glucose units with an average MW of 30 kD. Since polysaccharides are notoriously achromophoric, the data thus far offered no explanation as to the origin of the purple pigmentation.

In Physical Methods in Food Analysis; Tunick, M., et al.;
ACS Symposium Series; American Chemical Society: Washington, DC, 2013.

Downloaded by PURDUE UNIVERSITY on July 29, 2013 | http://pubs.acs.org
Publication Date (Web): July 24, 2013 | doi: 10.1021/bk-2013-1138.ch008

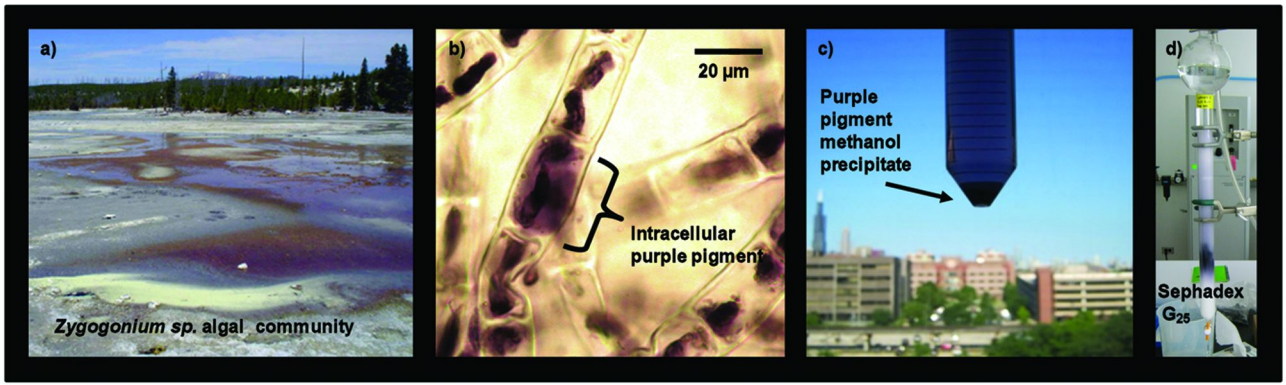

Figure 11. (a) A Zygogonium sp. algal mat community at Dragon Spring in Yellowstone National Park (WY) courtesy of Gill Geesey. (b) Light microscopy showing purple pigment within the intracellular compartment of an algal cell. (c) Pellet of purple pigment obtained after methanol precipitation. (d) Purification of precipitated pigment using the size-exclusion material Sephadex G_{25}. (see color insert)

Downloaded by PURDUE UNIVERSITY on July 29, 2013 | http://pubs.acs.org
Publication Date (Web): July 24, 2013 | doi: 10.1021/bk-2013-1138.ch008

Additional experiments, such as scanning electron microscopy with X-ray microanalysis, indicated the presence of iron in the sample. Also, acidic hydrolysis of the polysaccharide followed by HPLC-PDA-MS analysis revealed a minor presence of gallic acid. The total iron and gallic acid were quantitated using the colorimetric 1,10-phenanthroline method and UPLC-MS/MS, respectively, and were found to be in a molar ration of ~1:2 molar ratio and to account for ~15% (wt/wt) of the pigment. Electron spin resonance spectroscopy indicated the presence of high-spin ferric iron in the sample (*g* value = 4.3). To probe the nature and bonding of the iron in the sample, a Mössbauer spectrum was acquired at Argonne National Labs. As shown in Figure 12, the hyperfine parameters for the iron obtained from Mössbauer spectroscopy at 300 K (Q.S. = 1.08, I.S. = 0.31) were consistent with published data for ferric iron bound to polyphenolic moieties in a *bis* configuration ($Fe^{3+}L_2$) (*37*, *38*) and were close to values published for ferric $(gallate)_2$ complex (*37*). The UV-Vis spectrum of an aqueous preparation of Fe^{3+} and gallic acid in a 1:2 molar ratio compares closely with the UV-Vis spectrum of the natural pigment. These studies indicate the purple pigmentation of the highly branched glucose polysaccharide complex isolated from the *Zygogonium sp.* alga is largely if not completely due to the presence of ferric $(gallate)_2$ complexes.

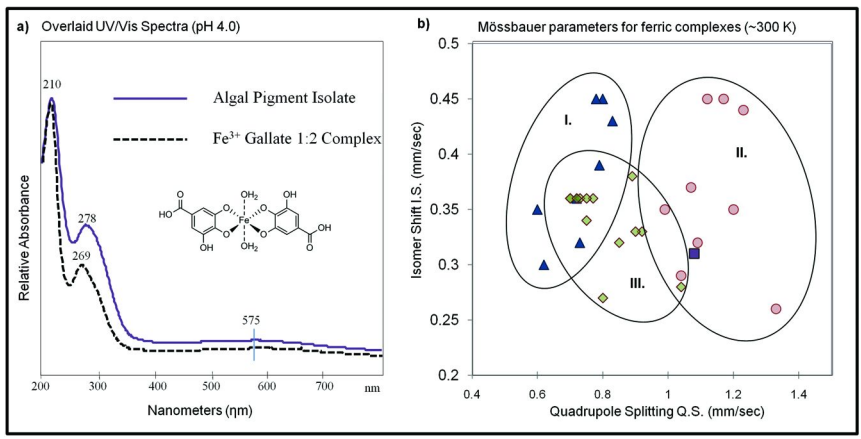

Figure 12. (a) Overlaid UV-Vis spectra (H_20, pH 4.0) for the natural algal pigment isolate and a synthetic ferric gallate 1:2 complex. The structure of the synthetic material is shown. (b) A plot of the Mössbauer hyperfine parameters (Q.S. versus I.S.) for a representative sampling of ferric catecholate and ferric polysaccharide compounds reported in the literature for comparison with the parameters obtained for the natural pigment (•). Data were collected at ~300 K. (Group I. ▲ = 1:1 Fe^{3+} catecholate complexes, Group II. • = 1:2 Fe^{3+} catecholate complexes, Group III. ♦ = Fe^{3+} polysaccharide complexes). The literature datapoint closest in value to the natural pigment corresponds to $Fe^{3+}(gallate)_2$ (37). (see color insert)

Conclusion

The literature review and research presented here demonstrate the continuing discovery of natural pigments from underexplored sources such as from marine microbes, extremophiles, and understudied terrestrial plants. This research approach describes useful analytical methodology for the rapid discovery new natural pigments through examples of isolation and characterization. While this work is focused on the discovery of natural blue and purple colorants for food and beverage use, natural pigmented compounds have many other potential commercial, medical and research applications. Therefore, pigments encountered during any natural product research program, which are often ignored and discarded, can instead be investigated for possible commercial or scientific applications.

Downloaded by PURDUE UNIVERSITY on July 29, 2013 | http://pubs.acs.org
Publication Date (Web): July 24, 2013 | doi: 10.1021/bk-2013-1138.ch008

Acknowledgments

We would like to thank Dr. Cathy Culver of PepsiCo (Valhalla, NY) for supporting this project, Dr. Nakashima at San-Ei Gen (Osaka, Japan) for providing the Kusagi berry extract, Dr. Gill Geesey of Montana State University (Bozeman, MT) for sample collection from Yellowstone National Park, and Dr. Ercan Alp of Argonne National Laboratory (Argonne, IL) for assistance with the acquisition of the Mössbauer spectrum. This work was supported by PepsiCo and Shimadzu.

References

1. Delgado-Vargas, F.; Paredes-Lopez, O. *Natural Colorants for Food and Nutraceutical Uses*, 1st ed.; CRC Press: Boca Raton, FL, 2003.
2. Dufosse, L. *Food Technol. Biotechnol.* **2006**, *44*, 313–321.
3. Sharma, V.; McKone, H. T.; Markow, P. G. *J. Chem. Educ.* **2011**, *88*, 24–28.
4. Downham, A.; Collins, P. *Int. J. Food Sci. Technol.* **2000**, *35*, 5–22.
5. Wissgott, U.; Bortlik, K. *Trends Food Sci. Technol.* **1996**, *7*, 298–302.
6. Handelman, G. J.; Nightingale, Z. D.; Lichtenstein, A. H.; Schaefer, E. J.; Blumberg, J. B. *Am. J. Clin. Nutr.* **1999**, *70*, 247–251.
7. Raja, R.; Hemaiswarya, S.; Rengasamy, R. *Appl. Microbiol. Biotechnol.* **2007**, *74*, 517–523.
8. Mortensen, A. *Pure Appl. Chem.* **2006**, *78*, 1477–1491.
9. Jackman, R. L.; Yada, R. Y.; Tung, M. A.; Speers, R. A. *J. Food Biochem.* **1987**, *11*, 201–247.
10. Castaneda-Ovando, A.; Pacheco-Hernandez, M. L.; Paez-Hernandez, M. E.; Rodriguez, J. A.; Galan-Vidal, C. A. *Food Chem.* **2009**, *113*, 859–871.
11. Romay, C.; Armesto, J.; Remirez, D.; Gonzalez, R.; Ledon, N.; Garcıa, I. *Inflammation Res.* **1998**, *47*, 36–41.
12. Romay, C.; González, R.; Ledón, N.; Remirez, D.; Rimbau, V. *Curr. Protein Pept. Sci.* **2003**, *4*, 207–216.
13. Jespersen, L.; Lene D. Strømdahl, L. D.; Olsen, K.; Skibsted, L. H. *Eur. Food Res. Technol.* **2005**, *220*, 261–266.

14. Chan, G.; Francis, T.; Thureen, D. R.; Offen, P. H.; Pierce, N. J.; Westley, J. W.; Johnson, R. K. *J. Org. Chem.* **1993**, *58*, 2544–2546.
15. Hughes, C. C.; MacMillan, J. B.; Gaudêncio, S. P.; Jensen, P. R.; Fenical, W. *Angew. Chem., Int. Ed.* **2009**, *48*, 725–727.
16. Spitzner, D.; Htifle, G.; Klein, I.; Pohlan, S.; Ammermann, D.; Jaenicke, L. *Tetrahedron Lett.* **1998**, *39*, 4003–4006.
17. Grossart, H-P.; Thorwest, M.; Plitzko, I.; Brinkhoff, T.; Simon, M.; Zeeck, A. *Int. J. Microbiol.* **2009** Article ID 701735.
18. Plitzko I. Ph. D. Thesis, University of Gottingen, Gottingen, DE, 2007.
19. Chen, D.; Yu, S.; van Ofwegen, L.; Proksch, P.; Lin, W. *J. Agric. Food Chem.* **2012**, *60*, 112–123.
20. Bulina, M. E.; Lukyanov, K. A.; Yampolsky, I. V.; Chudakov, D. M.; Staroverov, D. B.; Shcheglov, A. S.; Gurskaya, N. G.; Lukyanov, S. *J. Biol. Chem.* **2004**, *279*, 43367–43370.
21. Kobayashi, H.; Nogi, Y.; Horikoshi, K. *Extremophiles* **2007**, *11*, 245–250.
22. Tswett, M. S. *Proc. Warsaw Soc. Nat., Biol.* **1905**, *14*, 20–39.
23. Sogin, M. L.; Morrison, H. G.; Huber, J. A.; Welch, D. M.; Huse, S. M.; Neal, P. R.; Arrieta, J. M.; Herndl, G. J. *Proc. Natl. Acad. Sci. U.S.A.* **2006**, *103*, 12115–12120.
24. Jensen, P. R.; Fenical, W. *Annu. Rev. Microbiol.* **1994**, *48*, 559–584.
25. Bérdy, J. *J. Antibiot.* **2005**, *58*, 1–26.
26. Subramani, R.; Aalbersberg, W. *Microbiol. Res.* **2012**, *167*, 571–580.
27. Duran, N.; Justo, G. Z.; Ferreira, C. V.; Melo, P. S.; Cordi, L.; Martins, D. *Biotechnol. Appl. Biochem.* **2007**, *48*, 127–133.
28. Hirayama, K.; Akashi, S.; Ando, T.; Horino, I.; Etoh, Y.; Morioka, H.; Shibai, H.; Murai, A. *Biol. Mass Spectrom.* **1987**, *14*, 305–312.
29. Zhang, H.; Zhan, J.; Su, K.; Zhang, Y. *Food Chem.* **2006**, *95*, 186–192.
30. Maskey, R. P.; Grün-Wollny, I.; Laatsch, H. *Nat. Prod. Res.* **2005**, *19*, 137–142.
31. Iwadare, S.; Shizuri, Y.; Sasaki, K.; Hirata, Y. *Tetrahedron* **1974**, *30*, 4105–4111.
32. Koda, T.; Ichi, T.; Odake, K.; Furuta, H.; Sekiya, J. *Biosci., Biotechnol., Biochem.* **1992**, *56*, 2020–2022.
33. Ichi, T.; Shimizu, T.; Yoshihira, K. In *Biotechnology in Agriculture and Forestry 37: Medicinal and Aromatic Plants IX*; Bajaj, Y. P. S.; Springer: Berlin, DE, 1996; Vol. 27, pp 108−126.
34. Lagerheim, G. Über das Phycoporphyrin, einen Conjugaten-farbstoff. *Videnskabs-Selskabets Skrifter I. Math. Naturv. Kl* **1895**, *5*, 3–13.
35. Alston, R. E. *Am. J. Bot.* **1958**, *45*, 688–692.
36. Holzinger, A.; Tschaikner, A.; Remias, D. *Protoplasma* **2010**, *243*, 15–24.
37. Gust, J.; Sewalski, J. *Corros. Sci.* **1994**, *50*, 355–366.
38. Jaen, J. A.; Garcıa de Saldana, E.; Hernandez, C. *Hyperfine Interact.* **1999**, *122*, 139–145.

Downloaded by PURDUE UNIVERSITY on July 29, 2013 | http://pubs.acs.org
Publication Date (Web): July 24, 2013 | doi: 10.1021/bk-2013-1138.ch008

Downloaded by UNIV OF MICHIGAN ANN ARBOR on July 29, 2013 | http://pubs.acs.org
Publication Date (Web): July 24, 2013 | doi: 10.1021/bk-2013-1138.ch009

Chapter 9

Resonance Raman Study on the pH Dependence on Grape Anthocyanins

A. E. Burns,*,[1] J-P. Mazauric,[2] and V. Cheynier[2]

[1]Department of Chemistry, Kent State University Stark Campus, 6000 Frank Avenue, North Canton, Ohio 44720
[2]INRA, UMR Sciences pour l'Enologie, 2 Place Viala, 34060 Montpellier, France
***E-mail: aburns@kent.edu.**

Vibrational spectroscopy was used to study the different forms of anthocyanins at various pH. The Resonance Raman (RR) spectra of three grape anthocyanins are reported as a function of pH, using blue light with a wavelength of 433 nm. This light did not eliminate fluorescence but reduced it enough to observe a sufficient Raman signal. The Raman spectra clearly show differences in the anthocyanins at the different pH values. At an acidic pH below 3, the red flavylium cation form is observed, with its strong RR band at 1590 cm^{-1} and broad peak at 1350 cm^{-1}. As the pH is increased to 7 or 8, the flavylium ion can transform into a clear carbinol pseudobase or to a blue quinonoidal base form. This is observed with the 1590 cm^{-1} peak vanishing and the 1350 cm^{-1} peak separating into two bands. In addition, at pH above 6, the band at 1650 cm^{-1} broadens due to a C=O vibration and a band at 1200 cm^{-1} due to a vinyl ether stretch, both existing in the quinonoidal base only.

© 2013 American Chemical Society
In Physical Methods in Food Analysis; Tunick, M., et al.;
ACS Symposium Series; American Chemical Society: Washington, DC, 2013.

Downloaded by UNIV OF MICHIGAN ANN ARBOR on July 29, 2013 | http://pubs.acs.org
Publication Date (Web): July 24, 2013 | doi: 10.1021/bk-2013-1138.ch009

Introduction

Anthocyanins are found in many fruits, vegetables, and flowers, producing beautiful blue and red colors (*1*). Most of the anthocyanins exist as either mono or di-glucosides, meaning there is one or two glucose molecules attached to the anthocyanin molecule. There is enormous information on these chemicals in terms of their antioxidant health benefits, and thus they are classified as phytochemicals. Many studies have also investigated their structure and reactions.

This study focuses only on anthocyanins found in grapes, of which there are five, and all are mono-glucosides. The most widely studied of these five are malvidin-3-glucoside, delphinidin-3-glucoside, and cyanidin-3-glucoside, due to the ease of separating the molecules using standard analytical techniques. The various grape anthocyanin mono-glucosides are shown in Figure 1.

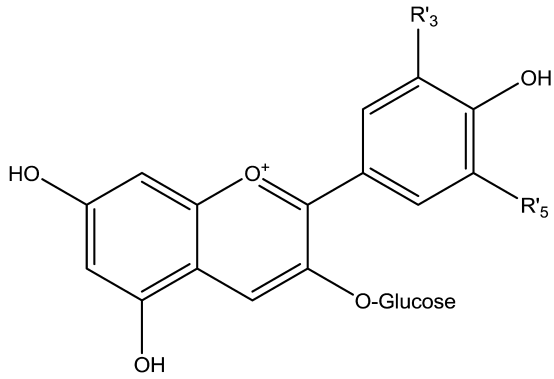

	R'_3	R'_5		
	H	H	pelargonidin	
	OH	H	cyanidin	
Names	OCH_3	H	peonidin	found in grapes
	OH	OH	delphinidin	
	OH	OCH_3	petunidin	
	OCH_3	OCH_3	malvidin	

Figure 1. The basic structure of anthocyaniins, all shown with a glucose attached.

Anthocyanins exist in 4 forms, depending on the pH of the solution. These forms and the conditions and criteria between the forms have been studied over the years. The spectroscopic techniques used to deduce these forms have been UV-Vis (1), NMR (*2*), and even Raman (*3–5*) These 4 forms are shown in Figure 2. The most notable form in grapes, due to its red color, is the flavylium cation form. This form exists exclusively at low pH. As the pH increases towards 4 or 5, the carbinol pseudobase and chalcone forms exist, in a tautomeric relationship. These intermediate pH forms are colorless. At a pH above 6, the blue color quinonoidal base form exists. All of these forms have equilibria between them (*6*), as shown in Figure 2

Downloaded by UNIV OF MICHIGAN ANN ARBOR on July 29, 2013 | http://pubs.acs.org
Publication Date (Web): July 24, 2013 | doi: 10.1021/bk-2013-1138.ch009

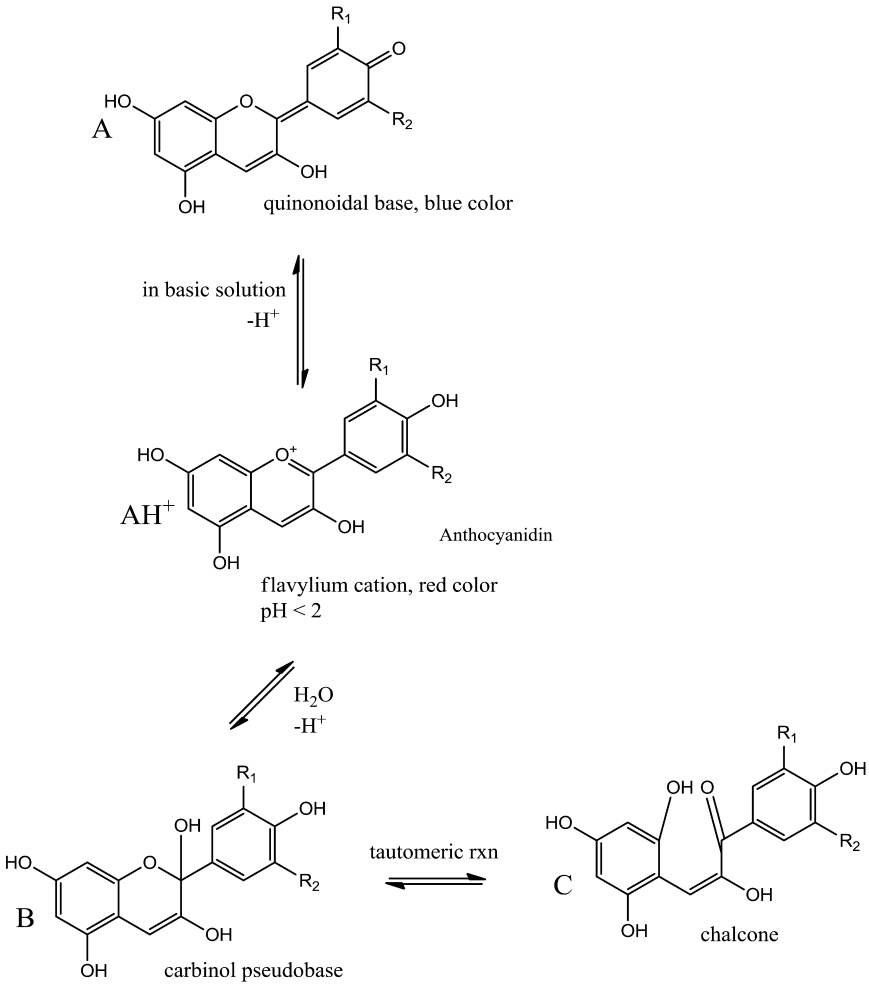

Figure 2. The structures of the various forms of the anthocyanidins as a function of pH.

The excitement of vibrational studies on grape anthocyanins is not only due to the various forms of the anthocyanins, but for the potential of investigating their reactions within the grape cells. UV-Vis and NMR are not sensitive enough to study reactions within cells, whereas vibrational spectroscopy might be able to do this. However, before attempting to study anthocyanin reactions within cells, some fundamental information must be obtained. One first must be able to determine and identify the anthocyanin form based on pH. In addition, the ability to observe an acylated product is also critical, as the addition of an acid to an anthocyanin produces an acylated product. This reaction occurs inside the cell, and the ability to observe this reaction would lead to a much deeper understanding into the genetics and properties of anthocyanins.

Raman spectroscopy is a form of vibrational spectroscopy, as is IR. With Raman, the molecule is excited with light in the Vis region of the spectrum, promoting an electron from a ground electronic state and ground vibrational level to a different electronic level before it scatters and drops in energy to the ground electronic state but to a new vibrational quantum level, the rule being $\Delta v = \pm 1$. For IR, the energy used to excite the electron is in the infrared region, and only promotes an electron from its ground vibrational state to a higher vibrational level, also with the quantum mechanical rule of $\Delta v = \pm 1$. The difference between normal Raman and Resonance Raman is due to the electronic excitation. For normal Raman, the excited electronic level is a virtual level, whereas for RR, the excited electronic level is a true electronic excited state. This is seen in Figure 3. By exciting a sample to an electronic excited state, the Raman effect is enhanced by orders of magnitude due to coupling from modes of motion such as changes in bond lengths and angles from the excited state relative to the ground state. This is critical when dealing with low concentrations of solute molecules.

Downloaded by UNIV OF MICHIGAN ANN ARBOR on July 29, 2013 | http://pubs.acs.org
Publication Date (Web): July 24, 2013 | doi: 10.1021/bk-2013-1138.ch009

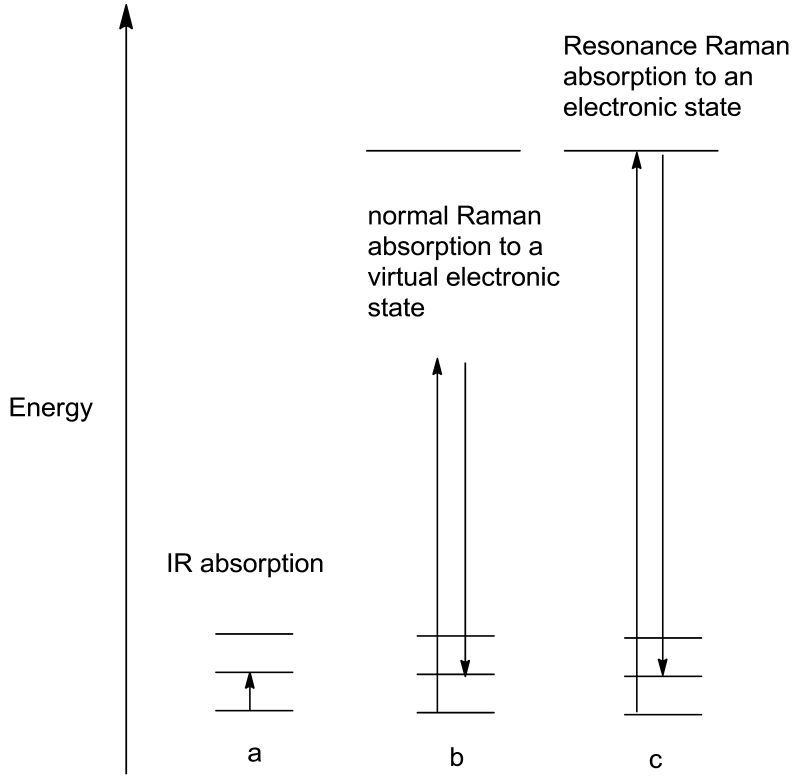

Figure 3. The energy levels of IR and Raman absorption.

In Physical Methods in Food Analysis; Tunick, M., et al.;
ACS Symposium Series; American Chemical Society: Washington, DC, 2013.

Experimental

The anthocyanins were obtained from skin extraction of Vitis vinifera Aliconte Bouschet grapes. The technique has been described extensively previously (*7*), but will be briefly discussed here. The grapes, including the skins, were frozen in liquid nitrogen, and then ground. The powder was extracted with an ethanol/water and 2% acetic acid solution overnight. The extract was sieved and filtered through a GF/C glass microfiber. The liquid extract was then concentrated under vacuum before undergoing HPLC (960 LC, Varian) to isolate the anthocyanins. The anthocyanins were checked with a diode array detector attached to the HPLC. In addition, anthocyanins purchased from Extransynthese (Genay France), were used for comparing the Raman spectra, which provided proof of purity of the extracted samples.

The Raman spectrometer used was a Horiba Jobin Yvon LabRam Aramis IR^2, which included micro-Raman and IR capabilities. All spectra shown in this work used the micro-Raman set-up, due to use of liquid samples. The laser used for this work was a blue diode laser with a wavelength of 433 nm, providing for Resonance Raman, and minimizing fluorescence. Two other laser options for this spectrometer were a Helium-Neon laser at 633nm and a diode laser at 785 nm. The power for solid samples was 90μW and for liquid samples 8-10 μW. The detector was a CCD detector cooled by a Pelletier Nodule at -70°C. The Raman arrangement used in this work was backscattering through the microscope objective.

Solid anthocyanin spectra were taken by placing the sample directly onto the Raman sample stage on a glass microscope slide, although their spectra are not shown in this work. Liquid Raman samples were prepared immediately prior to obtaining the spectra, due to the sensitivity of the liquid anthocyanins, and then placed on the microscope slide. The liquid anthocyanin samples were produced by adding one drop of methanol to a few micrograms of anthocyanin sample. Then, a few drops of appropriate buffer were added to maintain the desired pH and to minimize the amount of liquid, especially water. The concentration of the samples was in the range of 10^{-3}-10^{-4}M.

UV-Vis spectra on the liquid samples were taken with a Safas spectrometer having a 10 mm path length and quartz cells. The liquid samples were prepared as stated above.

Results and Discussion

Raman spectra taken with the lasers at 633 nm or 785 nm were not good. This is a two-fold problem. The first is that the Raman scattering probability goes according to the wavelength λ, as $1/\lambda^4$, thus using red light (633 nm or even 785 nm) instead of blue (433 nm), causes the Raman effect to be considerably weaker, especially with low concentrations of solute molecules. In addition, there is more fluorescence at higher wavelength. The IR spectra were not useful, as there is too much water in the solutions, which is highly absorbed, thus making the spectra useless for molecular understanding.

In Physical Methods in Food Analysis; Tunick, M., et al.;
ACS Symposium Series; American Chemical Society: Washington, DC, 2013.

Downloaded by UNIV OF MICHIGAN ANN ARBOR on July 29, 2013 | http://pubs.acs.org
Publication Date (Web): July 24, 2013 | doi: 10.1021/bk-2013-1138.ch009

Downloaded by UNIV OF MICHIGAN ANN ARBOR on July 29, 2013 | http://pubs.acs.org
Publication Date (Web): July 24, 2013 | doi: 10.1021/bk-2013-1138.ch009

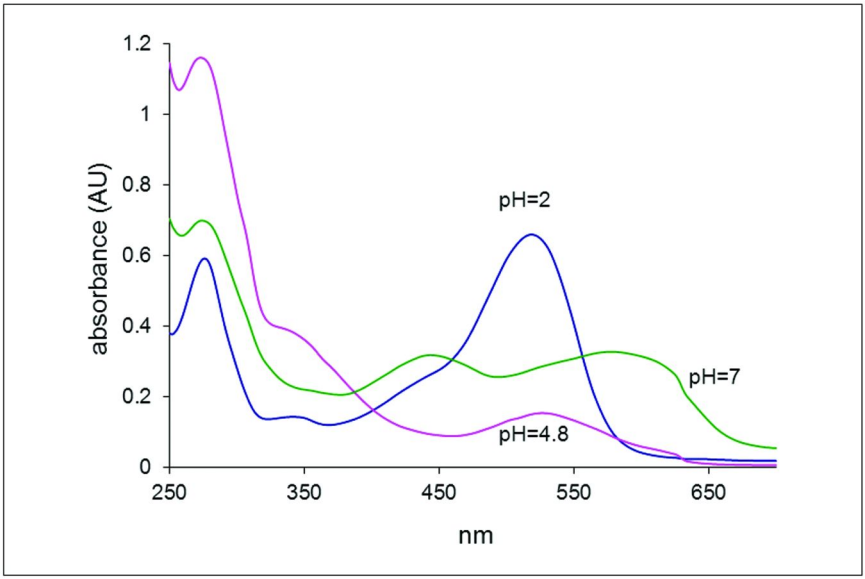

Figure 4. The UV-Vis absorbance spectra of mal3glu as a function of pH.

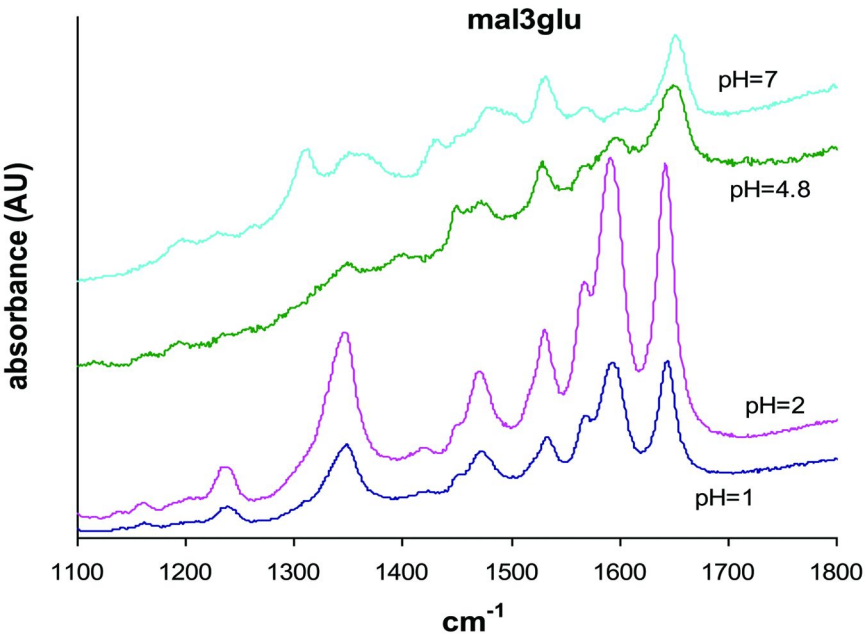

Figure 5. The RR spectra of mal3glu as a function of pH. The data are offset to make it easier to observe the spectra.

Figure 4 shows the UV-Vis spectra of malvidin-3-glucose (mal3glu) at different pH values and why the RR effect occurs at 433 nm, as there is significant absorption, whereas at 633 there is insignificant absorption. Thus, the 433 nm laser does produce the needed RR effect and was used for all the reported spectra. Although not seen, the UV-Vis spectra for the other anthocyanins as a function of pH is the same.

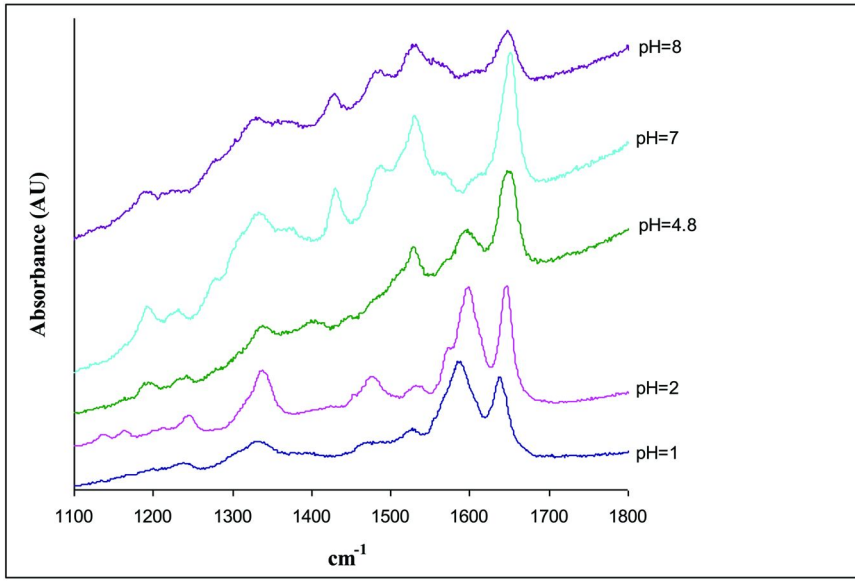

Figure 6. The RR spectra of cyan3glu as a function of pH. The data are offset to make it easier to observe the spectra.

Downloaded by UNIV OF MICHIGAN ANN ARBOR on July 29, 2013 | http://pubs.acs.org
Publication Date (Web): July 24, 2013 | doi: 10.1021/bk-2013-1138.ch009

Figures 5-7 show the RR spectra of the 3 anthocyanins at varying pH values. For all three anthocyanins, there is a clear difference in the RR spectra of the anthocyanin forms as a function of pH. The absorption band at 1590 cm^{-1}, which is due to the flavylium unit of the anthocyanin (*8*), clearly changes as the pH is increased. At low pH, it is a strong band, however, as the pH increases to 7 the band vanishes as the flavylium unit is lost to the anthocyanin's quinonoidal base form at the higher pH. The band at 1650 cm^{-1} also changes. This band is due to C=C and to C=O stretching. All pH values of the anthocyanin forms contain C=C, however only the quinonoidal base form exhibits the C=O, and that is why the band is broadened at higher pH. The 1300 – 1400 cm^{-1} exhibits changes with pH. At low pH, there is a peak at 1350 cm^{-1}, which has been attributed to the C-C inter-ring band (4). As the pH increases towards 8, the peak broadens and separates into two bands. This is due to the changing of the aromaticity and delocalization of the C=C in the benzene rings of each anthocyanin form, from the flavylium cation through

the carbinol and then to the quinoidol base, both of which lose this delocalization. In addition, at higher pH's, a band at 1520 cm^{-1} grows in size, due to C=C of a nonaromatic organic molecule (*9*). The peak at 1200 cm^{-1}, which is only seen at high pH, is also important, as it represents a C-O-C bonding unit (*10*, *11*). This bonding unit is found in vinyl ethers, something that is not found in the flavylium form but found in the carbinol and quinoidal base forms of the anthocyanin.

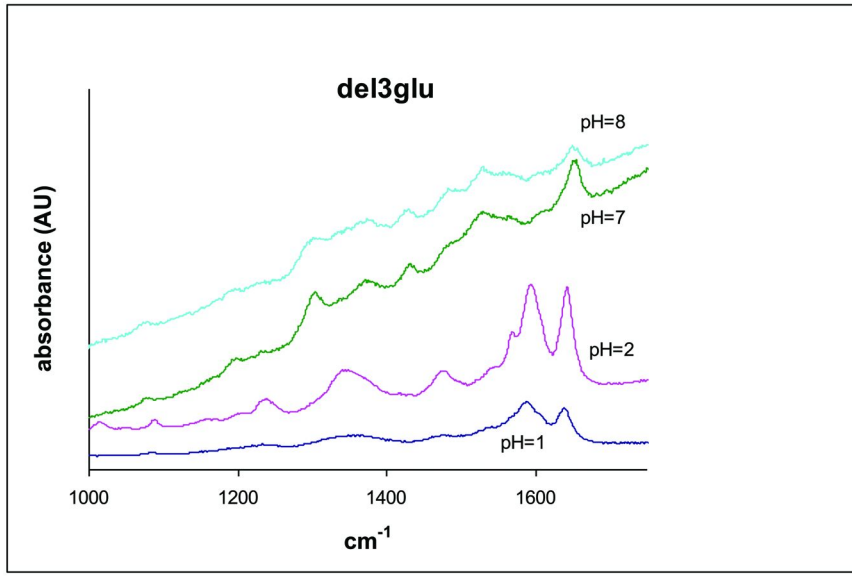

Figure 7. The RR spectra of del3glu as a function of pH. The data are offset to make it easier to observe the spectra.

RR and IR spectra of the solid anthocyanins were also performed. These spectra are not shown due to the inability of obtaining various pH with the solids, and thus were not relevant to this work.

Conclusion

Using RR spectroscopy, it has been clearly shown that the different forms of the anthocyanins exist at various pH. The work agrees with previous experimental work using NMR and UV-Vis. Hopefully, the investigation of anthocyanins in grapes at the cellular level to uncover mechanisms leading to the understanding of acylation of these molecules may be continued. However, before this can be achieved, different laser excitation wavelengths will be needed, in order to obtain better sensitivity.

In Physical Methods in Food Analysis; Tunick, M., et al.;
ACS Symposium Series; American Chemical Society: Washington, DC, 2013.

Downloaded by UNIV OF MICHIGAN ANN ARBOR on July 29, 2013 | http://pubs.acs.org
Publication Date (Web): July 24, 2013 | doi: 10.1021/bk-2013-1138.ch009

Acknowledgments

Many colleagues at INRA were extremely helpful throughout this project. One of us (AB) is grateful to Kent State University Stark Campus for allowing a sabbatical and for a Region Languedoc-Roussillon Visiting Scholar Fellowship. Mr. David Bourgogne at University Montpellier 2, performed the Raman spectroscopy, and his efforts were most valuable.

References

1. Harborne, J. B. In *Plant Pigments*; Goodwin, T. W., Ed.; Academic Press: London, 1988; pp 299−343.
2. Cheminat, A.; Brouillard, R. *Tetrahedron Lett.* **1986**, *27*, 4457–4460.
3. Merlin, J.-C.; Statoua, A.; Brouillard, R. *Phytochemistry* **1985**, *24*, 1575–1581.
4. Merlin, J.-C.; Statoua, A.; Cornard, J-P.; Saidi-Idrissi, M.; Brouillard, R. *Phytochemistry* **1994**, *35*, 227–232.
5. Merlin, J.-C.; Cornard, J. P.; Stastoua, A.; Saidi-Idrissi, M.; Lautie, M. F.; Brouillard, R. *Spectrochim. Acta.* **1994**, *50A*, 703–712.
6. Brouillard, R.; Delaporte, B. *J. Am. Chem. Soc.* **1977**, *99*, 8461–8468.
7. Vidal, S.; Hayasaka, Y.; Meudec, E.; Cheynier, V.; Skouroumounis, G. *J. Agric. Food Chem.* **2004**, *52*, 713–719.
8. Semenov, A. D.; Dorofeenko, G. N.; Dulenko, V. I. *Chem. Heterocycl. Compd.* **1966**, *2*, 10–13.
9. Withnall, R.; Chowdry, B. Z.; Silver, J.; Edwards, H. G. M.; de Oliveira, L. R. C. *Spectrochim. Acta* **2003**, *59A*, 2207–2212.
10. Meshcheryakov, A. P.; Glukhovtsev, V. G. *Russ. Chem. Bull.* **1960**, *9*, 1891–1893.
11. Frolov, Y. L.; Vashchenko, A. V. *J. Struct. Chem.* **2009**, *50*, 795–804.

Downloaded by UNIV OF MICHIGAN ANN ARBOR on July 29, 2013 | http://pubs.acs.org
Publication Date (Web): July 24, 2013 | doi: 10.1021/bk-2013-1138.ch009

Downloaded by PURDUE UNIVERSITY on July 29, 2013 | http://pubs.acs.org
Publication Date (Web): July 24, 2013 | doi: 10.1021/bk-2013-1138.ch010

Chapter 10

Polydiacetylene-Based Smart Packaging

Sarah C. Hill,[1] Yamin Htet,[1] Jennifer Kauffman,[1] Inyee Y. Han,[2] Paul L. Dawson,[2] William T. Pennington,[*,1] and Timothy W. Hanks[3]

[1]Department of Chemistry, Clemson University, Clemson, South Carolina 29634
[2]Department of Food, Nutrition & Packaging Sciences, Clemson University, Clemson, South Carolina 29634
[3]Department of Chemistry, Furman University, Greenville, South Carolina 29613
[*]E-mail: billp@clemson.edu.

Blends of polydiacetylenes (PDAs), such as 3- and 4-BCMU and PCDA in host polymers, Tecoflex® and polylactic acid were prepared and their potential applicability as active sensors in food packaging are described. A striking chromic transformation from deep blue to bright red, accompanied by a characteristic change in the Raman spectra of the PDAs occurs as a result of environmental stresses, such as heating, mechanical shear, exposure to solvents and other agents. Modification of the pendant groups of the PDA can expand the triggering stresses to include toxins, bacteria and other chemical and biological entities. Mechanical impact sensors and thermal and environmental history recorders have been prepared. The potential application of the polymer blends as photolithographic receptors has also been explored. Incorporation of the PDA sensing systems into textiles, such as calcium alginate and other materials allows the preparation of intelligent packaging, smart labels, and sanitation monitors for food processing, shipment, storage, and preparation.

© 2013 American Chemical Society
In Physical Methods in Food Analysis; Tunick, M., et al.;
ACS Symposium Series; American Chemical Society: Washington, DC, 2013.

Introduction

Smart Food Packaging

Food packaging represents an underexplored area for technological innovation and intervention that could dramatically address food safety concerns. Active, or "smart" packaging is defined as materials in intimate contact with a food item that can prevent, detect or respond to undesired changes in the product (*1*). This might involve anything from the controlled release of compounds for product preservation, surface contamination containment, or sensory enhancement. Smart packaging could also be used to detect problems with the product, such as bacterial contamination or decomposition. It could also detect product mishandling such as exposure to temperature extremes or impacts that could compromise either the packaging or the product. Here, we are primarily concerned with the development of inexpensive packaging that can readily sense problems with packaged foodstuffs.

The magnitude of the food safety challenge can be seen by considering the effects of pathogens introduced either before or after product packaging on human health. The U.S. Center for Disease Control estimates that 48 million people in the U.S. (1 in 6) contract a food borne illness each year, with some 128,000 requiring hospitalization and 3000 dying (*2*). Furthermore, the USDA-ARS has reported that the cost of foodborne illness from meat and poultry sources accounts for between $4.5 and $7.5 billion each year (*3*). The annual cost of salmonellosis alone is $0.6 to 3.5 billion per year in lost wages, medical costs while campylobacteriosis costs 0.6 to $1.0 billion each year in lost wages and medical costs. Besides the obvious fact that such events have serious health consequences, they can also have profound adverse economic impacts on the agricultural and food retail sectors. Post-process contamination, packaging defects and mishandling during transport accounts for as much as two thirds of serious food recalls due to bacterial contamination (*4*). Detection needs have also increased due to the risk of intentional contamination by bio-terrorists. With increased bio-terrorism threats to the general public, a variety of new generation detection and sensing systems for food-borne pathogenic agents are needed.

Downloaded by PURDUE UNIVERSITY on July 29, 2013 | http://pubs.acs.org
Publication Date (Web): July 24, 2013 | doi: 10.1021/bk-2013-1138.ch010

Polydiacetylenes

Recently, a class of materials known as polydiacetylenes (PDAs) have come to the attention of researchers concerned with food safety (*5*). PDAs are generally formed from the topotactic polymerization of substituted 1,3-butadiynes. The reaction has rather strict geometrical requirements, as shown in Figure 1 (*6*, *7*). This organization can be achieved in the solid state, thin films (*8*), liposomes (*9*, *10*), and in self-assembled monolayers (*11*). The efficiency of the polymerization reaction is highly sensitive to the substituents on the 1,3-butadiyene monomers, since they influence the packing of the monomers.

In Physical Methods in Food Analysis; Tunick, M., et al.;
ACS Symposium Series; American Chemical Society: Washington, DC, 2013.

PDAs display many interesting physical and optical properties that have made them the subject of numerous investigations over the past forty years (*12*). Of particular interest to this proposal are the changes in the visible and vibrational spectra of the polymers in response to stress along the polymer backbone. The potential use of these changes in the construction of molecular and nanoscale sensors has been widely recognized and has prompted much investigation.

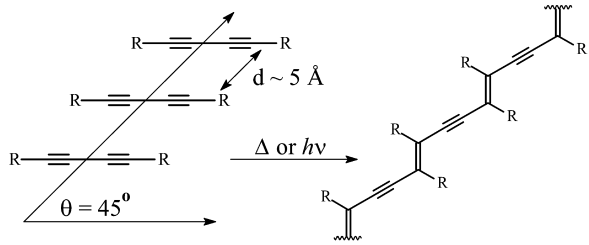

Figure 1. Geometrical requirements for topotactic polymerization of diacetylenes.

Downloaded by PURDUE UNIVERSITY on July 29, 2013 | http://pubs.acs.org
Publication Date (Web): July 24, 2013 | doi: 10.1021/bk-2013-1138.ch010

Perhaps the most striking feature of PDAs is their intense color, due primarily to the π – to – π^* transition of the polymer backbone. Often, the initially formed PDA is a deep blue, with an absorption maxima around 640 nm, though other features are also apparent. Many PDAs undergo a phase transition upon heating in which the material becomes bright red, with an absorption maxima of around 540 nm (*13*). While some gradual color change begins to appear within a few degrees of the triggering temperature, as the temperature is reached the color change is dramatic and in most cases irreversible. The temperature of this transition depends upon the nature of the pendant groups (R and R′, Figure 1) and the physical form of the PDA, but is often in the range of 50 – 100 °C. Heating to higher temperatures can lead to a second transition, giving a yellow material.

The mechanism of the thermochromism has been the subject of some debate and is not completely understood. It is now generally agreed that the organization of the pendant groups plays a role, probably leading to the twisting of the backbone out of complete planarity. Thus, the blue form has a perfectly planar backbone, while the red form has some degree of twisting, which shortens the effective conjugation length. In many (but not all) cases, conversion to the red form is irreversible, indicating that this is a lower energy geometry. The yellow form has little conjugation. It is observed upon heating to very high temperatures or in PDA solutions with a good solvent. In the former case, formation of the yellow phase is irreversible, while in solution, addition of non-solvent can regenerate the red form (this is primarily a random coil – rigid rod transition, though aggregation may also be involved).

Polydiacetylenes as Sensing Platforms

Color change in PDAs is not limited to thermal stimuli. Depending on the system, color change may be effected by pH, biological entities, solvent, or mechanical stress. This feature has driven the development of PDA-based sensors designed for specific applications. For example, in the early 1990's Charyech and co-workers demonstrated that appropriately derivatized PDAs monolayers could be used to detect the influenza virus (*14*). Related monolayer and vesicle sensors for toxins, glucose, and other biological agents were developed shortly thereafter (*15*). This has become an active area of research, with sensors being designed for an ever increasing variety of species, and techniques being developed to distinguish between specific pathogens (*16*, *17*).

Another technique that has been used in conjunction with PDAs for sensing applications is Raman spectroscopy (*18*). Historically, this has been done under resonance Raman conditions by using lasers that excite into the electronic absorption of the PDA backbone. Only four vibrational modes, each associated with either the acetylenic or olefinic moieties, undergo resonance enhancement, giving very intense, but simple spectra. The most important of them for analytical purposes is the acetylenic stretch, which is very intense and comes in a portion of the spectrum (~ 2100 cm^{-1}) that is free of other bands. In the late 1970's, Mitra and coworkers showed that this vibrational mode is highly sensitive to deformation of the polymer backbone (*19*). In single PDA crystals, this band shifts by approximate 20 cm^{-1} per 1% strain regardless of the pendant groups (*20*, *21*).

This shift in the vibrational frequency is unrelated to the change in the visible spectrum. It is due to the stretching of the polymer backbone and the change in the force constant of the acetylenic bond (*19*, *22*). The linear shift/strain relationship is only valid up to 1 or 2% strain, which is far less than that required for the visible mechanochromism (*23*).

Raman has been used to measure the strain in isolated PDA chains in a crystalline matrix of the DA monomer (*24*) and under shear in solution (*25*), but more commonly, PDA single crystals and crystalline fibers have been investigated. An important development was the use of PDA crystals to map strain in resins and laminates (*26*, *27*). While highly sensitive, this approach is not without problems as stress can be relieved by twinning of the crystal as well as by deformation. In addition, variations in the sensitivity have been observed due to the difficulty in controlling the adhesion at the PDA/polymer interface, meaning a given crystal must be calibrated *in situ*. The use of PDA crystals can also have a major detrimental effect on the strength of laminates, limiting their utility in critical components. Alternatively, the micromechanics of polymeric objects can be investigated with diacetylene-containing copolymers. The DA moieties phase separate into hard blocks, and are sufficiently organized to be polymerized. The thermal and mechanochromism has been studied by optical methods at high strain (*23*, *28*, *29*), and also by Raman techniques at lower strain (*30–32*). Diacetylene-containing polyesters have also been incorporated as a component in a polymer blend with a polyolefin as a model system (*33*, *34*). Thus, PDAs with different morphologies have a proven record as strain sensors.

Downloaded by PURDUE UNIVERSITY on July 29, 2013 | http://pubs.acs.org
Publication Date (Web): July 24, 2013 | doi: 10.1021/bk-2013-1138.ch010

Downloaded by PURDUE UNIVERSITY on July 29, 2013 | http://pubs.acs.org
Publication Date (Web): July 24, 2013 | doi: 10.1021/bk-2013-1138.ch010

PDAs in Polyurethanes and Polylactic Acid

Structure of PDA/Host Polymer Blends – BCMU/Tecoflex®

In order to make use of the chromatographic properties of PDAs for smart packaging applications new approaches to their incorporation must be explored. In particular, the use of copolymers of existing packaging materials and PDAs requires not only new, significantly more expensive, synthetic routes, but also revamping of processing conditions and likely compromises to the physical properties of the packaging. Another approach is to encorporate small amounts of PDAs into existing polymers. For example, we have looked at the incorporation of 3- and 4-butoxymethylcarbonylurethanes (3-, 4-BCMU) and their polymers into the engineering urethane which goes under the trade name Tecoflex® (Figure 2). Both the BCMU and the host polymer contain urethane groups, which provide for some mutual affinity. Both the 3- and 4-BCMUs are readily photopolymerized to the corresponding PDAs.

At low loadings (1%) the incorporation of the BCMU monomers had no statistical effect on the tensile strength of the host polymer and actually appeared to slightly increase the thermal stability as measured by TGA, even up to loading levels as high as 40%, though a lowering of the glass transition temperature was noted as the BCMU acted like a plasticizer under these conditions.

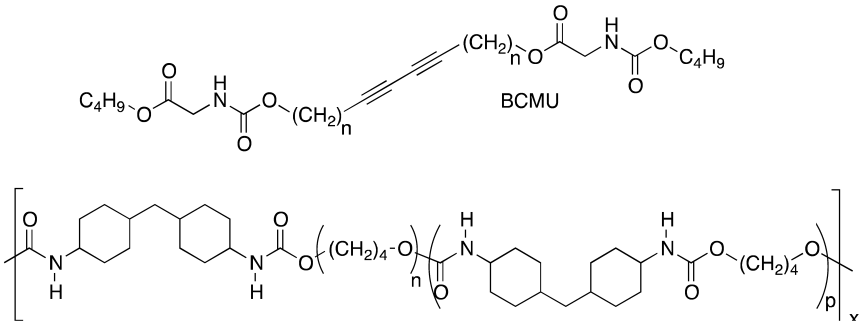

Figure 2. Structures of the PDA precursor BCMUs and the segmented urethane host polymer Tecoflex®.

The polymers derived from the BCMUs (BCMUp) could be incorporated into the Tecoflex as well by dissolving both polymers in chloroform and casting thin films. The BCMU polymers adopt a random coil geometry in this solvent as evidenced by the polymers changing from their original blue color to yellow. However, when blended with the Tecoflex, they each adopted their thermodynamically more stable ridged rod geometries; blue in the case of 3-BCMUp and red with 4-BCMUp (Figure 3). The PDA backbone vibrational modes undergo resonance enhancement (particularly in the blue form), and are thus detectable at loadings of a fraction of a percent. The acetylene stretching vibration around 2100 cm^{-1} is particularly valuable.

In Physical Methods in Food Analysis; Tunick, M., et al.;
ACS Symposium Series; American Chemical Society: Washington, DC, 2013.

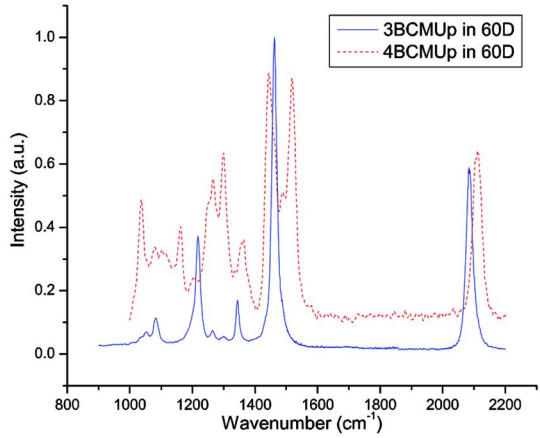

Figure 3. Normalized Raman spectra of 1% 3-BCMUp (red, dash) and 4-BCMUp in 60D Tecoflex® (blue, solid).

X-ray powder diffraction is unable to detect BCMUp phase separated aggregates at loading levels below 10%, though the clearly appear at this threshold. Optical microscopic examination of the films at just 1% loading showed both crystalline aggregates and a relatively uniform background indicating either very small aggregates or solubilized BCMUp chains (blends below 0.5% BCMUp appeared homogeneous and aggregate-free). The extent of large aggregation was a direct function of the concentration of "hard" segments in the Tecoflex. Figure 4 shows photomicrographs of four Tecoflex polymers in order of decreasing hard segment content.

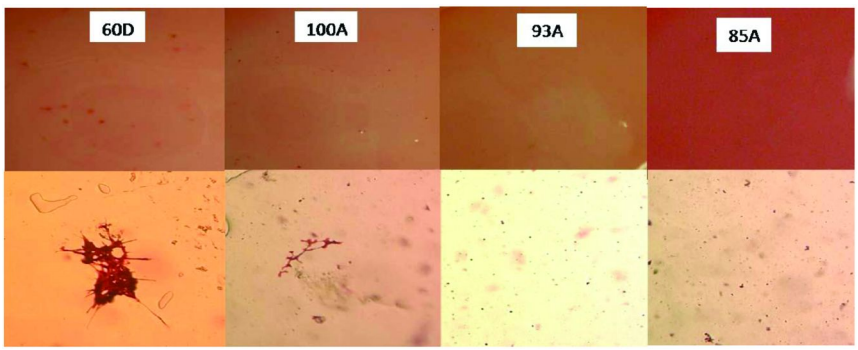

Figure 4. Photographs (top) and photomicrographs (500X, bottom) of 1% 4-BCMUp Tecoflex® 60D, 100A, 93A and 85A blend films. The Tecoflex formulations are ordered from high to low hard segment content.

In Physical Methods in Food Analysis; Tunick, M., et al.;
ACS Symposium Series; American Chemical Society: Washington, DC, 2013.

Downloaded by PURDUE UNIVERSITY on July 29, 2013 | http://pubs.acs.org
Publication Date (Web): July 24, 2013 | doi: 10.1021/bk-2013-1138.ch010

Downloaded by PURDUE UNIVERSITY on July 29, 2013 | http://pubs.acs.org
Publication Date (Web): July 24, 2013 | doi: 10.1021/bk-2013-1138.ch010

Environmental Sensing in BCMU/Tecoflex Blends

While previous work has shown that the alkyne stretching frequency of macroscopic PDA crystals or coatings on glass fibers could be used to measure tensile strain in host polymers, our attempts to collect such data in BCMUp/Tecoflex blends were of limited success. Increased stress did decrease the stretching frequency as has been previously reported, but the results were both highly variable and the trends were close to the noise level. Indeed, as others have observed, the resolution of the PDA sensor in this application is limited (*35*). It seems unlikely that simple blends of PDAs and packaging polymers will allow for the monitoring of strain in food packaging.

Another interesting application of DA and PDA as sensors in in the areas of temperature and impact sensing. At relatively high levels of loading, BCMU monomers bloom to the surface of Tecoflex films, forming highly crystalline and surprisingly well-adheared coatings (Figure 5). Upon irradiation with UV light, these coatings readily polymerize and display clear grain boundaries.

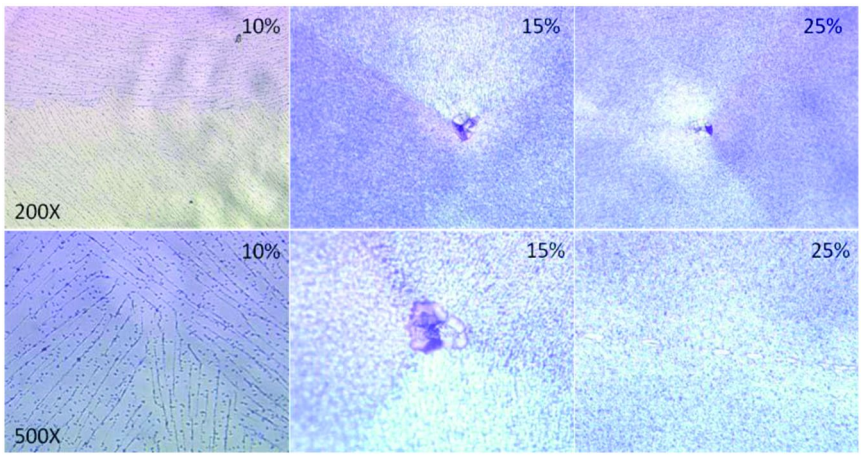

Figure 5. Photomicrographs of 4-BCMUm in 60D Tecoflex® at 10%, 15% & 25%; magnifications 200X & 500X.

These coatings could easily form a thin interlayer in a packaging system, providing an indication of the thermal history of a packaged product. Figure 6 shows the conversion of a pBCMU/Tecoflex blend upon exposure to elevated temperatures over time. While these temperatures are unlikely to be observed with food products under normal transportation conditions. Modifications of the monomer structure allow adjustment of the thermal window and could provide direct evidence of mishandling of food products.

In Physical Methods in Food Analysis; Tunick, M., et al.;
ACS Symposium Series; American Chemical Society: Washington, DC, 2013.

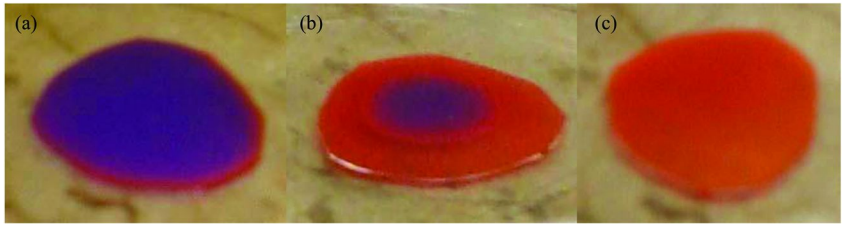

Figure 6. Photographs of 30% 4-BCMUm in 60D as polymerized by UV (a, blue) and after exposure to 75°C for one minute (b, red with blue center) and two minutes (c, red).

Downloaded by PURDUE UNIVERSITY on July 29, 2013 | http://pubs.acs.org
Publication Date (Web): July 24, 2013 | doi: 10.1021/bk-2013-1138.ch010

Another area of concern with the transportation of food products, especially produce, is physical mishandling. Mechanical damange to products is not always immediately visible, but can result in accelerated product degredation and eventual visual deterioration (bruises on bananas), or physical degradation (soft spots on apples) that can deter consumers. The most common cause of physical damage is sudden impact. Containers are typically sealed during transport so damage cannot be detected (*36*). Even upon arrival it can be particularly difficult to immediately detect the results of such damage in produce with a thick skin (*37*).

Sheer-induced mechanochromism of PDAs was reported by Burns in 2001 (*38*), and later by others, but we have found that sudden impacts can also cause the transformation of DAs in polymer hosts. This leads to a novel impact sensing mechanism that warrents detailed examination. In this case, films were prepared from 20% 4-BCMU PDA in 60D Tecoflex® film and a 100 g dart was dropped onto the surface from various heights. As discussed above, the 20% incorporation of monomeric BCMU results in substantial blooming to the surface and self-assembly into crystalline domains. Figure 7 shows the results of the impact.

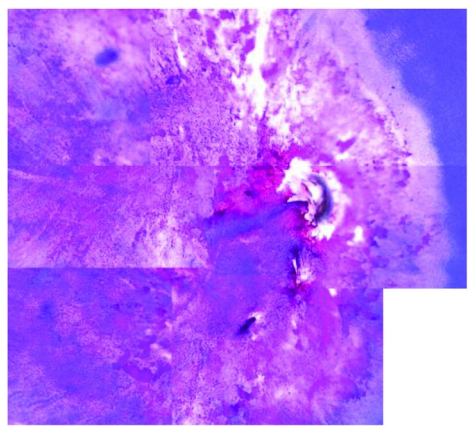

Figure 7. Photomicrograph of impact area on a sample from a height of 20.75 cm with a 100 g dart on a 20% 4-BCMUm blend with 60D Tecoflex®.

Mapping of the film by Raman spectroscopy shows that the impact extends beyond the immediate contact area of the dart. Refinement of this technique may allow for the incorporation of fine sensor layers within food packaging wrappers that will not only immediately identify mishandling of food products, but also identify sub-lot portions that may have been affected by the insult.

PCDA Blends with Tecoflex® and PLA

In addition to the BCMU/Tecoflex® blends discussed above, we have also incorporated the amphilic diacetylene, 10,12-pentacosadiynoic acid (PCDA) into Tecoflex® and polylactic acid (PLA) host polymers (Figure 8). PLA is a compostable polymer made from corn and other plant sources which is heavily used in the food and medical industries due to its low cost, ready availability from renewable resources, biodegradability and biocompatibility. Like BCMU, PCDA monomer is incorporated into the host polymers with little to no effect on the physical properties of the host, and at higher load levels the monomer blooms to the surface to form a robust, semicrystalline coating (Figure 9) that is responsive to temperature and to mechanical impact.

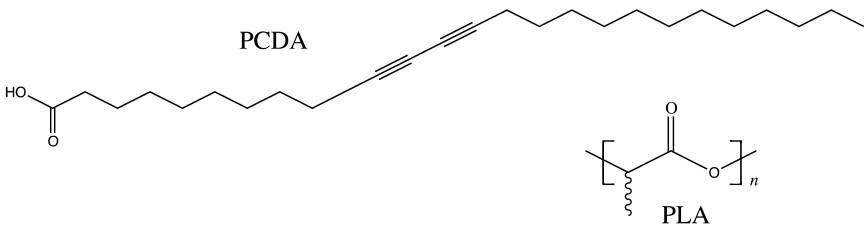

Figure 8. Structures of the PDA precursor PCDA and the host polymer PLA.

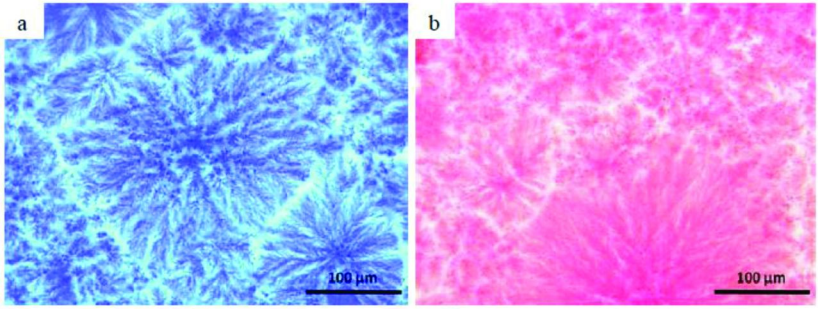

Figure 9. Photomicrograph of PLA blend with 1% PCDA (a) as polymerizes and (b) after heating to 60°C for 10 seconds.

Downloaded by PURDUE UNIVERSITY on July 29, 2013 | http://pubs.acs.org
Publication Date (Web): July 24, 2013 | doi: 10.1021/bk-2013-1138.ch010

Irradiation of the coating polymerizes the PCDA monomers to blue PDA polymer, and the degree of polymerization increases linearly with time over a range of approximately 5 minutes. Figure 10 shows UV/Vis spectra versus irradiation time for the 640 nm absorption of the blue form (Figure 10a), and the linear relationship of absorption intensity versus irradiation time (10b).

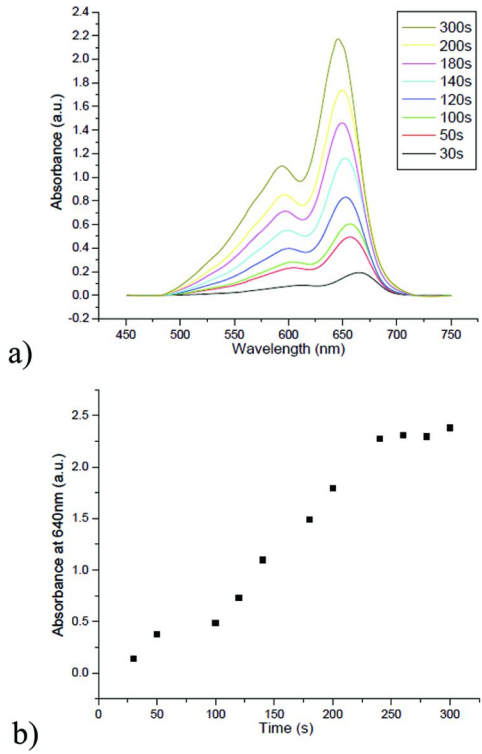

Figure 10. 1% PCDA in PLA. a) Overlay of 640 nm absorbance as a function of 254 nm irradiation time. b) Plot of absorbance versus irradiation time.

As previously discussed the nature of the monomer structure allows for adjustment of the thermal window. PCDA transforms from blue to red at a much lower temperature than BCMU. This is most likely due to the more flexible nature of PCDA and to its possessing a strong attachment site at only one end of the monomer. With additional modification to enhance or diminish these characteristics the thermal trigger temperature can be adjusted to provide a graded thermal history sensor for food transport and storage.

The coating formed by higher load levels behaves like those formed by BCMU/Tecoflex® blends. Upon polymerization a deep blue coating is formed which transforms to the red form upon mechanical impact. Figure 11a shows a 5% PCDA/Tecoflex® film after being impacted by a 100 g drop dart from heights ranging from 3 to 50 cms. The PCDA coating is more sensitive to impact than

In Physical Methods in Food Analysis; Tunick, M., et al.;
ACS Symposium Series; American Chemical Society: Washington, DC, 2013.

Downloaded by PURDUE UNIVERSITY on July 29, 2013 | http://pubs.acs.org
Publication Date (Web): July 24, 2013 | doi: 10.1021/bk-2013-1138.ch010

BCMU, as no visible color was observed for BCMU at heights of less than ~7 cm, while PCDA transforms to give a red spot at the smallest height allowed by the instrument. It is speculated that this difference is related to the same factors that lower the thermal trigger point of PCDA relative to BCMU. At lower load levels (0.5-2%), PCDA behaves quite differently, as irradiation for even 20 minutes, does not result in an observable color change. However, dart impact over the same height range as for the 5% PCDA/Tecoflex® film results in vivid red impact spots (Figure 11b).

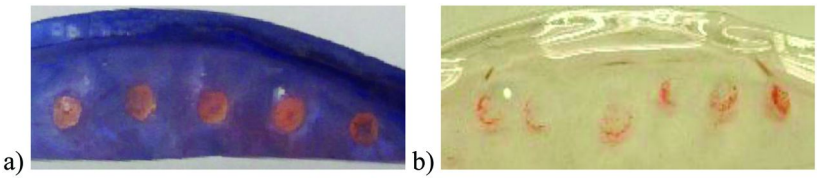

Figure 11. Drop dart impact spots over a height range of 3 to 50 cm (increasing from left to right) for a) 5%PCDA/Tecoflex® film, and b) 1%PCDA/Tecoflex® film.

In order to verify that the color of the impact sites on the transparent film were the result of the red form of PCDA, Raman analysis was performed (Figure 12). The observation of the acetylinic stretch at 2111 cm^{-1} provides indisputable evidence of the the mechanochromic transformation at the impact sites.

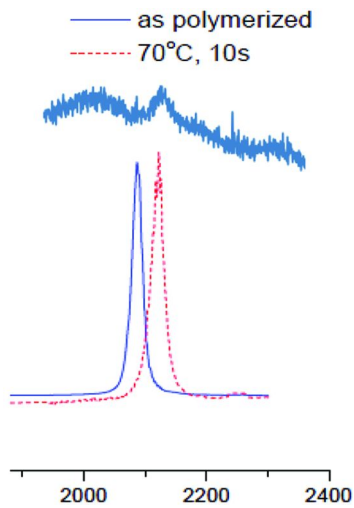

Figure 12. Raman spectrum of 1% PCDA/Techoflex® impact sites compared with irradiated and heated PCDA.

In Physical Methods in Food Analysis; Tunick, M., et al.;
ACS Symposium Series; American Chemical Society: Washington, DC, 2013.

Downloaded by PURDUE UNIVERSITY on July 29, 2013 | http://pubs.acs.org
Publication Date (Web): July 24, 2013 | doi: 10.1021/bk-2013-1138.ch010

The transparency of the low load PCDA films could be due to a greater degree of incorporation of the monomer within Tecoflex®, i.e the amount of monomer is below the bloom threshold, however, given the lower compatibility of the attractive sites of PCDA versus BCMU for Tecoflex®, this seems unlikely. It is also possible that the incorporated monomers of PCDA form much smaller aggregates than BCMU, preventing them from being visible. If this is the case, then impact must concentrate the aggregates enough to be visible as the transformed red polymer. The inability to see aggregates even under magnification makes this explanation unattractive as well. Continued investigation of this interesting phenomenon is underway. Regardless, the transparency of the low load PCDA/Tecoflex® blends could be advantageous for packaging applications, where the contents must be observable through the film, or in label design, where the blue color might be undesirable.

Downloaded by PURDUE UNIVERSITY on July 29, 2013 | http://pubs.acs.org
Publication Date (Web): July 24, 2013 | doi: 10.1021/bk-2013-1138.ch010

UV Photolithography of PDA/Host Polymer Blends

Selective polymerization of PDA/host blend films using masking techniques allow the design of micro and macro lithographic images. Star micro-images with diameter of ca. 700 μm were created by irradiation of a 1% PCDA/PLA film through an array mask designed for extrusion of polymeric fibers. Clear images with proper dimensions were isolated under magnification (Figure 13)

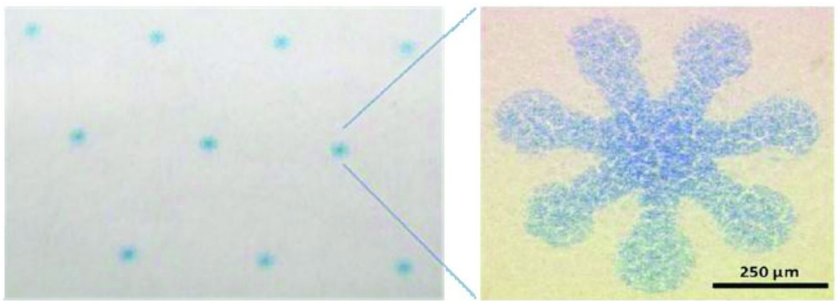

Figure 13. Micro-scale image obtained by 264 nm irradiation of 1% PCDA/PLA film through an array mask.

Bichromic images can be obtained by exploiting the thermochromic properties of PDAs. The "tiger paws" shown in Figure 14 were created by: a) UV irradiation of 1% PCDA/PLA through a paw-shaped aluminum foil mask for five minutes. b) Heating the film to 70°C for ten seconds, turning the image red/orange in color. c) After 72 hours, irradiation of the film resulted in polymerization of the film surrounding the paw. It is important to note that irradiation of the film immediately after the heating transformation did not produce a blue background. It is believed that the heating either causes the PCDA monomers to adopt an

amorphous structure which must then reorganize to a polymerizable morphology, or sublimation of the surface PCDA occurs, which then must be replenished through additional blooming. The deeper red color of the paw in Figure 13c versus the red-orange color of the paw in Figure 13b appears to be the result of polymerization of additional monomer within the paw region, providing support for the latter explanation.

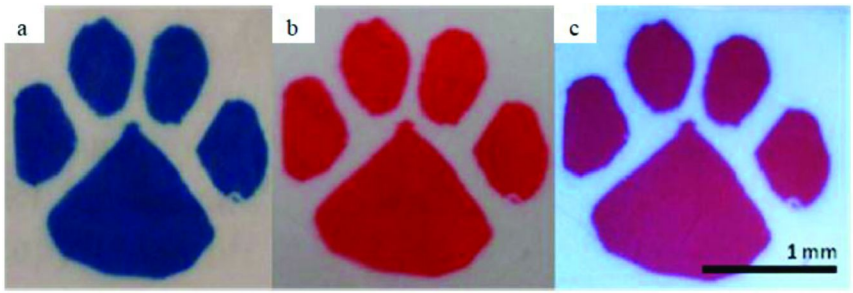

Figure 14. Macro-scale imaging of 1% PCDA/PLA film after: a) 264 nm irradiation through "tiger paw" mask, b) heating the film to 70°C for 10 seconds, c) after irradiation of the film 72 hours after heating.

The micro- and macro-lithography of PDA blends is important for their application in food packaging for several reasons. Patterned arrays provide the capability to produce a grid system within a packaging unit. On a macro scale this could be applied to cargo crates to identify impact history from improper handling, and on a micro scale might be incorporated into a tamper sensor or to indicate problems with individual compartments of a packaging unit. Manipulation of the patterns also allow the sensing system to be incorporated into label/logo designs for aesthetic appeal.

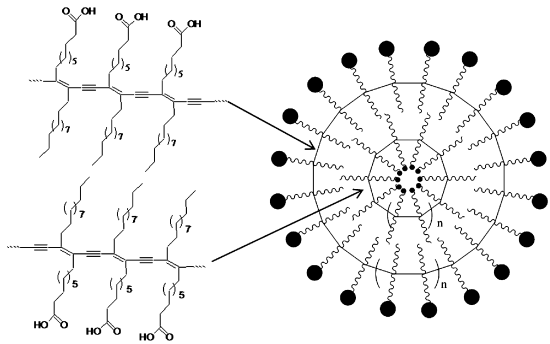

Figure 15. Polymerized PCDA liposomes.

In Physical Methods in Food Analysis; Tunick, M., et al.;
ACS Symposium Series; American Chemical Society: Washington, DC, 2013.

Downloaded by PURDUE UNIVERSITY on July 29, 2013 | http://pubs.acs.org
Publication Date (Web): July 24, 2013 | doi: 10.1021/bk-2013-1138.ch010

Functionalized PDAs for Bacterial Sensing

Due to their amphilic nature, molecules of PCDA can self assemble in water to form polymerizable liposomes, artificial structures consisting of a self-closed bilayer with an aqueous core (Figure 15) (*39*). Liposomes are of considerable fundamental scientific interest in fields ranging from mathematics and physics to biology and chemistry to pharmaceutics and medicine (*40*). The broad interest stems from their biological compatibility and the ease with which the structure may be modified to add functionality.

Indeed, the surface of PDA liposomes have been decorated with nucleic acids, sugars, antibodies or other functionalities, allowing them to serve as biosensors (*41*, *42*). The PDA polymer acts as a built-in reporter of interaction between the incorporated receptor and biological targets, measurable by a chromatic change in the visible absorption spectrum (Figure 16).

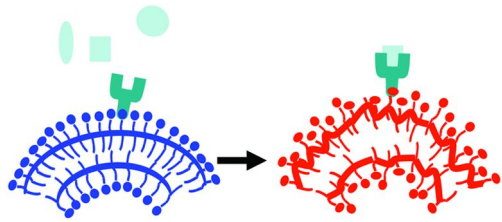

Figure 16. Biosensing using PDA systems: receptors for biological targets are covalently attached to the PDA; binding of ligands induce the blue-red transitions.

We have prepared PCDA liposomes decorated at a 5% loading level of PCDA molecules functionalized with tryptophan, tyrosine and other receptors. Figure 17 shows a suspension of tryptophan functionalized PCDA liposomes serving as an *E. Coli* sensor.

Figure 17. PCDA-Trp Liposome Solutions on a Ceramic Surface; the first and third samples were exposed to E. coli, producing a colorimetric response.

In Physical Methods in Food Analysis; Tunick, M., et al.;
ACS Symposium Series; American Chemical Society: Washington, DC, 2013.

Downloaded by PURDUE UNIVERSITY on July 29, 2013 | http://pubs.acs.org
Publication Date (Web): July 24, 2013 | doi: 10.1021/bk-2013-1138.ch010

Downloaded by PURDUE UNIVERSITY on July 29, 2013 | http://pubs.acs.org
Publication Date (Web): July 24, 2013 | doi: 10.1021/bk-2013-1138.ch010

PDA Sensor Attachment to Textile Surfaces

A unique advantage of the use of PDA in sensing platforms is the feasibility to incorporate the polymer in diverse matrices and configurations. For example, we have incorporated PDA liposomes into sodium alginate solutions and extruded them into a $CaCl_2$ solution (Figure 18a). The resulting calcium alginate / PDA composite was insoluble, enabling the production of high quality, robust fibers (Figure 18b). Importantly, the PDA liposomes remained blue through the extrusion and drying processes, yet were able to act as temperature and pH sensors (*39*). After swelling the fibers in an aqueous sodium chloride solution, larger molecular species, such as cyclodextrin (acting as a bacteria mimic), could be detected. These results are important since alginate is a naturally occurring, biocompatible, and biodegradable material that is approved for use in food products and biomedical implants. For example, alginate fibers can be spun into bandages that have the unique feature of slowly exchanging calcium for sodium in the blood. The coupling of the PDA matrix to the alginate fibers offers the possibility for construction of "intelligent packaging" for monitoring bacterial contaminations in foods (as well as changes in other environmental parameters, such as heat, humidity, salts and others). Likewise, dipsticks, swabs, and wipes woven from PDA/alginate fibers could be employed for reporting on the presence of bacteria and toxins on foods and upon food preparation surfaces.

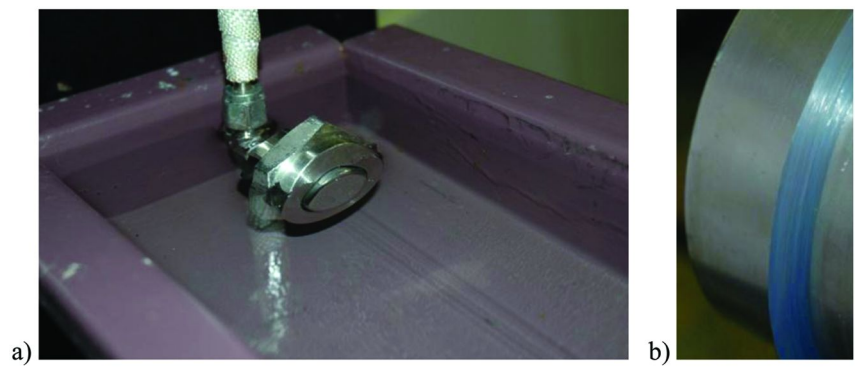

Figure 18. a) Extrusion of sodium alginate/PCDA into a $CaCl_2$(aq) bath, to form (b) robust PCDA-doped calcium alginate fibers.

Conclusions

Polydiacetylenes (PDAs) are conjugated polymers formed by the topotactic polymerization of 1,3-butadiynes in ordered solids such as crystals, thin films, liposomes and self-assembled monolayers. PDAs display interesting chromic transitions as a result of stress along the polymer backbone, transforming from an "as polymerized" deep blue material to a more stable conformation, which is

bright-red. The color change, which is accompanied by a characteristic change in the Raman spectra, is typically the result of thermal, pH, solvent, or mechanical stress. Modification of the polymer pendant groups expands the possible stimuli to biological entities, toxins or any other agent that can effect stress in the backbone through interaction with the pendant group. These chromatic properties, as well as changes in the their fluorescence, can form the basis of sensor platforms for a wide variety of applications.

We have incorporated the PDAs, 3- and 4-BCMU and PCDA into host polymers, Tecoflex® and Polylactic Acid (PLA) and have found that the optical responses of the PDAs are maintained. These polymer blends have great potential for use in food packaging, as sensors to indicate and record environmental history, shear-induced damage to, and contamination or spoilage of package contents.

In order to realize the utility of these sensors to for smart labeling and intelligent packaging, several technical challenges must be addressed. First and foremost, it is necessary to ensure that the sensor is triggered only by the stimulus that is of interest. For example, an impact sensor that is triggered by exposure to thermal conditions that could be experienced by the packaging under normal transportation conditions is of little use. It is also critical that the sensing system be physically positioned to detect the stimulus. A packaging material designed to detect bacterial contamination in a food product may fail if the pathogens and their byproducts are contained deep within the product and do not make their way to the interface with the packaging materials. Producers will not be interested in a smart package unless it is both robust and has a very low chance of failure. While these issues can be overcome by designing materials based upon a detailed understanding of the product performance requirements and coupling them with other packaging components (UV absorbing layers, semi-permeable membranes, etc), the sensitivity of the PDAs to stress and temperature limit the processing methodologies that can be used. A key observation in this work is that the polymerization step should be performed as late in the composite manufacturing process as is possible to avoid inadvertent triggering of the colorimetric response.

Despite these caveats, the simplicity of the PDA response and their wide versatility in both the stimuli that may be detected and the structural forms in which they may be deployed ensure that practical sensing platforms will be developed.

Downloaded by PURDUE UNIVERSITY on July 29, 2013 | http://pubs.acs.org
Publication Date (Web): July 24, 2013 | doi: 10.1021/bk-2013-1138.ch010

References

1. Imran, M.; Revol-Junelles, A.-M.; Martyn, A.; Tehrany, E. A.; Jacquot, M.; Linder, M.; Desobry, S. *Crit. Rev. Food Sci. Nutr.* **2010**, *50*, 799.
2. http://www.cdc.gov/foodborneburden/2011-foodborne-estimates.html.
3. Huang, S.; Huang, K. *United States Department of Agriculture Economic Research Service* **2007**, FTS-328-01.
4. Gounadaki, A. S.; Skandamis, P. N.; Drosinos, E. H.; Nychas, G. J. E. *J. Food Protect.* **2007**, *70*, 2313.
5. Pires, A. C. S.; Soares, N. de F.; da Silva, L. H. M.; Andrade, N. J.; Silerira, M. F. A.; de Caralho, A. F. *Food Bioprocess. Technol.* **2010**, *3*, 172.

6. Baughman, R. H.; Yee, K. C. *J. Polym. Sci., D: Macromol. Rev.* **1978**, *13*, 219.
7. *Polydiacetylenes: Synthesis, Structure and Electronic Properties*; Bloor, D., Chance, R. R., Eds.; Martinus Nijhoff: Boston, 1985.
8. Carpick, R. W.; Sasaki, D. Y.; Eriksson, M. A.; Burns, A. R. *J. Phys.: Condens. Matter.* **2004**, *16*, R679.
9. Okada, S.; Peng, S.; Spevak, W.; Charych, D. *Acc. Chem. Res.* **1998**, *31*, 229.
10. Bloor, D. *Macromol. Chem. Phys.* **2001**, *202*, 1410.
11. Giorgetti, E.; Muniz-Miranda, M.; Margheri, G.; Giusti, A.; Sottini, S.; Alloisio, M.; Cuniberti, C.; Dellepiane, G. *Langmuir* **2006**, *22*, 1129.
12. *Crystallographically Ordered Polymers*; Sandman, D. J., Ed.; ACS Symposium Series 337; American Chemical Society: Washington, DC, 1987.
13. For a recent review, see: Carpick, R. W.; Sasaki, D. Y.; Marcus, M. S.; Eriksson, M. A.; Burns, A. R. *J. Phys. Condens. Matter* **2004**, *16*, R679.
14. Charych, D. H.; Nagy, J. O.; Spevak, W.; Bednarskik, M. D. *Science* **1993**, *261*, 585.
15. Jelinek, R. *Drug Dev. Res.* **2000**, *497*.
16. Rangin, M.; Basu, A. *J. Am. Chem. Soc.* **2004**, *126*, 5038.
17. Scindia, Y.; Silbert, L.; Volinsky, R.; Kolusheva, S.; Jelinek, R. *Langmuir* **2007**, *23*, 4682.
18. Materny, A.; Chen, T.; Vierheilig, A.; Kiefer, W. *J. Raman Spectrosc.* **2001**, *32*, 425.
19. Mitra, V. K.; Risen, W. M.; Baughman, R. H. *J. Chem. Phys.* **1977**, 2731.
20. Galiotis C. Ph.D. Thesis, University of London, London, 1982.
21. Young, R. J.; Eichhorn, S. J. *Polymer* **2007**, *48*, 2.
22. Batchelder, D. N.; Bloor, D. *J. Polym. Sci., Polym. Phys. Ed.* **1979**, *17*, 569.
23. Nallicheri, R. A.; Rubner, M. F. *Macromolecules* **1991**, *24*, 517.
24. Spagnoli, S.; Berrehar, J.; Fave, J.-L.; Schott, M. *Chem. Phys.* **2007**, *333*, 254.
25. Dunstan, D. E.; Hill, E. K.; Wei, Y. *Macromolecules* **2004**, *37*, 1663.
26. Fisher, N. E.; Sharpe, D. J.; Batchelder, D. N. *Meas. Sci. Technol.* **1994**, *5*, 1325 and references therein.
27. Galiotis, C.; Batchelder, D. N.; Robinson, I. M.; Young, R. J. *J. Mater. Sci.* **1987**, *22*, 3642.
28. Rubner, M. F. *Macromolecules* **1986**, *19*, 2129.
29. Rubner, M. F.; Sandman, D. J.; Velazquez, C. *Macromolecules* **1987**, *20*, 1296.
30. Hu, X.; Stanford, J. L.; Day, R. J.; Young, R. J. *Macromolecules* **1992**, *25*, 672.
31. Hu, X.; Stanford, J. L.; Day, R. J.; Young, R. J. *Macromolecules* **1992**, *25*, 684.
32. Hu, X.; Breach, C. D.; Young, R. J. *Polym. Commun.* **1997**, *38*, 981.
33. Lovell, P. A.; Stanford, J. L.; Wang, Y. –F.; Young, R. J. *Macromolecules* **1998**, *31*, 842.
34. Hu, X.; Li, X. *J. Polym. Sci., B.: Polym. Phys.* **2002**, *40*, 2354.

Downloaded by PURDUE UNIVERSITY on July 29, 2013 | http://pubs.acs.org
Publication Date (Web): July 24, 2013 | doi: 10.1021/bk-2013-1138.ch010

35. Sutrisno, W.; Stanford, J. L.; Lovell, P. A. *Jurnal Fisika Dan Aplikasinya* **2005**, *1*, 050104-1.
36. Lamberti, M.; Escher, F. *Food Rev. Int.* **2007**, *23*, 407.
37. Montero, C. R. S.; Schwarz, L. L.; dos Santos, L. C.; Andreazza, C. S.; Kechinski, C. P.; Bender, R. J. *Pesqui. Agropecu. Bras.* **2009**, *44*, 1636.
38. Burns, A.; Carpick, R.; Sasaki, D.; Shelnutt, J.; Haddad, R. *Tribol. Lett.* **2001**, *10*, 89–96.
39. Kauffman, J. S.; Ellerbrock, B. M.; Stevens, K. A.; Brown, P. J.; Pennington, W. T.; Hanks, T. W. *Appl. Mater. Interface* **2009**, *1*, 1287.
40. Lasic, D. D. Applications of Liposomes. In *Handbook of Biological Physics*; Lipowsky, R., Sackmann, E., Eds., Elsevier Science: New York, 1995.
41. Kolusheva, S.; Shahal, T.; Jelinek, R. *Biochemistry* **2000**, *39*, 15851–15859.
42. Volinsky, R.; Kolusheva, S.; Berman, A.; Jelenik, R. *Langmuir* **2004**, *20*, 11084.

Downloaded by PURDUE UNIVERSITY on July 29, 2013 | http://pubs.acs.org
Publication Date (Web): July 24, 2013 | doi: 10.1021/bk-2013-1138.ch010

Editors' Biographies

Michael H. Tunick

Michael H. Tunick received a B.S. in Chemistry from Drexel University in 1977 and a Ph.D. in Physical-Analytical Chemistry from Temple University in 1985. Since then he has been a research chemist at the Eastern Regional Research Center of the U.S. Department of Agriculture in Wyndmoor, PA, where he is with the Dairy & Functional Foods Research Unit. He investigates the chemistry of cheese and bioactive compounds in milk, and has co-authored over 100 publications. He is the Secretary and a Past Chair of the ACS Division of Agricultural and Food Chemistry, and was named an ACS Fellow in 2011.

Charles I. Onwulata

Charles I. Onwulata is Director of the Office of the Chief Scientist for the United States Department of Agriculture's (USDA) Research, Education, and Economics mission area. Before this appointment, he was a Lead Scientist and Food Technologist for the dairy research program at the USDA, ARS, Eastern Regional Research Center, Wyndmoor, PA. Dr. Onwulata was also the Coordinator of the Center of Excellence in Extrusion and Polymer Rheology there. Dr. Onwulata is a Fellow of the Institute of Food Technologists. He received his Ph.D. in 1991 in Food Science and Agricultural Engineering from University of Missouri-Columbia.

Downloaded by UNIV OF ROCHESTER on July 29, 2013 | http://pubs.acs.org
Publication Date (Web): July 24, 2013 | doi: 10.1021/bk-2013-1138.ot001

© 2013 American Chemical Society
In Physical Methods in Food Analysis; Tunick, M., et al.;
ACS Symposium Series; American Chemical Society: Washington, DC, 2013.

Subject Index

In Physical Methods in Food Analysis; Tunick, M., et al.;
ACS Symposium Series; American Chemical Society: Washington, DC, 2013.

Downloaded by 137.207.120.173 on July 29, 2013 | http://pubs.acs.org
Publication Date (Web): July 24, 2013 | doi: 10.1021/bk-2013-1138.ix002

G

H

M

N

O

P

Downloaded by 137.207.120.173 on July 29, 2013 | http://pubs.acs.org
Publication Date (Web): July 24, 2013 | doi: 10.1021/bk-2013-1138.ix002

In Physical Methods in Food Analysis; Tunick, M., et al.;
ACS Symposium Series; American Chemical Society: Washington, DC, 2013.

Q

R

S

Downloaded by 137.207.120.173 on July 29, 2013 | http://pubs.acs.org
Publication Date (Web): July 24, 2013 | doi: 10.1021/bk-2013-1138.ix002

In Physical Methods in Food Analysis; Tunick, M., et al.;
ACS Symposium Series; American Chemical Society: Washington, DC, 2013.

Downloaded by 137.207.120.173 on July 29, 2013 | http://pubs.acs.org
Publication Date (Web): July 24, 2013 | doi: 10.1021/bk-2013-1138.ix002

In Physical Methods in Food Analysis; Tunick, M., et al.;
ACS Symposium Series; American Chemical Society: Washington, DC, 2013.